SOURCE PARAMETERS OF A MICROEARTHQUAKE SWARM IN TURKEY

John H. Lovell
B.Sc. University of London

Master of Philosophy
University of Edinburgh
1989

Declaration

I, John Lovell, declare that this thesis was entirely my own composition, and that, except where expressly stated to the contrary, the work described herein was completely carried out and written by myself.

Acknowledgements

The data upon which this thesis is based were collected during a seven-month field project in northwest Turkey in 1984. This, the third Turkish Dilatancy Project, was financed chiefly by the UK Overseas Development Administration, and carried out with my colleagues at the British Geological Survey, Edinburgh and at Kandilli Observatory, Istanbul. They were Stuart Crampin, Russ Evans, Alan Logan, Alistair Miller, David Booth, Sheila Peacock, John McDonald, David Beamish, Martin Russell, Balamir Üçer and Nafiz Kafadar, and are warmly thanked for helping me in so many ways.

The projects, although arduous at the time, have been very productive scientifically, and have also led to a fruitful working environment and warm and lasting friendships between the two parties of scientists, in spite of logistical problems and the difficulty of maintaining relationships over the distances involved. Throughout, the British team was shown nothing but warmth and hospitality by the Turkish people, with the sole exception of one occasion when a three-component seismic station was deliberately vandalised in an area where certain individuals were known to be hostile to investigations of any kind.

This research was undertaken part-time, and supervised jointly by Prof. K. Creer of Edinburgh University and Dr. S. Crampin of the British Geological Survey. I am grateful to Dr. Chris Browitt and the BGS management for permission to use BGS data and facilities for the production of this thesis, and also for a considerable degree of financial support.

The analysis was carried out under the supervision of Dr. Stuart Crampin, who, throughout, has given guidance and much encouragement, and without whose help and enthusiasm this thesis would not have been produced. Special thanks, too, are due to Russ Evans, Alan Logan and Charlie Fyfe, with all of whom I worked closely at some time or other. They were all unstinting in their efforts to help me with the geophysical and computing problems encountered. Many other colleagues have contributed advice and useful discussion at various times; all of them are warmly thanked. Prominent among these have been David

Booth and Peter Marrow. I hope that any omitted will not attribute this to ingratitude.

I would like to thank the proof-readers - Derek Abraham, David Booth, Peter Marrow, and Chris Thomas for pointing out the errors and inaccuracies in drafts of this thesis. Any mistakes remain my responsibility.

Last, but not least, thanks are due to my wife, Hélène, who, throughout the production of this thesis, has provided encouragement when the call of the mountains and the sea was almost too strong.

Abstract

A persistent swarm of microearthquakes located in a seismic gap near the North Anatolian Fault in Turkey has been monitored in detail by three Turkish Dilatancy Projects. Their purpose was to use the swarm as a natural data source with which to investigate shear-wave properties, to develop the hypothesis of extensive-dilatancy anisotropy, and (hopefully) to seek methods of earthquake prediction.

The introduction reviews the third project (TDP3) in 1984, in which the author participated, in the context of the long collaboration between the British Geological Survey and Kandilli Observatory, and the seismotectonics of that part of northwest Anatolia at risk from large earthquakes. The acquisition of the data set is described, and the method of earthquake prediction reviewed.

Succeeding chapters describe the theory and methods used by the author in the routine analysis of the data - the production of earthquake locations, magnitudes and fault-plane solutions. TDP3 utilised digital recording techniques and a greater number of three-component seismometers in a more closely spaced network directly above the microearthquake swarm than the previous projects. The increased resolution obtained has enabled the results of the previous projects to be confirmed and refined, and it is shown that the locations, magnitudes and fault-plane solutions are very similar to those found previously, and that the swarm's character has changed little in the period during which it was observed by the networks, even allowing for differences in network geometry and different operators. The use of the present fault-plane solutions in deriving and confirming the directions of the local tectonic stress is demonstrated, and the independent confirmation of these directions using polarization directions of split shear-waves is shown.

The clustering in space and time of microearthquakes in the swarm is described. Many, perhaps most, of the events in this swarm belong to clusters, some of which can be further sub-divided. It is suggested that detailed studies of such swarms will reveal much about the poorly-understood properties of the source regions of these microearthquakes, and, by extension, may reveal more of those of larger earthquakes.

Contents

Chapter 1

Description of the Turkish Dilatancy Projects

1.1 Introduction

This thesis describes the operation of, and results obtained from, a multidisciplinary geophysical experiment, during which a dense network of three-component seismograph stations monitored the seismicity of a section of the North Anatolian Fault, in northwest Turkey. The historical and tectonic context of the experiment will be illustrated in Chapter 1. The subsequent analysis of the large data set produced and the significance of the results obtained will be described in the succeeding chapters. The earthquake locations are the subject of Chapter 2, the magnitudes of Chapter 3, and the fault-plane solutions of Chapter 4. Chapter 5 describes new observations of clustering in space and time of earthquakes in a swarm. This formed the topic of the author's private research, interest in which was prompted throughout the project by discussion with various members of the research team. The location details of local earthquakes discussed in the text are presented in Appendix A. Appendix B summarises the published and oral presentations of this work and also discusses the author's function in the project. Published papers are bound into the end of this thesis as Appendix C.

The fieldwork upon which this thesis is based was carried out between March and November 1984, and was part of the third Turkish Dilatancy Project (TDP3). TDP3, a multidisciplinary project, was the culmination of a long history of fruitful collaboration between staff of the Edinburgh-based Global Seismology Research Group of the British Geological Survey (BGS) and counterparts at the Centre for Research and Development in Space and Earth Science of Boğaziçi University, Istanbul, Turkey. This latter organization was known as Kandilli Observatory before it was absorbed into Boğaziçi University, Istanbul. It is situated high on the Asian (east) bank of the Bosphorus, opposite the European city of Istanbul. It will be referred to as Kandilli in the text.

The previous two projects, TDP1 in 1979 and TDP2 in 1980, were devised to investigate a persistent swarm of microearthquakes located south of Izmit at the eastern end of the Marmara Sea, and to use data recorded to research a method of earthquake prediction. The swarm was identified by a network of seismometers situated in northwest Turkey. This network, consisting of twelve stations, run by Kandilli Observatory, and recording on paper drums, was set up in 1971, and augmented in 1978 by MARNET, financed by the UK Overseas Development Administration (ODA). MARNET, a much more extensive network, monitored the Marmara Sea area and northwest Anatolia (the name normally applied to Turkey-in-Asia), and provided a much more comprehensive data set with which to advance the science of earthquake prediction. The pattern of seismicity in western Turkey identified by these networks has enabled the complex tectonics of the Marmara Sea area to be described and put into the regional context of the northward movement of the African Plate with respect to the relatively stationary Eurasian Plate, and the consequent westward migration of the Anatolian or Turkish Plate along the line of the North Anatolian Fault (tectonic escape). It has also provided a data set with which to assess the seismic risk in western Turkey. Many such studies have been carried out, not only in the Mediterranean region but in other parts of the world. They are proving highly important in the development of building codes and emergency procedures, and emphasise the need for high-quality data sets, as throughout history, Turkey has suffered devastating earthquakes, and various cities in the Marmara area have on occasion been severely damaged.

Man has long tried to predict earthquakes, chiefly without success until very recently when earthquakes have been predicted using scientific principles in Japan, China (Raleigh *et al.* 1977), the USA (Bakun & Lindh 1985) and Mexico (Ohtake *et al.* 1977). The many methods of earthquake prediction have been reviewed by Rikitake (1976); some of these methods have been scientifically quantified and appear to offer the prospect of reliable earthquake prediction. The most promising for long-term prediction, at least in some areas, is the seismic gap principle. This was first suggested by Fedotov (1965; 1968), working in the USSR, and later, independently, by Mogi working on the circum-Pacific between Japan and Alaska, in a series of papers

culminating in Mogi (1969). The seismic gap principle, when combined with intensive but expensive local monitoring as suggested later (section 1.5.9), must surely lead to accurate earthquake prediction. A seismic gap is an area of low seismicity surrounded by areas exhibiting much higher levels of activity and where aseismic creep is not occurring. This phenomenon has been noted from many parts of the world, for example along the Pacific coast of South and Central America (Kelleher *et al.* 1973), in Japan, (Utsu 1972a, 1972b; Utsu 1974; Rikitake 1974; Ando 1975), in the USA (Allen *et al.* 1965; Brune & Allen 1967), in Turkey (Toksöz *et al.* 1979) and elsewhere. Areas at risk were identified by a study of the seismicity patterns and historical seismicity records, and, in the case of the USA, the seismic gaps were observed to coincide with the epicentral areas of the damaging 1857 Fort Tejon and 1906 San Francisco earthquakes. A knowledge of the recurrence times of large events can therefore lead to prediction of the likely location, and a rough idea of the time of an earthquake. At present this uncertainty is causing concern in California, where large urban areas are at risk from an expected large event, and demonstrates the need for a method which will give a more accurate idea of the time of the event. Such a method of earthquake prediction has been suggested (Crampin 1987b) and demonstrated in principle (Chen *et al.* 1987; Peacock *et al.* 1988; Booth *et al.* 1989) as a result of the long collaboration between BGS and Kandilli Observatory in earthquake research in the Marmara area. This significant achievement will be discussed further in a later section of this chapter (1.5.9).

The importance of the detailed analysis of earthquake shear-waves was gradually realised in the late 1970s, as BGS modelling work took place on the increasing numbers of recordings of shear-waves. The Turkish Dilatancy Projects were designed to use the microearthquake swarm as a source of shear-waves. The projects evolved with time, each using a greater number of three-component seismometers and a slightly different network configuration from the previous one, as the importance of the shear-wave window concept was realised (section 1.4.4). This evolution enabled the results of the preceding projects to be confirmed and refined. The network in use during the last project consisted of two single-component and nine three-component surface seismometers, had an aperture of about 15 km, and was sited

around 10 km above the swarm. It provided a dataset consisting of over 4000 earthquakes - locals, regionals and teleseisms.

This first chapter includes a description of the historical background of the projects, the seismicity and tectonics of the area, and the work involved in TDP3. It also summarises the method of earthquake prediction which was developed during the projects.

1.2 The study area

1.2.1 The Marmara Sea region

The Turkish Dilatancy Projects were carried out in a field area which lies south of Izmit in the hills formed by the southern limit of a half-graben structure running roughly east-west from Adapazarı through the Marmara Sea (Fig. 1.1). The country is of high relief, ranging from sea level up to well over 1500 m, in fact the highest station used in the TDP networks lies at 1604 m. The country rock consists chiefly of basaltic lava piles and ash flows, together with a few pale-coloured limestones, all of Palaeozoic age (Brinkmann 1976 and the author's observations). Most of western Anatolia is thought to consist of a patchwork of terranes which were amalgamated as a result of the closure of the Tethyan ocean (section 1.3.1). As a result of the rapid uplift to which this area has been subjected, intense dissection by the northward-flowing streams has taken place. Along the coastal areas, fans of coarse alluvial detritus, themselves highly uplifted and dissected, have been formed, and are of Eocene age. The low-lying, half-graben structure running along the coastal strip and eastwards from Izmit Bay through Adapazarı and Lake Sapanca is filled with an unknown thickness of unconsolidated muds and silts, probably overlying the Eocene fans. This sediment pile was found to cause some perturbation of seismic waves propagating through it. Consequently, readings from the two seismic stations unavoidably sited on these sediments were not used in earthquake locations because of the unknown, and perhaps variable, velocity structure. However, *P*-wave polarity readings from these stations were used in the construction of fault-plane solutions.

The 100 km coastal strip along the northeastern margin of the

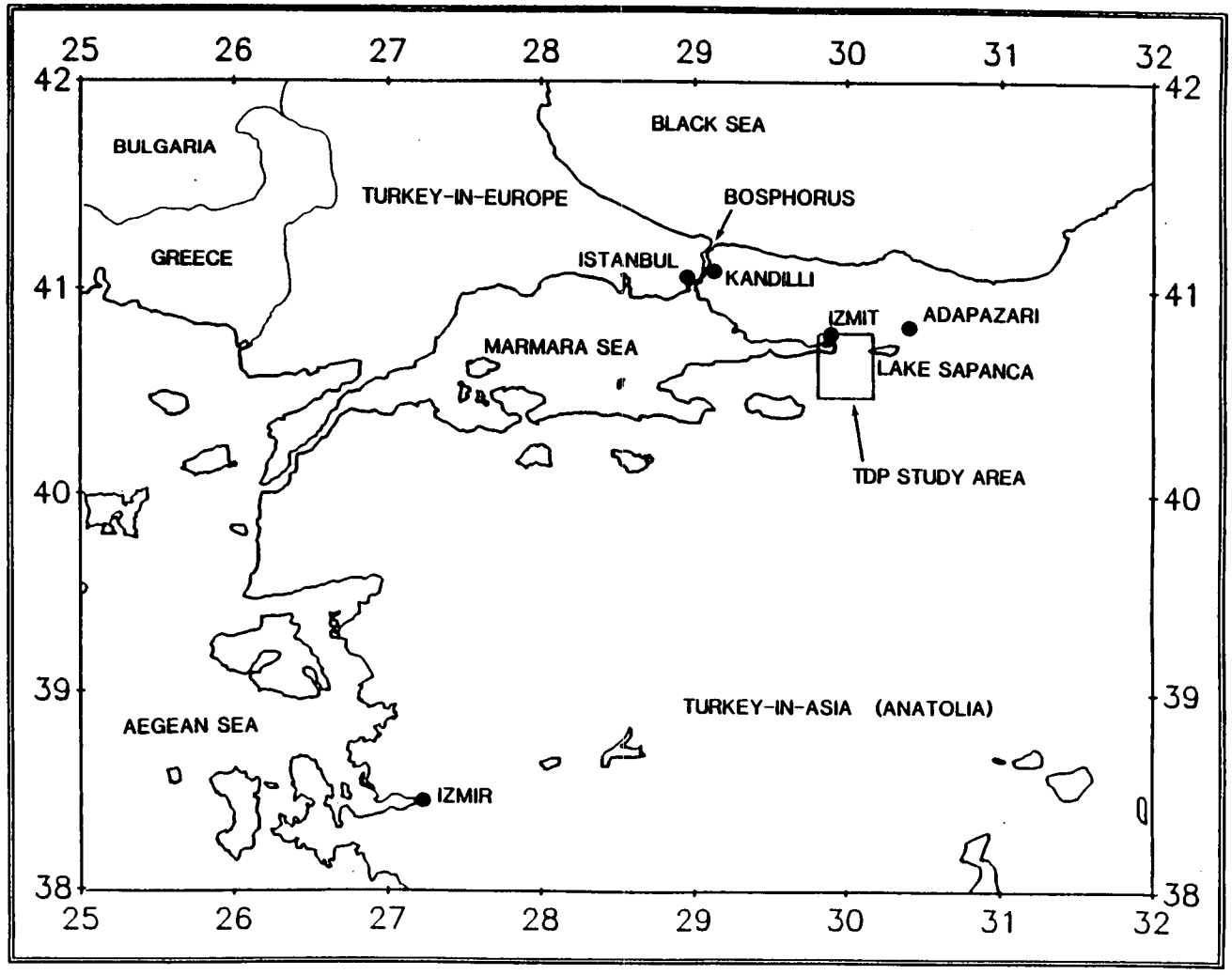

Figure 1.1 Geographical location of the TDP study area.

Marmara Sea between Istanbul and Izmit (Fig. 1.1) is heavily populated. Lines of communication between these two centres and Ankara and the interior run parallel with the shoreline. In addition, much of Turkey's industrial development has taken place here, relying on the large pool of labour and the ease of import and export by sea, road, rail and, latterly, air. A large part of Turkey's petrochemical industry is situated in a vast complex just west of Izmit (Fig. 1.1), and processes oil imported from the Middle East by sea and pipeline. The consequences to the populace and economy of major earthquake damage need no elaboration here. Kandilli Observatory staff have been able to use data from their networks to compile and enhance earthquake catalogues, and hence contribute to a better assessment of the earthquake risk in the area (Üçer *et al.* 1985).

1.2.2 History of seismic research in the area

Between 1970 and 1976, Kandilli staff installed a network of single-component Willmore Mk III seismometers over the western half of Turkey (Üçer *et al.* 1985). These instruments recorded on paper drums, and provided data which enabled Kandilli to monitor the overall seismicity of western Turkey and produce a short-term earthquake catalogue. Such earthquake catalogues, extended into the past by relocation of historical earthquakes, have been used by workers to assess earthquake risk, not only in Turkey and the Mediterranean region (for example, Karnik 1971; Burton 1979; Burton *et al.* 1984; Makropoulos & Burton 1984; Main & Burton 1988), but elsewhere in the world. The importance of a high-quality dataset can not be overemphasised, as Kandilli provides an information service to government departments and other interested parties on seismicity in general and earthquakes in particular, in much the same way as BGS does in the UK.

It was realised that with a station separation typically of around 150 km, the network (Fig. 1.2) could not produce the high resolution required. It was apparent that the seismicity over the area differed in character, being swarm-like in some regions but more continuous elsewhere. To provide more detailed data in the Marmara Sea area, (the populous and industrial area described in section 1.2.1), the Overseas Development Administration of the UK agreed to finance the

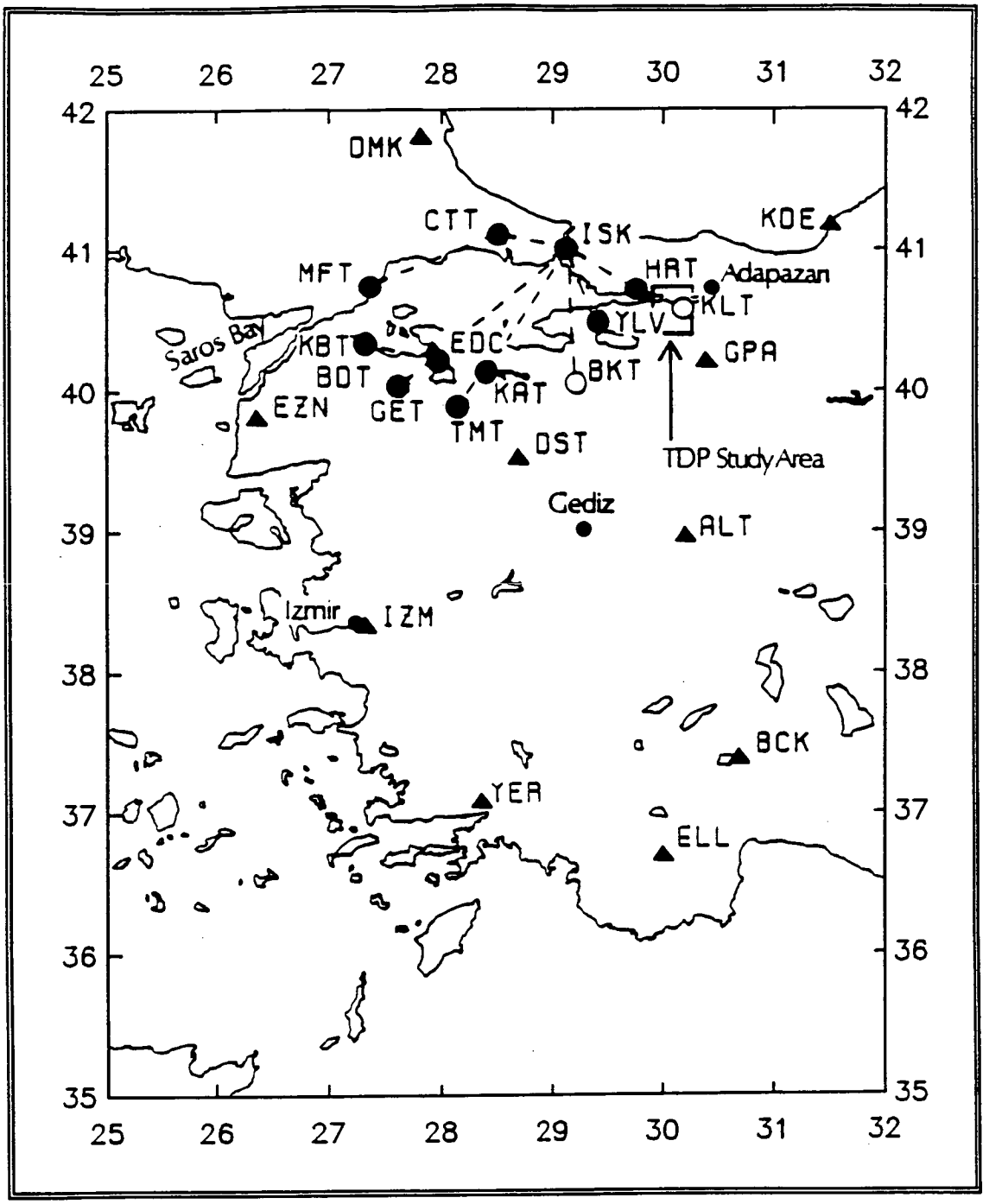

Figure 1.2 (after Üçer *et al.* 1985) Seismic stations operated by Kandilli Observatory in western Turkey. Circles indicate MARNET stations telemetered to Kandilli (ISK), triangles are ISK stations recording on paper drums. Solid symbols indicate current stations, open symbols those stations now abandoned.

installation and maintenance of a network of seismometers around the Marmara Sea coastal regions.

1.2.3 MARNET

With the financial backing of ODA, MARNET (Üçer *et al.* 1985) was installed in 1978 using instrumentation already proved on LOWNET (Crampin *et al.* 1970), and with the assistance of BGS personnel. A BGS engineer, A. Miller, spent five years on foreign service in Istanbul installing MARNET and providing backup and expertise. Since his departure from Turkey in 1982, ODA have financed the purchase of new equipment and annual visits by BGS staff to continue the maintenance and refinement of this network. Recently, an automatic triggering system, based on a PDP 11 minicomputer, and designed and developed by Dr J. R. Evans, has been installed on MARNET. This triggering system was under development during the TDP3 project (Evans *et al.* 1987 and section 1.5), and has since been used successfully on LOWNET in the UK, and in Kenya (Cooke *et al.* 1988).

MARNET consists of 12 stations, the locations shown in Fig. 1.2, each equipped with a Willmore Mk III seismometer, and radiolinked, via relay stations in some cases, to Kandilli Observatory (station ISK on Fig. 1.2). Trouble was experienced with two of the highest stations; they were susceptible to lightning damage, and were moved to safer ground which was unfortunate as they were particularly quiet and sensitive stations. Data are recorded on paper drums and analogue tape, and the recent addition of the digital triggered system should permit the prompt and more sophisticated analysis of events.

1.3 Seismotectonics of northwestern Turkey

The complex seismotectonics of the study area near Izmit cannot be thoroughly understood without some appreciation of the regional tectonic framework of the Aegean and eastern Mediterranean. Much of the structure and seismicity of this area, southern Europe, north Africa, the Middle East and Asia as far east as the Himalayas and China can be attributed to the closure of the Tethyan Ocean and the relative northward movement of the African, Arabian and Indian landmasses. The following section gives a brief introduction to those

events.

1.3.1 The Tethys

The Tethys (Dewey *et al.* 1973; Laubscher & Bernoulli 1977; Şengör 1984) was a complex, sub-tropical to tropical ocean, elongate east-west, and covering an area at least from present-day Iberia to eastern Asia. It is thought to have existed from about late Triassic times until its closure in the Tertiary. Its closure was brought about by the relative northward movement of the African and Arabian Plates (still joined at that time) towards the massive and relatively stationary Eurasian and Black Sea Plates. These events were intimately associated with the opening of the North Atlantic Ocean, the rotation of the Iberian Peninsula and the formation of the Alpine and Himalayan orogenic belts. As the Tethys closed, pieces of continent (terranes) were swept together (accreted) to form much of Turkey. Evidence for this accretion may be found in the Turkish ophiolite zones (Brinkmann 1976), which are thought to represent incompletely subducted or uplifted ocean floor sediments, basalts and mantle rocks, but which are not necessarily of the same age. The eventual collision between Africa and the Eurasian landmass resulted in the initiation of the North and East Anatolian Faults, as the Turkish or Anatolian Plate was squeezed westwards, as shown in Fig. 1.3, and as the Arabian Plate broke away from Africa and commenced movement northeastwards. The exact dating of these events is the subject of much discussion (Şengör *et al.* 1985). The westward movement of Turkey in response to this collision is termed 'tectonic escape' (Burke & Şengör 1986). An analogous process takes place farther east, where a large fragment of southern China is being squeezed eastwards along major faults into the Pacific and Philippine Plates (Tapponier *et al.* 1986). A fuller review of the Tethyan events can be found in Dewey *et al.* 1973, and Şengör 1984, and is outside the scope of this work.

1.3.2 The North Anatolian Fault

The North Anatolian Fault (hereinafter abbreviated to NAF) is a prominent, east-west trending, dextral strike-slip fault (Fig. 1.3). A thorough review of its characteristics may be found in Barka &

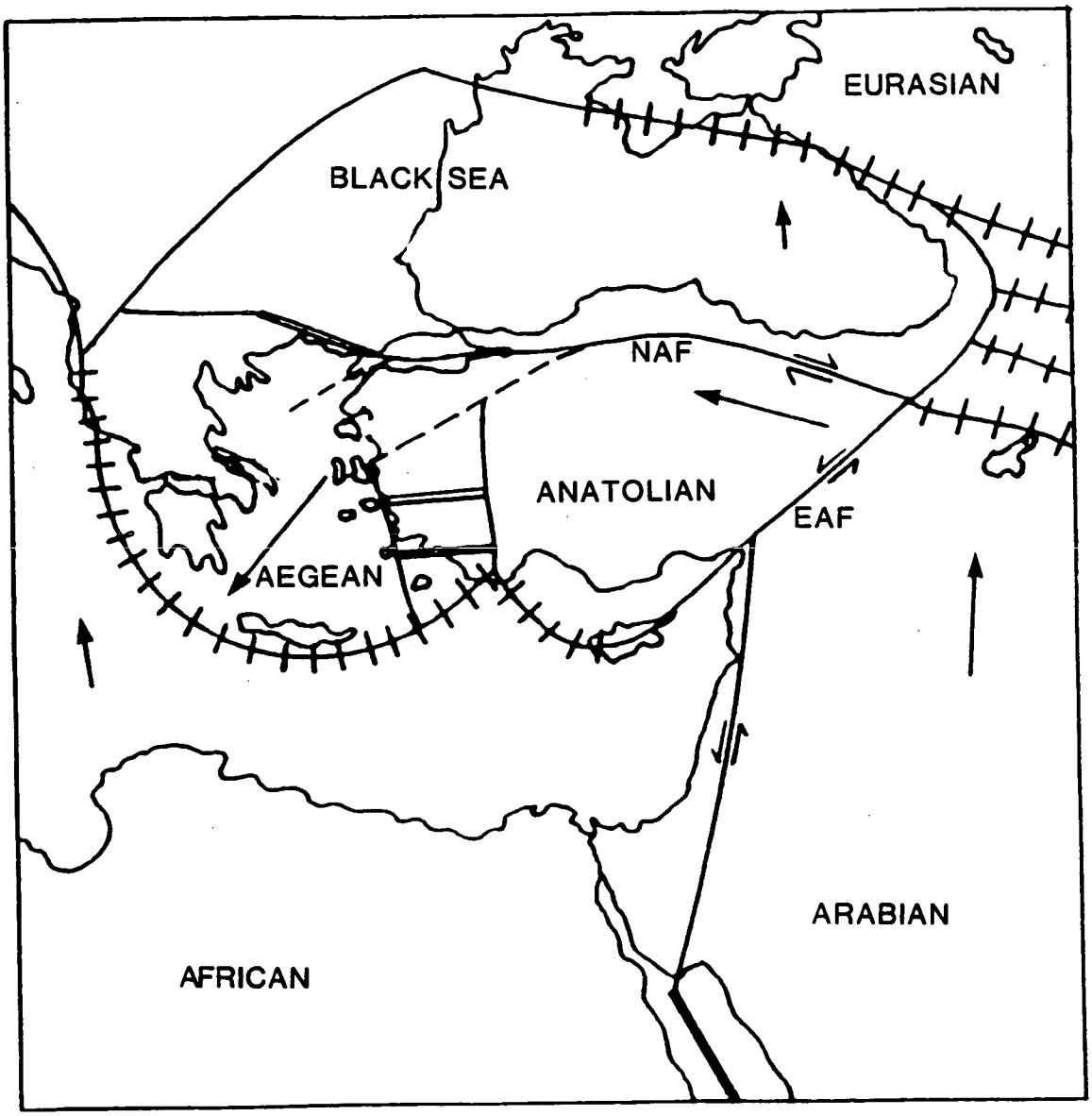

Figure 1.3 (based on McKenzie 1972 and Logan 1987) Generalised outline of the plates in the eastern Mediterranean region. Arrows indicate the direction of motion of each plate relative to the Eurasian plate, and their lengths are proportional to the relative plate velocities. Transcurrent faulting is indicated by a single line (dashed where uncertain), normal faulting by a double line, and thrusting and subduction by a single line with bars. NAF and EAF indicate respectively the North and East Anatolian Faults.

Kadinsky-Cade (1988). Estimates of its offset vary between 90 km (Dewey & Şengör 1979) and 120 km (Le Pichon & Angelier 1979), but later workers suggest the figures of between 15 and 40 km (Barka & Kadinsky-Cade 1988). It separates the massive and relatively stationary Eurasian-Black Sea Plate to the north from the westward-migrating Anatolian plate to the south. The westward movement of the Anatolian Plate occurs along the NAF in the same way as similar motion takes place between the Anatolian and Arabian Plates along the sinistral East Anatolian Fault. Both faults are associated with high seismicity, and have been frequently compared with the San Andreas Fault in California, for example, by Allen (1975). The NAF was initiated in the Middle to Upper Miocene (Dewey & Şengör 1979; Le Pichon & Angelier 1979), about 13 million years ago.

From its junction with the East Anatolian Fault westwards to the Adapazari area, near Izmit (Figs 1.3 & 1.4), the NAF is a classical strike-slip fault, and forms a well-defined zone of parallel rifts with tensional features such as pull-apart basins, sag ponds, normal faults, and is associated with minor recent volcanism (Ambraseys 1970; Dewey & Şengör 1979; Şengör 1979; Şengör & Canitez 1982).

The nature of the NAF changes at the eastern extremity of the Marmara Sea. On the basis of their associated seismicity, three distinct lineations have been recognised radiating from this area of trifurcation (Crampin & Üçer 1975; Üçer *et al.* 1985). The northern branch of the NAF continues in a direct line westwards as a graben structure, forming Lake Sapanca, Izmit Bay and a deep trough in the Marmara Sea. It reappears as a south-west trending strike-slip fault on the north-west shore of the Marmara Sea, and continues into the Aegean Sea as a deep trough.

The middle lineation follows the southern shore of the Marmara Sea westwards, changing strike to south-west towards the western extremity of the sea. Although it is less well-defined seismically than the other two lineations, it is well outlined by surface geology (Dewey & Şengör 1979).

The southern lineation strikes south-west from the trifurcation area. It follows approximately the line of the Izmir-Ankara

ophiolitic suture zone, (Şengör & Yilmaz 1981).

Farther west, movement on the two southern branches of the NAF is taken up in the extensional zone of western Anatolia and the Aegean Sea. The Aegean is a complex area, and there is much debate about its detailed structure. It is an area of predominantly normal faulting, thin crust (Makris 1976), and high heat flow, and the extension is probably driven by the continuing subduction of the African Plate beneath the Hellenic Arc (Makropoulos & Burton 1984), and associated slab-pull. Modern ideas have been reviewed by Main (1985). The northern branch of the NAF continues westwards into the North Aegean Trough. A suggestion was made (McKenzie 1972), but later retracted (McKenzie 1978), that the fault continued westwards into central Greece. Seismic evidence (focal depths) indicates that this is probably not the case (Makropoulos & Burton 1984), and it possibly continues northwestwards into Yugoslavia (Dr. J. R. Evans, personal communication).

1.3.3 The Marmara Block

The swarm of small earthquakes identified by MARNET near the NAF was monitored during the Turkish Dilatancy Projects, TDP1 in 1979, TDP2 in 1980 (Crampin *et al.* 1985) and TDP3 (Evans *et al.* 1987) in 1984. This persistent swarm of microearthquakes is associated with the southern limb of a graben structure beneath the hills south-east of Izmit, at the eastern end of the Marmara Sea (Fig. 1.4). Here the nature of the NAF changes, and it has been suggested (Evans *et al.* 1985) that this is a key area for understanding the complex tectonics of western Anatolia.

Recognition of the three seismically-defined lineations outlining the NAF in the study area has led Evans *et al.* (1985) and Crampin & Evans (1986) to postulate the existence of the Marmara Block (Fig. 1.4) as a distinct seismotectonic unit. This wedge-shaped zone of accommodation is trapped between the Eurasian and Anatolian Plates, and is being rotated and internally sheared by the westward movement of the Anatolian Plate as it is pushed against the bulge of Thrace. Seismicity associated with the Marmara Block is typically low-magnitude and persistent, and displays marked clustering. Its

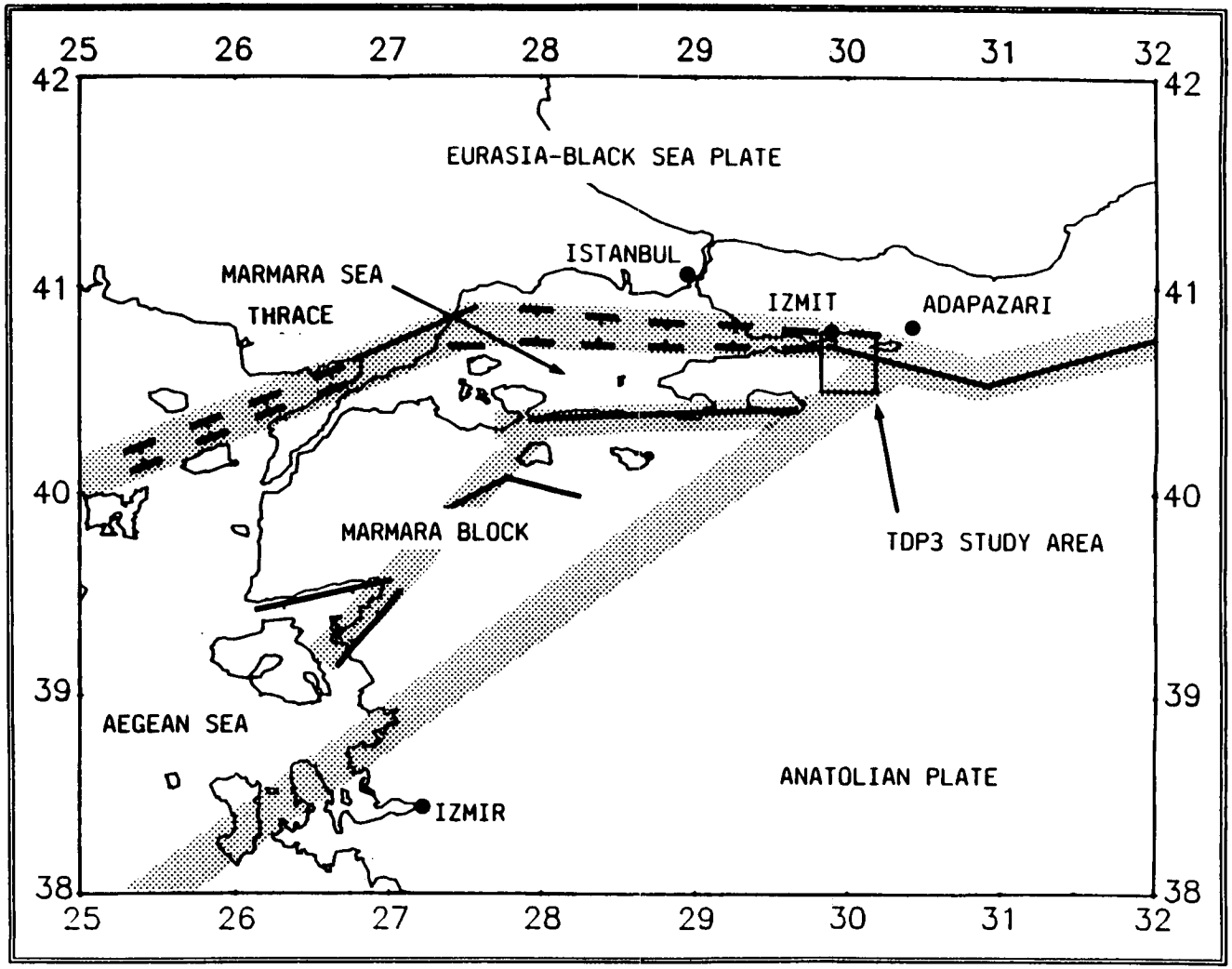

Figure 1.4 (after Crampin & Evans 1986) Location and simplified tectonics of TDP3 study area; solid and dashed lines show the trace of the North Anatolian Fault and its subsidiary faults on land and under water respectively.

character is therefore somewhat different from that of the rest of western Anatolia, which generally displays the more usual foreshock/mainshock/aftershock sequences, and suggests that the Marmara Block behaves as a discrete tectonic unit (Crampin & Evans 1986). Crampin & Booth (1985) conclude that sub-horizontal tension provides the main driving force for movement on the NAF in this area, and this is confirmed by the geometry of the plate motions (Crampin & Evans 1986).

An alternative theory for the structure in this area has recently been proposed by Barka & Kadinsky-Cade (1988). Using geological information projected beneath the Marmara Sea with seismic reflections and bathymetric data, they suggest that much of the northern Marmara Sea floor area consists of discontinuous pull-apart basins separated by strike-slip and normal faults. The pull-apart basins correspond with bathymetric lows, and are associated with seismicity and extensional focal mechanisms. They also suggest that the graben structure running east-west through Izmit Bay is rather more complicated, and is, in fact, a combination of strike-slip and normal faulting.

There appears to be no incompatibility between these alternative hypotheses except for the underlying driving mechanism. Both suggest deformation similar in nature in the area, but the Marmara Block postulation appears to fit the seismic data rather better, and also fits the Marmara area into its regional context. It is clear that more data will enable the true nature of this complex area to be resolved.

1.3.5 Other earth science research in the area

In addition to the BGS/Kandilli collaborative projects in seismology and geomagnetism, various other geophysical and geological projects have taken place in the area. Farther east, near Adapazari (Fig. 1.4), a German/Turkish group is collaborating in a wide range of studies (Zschau *et al.* 1981, 1982). Their instruments are monitoring seismicity, geomagnetism, tilt and groundwater chemistry along a section of the North Anatolian Fault a few km east of its trifurcation point. A regional microgravimetric survey is being

carried out by a University of Edinburgh/Technical University of Istanbul (ITU) team between Bolu, Bursa and Istanbul (see Fig. 1.12), (Russell 1988); their investigations are still in progress.

Small-scale geological projects have been undertaken in the vicinity of the study area. These are generally very local, and the results inaccessible to western workers. The geological map of the region is at a scale of 1:1,000,000, and there is a pressing need for a modern survey, oriented towards structure and tectonics. This, together with heat flow measurements, so far not undertaken, would enable a comprehensive synthesis of the complicated tectonics and structure of the area to be attempted, and could well result in a better understanding of the Izmit seismic gap (section 1.4.1).

1.4 TDP1 and TDP2

1.4.1 Introduction

Only the largest events in the swarm of microearthquakes near Izmit identified by MARNET (section 1.2.3) could be located by that network. Resolution was to only about ±10 km (Crampin *et al.* 1985). This was considered inadequate for the purposes of shear-wave analysis. Accordingly, with financial support from ODA, and with the collaboration of colleagues at Kandilli Observatory, field projects in that area were planned. The area was relatively aseismic, and had been designated as a seismic gap by Toksöz *et al.* (1979). Seismicity along the NAF is cyclic (Ambraseys 1970), and historical evidence points to at least two previous cycles of activity (Barka & Kadinsky-Cade 1988). It has been noted by various authors, for example, Pamir 1944; Ambraseys & Zatopek 1969; Dewey 1976; Toksöz *et al.* 1979, that the latest major earthquake epicentres on the NAF formed a sequence migrating westwards, starting with the 1939 Erzincan event and ending with the 1967 Mudurnu event. Surface breaks of these earthquakes extend as far west as Lake Sapanca. There is then a break between this sequence and the 1963 Çinarcik event to the west. The swarm studied by the TDP experiments lies within this gap, which, unless the accumulated strain is being aseismically accommodated, must expect a large earthquake in the future. Further evidence for this theory lies in the fact that similar swarms

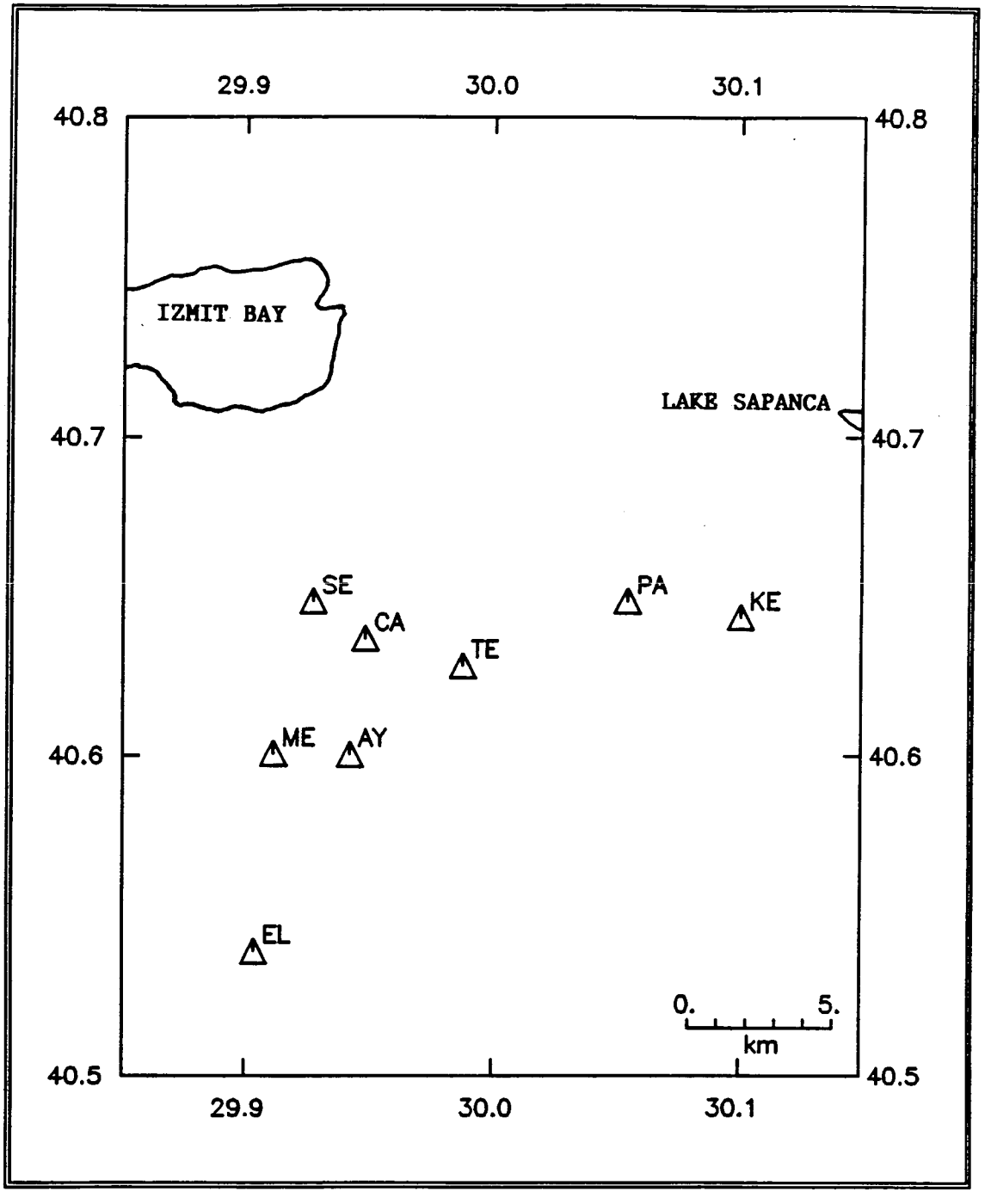

Figure 1.5 Stations used during TDP1, 1979

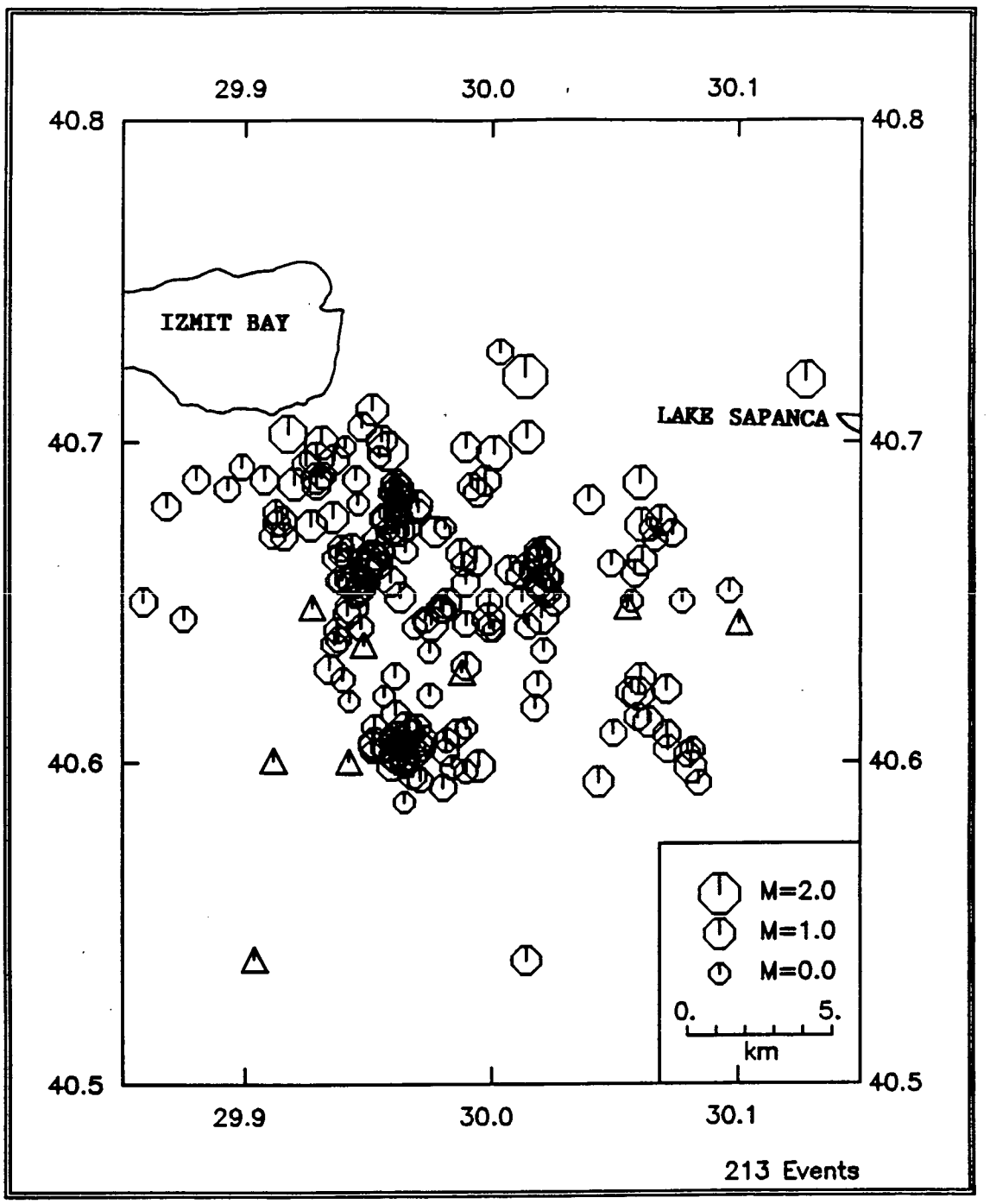

Figure 1.6 Events located during the six-week TDP1 experiment, 1979

identified farther west by MARNET seem to be associated with the epicentres of the large 1912 Mürefte and the 1935 Marmara Island earthquakes (Crampin & Evans 1986). Additionally, no large event has occurred in the Izmit area this century (Barka & Kadinsky-Cade 1988).

1.4.2 TDP1

During TDP1, in 1979, after a brief trial with a few vertical seismometer stations to locate the swarm of earthquakes, a network of up to eight three-component seismometers was deployed in that area, with the base station situated at station SE (Fig. 1.5). Instrumentation was the same as that used in TDP3 (see section 1.5.3). It was operational for six weeks. The velocity structure of the area was found by timing local quarry blasts. This structure was used for locating events in all three TDP experiments. The locations of the events are shown in Fig. 1.6. It was found that the network was slightly off-centre from the swarm, however, and the epicentres slightly deeper than anticipated, and a further project was planned.

1.4.3 TDP2

The TDP2 network of nine three-component seismometers (Fig. 1.7) was deployed over a larger area than that used in TDP2, in order to increase coverage of the upper focal sphere. The stations were radiolinked to a PTT microwave station near Izmit (IZ), and were operational for nine weeks in 1980. Epicentres located by this network are shown in Fig. 1.8. Some of the stations were found to be too remote from the earthquake epicentres, and the shear-waves propagating to them were incident at the surface at too high an angle. The significance of this was not fully realised until the results were processed (Crampin & Booth 1985; Evans 1984). The shear-wave arrival was frequently masked by the *P*-wave coda, making polarization reading difficult. However, the increased coverage of the focal hemisphere provided improved the fault-plane solutions.

1.4.4 Results of TDP1 and TDP2

The results obtained from TDP1 and TDP2 were very similar. The level of activity in the latter appears to be slightly less, but this

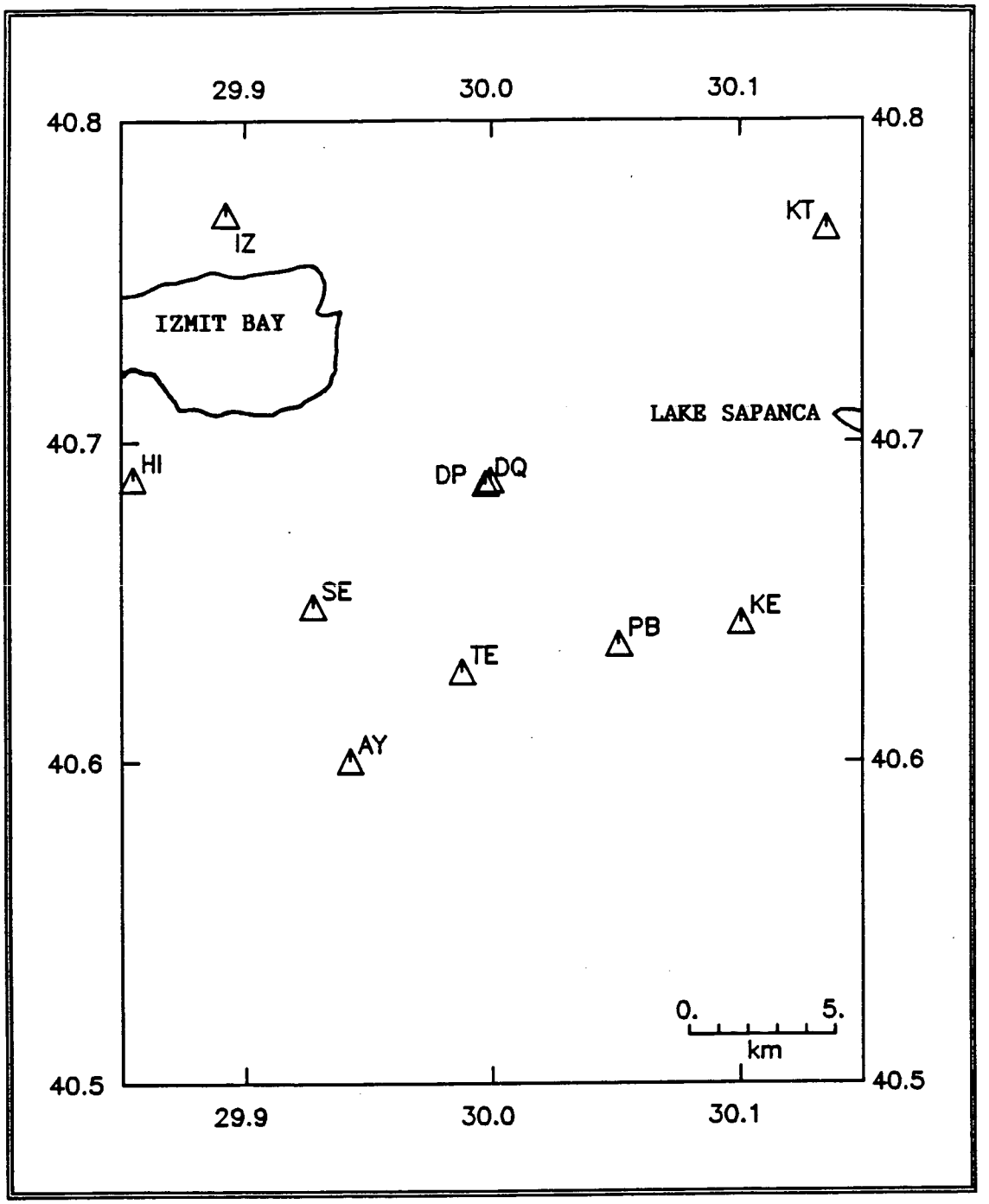

Figure 1.7 Stations used during the two-month TDP2 experiment, 1980. Note that stations DP and DQ have been separated on the map for clarity.

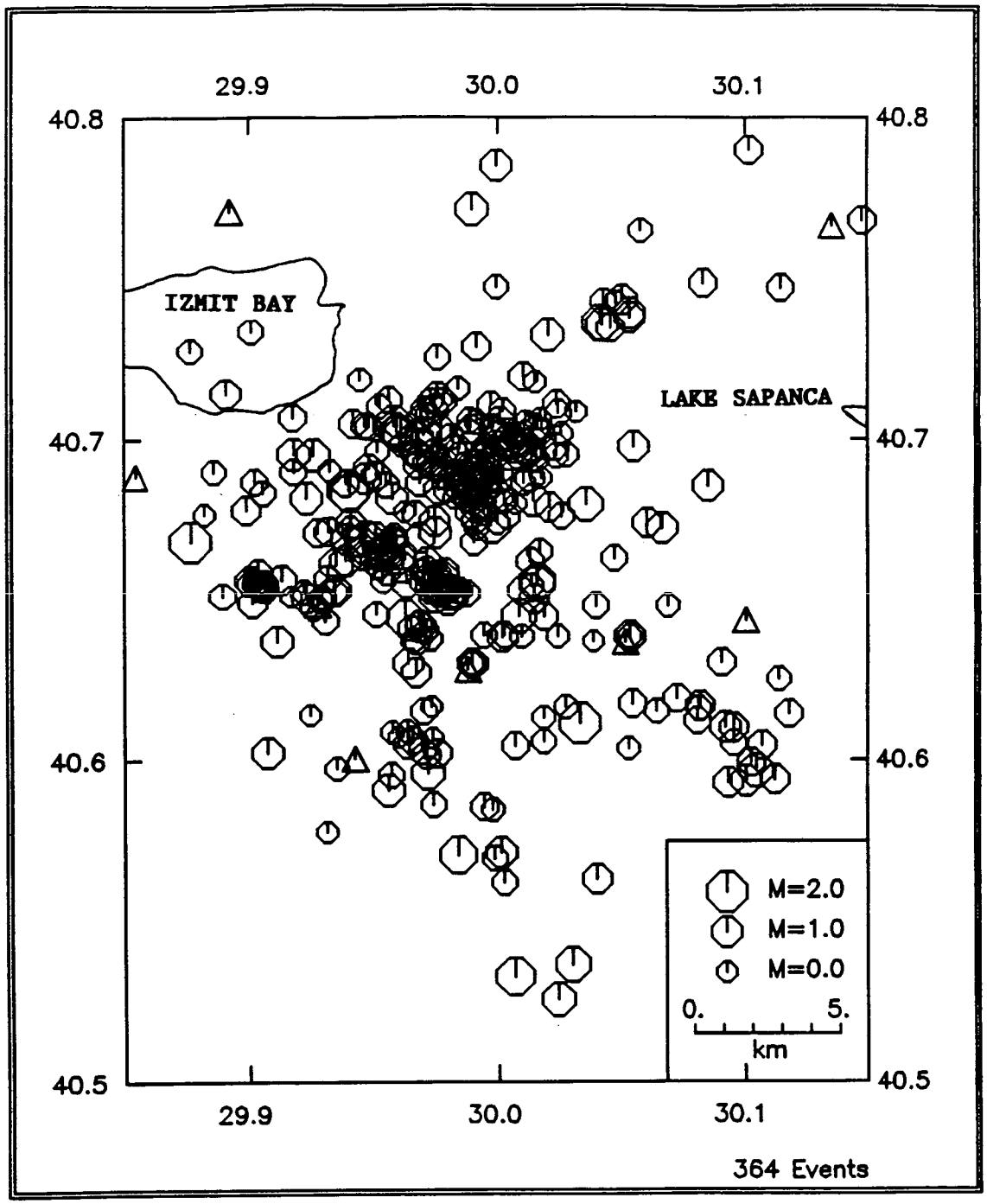

Figure 1.8 Events located during the two-month TDP2 experiment, 1980.

may be a reflection of the differing network geometry and periods of operation. The various other geophysical parameters derived, such as locations, magnitudes, stress directions, polarization directions of the leading split shear-waves, and fault-plane solutions were all confirmed (Lovell *et al.* 1987) by the better resolution obtained in the later, longer and more comprehensive study, TDP3, on which this thesis is based. The succeeding chapters discuss the TDP3 results in detail, and will include a comparison with the preceding studies.

The concept of the shear-wave window (Evans 1984) was an important development from the two projects. It became apparent that some shear-wave arrivals were severely modified by contact with the free surface, so much so that any polarization readings were unreliable or impossible. This phenomenon was studied, and it was realised that this shear-wave perturbation occurred when shear-waves were incident at the surface at high angles. The critical angle of incidence below which shear-wave arrivals are unaffected is approximately 35°, or $\mathrm{Sin}^{-1}(V_s/V_p)$, where V_s and V_p are the velocities of shear- and *P*-waves respectively, assuming a Poisson's Ratio of 0.25 for the propagation medium. It follows that shear-waves should always be observed within the shear-wave window - that roughly circular area of ground above the shear-wave source where incidence angles are always less than the critical angle (shown schematically in Figure 1.9). However, some topographic influences can be seen, even within the shear-wave window, especially in areas of high relief. This effect was observed at stations PA and PB in the projects (Crampin & Booth 1985; Booth *et al.* 1985). The stations are only a kilometre or two apart, yet the polarization directions of the leading split shear-waves (explained fully in section 1.5.9) were about 60° different. At first, this was attributed to perturbation of the local stress field by a large local earthquake which occurred between the projects. It is now known that this was the effect of local topography on the shear-waves. These topographic effects were again observed and confirmed in TDP3 (section 1.5).

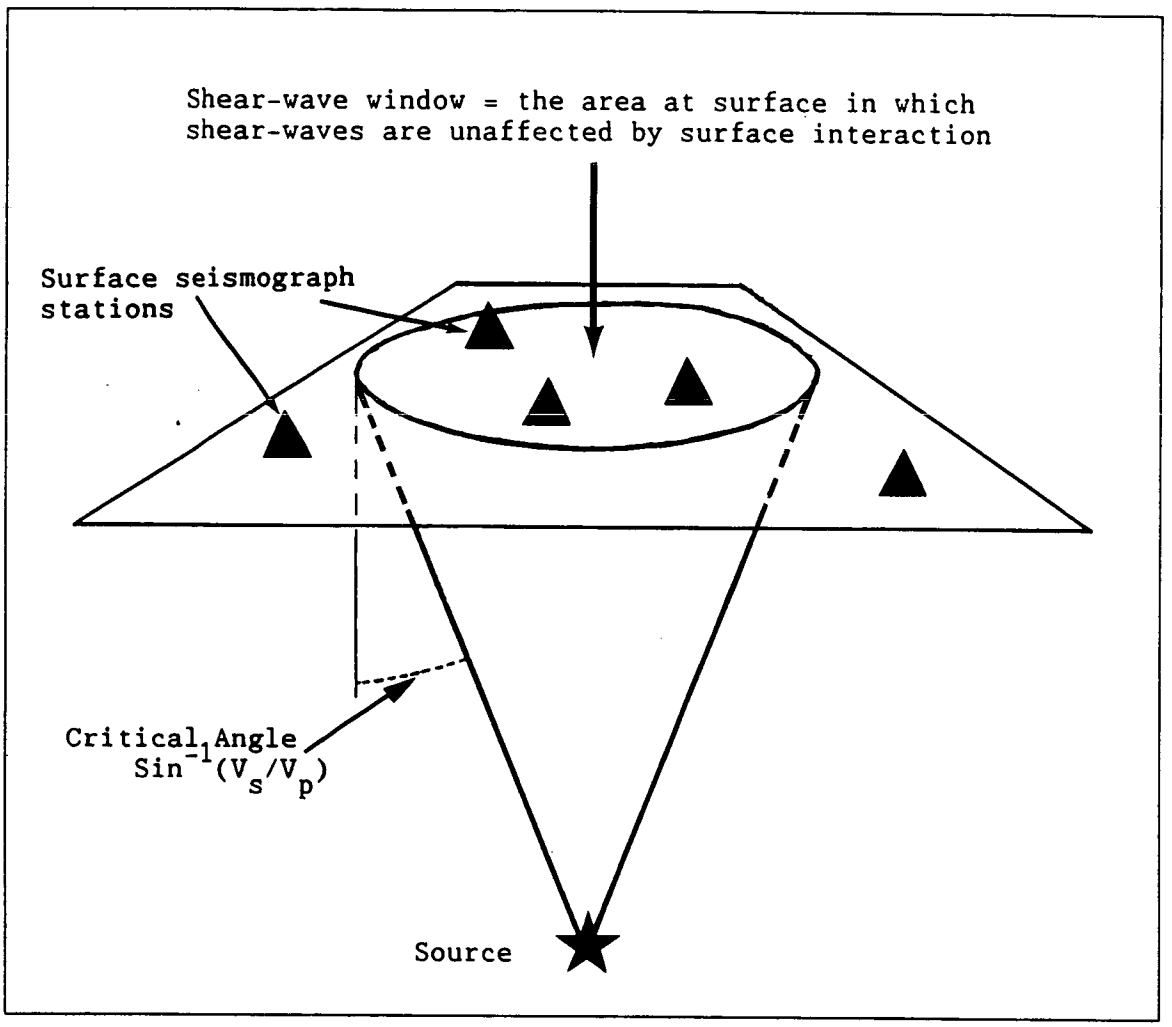

Figure 1.9 Diagrammatic illustration of the shear-wave window

1.5 TDP3, 1984

1.5.1 Introduction

Planning for TDP3 began soon after the analysis of the results of the previous projects, TDP1 in 1979 and TDP2 in 1980 (section 1.4). As TDP3 was planned as a multidisciplinary project, involving staff of the Global Seismology and Geomagnetism Research Groups of BGS as well as Turkish counterparts, early liason avoided unnecessary duplication of effort. Wherever possible, equipment packing, shipping, vehicle purchase and conversion, and documentation such as visas, work permits, and medical and customs matters were dealt with centrally, chiefly by the author. A reconnaissance visit to Turkey was made in late 1983 by Drs. D. Beamish and J. R. Evans of the Geomagnetism and Global Seismology Research Groups respectively. During this visit, talks were held with Kandilli staff and the British Council, and with various Turkish Government Ministries in Ankara, from whom the necessary permission, such as for radio operation, access to school buildings, etc., was obtained. Plans were also made about the disposition of new seismic and geomagnetic stations, and about the general aims and execution of the project.

By mid-1983, much of the equipment necessary had either been purchased, ordered, or constructed in-house. The long task of checking, calibrating and packing was complete by early 1984, and in March, 1984, the equipment, worth about £500,000 and weighing around 5 tonnes, was despatched overland to Istanbul. Shortly after this, two Land Rovers were driven out by four members of the party. The remaining members arrived by car a few days later. The British Council in Istanbul had arranged customs clearance of the equipment, which was delivered direct to Kandilli, arriving a matter of hours before the Land Rover party.

Preparation for field work was commenced by unpacking all the equipment, and installing it in the laboratories provided at Kandilli (section 1.5.2). All equipment was examined, and tested. The 45 seismometers were reset to a free period of 1 sec, and their sensivities re-measured. The amplifier/modulator damping factors were checked, and the gains set to a position corresponding to a damping

factor of 0.6. The radio transmitter and receiver frequencies and outputs were reset. Meanwhile, purchases were made locally of such items as wood for pit liners, cement, wire, plugs, scaffold pipe and clips for antenna masts, water pipe and various other equipment necessary. Some of this was used by the workshop staff at Kandilli to fabricate equipment used during the network installation.

The TDP3 experiment was under the overall direction of Dr. S. Crampin in Edinburgh. The Global Seismology Research Group staff in Turkey consisted of Dr. J. R. Evans, A. Miller, the author and A. L. L. (now Dr.) Logan. Working visits were made to Turkey at various times by Dr. S. Crampin, Dr. D. C. Booth and Miss (now Dr.) S. Peacock. The Geomagnetism Research Group team comprised Dr. D. Beamish, J. McDonald and M. (now Dr.) Russell.

1.5.2 Kandilli Observatory

Kandilli Observatory, now part of Boğaziçi University, Istanbul, is situated in an elevated position overlooking the Bosphorus, on the Asian side of this busy waterway. Two laboratories were made available to the BGS party. In one, the Seismology team installed desks and testbenches, where instruments could be tested and repaired. A PDP 11 minicomputer and tape playout facilities were installed, and used for preliminary data analysis. The Geomagnetism group set up a similar lab. These labs were shaded, so extreme temperatures were no problem, and were regularly and scrupulously cleaned because of the delicate nature of some of the instruments serviced there. Radio contact with the base station at Hereke, and sometimes with field parties, was possible, and a listening watch was kept at Kandilli at all times.

Kandilli staff normally accompanied BGS personnel on field trips. An element of training and instruction was built into the projects, and, at various times, students from neighbouring institutions participated in station visits and normal analysis procedures. Since the last project, a technician from Kandilli has spent a six-week training period at BGS, Edinburgh, working primarily with BGS technicians on instrument design and servicing, and gaining expertise invaluable in the smooth running of a sophisticated network.

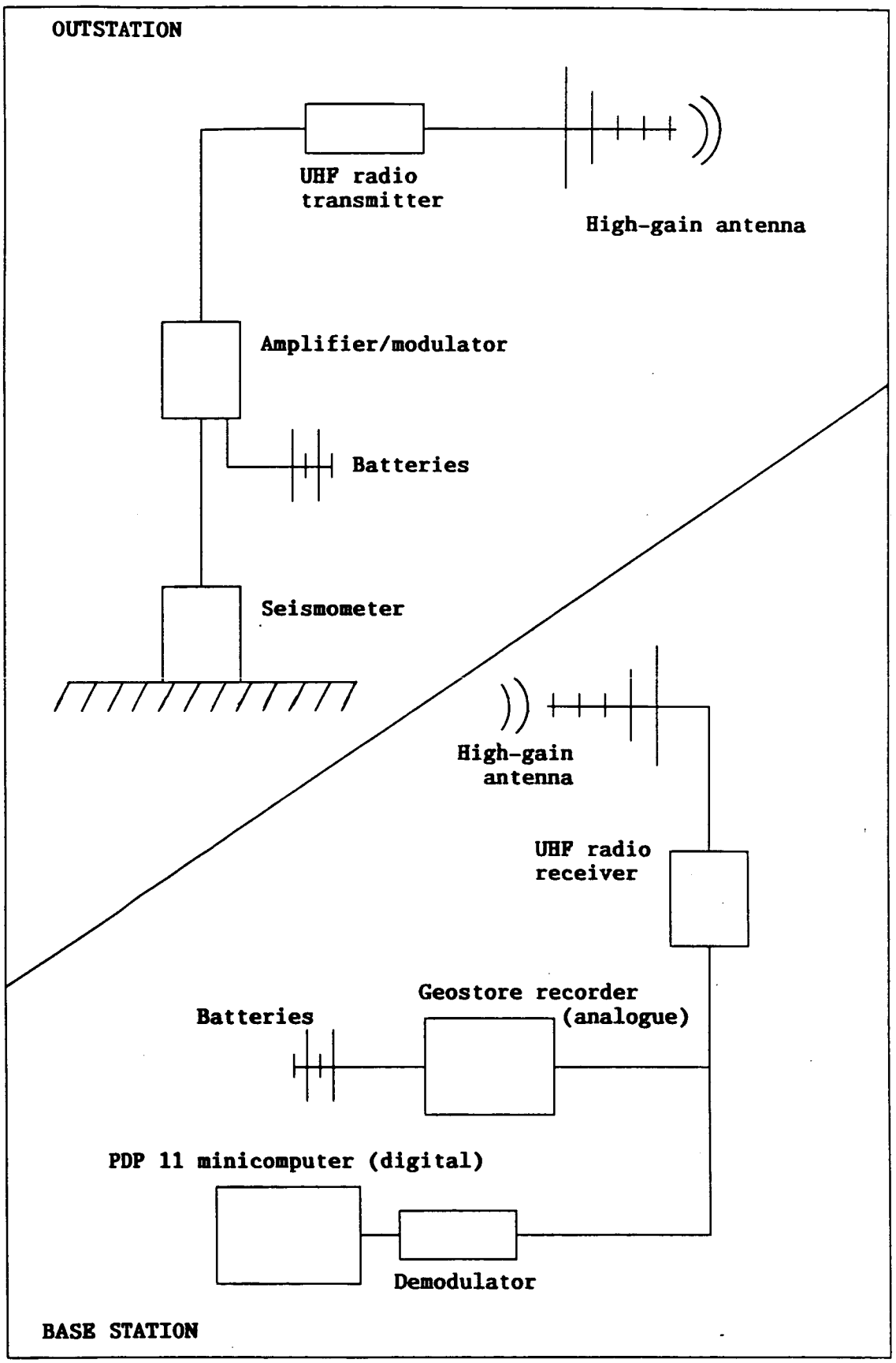

Figure 1.10 Diagrammatic representation of the instrumental setup.

The performance of the seismometer network installed in the Izmit area was monitored at Kandilli. Paper playouts of events were made, phase-arrival times measured and the minicomputer used to produce event locations using the standard program HYPO71 (Lee & Lahr 1975). The full analysis procedure will be described in section 1.5.8.

1.5.3 Outstations

Instrumentation was generally the same as used previously in TDP1 and TDP2 (section 1.4). Figure 1.10 shows the outstation and base station instruments in diagrammatic form. Each seismograph station was equipped with either one or three Willmore Mk III seismometers, set to a free period of 1 sec. prior to installation, and with known sensivities. These seismometers have been in use on LOWNET in the UK (Crampin *et al.* 1970; Browitt *et al.* 1985) for many years, and are well-suited for field use. They have an output proportional to ground velocity in the frequency range of the microearthquakes recorded in this part of Turkey (around 5 to 20 Hz). The velocity response of the seismometer/Geostore recording system is flat between 2 and 26 Hz (Turbitt & Stewart 1982). Every effort was made to keep the network configuration stable during the project, chiefly for administrative convenience. The signal from the seismometer was fed into a Racal FM amplifier/modulator, fitted with a feedback circuit to produce a damping factor of 0.6. A few Earth Data 9690 digital amp/mods were used at some stations. Power for these outstations was provided by 12v dry cells, which were kept charged using local mains supplies. Some of these supplies proved less than reliable, and, in retrospect, solar panels could, with advantage, have been used. Some outstations were remote from any mains supply. These were powered by a bank of air cells, which lasted for considerable periods, obviating the necessity for frequent visits to such stations to change batteries.

The TDP3 stations (Fig. 1.11) reoccupied many sites which were used in the previous projects. For example, schools at SE, TE, PB, and DP were used again, together with a hill site at PA. Table 1.1 shows details of all sites used in the projects. Where necessary, the old pits were renovated or new ones installed. New sites, considered necessary to tailor the network to the pattern of seismicity

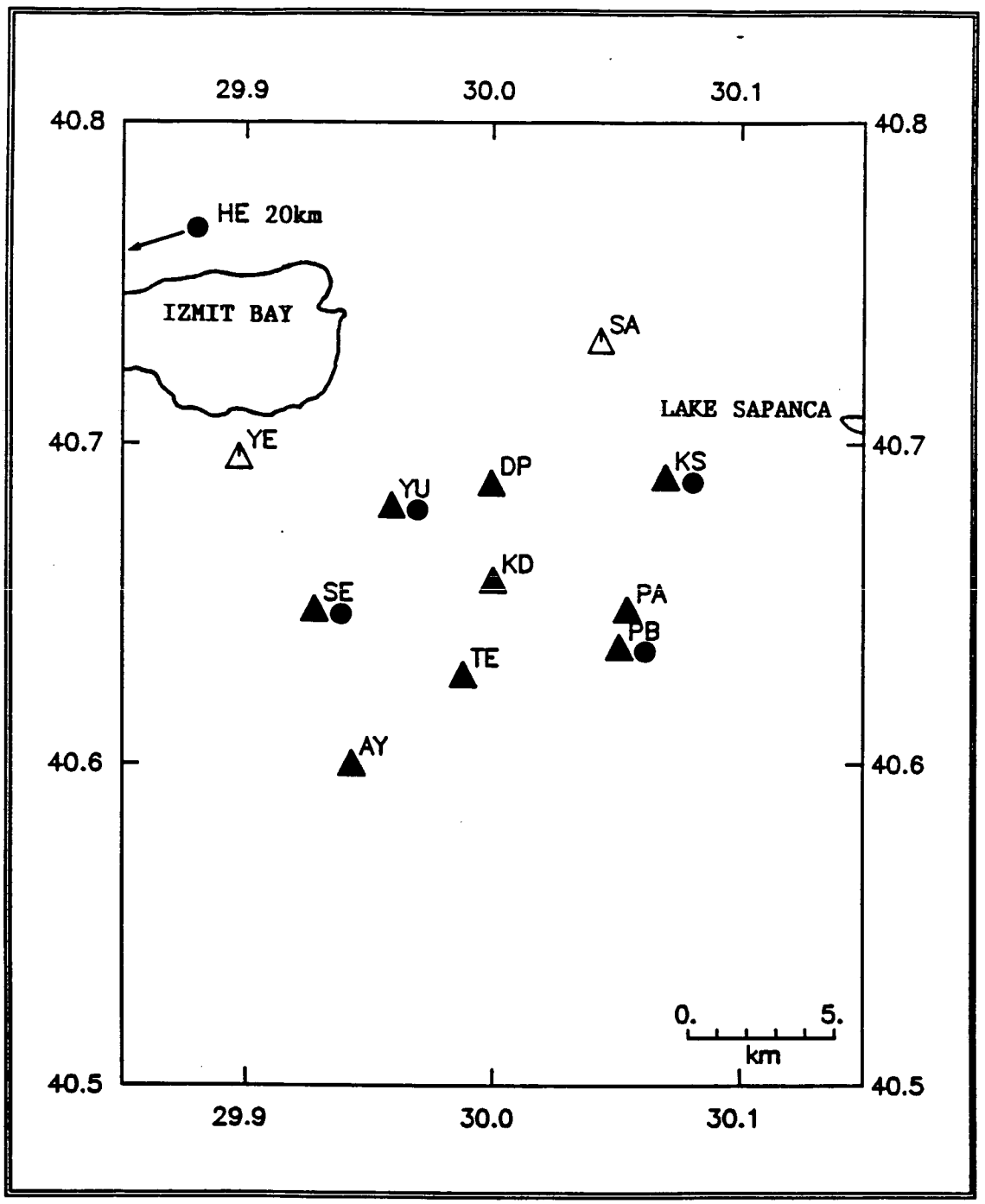

Figure 1.11 Stations used during TDP3. Filled and unfilled triangles represent three-component and single component stations respectively. Geomagnetic stations are shown as dots. The base station is arrowed.

identified in the previous projects, had been identified during a preliminary visit to Turkey by Drs J. R. Evans and D. Beamish, in late 1983. They were accurately surveyed using a theodolite. Great care was taken to ensure good instrument/ground coupling by digging as close to bedrock as possible. This frequently entailed the excavation of considerable quantities of topsoil or deep-weathered lavas. Cement foundations were laid, unless the station was sited on a concrete floor in a school or other building. Drains were installed as necessary, much to the amazement of local people, who pointed out

Station	Latitude (°N)	Longitude (°E)	Altitude (m)	Years used (*) 1979 TDP1	1980 TDP2	1984 TDP3
SE	40.6485	29.9275	614	*	*	*
TE	40.6283	29.9880	648	*	*	*
AY	40.6005	29.9425	995	*	*	*
PA	40.6485	30.0547	900	*		*
PB	40.6368	30.0515	847		*	*
DP	40.6882	29.9995	190		*	*
DQ	40.6882	29.9995	190		*	
KS	40.6900	30.0700	140			*
YU	40.6810	29.9587	380			*
SA	40.7325	30.0438	44			*
YE	40.6960	29.8973	47			*
KD	40.6577	30.0002	593			*
KE	40.6435	30.1005	1604	*	*	
CA	40.6368	29.9485	444	*		
ME	40.6007	29.9117	994	*		
EL	40.5390	29.9040	1233	*		
IZ	40.7708	29.8925	180		*	
HE	40.8022	29.6732	582		*	
HF	40.8022	29.6732	582		*	
HI	40.6885	29.8547	95		*	
KT	40.7665	30.1353	90		*	

Table 1.1. Seismograph stations used in the TDP experiments

that summer was imminent. However, this attention to detail was proved necessary, as some pits flooded several times, and it only backfired once when a small rodent crawled up the drainpipe and gnawed through the power cable, thus putting the station out of action. The north-south and east-west components of three-component seismometer stations were accurately oriented using a theodolite together with a hand-bearing compass with which an accurate bearing

was taken on a distant object, and an aligning cradle which was fitted to the top of the seismometer case. Due allowance was made for magnetic variation; an up-to-data figure for this was obtained from Kandilli Observatory, who are responsible for the monitoring of magnetic variation in the same way as BGS are in the UK. These horizontal components were then accurately levelled with the aid of a dentist's mirror. The vertical seismometers were readily aligned by moving them slightly in a small depression moulded into their cement foundations, their levelling bubbles being easily seen. Polarities of the seismometers were then checked with a field test box, and the rest of the equipment (amp/mods, batteries, etc.) installed. Particular care was taken with wiring used to take mains electricity from the supplies to the battery chargers. Strain relief cables and high quality wire, connectors and insulating materials were used, as the team relied very much on the good will of school teachers and the local population, and an accident might have jeopardised the operation. As a final precaution, the seismometer pits and battery boxes were padlocked.

Outstations were visited routinely, or whenever problems were identified by monitoring the stations' outputs at the base station Geostore or with a scanning receiver. A log was kept of all visits, and proved useful in identifying areas where radio contact was possible between the field party's Land Rover and the base station at Hereke, or even with Kandilli Observatory. During these routine visits, the station was checked rigorously. Checks were made on battery voltage, charger current, radio output and frequency, and, on those occasions when instrument changes were necessary, on seismometer polarity and amp/mod gain. The more experienced members of the team ensured that no field party ever departed without being in radio contact with base, or without a full set of tools and spare instruments. This attention to detail contributed greatly to the overall reliability of the network, especially as great problems were experienced with the radiolinks. These quickly went out of tune, probably because of poor crystal toleration of the extremes of temperature encountered, and required constant attention.

Data from the stations were radiolinked to the base station at Hereke using UHF FM systems. Some problems with adjacent channel

interference were experienced as a consequence of operating at very close frequency spacings (25 KHz) in the 1 MHz bandwidth (458.0 to 459.0 MHz) allocated to us by the authorities, and as a result of the near-parallel ray paths from the outstations to the base station, even though similar or near-frequency radiolinks were sited as far apart as possible in the network. These problems were recognised early in the project, and steps taken to minimise their effect. Events subsequently located by the outstation network are shown in Figure 1.12.

1.5.4 The base station

The base station was located in a building used by the Turkish telecommunications service (PTT) as a microwave relay station. It is situated at Hereke, on hills above the northern shore of Izmit Bay, a few km west of Izmit, and facing across Izmit Bay towards the network, 20 km away. The premises were used previously, and we are grateful to the Turkish PTT for giving us every facility. A shaded room with mains power was allocated to us for the duration of the project, and every assistance given by the staff on site.

The receiving antennae were erected on scaffolding constructed outside the building, and giving approximate line-of-sight to most of the outstations. Instrumentation in the base station is shown diagrammatically in Fig. 1.10 (page 25). Signals were cabled into the laboratory, where they were recorded on Geostore analogue tape recorders and fed, in parallel, into the digital triggered system developed previously, and refined during the project. The Geostore tape recorder is a robust instrument, capable of being hermetically sealed when used under arduous field conditions. Three Geostores were used in the base station. Each has a capacity of 10 seismic and two flutter compensation channels, together with an internal clock and a channel for an external absolute time-standard. For this project, the internal clock signal from the master Geostore was fed into all Geostores, and this time code used for all subsequent timings. To give real time, a time code signal from an external source was recorded too. Some trouble was experienced in obtaining a reliable signal from MSF, Rugby, and the Omega time signal from Norway, so a signal from Radio Moscow was recorded onto the tapes via a small

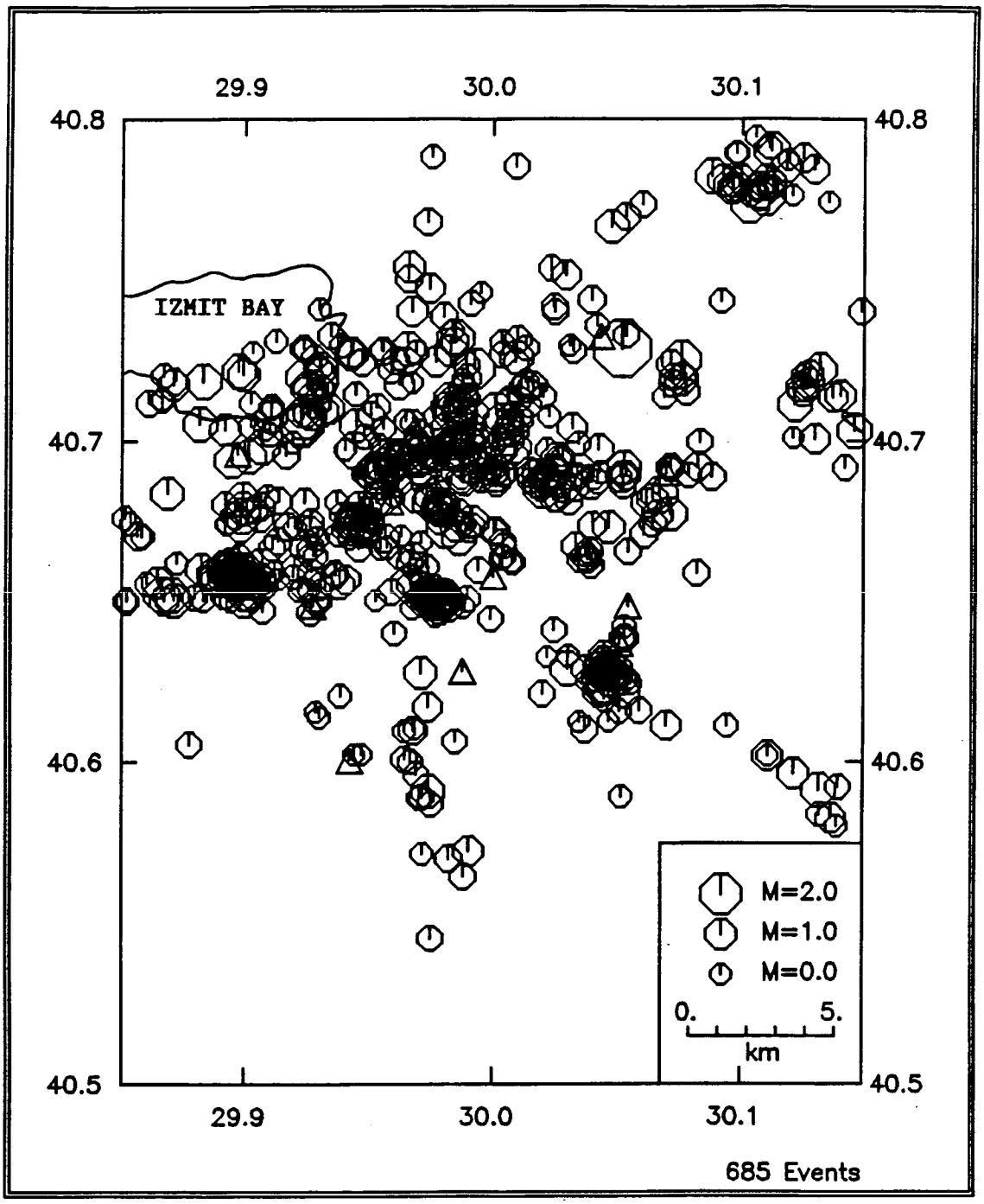

Figure 1.12 Events located during the seven-month TDP3 experiment, 1984.

circuit constructed by Dr J. R. Evans. The Geostores were run at a speed of 15/160 inches per sec., giving a tape duration of about three and a half days with 1/2 inch, 2400 ft. tapes. The Geostore heads were cleaned and the signals from all stations monitored at each tape change. A total of 159 data tapes was collected. Signals from three-component seismometer sets were recorded on adjacent tracks on the same Geostore head, to minimise timing errors which are known to occur as a result of head misalignment. Errors of up to 0.05 seconds can be systematically introduced, and this is of the order of the reading and residual errors of the arrival-time data. The head alignments on each Geostore were measured by injecting a 1 Hz monotone from a signal generator into all channels and recording the results at the beginning, in the middle, and at the end of a tape. In this way the consistency of the recording speed could be checked also. The tape segments were digitized using the same replay system as that used for digitization of the rest of the data tapes, and the delays between channels measured using the standard 'Pick' program (Evans 1986b). The head alignments were calibrated, and the maximum error between adjacent horizontal components estimated to be 0.002 seconds (Evans *et al.* 1987), that is, that the errors found were so small that timing corrections were unnecessary. The Geostore speed was also found to be consistent.

The incoming seismic signals were also fed, via a demodulator box, into the PDP 11-based digital triggered system. This system was mains powered but with a battery-powered Uninterruptible Power Supply (UPS) backup. Events recorded were archived on to digital tapes. Development of this system, particularly of the triggering algorithm, was continued throughout the project by Dr. J. R. Evans, and it has since been successfully used elsewhere (see section 1.2.3). An identical system is now in use at Kandilli Observatory, where it is used to monitor MARNET.

1.5.5 Büyükçekmece and Harmancik networks

Two other earthquake swarms had been identified by MARNET, (Crampin & Üçer 1975; Üçer et al. 1985) and it was decided to investigate their shear-wave propagation in more detail. Their tectonic setting was different from that of the Izmit swarm as

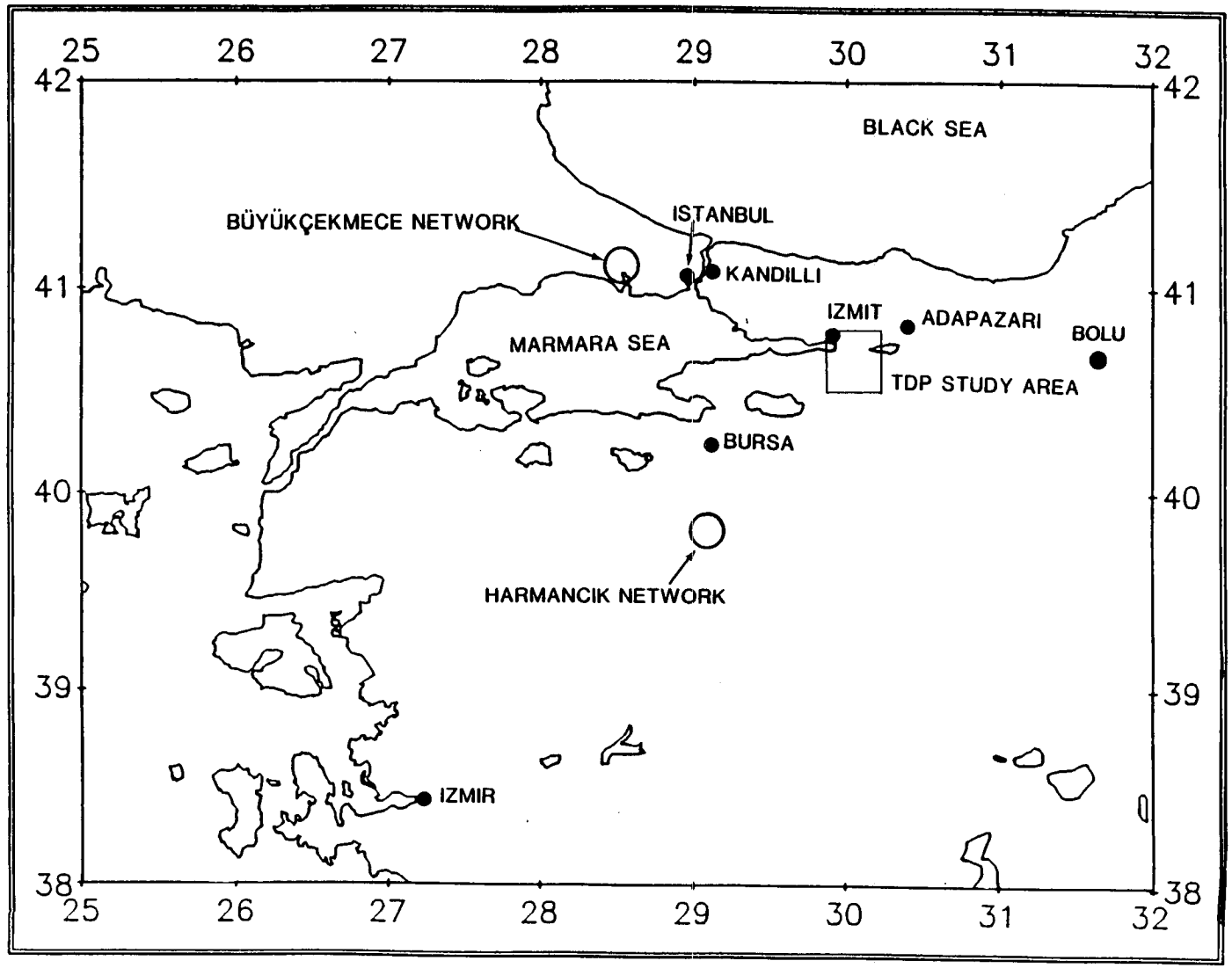

Figure 1.13 The locations of the subsidiary networks used during TDP3.

neither was associated with the east-west graben structure of the Marmara region but each was influenced by the same stress regime (Evans *et al.* 1987).

A small network of vertical seismometers was installed around Büyükçekmece, about 40 km west of Istanbul (Fig. 1.13). These instruments were radiolinked to Kandilli Observatory. A normal fault mapped at surface was thought to be the location of the swarm (Evans *et al.* 1987), but the network was dismantled after two months when it became apparent that only local quarry blasts were being detected.

The second swarm was to the south of Bursa (Fig. 1.13), and was thought (Evans *et al.* 1987) to originate near the southern branch of the NAF striking southwestwards towards Izmit (section 1.3.2). Four vertical instruments were radiolinked to a Geostore recorder. Only a few events were detected, however. These were generally regional events, and the network was dismantled, chiefly because of the pressing need for spare radiolinks to replace those proving less than reliable in the main Izmit network.

1.5.6 The Yuvacik array

To study the effects of topography and azimuth on incident waveforms, a cruciform array of six three-component stations, with a station separation of 220 m, was installed on an expanse of flat ground just northeast of station YU (Fig. 1.11), in close proximity to some of the more intense swarm activity (Evans *et al.* 1987). The long axis was aligned NE. The array was accurately surveyed in, and great care was taken during its installation. Digital equipment was used throughout this array. Data channels were wirelinked into a PDP 11 minicomputer installed in a van parked at the roadside. This computer acted as a triggered system, and events were periodically archived to tape. The array worked faultlessly for two months. These data are currently being analysed (Evans 1989). Preliminary results show that differences in shear waveform can be detected in time domain records across the array. It is suggested that the use of this technique will become increasingly important in future shear waveform studies.

1.5.7 The TDP3 Geomagnetic experiment

In addition to the large-scale seismic experiment in the Izmit area, a parallel geomagnetic investigation was planned in the same area in collaboration with the Technical University of Istanbul. The aim was to record variations in the Earth's electromagnetic fields and conductivity, using a long-term magnetotelluric array, as suggested by Beamish (1982), and described by Beamish & Riddick (1985a, 1985b). These variations are related to the crust's accommodation to changes in stress by movement of fluids through cracks, and it is thought that a knowledge of these changes might assist in earthquake prediction (Beamish 1982).

Time variations in the Earth's magnetic field generate or induce electric currents in the rocks of the crust. The electrical conductivity of crustal rocks is measured using the ratio between the induced (telluric) electric fields and the inducing (magnetic) fields. Four outstations, at locations KS, SE, YU and PB of Figure 1.11, were installed alongside seismic instruments. Each outstation consisted of one sensitive, three-component fluxgate magnetometer, shielded from vibration, and four, non-polarizing copper/copper sulphate electrodes buried in the earth to minimise temperature variations. An identical installation was made at the base station at Hereke, HE in Fig. 1.11, to provide a comparison remote from the earthquake swarm under investigation. Thus, each geomagnetic station measured five components of the Earth's electromagnetic field. Measurements were taken every five seconds, and radiolinked to the base station. Data were then processed to provide a response function which is determined by the conductivity structure of the Earth, and a search made for temporal changes. It was intended also to search for earthquake precursors by analysing the seismic and geomagnetic data sets in parallel. Results of the geomagnetic experiment have been summarised by Evans *et al.* (1987), and Russell (1988). The conductivity structure of the crust in this area derived from this experiment may have a bearing on the earthquake hypocentres determined by the seismic network. This will be discussed further in Chapter 2.

1.5.8 Data analysis

Over 150 data tapes were accumulated during TDP3, as well as tapes recorded during the operation of subsidiary networks (section 1.5.5 and 1.5.6) and triggered system archives. Some preliminary processing was carried out at Kandilli Observatory to monitor the performance of the network and the data quality. After the experiment, the equipment was transported back to BGS, Edinburgh, where bulk data processing was carried out, principally by the author during working hours, but also privately as the subject for this thesis.

Data were recorded as 50 sets of three tapes, as three Geostores were used to record the incoming data signals. A replay unit was set up, and two out of each set of three tapes were analysed. Data tapes were played back at 80 times real time. This brought the earthquake frequencies into the audible spectrum, and the events could be identified using headphones to listen to two channels from each tape. The stations listened to were as widely separated as possible so that arrivals from local and other events could be easily discriminated, as arrivals from teleseismic events arrive almost simultaneously at all stations in a local network. The freedom from noise was also important. By implication, this means that some very small events may have been only detected on a few stations in one part of the network. These events were rejected as being probably too small to be of use. A rough event timing was made from the Geostore time code.

Comparison of the two picking lists then enabled events to be identified. Paper playouts were made of all events. The time code from the master Geostore was then used in the digitization of the events at 100 samples per sec. on a PDP 11 minicomputer, using software (Evans 1980), and an interface unit (Evans & Miller 1986) developed in-house. High sampling rates were necessary to give sufficient resolution to show the abrupt changes of direction when shear-wave polarization diagrams were plotted.

A PDP 11 minicomputer was used for all subsequent analysis. A suite of programs written by Dr. J. R. Evans (Evans 1986a, 1986b) was used to display the digitised files sequentially on a high-resolution graphics screen and pick *P*- and the first shear-wave arrivals to

1/100 sec. Paper plots were made of local events for archive purposes. Plots of shear-wave particle motions were made for further analysis. Event locations were calculated using HYP071 (Lee & Lahr 1975) adapted to run on the PDP 11. Most analysis was carried out by the author as part of this thesis, and the techniques involved will be described in the relevant chapters.

1.5.9 Earthquake prediction

Traditionally, most seismic observations have been undertaken on *P*-waves recorded on vertical component instruments. More recently however, there has been increasing use of digital, three-component instruments, especially in petroleum exploration, as the importance of shear-wave analysis has been realised. *P*-waves are compressional waves vibrating in the direction of propagation. They are relatively insensitive to the three-dimensional structure of the rocks through which they propagate. Shear-waves, however, vibrate in a plane at right angles to their direction of propagation, and are highly sensitive to the three-dimensional structure of the propagation medium. Shear-waves typically contain at least three times as much information as the equivalent *P*-wavetrain (Crampin 1978). The large amount of data, particularly the three-component data, recorded during the Turkish Dilatancy Projects (section 1.5), and elsewhere, has enabled the techniques for detailed analysis of the shear-waves to be developed.

It was noticed that the shear-waves recorded on three-component instruments showed two distinct arrivals. This phenomenon is called shear-wave splitting. This behaviour was modelled by propagating shear-waves through a homogeneous, elastic solid which had the same elastic properties as the rock through which the shear-waves propagated (Crampin 1984). The modelling indicates that the behaviour of shear-waves can be explained if they propagate through rock containing distributions of fluid-filled cracks and microcracks which are constrained by the current tectonic stress into sub-parallel, sub-vertical alignments. The rock is then anisotropic to seismic waves. This property is analogous to the optical anisotropy or birefringence observed in many minerals. The distributions of stress-aligned cracks are called Extensive-Dilatancy Anisotropy or

EDA (Crampin 1984; Crampin *et al.* 1984). The behaviour of a shear-wave propagating through such an anisotropic region is shown schematically in Fig. 1.14. When a shear-wave, generated either by an earthquake or an artificial source, enters the anisotropic region, it splits into two (or more) components, each with a different velocity and direction of polarization (shear-wave splitting). The velocity difference between the split waves introduces a characteristic signature into the wavetrain as the components separate in time. This distinctive signature is preserved, and can be recognised whenever the waves are recorded and displayed in polarization diagrams. Additionally, the direction of polarization of the leading, or faster, split shear-wave is parallel to the direction of the maximum compressive component of the tectonic stress. The implications of shear-wave analysis are far-reaching, and have been described in detail by Crampin (1987a).

Shear-waves displaying splitting and with polarizations distinctively aligned were first described from an area around the North Anatolian Fault in the Turkish Dilatancy Projects, (see above). Here, tectonic stress directions derived from shear-wave analysis agree very closely with those derived independently from earthquake fault-plane solutions (Evans *et al.* 1985: Lovell *et al.* 1987).

Since these initial observations, shear-wave splitting has been reported from many parts of the world, not just from earthquake observations but also from exploration techniques employed by the hydrocarbon industry. These observations are reviewed by Crampin (1987b). In many of these areas, compressive stress directions derived from earthquake fault-plane solutions, confirmed by local tectonics, or directly measured, have shown alignment parallel with the polarization direction of the leading split shear-wave (Crampin 1987b). It is now thought that EDA is ubiquitous in the upper 10-20 km of the Earth's brittle crust (Crampin 1987b).

The science of earthquake prediction appears to have been greatly advanced by these discoveries. A method has been suggested whereby the stress in an area is closely monitored either by a study of shear-waves from earthquakes, or, preferably, from periodic shooting of vertical seismic profiles. Any temporal change in stress direction

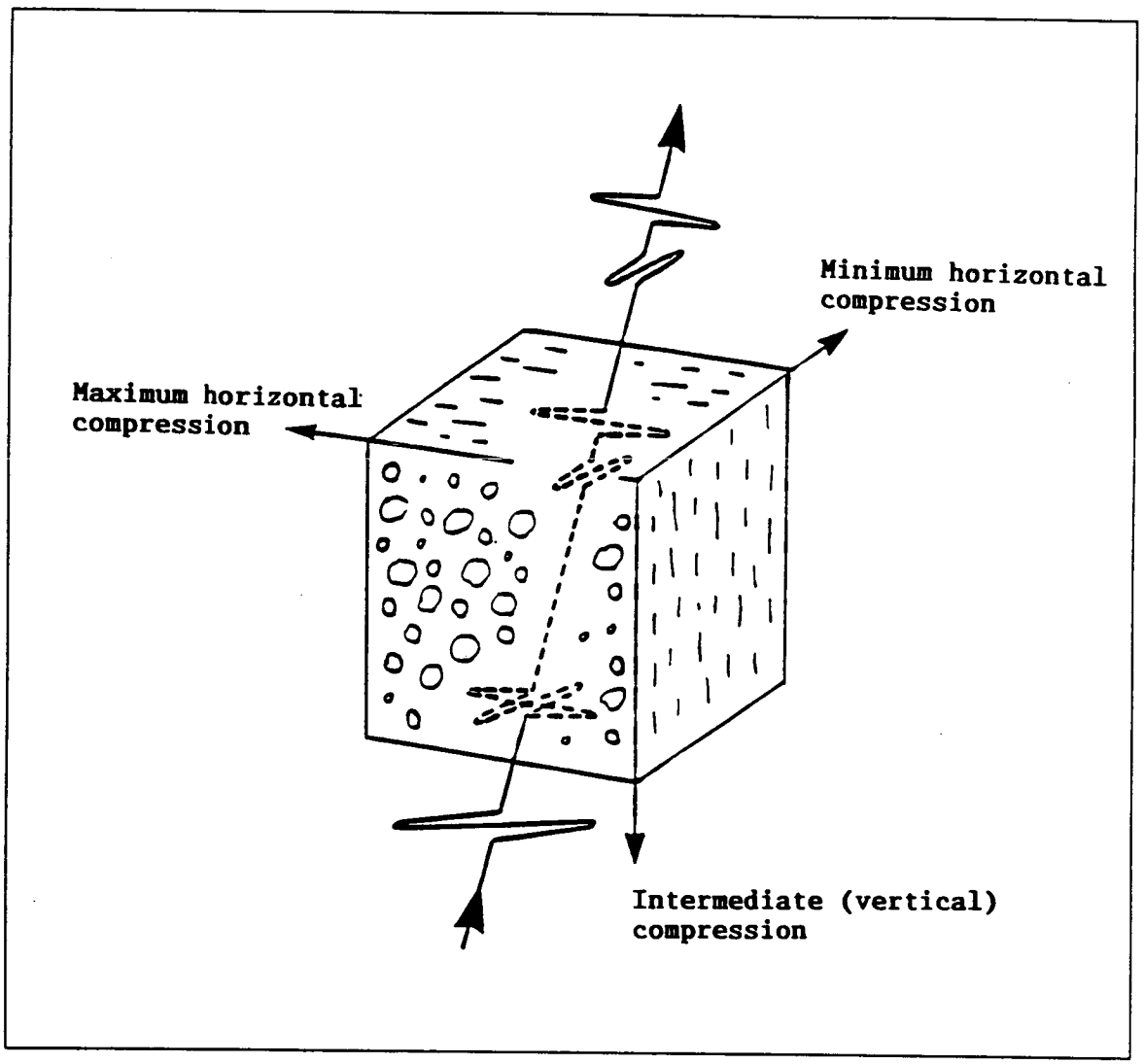

Figure 1.14 (after Crampin 1987a) Diagrammatic representation of shear-wave splitting.

or magnitude, thought to be earthquake precursors, would have an effect on the EDA-cracks present and hence on the shear-waves propagating through the area. This change could be easily detected using appropriate techniques. This method should be even more powerful in a seismic gap (such as the Izmit area or at various locations along the San Andreas fault), has yet to be tried, and would require a large investment of finance and instrumentation. However, temporal changes in delays between split shear-waves have been reported from California (Peacock *et al.* 1988: Crampin *et al.* 1989), and, less clearly, from Turkey (Chen *et al.* 1987).

1.6 Summary

Since their inception in 1979, the Turkish Dilatancy Projects have evolved with time as various factors influencing the observation of shear-waves became apparent. The final, multidisciplinary, project in summer 1984, produced a large quantity of high-quality, digital data. Credit must be given to the staff concerned whose care and efforts in the planning, equipment testing, calibration, and field stages made this possible. The projects have been a model of international cooperation in scientific research for the ultimate benefit of mankind. Some of the data have not yet been analysed fully; this is planned for the near future.

This chapter has described the TDP3 experiment, in which the author played a large part, in terms of the previous two projects, other geophysical experiments in the same area, and the seismotectonic framework of that part of northwest Anatolia around the Marmara Sea thought to be at risk from a large earthquake.

Succeeding chapters will describe the analysis, by the author, of the large data set collected during the TDP3 project, and will relate the results to those found in the two previous projects carried out in the same area. The locations and magnitudes will be described in, respectively, Chapters 2 and 3, and it will also be shown that the swarm's activity has changed little in character between 1979 and 1984 (the period during which the swarm was monitored). The fault-plane solutions to be described in Chapter 4 will be shown to be similar to those found previously, but with the addition of a

small additional set of suggested fault-planes. The clustering in space and time, described in Chapter 5, is a recently-observed phenomenon in low-magnitude swarms. The clustering will be described in detail, and conclusions consistent with the available data set will be drawn. Further monitoring would be required to enable these results to be elaborated upon.

Chapter 2

Earthquake locations

2.1 Introduction

The absolute locations, magnitudes and origin times of most earthquakes are routinely calculated as soon as they are detected by world-wide and local monitoring stations. In the past, timings of *P*- and shear-wave arrivals were made from paper playouts, but nowadays, for specialised studies, the digitised event files are displayed on high-resolution graphics screens from which extremely accurate arrival times can be read directly. In this chapter, a brief review of the location method used will be given. The hypocentral locations determined will be described and discussed in the light of the local tectonics, compared with previous results, and linked with the preliminary results of the TDP3 geomagnetic project.

2.2 The method

Most modern earthquake location methods use a computer program which requires as input a file containing the *P*- and shear-wave arrival times together with a crustal model, the station coordinates and station elevation corrections. Output from the program includes the latitude, longitude, depth, origin time and, frequently, the magnitude of the earthquake, together with some estimate of the fit of the arrival-times to the crustal model used. The choice of program depends mainly on the computing facilities available. Such a location program is HYP071 (Lee & Lahr 1975), which has been in use in BGS for many years. Although designed for use on a mainframe computer and with regional networks, this program was adapted for use on a PDP 11 minicomputer by Dr. J. R. Evans for the TDP projects, and has proved reliable. Various other location programs have been tried, including one which would work on a personal computer, but none offered any real advantage over HYP071, and they will not be discussed further here.

The region is underlain by a variety of rock types, chiefly

volcanics, of differing ages and with a complex structure. Such geological complexity is not reflected in the seismograms, however, which are generally clean and contain the impulsive *P*- and shear-wave arrivals well suited to arrival-time and shear-wave analysis (examples of seismograms will be shown in Chapter 5). This is because the *P*- and shear-wave raypaths are direct, and contain no refracted arrivals, as the network was situated within the shear-wave window directly above the earthquake swarm. Additionally, the surface layer may be very thin, as solid rock crops out at surface over much of the area, there is little drift and weathering may not be deep. This may also have contributed in a small way to the high quality of the seismic records because of the lack of reverberations and consequent noise.

After digitisation, the event files were displayed sequentially on the high-resolution graphics screen of a PDP 11 minicomputer, using a suite of in-house programs (Evans 1986b). The arrival times were picked directly from the screen using a cursor. The *P*-arrivals could generally be timed to within 1/100 sec, corresponding to one sample. On those occasions when the signal to noise ratio was very high, interpolation between sample points was possible. Most shear-wave arrivals were impulsive, and could be clearly identified emerging from the *P*-coda, but could not be timed with the same precision as the *P*-arrivals. Each pick was weighted according to its quality - from 0 (clear and impulsive arrival) to 4 (useless for location purposes), and the polarity of the *P*-arrival was noted so that fault-plane solutions could be obtained. The weighted arrival times were subsequently used as an input file for the location program.

The crustal model taken was the simple, plane-layered isotropic model used for both TDP1 and TDP2 locations (Crampin *et al.* 1985). This was determined by the accurate timing of quarry blasts recorded by the network during TDP1, and consists of a 1 km thick surface layer with *P*- and shear-wave velocities of 5.1 and 2.9 km/sec respectively, overlying an isotropic half-space with *P*- and shear-wave velocities of 5.7 and 3.3 km/sec. A Poisson's ratio of 0.25 was assumed. Although this model is very simple, it appeared to give reliable locations, but, as in all location calculations, the ultimate accuracy of hypocentral locations depends primarily on the

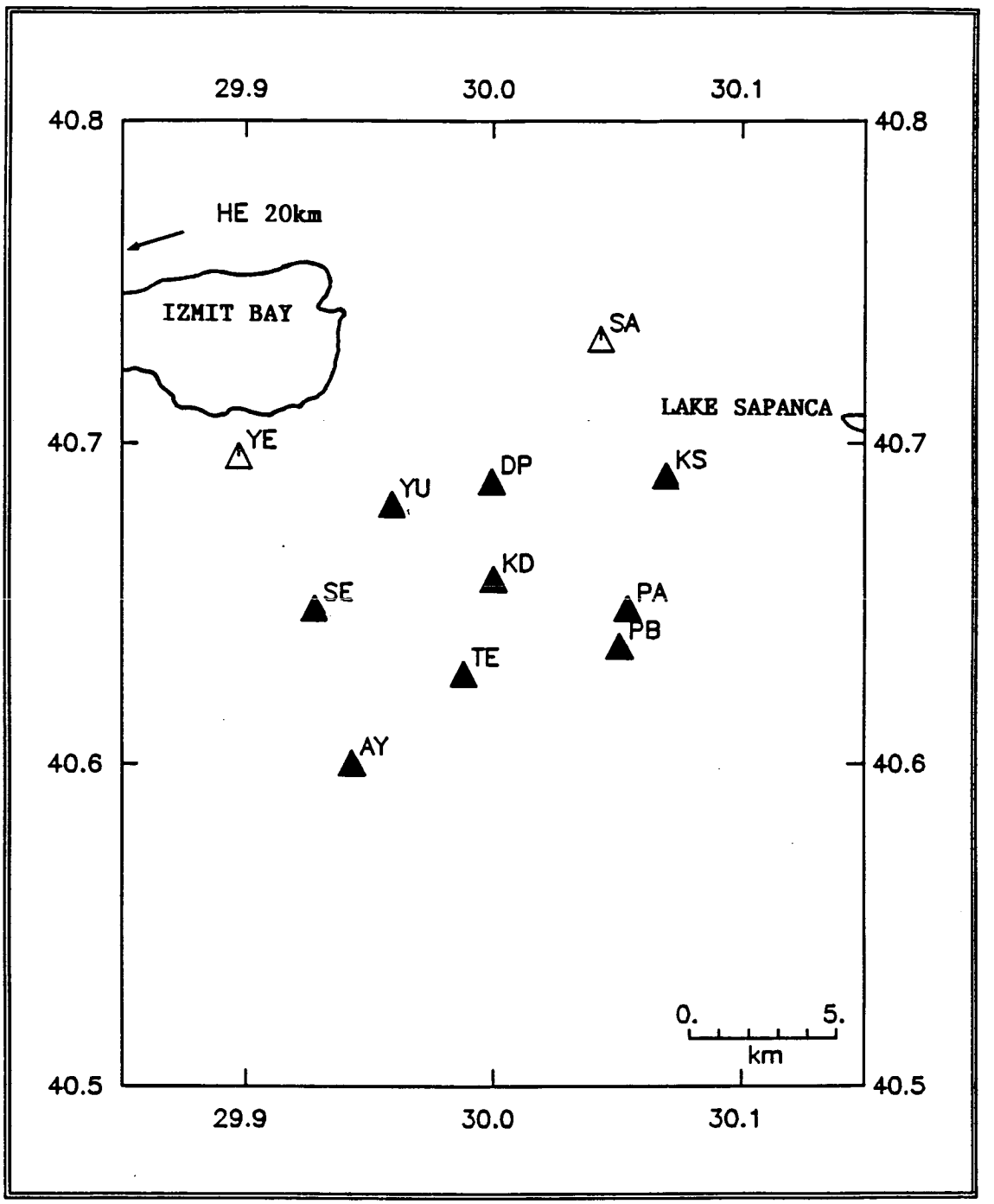

Figure 2.1 Stations used during TDP3. Filled and unfilled triangles represent three- and single-component stations respectively. The base station is arrowed.

accuracy of this crustal model. Further refinement of the locations would require a more complex model with much more crustal information, such as borehole and geophysical data, which are unavailable.

The coordinates and number of components of the seismic stations used during TDP3 are shown in Table 2.1, and the station locations in Figure 2.1.

Station	Latitude (°N)	Longitude (°E)	Altitude (metres)	Number of components
SE	40.6485	29.9275	614	3
TE	40.6283	29.9880	648	3
AY	40.6005	29.9425	995	3
PA	40.6485	30.0547	900	3
PB	40.6368	30.0515	847	3
DP	40.6882	29.9995	190	3
KS	40.6900	30.0700	140	3
YU	40.6810	29.9587	380	3
SA	40.7325	30.0438	44	1
YE	40.6960	29.8973	47	1
KD	40.6577	30.0002	593	3

Table 2.1 Coordinates of seismic stations used in the TDP3 experiment.

Where possible, data from nine out of the 11 seismic stations shown in Table 2.1 were used for the location calculations. Most of these provided consistent and high-quality records from which accurate arrival times could be picked. The exceptions were the two single-component stations, SA and YE (Fig. 2.1 and Table 2.1), situated in the north of the network. These stations had been installed to give more control over the locations of nodal planes of fault-plane solutions (Chapter 4). They were both sited in village schools, with consequent cultural noise at times, but were also unavoidably situated on the low ground, north of the main fault scarp, which forms part of the half-graben structure in this area (see Chapter 1). The Oligocene-Recent sediments underlying this area consist primarily of unconsolidated alluvial fans derived from the high ground to the south, together with lacustrine and marine alluvium consisting of sands, silts and clays. These sediments were of an unknown thickness and structure. Such unconsolidated deposits

have low seismic velocities and therefore cause perturbation of seismic waves. This was found to be the case here, as when data from these two stations were included in the location calculations, unknown and varying delays were introduced which appeared to degrade the locations by increasing the RMS (section 2.2.1), so these stations were not used for location calculations. However, *P*-wave polarities are unaffected by passage through sediment piles, and readings were used in deriving fault-plane solutions.

The seismic signals from all stations were examined to see if any others were susceptible to unknown and varying introduced delays in the same way as stations SA and YE had been affected. Although many stations exhibited very characteristic seismograms, no evidence of any varying delay was found, and so all remaining stations were used in location calculations. Station SE (Fig. 2.1) shows a very strong tendency to exhibit a local SP phase (Chen *et al.* 1987). Additionally, seismograms recorded at station DP (Fig. 2.1) exhibit a high-frequency ringing. This phenomenon was investigated during TDP2 by the installation of station DQ (Chapter 1, Fig. 1.7) a few yards away to see if this was due to the building in which DP was situated (Dr. J. R. Evans, personal communication). It is now realised that the ringing is due to a local geological peculiarity of an anomalously thick soil layer held in place upon a ledge of solid rock, as both stations are situated on a gentle slope which locally displays evidence of soil creep or small-scale land slip.

2.2.1 Location process

The earthquake locations were calculated using HYP071 (Lee & Lahr 1975). This program uses as input a file containing the weighted *P*- and shear-wave arrival times, the crustal model and the station coordinates. Using the crustal model, an assumed origin time and a trial hypocentre, the program calculates arrival times at each station, compares these with the observed values, and notes the differences (the residuals). It then attempts to adjust the trial hypocentre in four dimensions (time, depth, latitude and longitude) by applying regression analysis or least mean squares fit to the residuals, and tests to see if any reduction in the residuals is statistically significant. If so, this new hypocentre becomes the

trial hypocentre, and the regression analysis is repeated. In this way the program iterates towards the final hypocentre in a way controlled by certain variable test values which are used to modify the program operation. These test values were kept the same as those used in the previous TDP location calculations, so that locations could be directly comparable. HYPO71 terminates when certain conditions are met; after a specified number of iterations, or if the movement of the trial hypocentre is less than a certain specified amount, or if the RMS values cannot be improved after four iterations. Output is then produced containing the earthquake location.

The locations found by the above method are plotted in Figure 2.2, and summary location data are given in Appendix A. It should be noted that the errors quoted in columns ERZ, ERH and in particular Q, of Appendix A are not actual errors, but only statistical estimates of the quality of fit of the data to the crustal model, as it is possible to fit the model exactly with the barest minimum of data. A better estimate of the actual error may be found in the "DRMS cube" also output by the program, which shows the change in RMS values as the hypocentre, located at the centre of a cube, is moved towards the eight corners. However, the RMS and other error values given for events in Appendix A are all low. Typically, the RMS is below 0.08, and, taken together with the number of arrivals (column N, Appendix A), give some idea of the location accuracy. The TDP team have every confidence that the locations are as good as it is possible to get, given the care taken during station installation and surveying, and the careful data processing and analysis.

2.2.2 Locations in anisotropic regions

In addition to any errors associated with imprecise timing of arrivals and an overly simple crustal model, it has been shown (Doyle *et al.* 1982) that the focal depths and epicentres of local earthquakes may be systematically modified, in a way that might be mistaken for hypocentral migration, when dilatancy-induced anisotropy is present. Working on the TDP2 data-set, Doyle *et al.* (1985) inverted the *P*- and shear-wave arrival times, and calculated elastic tensors which were similar to those predicted from a system of

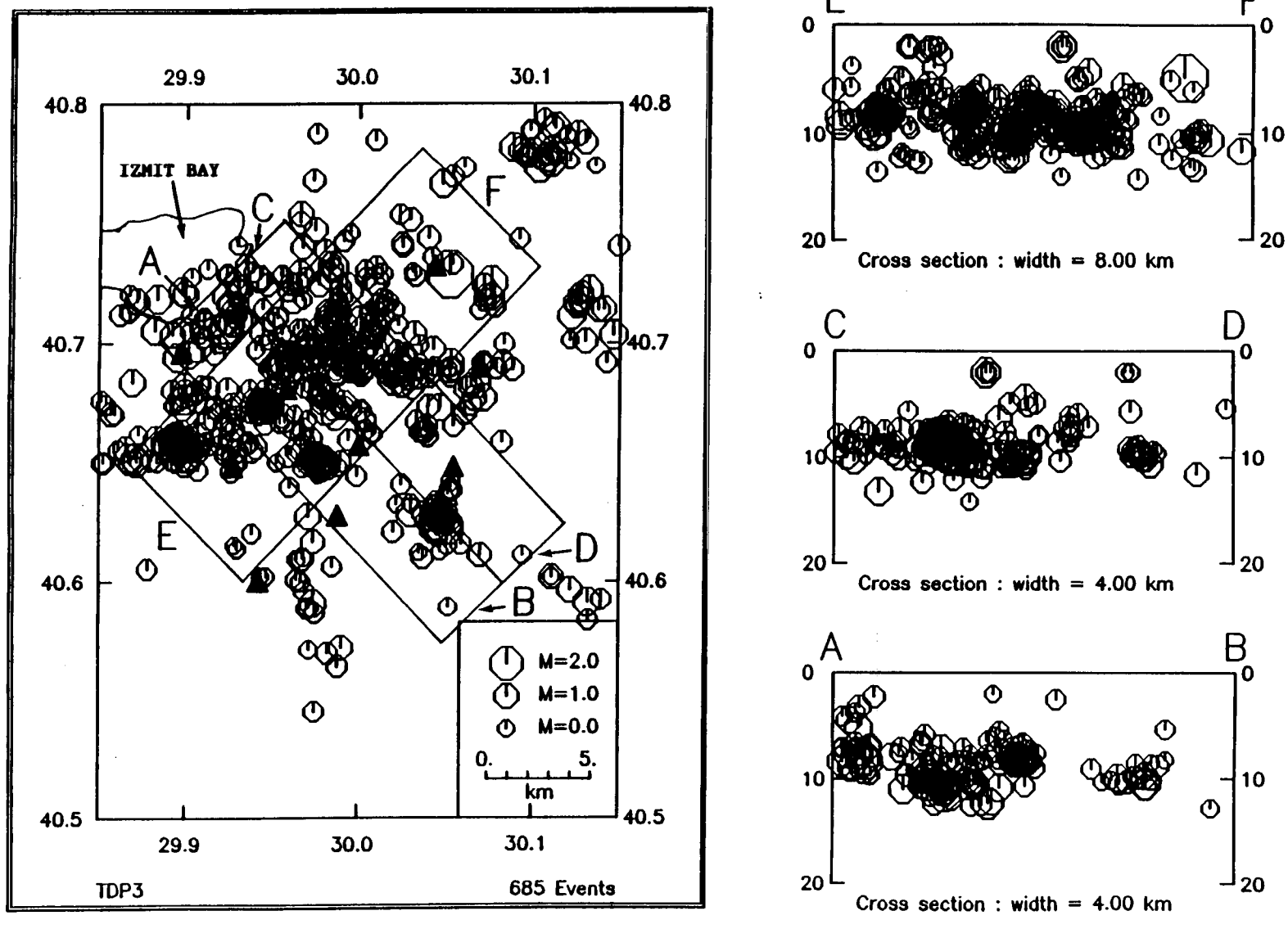

Figure 2.2 Epicentral plot and cross-sections for events located during TDP3.

vertical cracks whose normals lay between 10° and 30° east of north (Crampin & Booth 1985). The inversion method showed that the anisotropy was statistically significant, but, as the locations calculated in anisotropic media were little different from those derived using HYP071, the latter locations were used in all their subsequent analyses. The same argument is adopted here.

2.3 Locations

Over 4000 events were recorded and located during TDP3. However, as many of these events lie outside the map area, their locations are considered not reliable, and they will not be discussed further. The HYP071 locations of the local events determined within the map area together with mutually orthogonal cross-sections are shown in Figure 2.2, and the HYP071 summary location details are given in Appendix A. Note that earthquake locations are quoted as latitude and longitude by most location programs. This is meaningful on the regional or global scale, but inappropriate for a small swarm of events, when a plot is preferable. Here the locations are plotted on diagrams on which are superimposed some topographic features, rendering the locations much more comprehensible, and their comparison much easier.

The epicentres in Fig. 2.2 form a very closely-packed swarm south east of Izmit Bay (Lovell *et al.* 1987). This location is in the same area as the original swarm first located by MARNET (Üçer *et al.* 1985). The swarm is roughly 15 km in diameter, elongate in an ENE-WSW direction, and shows approximately the same level of activity as during the previous projects. In addition, the cross-sections for all three projects show that the depths of the better-located events are almost entirely confined to between around seven and 12 km (Lovell *et al.* 1987) although depths of earthquakes located using arrivals from the upper focal hemisphere may not be well-controlled (Crampin *et al.* 1985). The hypocentres appear to form an approximately horizontal sheet between these depths, and display close clustering of events in separate concentrations within the swarm. This observation will be discussed more fully in Chapter 5.

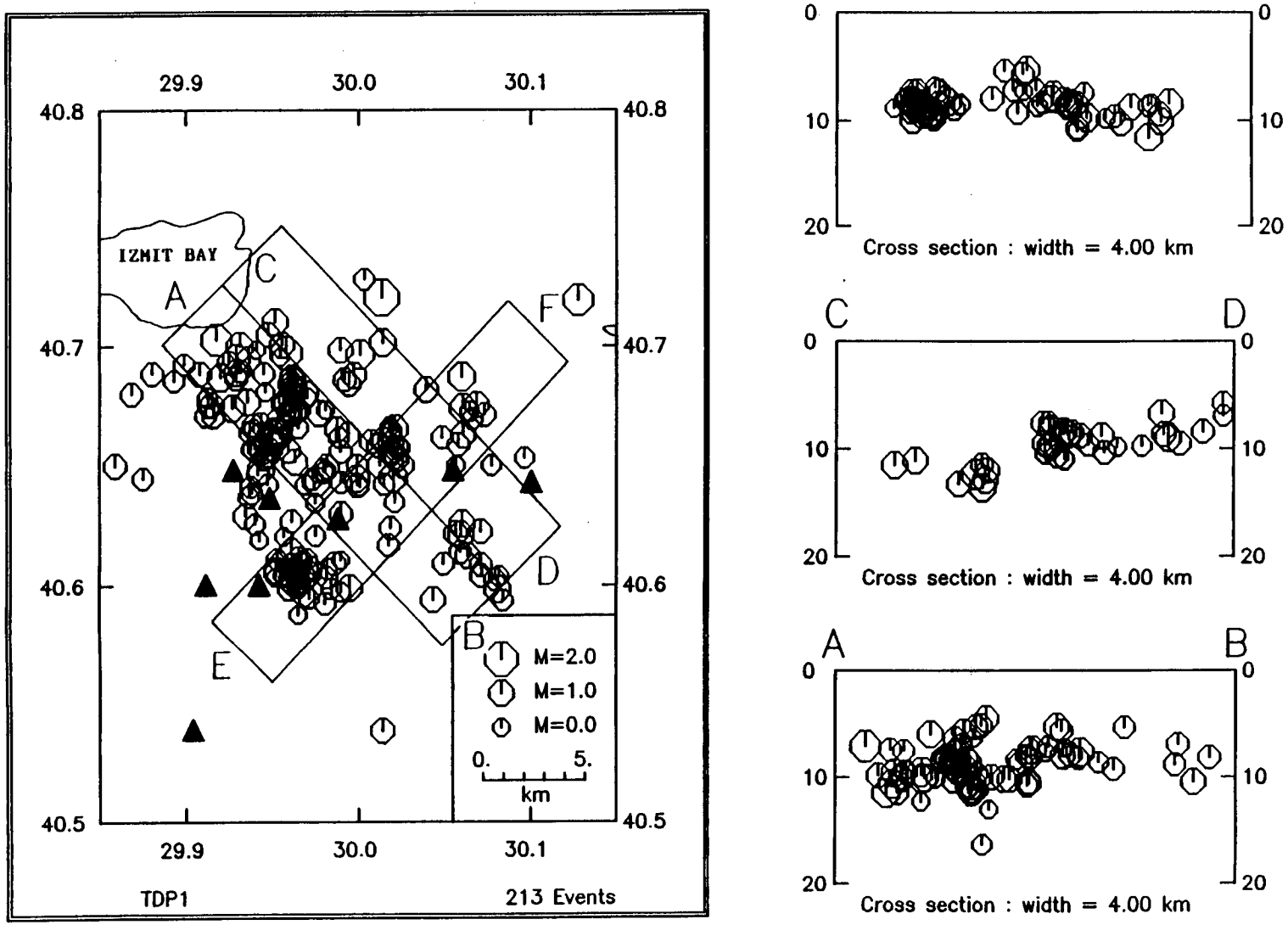

Figure 2.3 Epicentral plot and cross-sections for events located during TDP1.

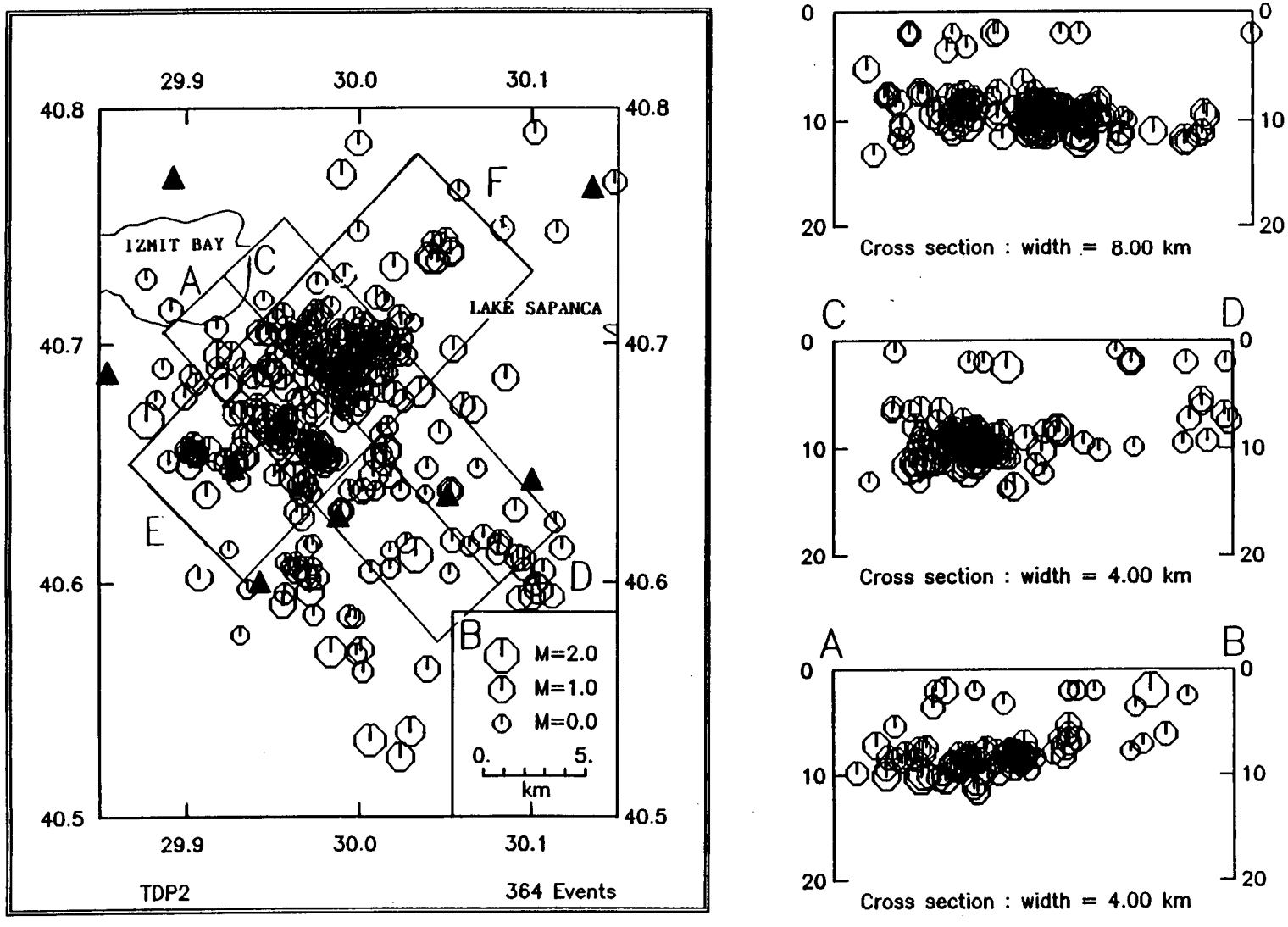

Figure 2.4 Epicentral plot and cross-sections for events located during TDP2.

2.4 Discussion and comparison with other projects

Hypocentral plots and cross-sections from the previous TDP experiments (TDP1, 1979, and TDP2, 1980) are given in Figures 2.3 and 2.4 (after Fig. 3 of Crampin *et al.* 1985). Cross-sections E-F of Figs. 2.3 and 2.4 have been drawn in different positions to reflect the differing shape of the swarm. A comparison of these figures with Fig. 2.1 reveals that even allowing for any systematic errors attributable to the differing network geometries, the swarm has changed little in position or character over the period of observation (five years). Any minor differences may be attributable to the differing periods of the observations (six weeks in TDP1, nine weeks in TDP2 and nearly seven months in TDP3). Each cross-section shows that the majority of events are closely confined to depths of between seven and 12 km. It might be expected that, in a region of active tectonism cut by a major fault, the earthquake hypocentres would be associated in some way with the major fault plane. In this case we might expect to see a plane of events dipping northwards and striking approximately east-west. No such evidence can be seen from the cross-sections in Figs. 2.2, 2.3 or 2.4, and instead the events appear to lie in an approximately horizontal sheet. This suggests great complexity in the seismogenic zone, and this will be discussed in Chapters 4 and 5. Here the resolution in locations is not sufficient to show structure within this sheet except for the clustering of events, which will be discussed in Chapter 5.

The sharp cutoff of events below about 12 km may be attributed to the presence of a maximum in crustal strength which marks the base of the seismogenic zone (Meissner & Strehlau 1982). Additional evidence for this argument is provided by the results of the TDP3 Geomagnetic experiment (Evans *et al.* 1987; Russell 1988, see also Chapter 1). The crustal resistivity around the seismic network south of the NAF graben was found to be much greater than that measured at the MT base station (HE on Fig. 2.1) north of the graben. Resistivity models for MT sites 2 and 3 (adjacent to seismograph stations SE and PB, Fig. 2.1) are presented in Fig 2.5. They show a two-fold crustal structure, with a 12 km thick homogeneous, conductive unit overlying a lower layer whose resistivity is an order of magnitude greater. The upper layer may represent the region permeated by the liquid-filled

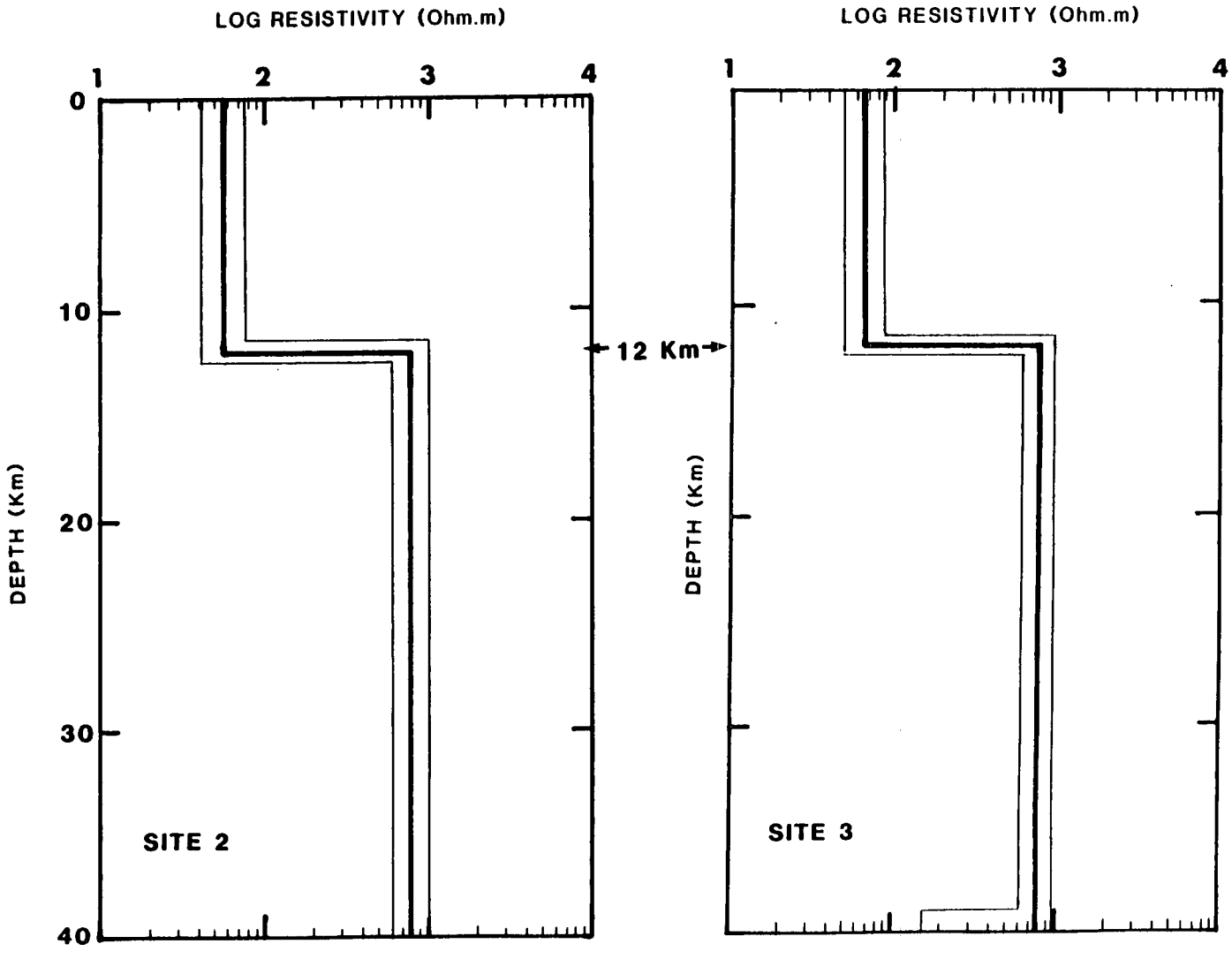

Figure 2.5 (after Russell 1988) 1-D crustal resistivity model for MT sites 2 and 3 (SE and PB of Fig. 2.1).

cracks of the EDA hypothesis (Crampin & Booth 1985), identified by shear-wave splitting observations, with the cutoff (arrowed in Fig. 2.5) representing the base of the seismogenic zone.

The TDP3 experiment has allowed the swarm of microearthquakes originally identified by MARNET to be closely examined and well located using the high-quality records which were the result of observing only direct raypaths within the shear-wave window. It has demonstrated that the swarm activity in the region has remained in much the same position over a number of years. It has also provided a large amount of data useful for the analysis of shear-waves, and was probably the first time that such a small-magnitude earthquake swarm has been so closely studied by a small-aperture network of three-component instruments. Further resolution of the hypocentres is not possible using HYP071 for the reasons outlined above - a relative relocation method is needed. Logan (1987) describes the use of such a method on this data set, and this will be briefly discussed in Chapter 5.

Chapter 3

Earthquake magnitudes

3.1 Introduction

The magnitude of an earthquake is a number, characteristic of that earthquake, and is ideally independent of the location and number of recording stations used to determine it. Its determination method should conform to some international standard so that comparisons can be made with other events. However, there are too many variables involved in magnitude calculation for there to be a universally-applicable exact method, and magnitude calculation formulae have been derived using, amongst other parameters, *P*- and shear-wave amplitudes and event durations. To fully represent the magnitude of an earthquake would require many determinations over all waves and frequencies emanating from the source region. Such a calculation is impractical, and approximate world-wide standards have been adopted. These, and the complex relationships between them, are exhaustively reviewed by Båth (1981). It is recognised that different methods of magnitude calculation are applicable depending on, for example, the period of the instruments used, and the location and size of the earthquake, and that calculations in each area are specific owing to the non-uniform, laterally-varying attenuation properties of the crust. Magnitudes bear little relation to the source of the earthquake, and are frequently replaced by seismic moment calculations which relate directly to the source. Seismic moments have not been calculated here, and could be the subject of further study.

Despite these generally negative comments, however, magnitudes are recognised as being a quick and convenient means of comparing approximately the sizes of earthquakes, and have been widely used. They are used here to demonstrate the very small variation in nature of the Izmit swarm, and have been carefully derived to permit comparison with microearthquakes elsewhere.

Throughout this thesis, the Izmit swarm has been discussed as

containing microearthquakes. After Richter's (1935) definition of the magnitude scale, seismologists were able to classify events more exactly, even more so after Hagiwara's (1964) magnitude classification was published. Hagiwara defined microearthquakes as those having magnitudes $1 \leq M_L < 3$, and ultra-microearthquakes as having magnitudes less than 1 (M_L, the Richter local magnitude, will be defined in section 3.2). Many swarms contain events of low magnitude, some have been recorded down to $-1.3M_L$ (Brune & Allen 1967), although magnitudes are more typically around $2M_L$, for example Eaton *et al.* (1970). Magnitudes in the Izmit swarm range from -0.5 to above $3M_L$, and the swarm will be discussed as a microearthquake swarm as the term ultra-microearthquake seems nowadays to have become redundant.

Most of the earthquakes occurring in the swarm studied by the TDP network, and whose locations were discussed in Chapter 2, were of such small magnitude that they would not have been detected by any other network except MARNET (Üçer *et al.* 1985). Indeed, even the larger TDP events are frequently smaller than microearthquakes studied elsewhere primarily for earthquake prediction purposes, for example those studied by Brune & Allen (1967) and Eaton *et al.* (1970). MARNET detected only the largest events of the swarm, those with magnitudes above around $2.6M_B$ as measured from the MARNET records (M_B - the body-wave magnitude scale - is calculated in a similar way to M_L but with a correction factor which incorporates both epicentral distance and depth). Events of this magnitude occur in the swarm infrequently, a few times a year at most, so their detection by the TDP networks was fortuitous as these were in operation for only fractions of the swarm's lifetime. It could be argued, then, that the swarm should be studied in isolation, and that magnitudes assigned to the events should be calculated almost arbitrarily. This argument, however, is not only unscientific, but it ignores the fact that studies of any activity, however localised, along a major crustal feature (here the North Anatolian Fault) need to be directly comparable with results elsewhere if any meaningful synthesis of work along the whole feature is to be attempted, or any comparison with events elsewhere is to be valid. It was therefore decided early in the TDP experiments that the event magnitudes should approximate to the local magnitude scale (Richter 1935).

3.2 Method of calculation

The local magnitude, M_L, of an earthquake was originally defined by Richter (1935) as

$$M_L = \mathrm{Log}_{10}\ (A/A_0)$$

where A is the maximum centre-to-peak amplitude of an earthquake record, measured in mm, on a standard seismometer, and A_0 is the maximum amplitude of the record of a zero magnitude earthquake recorded at the same distance. The standard seismometer used was a Wood-Anderson torsion instrument, with known pendulum period, magnification and damping factor. A_0 becomes a distance attenuation factor, and calibration curves were constructed so that the magnitude of most earthquakes could be related to this scale. The scale was originally strictly applicable only to Californian events, however, as differences in crustal structure, instrumentation, etc., made its wider application difficult. However, attempts to apply correction factors for different instruments and crustal structures were made in many areas, and the scale is in world-wide use today. In BGS, local magnitudes are calculated by taking the average of deflections on orthogonal horizontal instruments and correcting this to the equivalent deflection on a Wood-Anderson instrument. Here, a method similar to Richter's will be used to relate the magnitudes of the TDP events to the Richter local magnitude scale.

None of the programs in use at the time of data analysis would calculate magnitudes, so a method developed in the previous projects was used. The maximum centre-to-peak amplitudes of the shear-waves recorded on the north-south and east-west components were measured in millimetres from paper playouts of the events, and corrected according to the scale factor of the plot. The mean was taken, and an empirically-derived formula then used to calculate the magnitude at that station, and a mean taken for all stations used in the determination. The formula used was based on the general magnitude formula

$$Magnitude = \log(Amplitude/Period) + F$$

where F is a distance factor determined by observation.

Here, this formula was adjusted to take account of the properties of the Willmore seismometers, and the factor F became 0.4 (note that magnitudes are generally calculated to one place of decimals). This factor was found to adjust the magnitudes approximately to the local scale, and was derived from comparisons of determinations of previous local magnitudes and the M_B values measured for the very largest local events by MARNET, so the general formula became

$$Magnitude = \log(Amplitude/100) + 0.4$$

Many events saturated at least some of, and the largest events saturated all of the instruments, so a method was evolved to deal with these. The largest events recorded by MARNET during TDP1 and TDP2 were $3.1M_B$ and $2.6M_B$, but a $3.5M_B$ earthquake was located in the swarm area by MARNET in October 1980 after the TDP2 network was dismantled (Crampin *et al.* 1985). These body-wave magnitudes were estimated from MARNET records. Events of this magnitude recorded by the TDP3 network could therefore be assigned M_B values derived from MARNET records. However, for those events with local magnitudes between, say, 1.5 and 2.0, which partially or fully saturated the network, the MARNET magnitude method (duration) was found to be inaccurate. Magnitudes for these events were calculated by estimating the maximum shear-wave amplitudes by drawing the shape of the shear-wave envelope as accurately as possible. Amplitude measurements were then used to calculate the event magnitudes in the usual way. For those events where extrapolation of the envelope was considered too inaccurate, an approximate method based on record duration (as in M_B calculations) was adopted. However, such events were generally regionals, and are not discussed here.

3.3 Results

Earthquake magnitudes determined appear in Appendix A. They approximate to the Richter local magnitude scale and will be discussed as such. The magnitudes of some events became negative because of the logarithmic scale used. Many such events were only recorded on only a few stations (Appendix A, column N (no. of

arrivals)), and are therefore of little use in subsequent analysis, eg for fault-plane solutions. The inclusion in the data sets of many of these small events reflects to some extent the network geometry and sensivity and the selection criteria used by the analysts.

Figure 3.1 shows plots of event magnitudes against time for each of the TDP experiments. For the TDP3 data set, it can be seen that event magnitudes range from very low values (negative magnitudes have been corrected to zero by the plotting program) up to just over 2.0, with a few events above that magnitude, and with a sharp cutoff above $1.4M_L$. Events having magnitudes between 1.4 and $2.0M_L$ are relatively few compared with the number with magnitudes between 0.0 and $1.4M_L$; this may reflect inaccuracies caused by the crossover between those magnitudes calculated using the amplitude method and those determined with a combination of amplitude and event duration. Any internal trends in magnitude distribution are masked by the number of events detected, and any further study of the distribution of magnitudes would have to take account of the clustering of events in this swarm (discussed briefly in Chapter 2, and the subject of Chapter 5). The overall pattern seems very similar to the patterns for the previous two TDP experiments also presented in Figure 3.1, although magnitudes here have a greater range than those in the previous projects.

For the TDP3 data set, it does appear that a slight increase then a decrease in maximum magnitude is discernible. No such trend is visible in the other two data sets. The apparent lack of small events about two thirds of the way along Fig. 3.1(a) is spurious, and represents only a period of less rigorous network maintenance owing to the incapacitation of the project leader for six weeks or so. This was additionally unfortunate as it disrupted, to a small extent, the shear-wave polarization studies which were carried out later on the data (Chen *et al.* 1987), as these depend critically on the simultaneous operation of both horizontal components at a seismograph station. There appears to be an overall decrease in magnitudes between TDP1 and TDP2, after which a considerable increase takes place during TDP3. This may be a reflection of the work of different operators on data derived from networks with differing geometries (station location maps are presented as Chapter 1, Figs 1.5, 1.7 and 1.11). Chen *et al.* (1987), working on shear-wave polarizations,

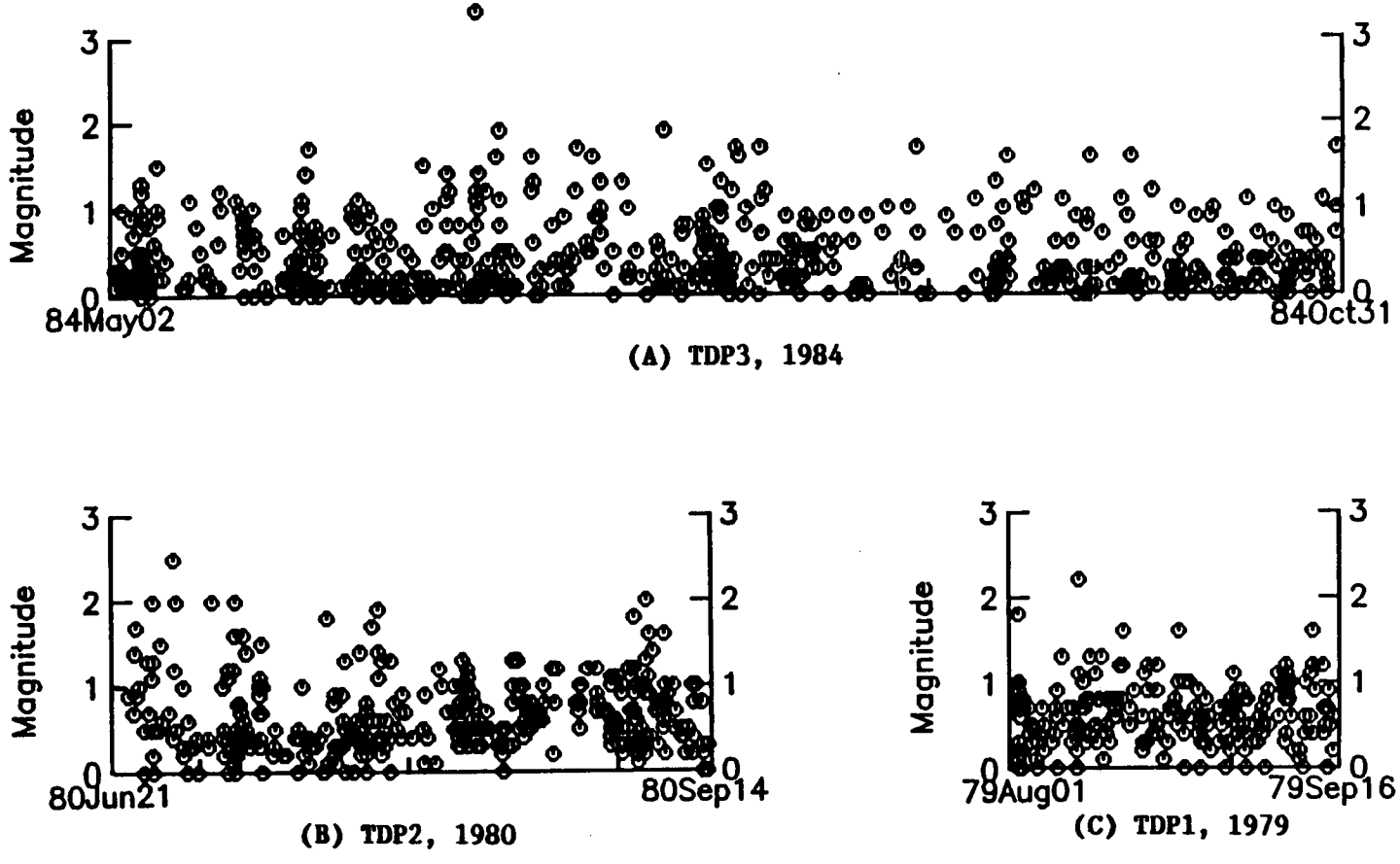

Figure 3.1 Plots of magnitude (M_L) against time for the three TDP experiments: (a) TDP3, in 1984, (b) TDP2, in 1980, and (c) TDP1, in 1979. The time axes are plotted at the same scale.

suggest a decrease in overall tectonic stress between TDP1 in 1979 and TDP3 in 1984. This may well correlate with the decrease in earthquake magnitudes observed between TDP1 and TDP2 (Figs 3.1(c) & 3.1(b)). Correlation with earthquake magnitudes in TDP3 is more tenuous as the TDP3 network was more closely packed over the swarm, and therefore more susceptible to saturation and consequent inaccuracy of the larger magnitudes. Few, if any, conclusions can be drawn from such observations, as any such conclusions would require constant and long-term monitoring with identical networks to be justified. This is not possible with the TDP networks, and the resolution of MARNET is insufficient to show up these trends.

The magnitude against time plot for TDP3 (Fig. 3.1(a)) shows the largest event to have a magnitude of $3.3M_L$. This event was also detected by MARNET, and assigned a magnitude of $3.3M_B$. Events of such magnitude occur rarely in this area, and are only detected by the TDP networks by chance as their recording times were short compared with the repeat time of such events which may perhaps be some other manifestation of the seismicity associated with the seismic gap, as discussed later. However, the similarity of magnitudes assigned lends credence to the method used here for magnitude determinations, although it is realised that the two scales are not directly related.

3.4 The magnitude-frequency relation

The relationship between the magnitude of an earthquake and its frequency of occurrence was derived by Gutenberg and Richter (1941) and expressed thus:

$$\text{Log } N = a - bM$$

where N = number of earthquakes of magnitude M or greater, and a and b are numerical constants. The slope, b, of the graph is called the b-value of an earthquake swarm, and is generally obtained from the Gutenberg-Richter (1941) relation.

In most cases, the b-value for a swarm lies between about 0.6 and 1.2 (Lee & Stewart 1981), although in theory it should equal unity. Studies of b-values have been carried out, primarily for earthquake

prediction purposes, and decreases have been noted before large earthquakes, for example, by Bufe (1970) and Stephens *et al.* (1980). Here the *b*-values derived from two TDP data sets are compared.

Cumulative magnitude-frequency curves for TDP2 and TDP3 are presented in Figure 3.2, where the log of the cumulative frequency is plotted against M_L in the conventional manner (TDP1 data have been omitted because of slight differences in magnitude calculation methods). Both graphs exhibit the typical shape, with a tail-off of events below a certain magnitude, called the completeness threshold, above which the data can be assumed to be complete. These thresholds reflect the differing network sensivities in each project, being at approximately 0.5 and $0.2M_L$ for TDP2 and TDP3 respectively. The expected scatter at the upper ends of the graphs is also observed, and probably means that the sample times are not sufficiently long, as larger events are much less frequent than those of smaller magnitude. Linear regression lines have been fitted to the straight parts of both curves in Fig. 3.2 above the completeness thresholds. Correlation coefficients and *b*-values for both are presented in Table 3.1.

Project	b-value	Correlation coeff.
TDP3	-1.02	-0.99
TDP2	-1.04	-0.99
TDP1	-1.3 to -1.6	

Table 3.1 *b*-values and correlation coefficients for the TDP data sets (values for TDP1 included for comparison).

The consistency between at least the TDP2 and TDP3 data sets is clear, with each having a *b*-value of unity and high correlation coefficients for the linear regression lines. TDP1 has a higher *b*-value, in fact it is difficult to draw a straight line on the data available. This reflects the fact that the TDP1 project was very much shorter than the later projects, and its data set is therefore less complete.

(A) TDP3, 1984

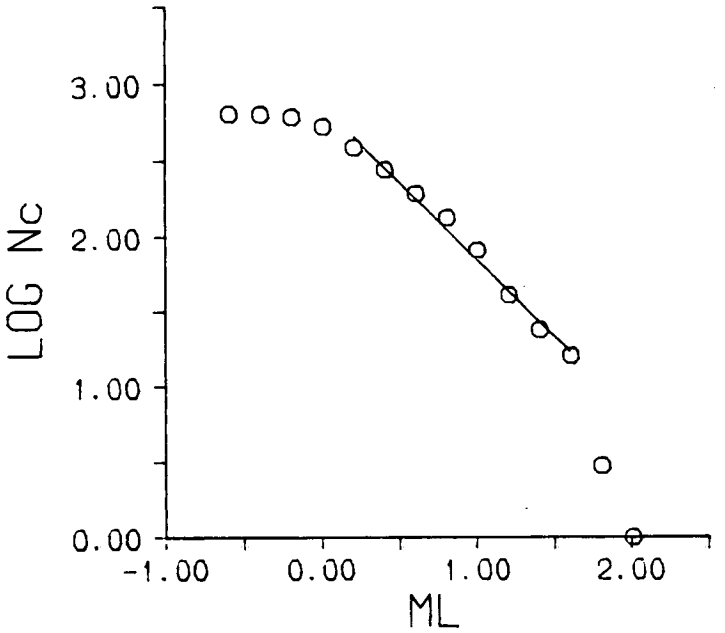

(B) TDP2, 1980

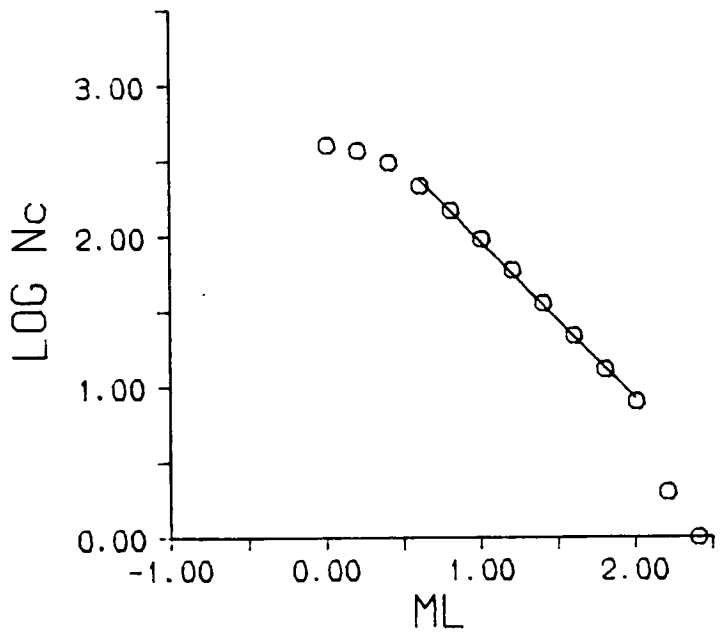

Figure 3.2 Cumulative magnitude-frequency plots (Log N_c vs M_L) and linear regression lines plotted above the completeness threshold for (a) TDP3 and (b) TDP2.

3.5 Discussion

It is difficult to compare the results from the three TDP projects directly, owing to the facts that different operators worked with the data sets, the projects operated for such short and different time windows compared with the lifetime of the swarm, and that the different station distributions used have given the networks differing sensitivities. In particular, the TDP3 network was closely spaced over the swarm, and may be expected to have located many more small events than the previous networks. This is reflected in the low completeness threshold of $0.2M_L$ in Fig. 3.2(a). However, the event magnitudes described in this chapter show a remarkable consistency in range, and the magnitude-frequency curves give such similar *b*-values that it must be concluded that the swarm shows very little variation in character with time, for the two later data sets at least. The magnitudes calculated for TDP1 are similar to the rest, and it is only the fact that this project was so much shorter than the others which prevents a rigorous comparison.

It must be remembered that this swarm has been active over at least five years, and therefore very long-term monitoring would be required to determine any true variations in its nature. Similar swarms to the west, for example the Marmara Island and Mürefte swarms (Crampin & Evans 1986), have been associated with the epicentres of large earthquakes in the past. These swarms are still active, and have been monitored by MARNET since its inception in 1978. As suggested in Chapter 1, it will be interesting to see if the expected large event is associated with the Izmit swarm.

The large events detected in the swarm area by MARNET (for example the 3.1 and $3.5M_B$ events, Crampin *et al.* (1985)) have a repeat time of perhaps six months or so. Such events were therefore only recorded by chance on the TDP networks. The largest event recorded during TDP3 (3.3 M_L, Fig. 3.1(a)) comes into this category. Such events saturate the network, and it is therefore not possible to determine if they are part of the swarm activity in this area, because they cannot be related to the clusters to which most other events are related by comparison of seismograms (see Chapter 5). Indeed, they are so large that their source dimensions may be incompatible with the few tens of metres

suggested by Logan (1987) for events in this swarm, and they may be part of a larger fault system influenced by the same tectonic regime. However they do occur within the swarm area, although their depths are subject to large errors as shear-wave readings could not be included in the calculations because of saturation problems. The magnitude-frequency curve for TDP3 (Fig. 3.2(a)) suggests a gap in the data set above about $2.0M_L$, and this adds weight to the preceding argument that such large events may not be directly related to the swarm. This could be the subject of further study. In particular, it would be interesting to deploy some less sensitive or strong motion instruments so that the magnitudes of the larger events could be more accurately determined without the saturation problems experienced previously. Alternatively, the presence but infrequent occurrence of such large events may just illustrate the fact that the data sets are not complete, and that a much longer monitoring period is required to reveal the true picture.

In conclusion, it can be stated that the magnitudes determined for the three data sets appear very similar, as broadly the same methods were used in each case. The swarm appears to be normal, as indicated by the consistent *b*-values obtained. Small differences may be attributed to the differing network sensivities and the different analysts who have examined the data.

Chapter 4

Fault-plane solutions

4.1 Introduction

Fault-plane solutions are produced as a matter of routine for many of the large earthquakes occurring in the world today. Such studies give important information about the sense and magnitude of relative motion of the causative faults at various plate boundaries. They are important if an overall picture is to be obtained, but also presuppose that the fault-plane can be unambiguously identified. This is generally the case for large earthquakes, but, for the swarm of microearthquakes studied here, surface breaks were not present, so fault-planes could not be positively identified. However, detailed studies of the many earthquakes considered likely to give well-constrained fault-plane solutions, and a knowledge of the tectonic regime, has enabled a previous synthesis of the local tectonics to be confirmed and refined.

In this chapter, the method used to produce fault-plane solutions will be described. The results obtained, and the confirmation and refinement of previous observations will be illustrated.

4.2 Fault-plane solutions

4.2.1 Method

The theoretical basis for the production of fault-plane solutions has been fully described by Aki & Richards (1980) and Lee & Stewart (1981), and simplified by Roberts (1985), who used the method to derive fault-plane solutions for small acoustic events in Cornwall. Only a brief summary only of the method is given here.

The fault-plane solution of an earthquake may be determined by several methods or combinations of methods. The most common method requires good quality recordings of *P*-wave first-motions at a range

of azimuths and distances around the source, and for small earthquakes this requires a large number of stations in the epicentral region. The TDP network fulfilled both these conditions.

A double-couple earthquake source is assumed here. This assumption has been shown to be valid for large earthquakes (Sykes 1967; Pearce 1977; Pearce & Rogers 1987). The same may not be true for some small events. Foulger & Long (1984), working with events with local magnitudes typically of around $0.0M_L$, pointed out that double-couple solutions were invalid for approximately half of the events. Similar conclusions were stated by Julian (1983). In both instances, (Iceland and Long Valley, California respectively), magmatism and not fault slip was suggested as the cause of the earthquakes, and linear vector dipole and compensated linear vector dipole (LVD and CLVD respectively) mechanisms were shown to fit the data. The TDP3 geomagnetic experiment (see Chapters 1 and 2) indicates that large-scale magmatism can be discounted in the seismogenic zone at between seven and 12 km depth. In a tensional environment, some magmatism might reasonably be expected. Pull-apart basins farther east on the North Anatolian Fault are associated with recent volcanism and hot spring activity (Dewey & Şengör 1979; Şengör 1979; Şengör & Canitez 1982). However, no such volcanic features are recognised in the study area, although hot spring activity occurs farther south near Bursa but is not really associated with the Izmit graben structure. Volcanic activity is not a prerequisite for these tensional areas. Weaver & Hill (1978) point to similar swarms associated with strike-slip faults in California, not all of which are associated with volcanism. It could be that small-scale dyke intrusion is occurring at the seismogenic depth, but is not observed using current geophysical methods, hence the need for further investigations (Chapter 6). Available evidence suggests that the events are associated with a complex series of faults, as their distribution on a series of dipping fault-planes was suggested by Logan (1987). Additionally, a careful review of the fault-plane solutions fails to show any which might, with certainty, be attributed to mechanisms other than double-couple.

The distributions of *P*- and shear-wave motions observed in the epicentral area around a double-couple earthquake source are shown in

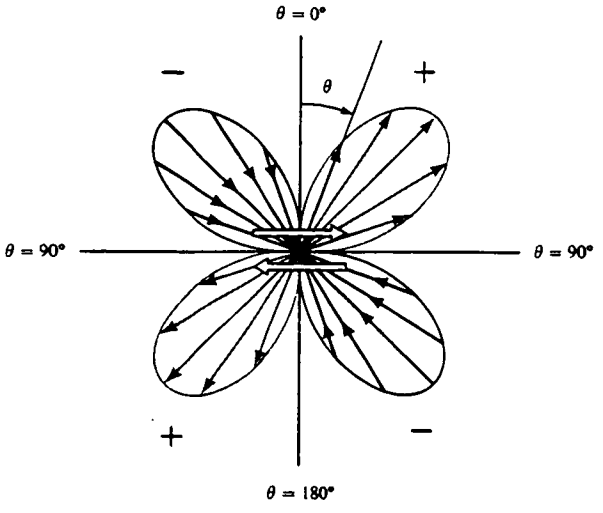

Figure 4.1(a) The far-field *P*-wave radiation pattern for a double-couple source. Arrows at centre show sense of shear, plus and minus signs denote compression (upwards) and dilatation (downwards) respectively. (after Aki & Richards 1980)

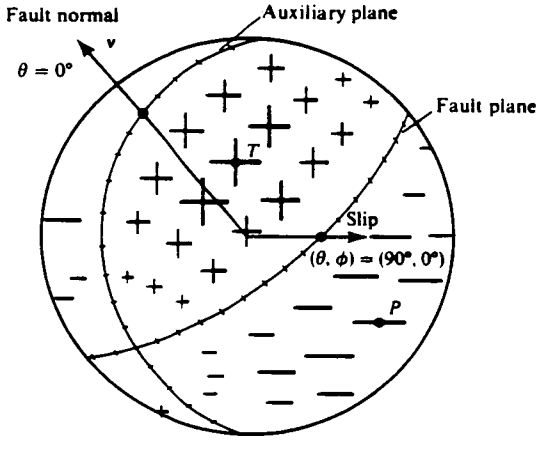

Figure 4.1(b) *P*-wave radiation pattern over equal-area projection of sphere centred on the origin. Amplitude denoted by size of symbols. Fault-, auxiliary planes, tensional (T) & compressional (P) axes marked. (after Aki & Richards 1980)

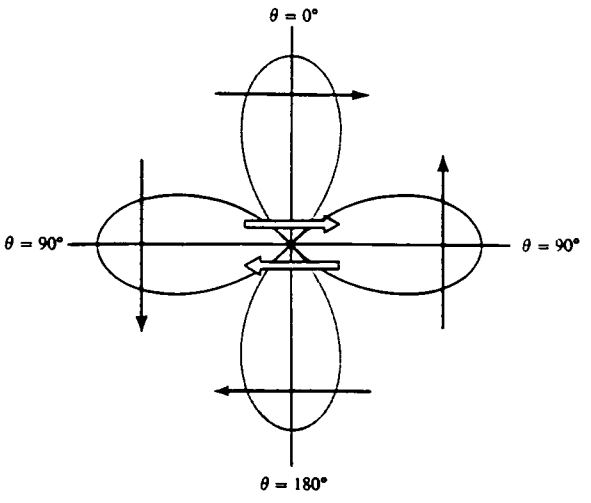

Figure 4.1(c) Shear-wave radiation pattern for a double-couple source. Arrows at centre show sense of shear, arrows on lobes show direction of displacement. (after Aki & Richards 1980)

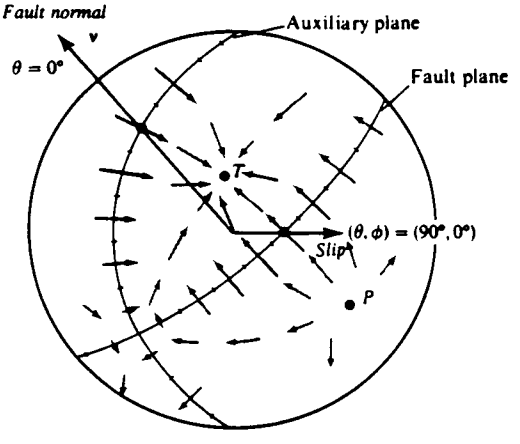

Figure 4.1(d) Shear-wave radiation pattern over equal-area projection of whole sphere centred on origin, arrows show variation in direction and amplitude of motion. (after Aki & Richards 1980)

Figures 4.1(a) and 4.1(c). Their more complex variations over the focal sphere are shown respectively in Figures 4.1(b) and Figure 4.1(d). These variations provide the basis for the derivation of a fault-plane solution.

It can be seen from Fig. 4.1(a) that the *P*-wave first motion pattern consists of alternate lobes of compressions (upward movements) and dilatations (downward movements), separated by orthogonal planes along which no *P*-wave motion is observed. These planes are the fault- and auxiliary-planes, and there is no way in which these can be differentiated solely from the fault-plane solution. This ambiguity in the source orientation must be resolved by using other evidence, which may be obtained from observation of surface deformation or displacement, or from the distribution of aftershocks (such as in Marrow & Roberts, 1985), or from the ellipticity of isoseismal lines. The shear-wave radiation patterns in Figures 4.1(c) and 4.1(d) show maximum amplitudes which coincide with the *P*-wave null points along the nodal lines. This amplitude variation can then be used to locate more accurately the nodal planes by looking at the ratio between the amplitudes of the shear- and *P*-waves; a high ratio indicates proximity to a nodal line.

The *P*-wave polarity recorded by the seismometer is plotted on to the surface of a sphere of small and arbitrary radius surrounding the earthquake source (the focal sphere), using appropriate symbols for compressions (ups) and dilatations (downs). If this information is to be plotted in its correct position on the focal sphere, the regional velocity structure and hence the azimuth and take-off angles between source and receiver must be well known (i.e. the earthquake must be well-located). An equal-area projection is then used to plot the *P*-wave polarity information on to a flat surface representing the surface of the focal sphere. In this case, equal-area projections of the *upper* focal hemisphere were used. This is logical as the seismograph stations were closely clustered directly above the earthquake swarm, and only direct, upward-going rays were being observed. The projection is then divided up using an equal-area net to draw great circles which separate the focal sphere into four quadrants, each containing either only compressions or dilatations. The strike, dip and rake of the fault- and auxiliary-planes are then

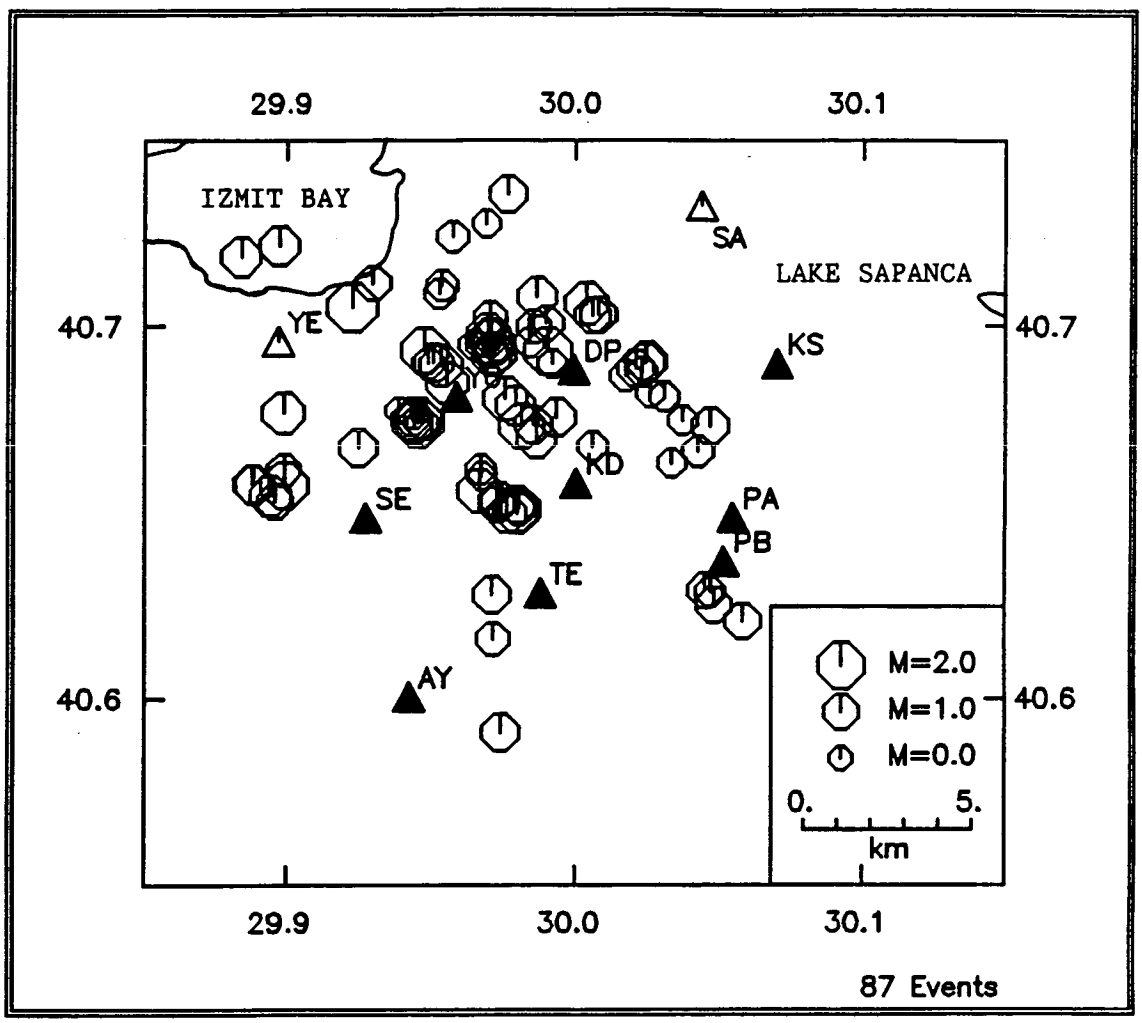

Figure 4.2 Epicentre map of the 87 events with at least six *P*-wave arrivals. Filled and open triangles represent respectively three- and single-component seismograph stations.

measured directly from the upper focal hemisphere projection, again using an equal-area net, and quoted using the sign conventions of Aki & Richards (1980).

Because of the size of the data set (over 600 local events), it was decided to concentrate analysis on those events which had at least 6 reasonable *P*-arrivals, and which could therefore be expected to give well-constrained fault-plane solutions. This reduced the number of events to 87, and their locations are presented in Figure 4.2. Readings of *P*-wave polarities were taken from the seismograms at the same time as the picking of arrival-times used for locations. Data from all stations were used; this includes the two single-component stations, SA and YE (Fig. 4.2), which were not used for location purposes for the reasons given in Chapter 2. The *P*-wave polarities at these stations were unaffected by the ray's passage through the sediment pile, and where possible, readings from these stations were used in the fault-plane solutions. All readings were given a confidence weight, and care taken to identify correctly the actual polarity, as it is known that in cases of high noise or low *P*-wave amplitude, the second *P*-wave cycle is frequently larger than the first, so giving rise to incorrect polarity readings (Aki & Richards 1980).

Fault-plane solutions were constructed for these 87 earthquakes, locations of which are presented in Figure 4.2. In general, these events were the largest and best-located, although unambiguous *P*-wave arrivals were not always present. In such cases nodal lines were drawn near to stations whose seismograms showed the high shear- to *P*-wave amplitude ratios which generally indicate the proximity of a nodal plane. In some cases when *P*-wave polarity readings were not available (for instance if the vertical component was inoperative for some reason) a large shear- to *P*-wave amplitude on the horizontal components was taken as indicating proximity to a nodal line. Many of the 87 events gave well-constrained solutions, and fault-plane solutions for the best 32 of these are shown in Figure 4.3. These 32 events are distinguished by having generally larger magnitudes and better azimuthal distributions of *P*-wave arrivals than the rest, and they include a representative selection of all the mechanisms observed.

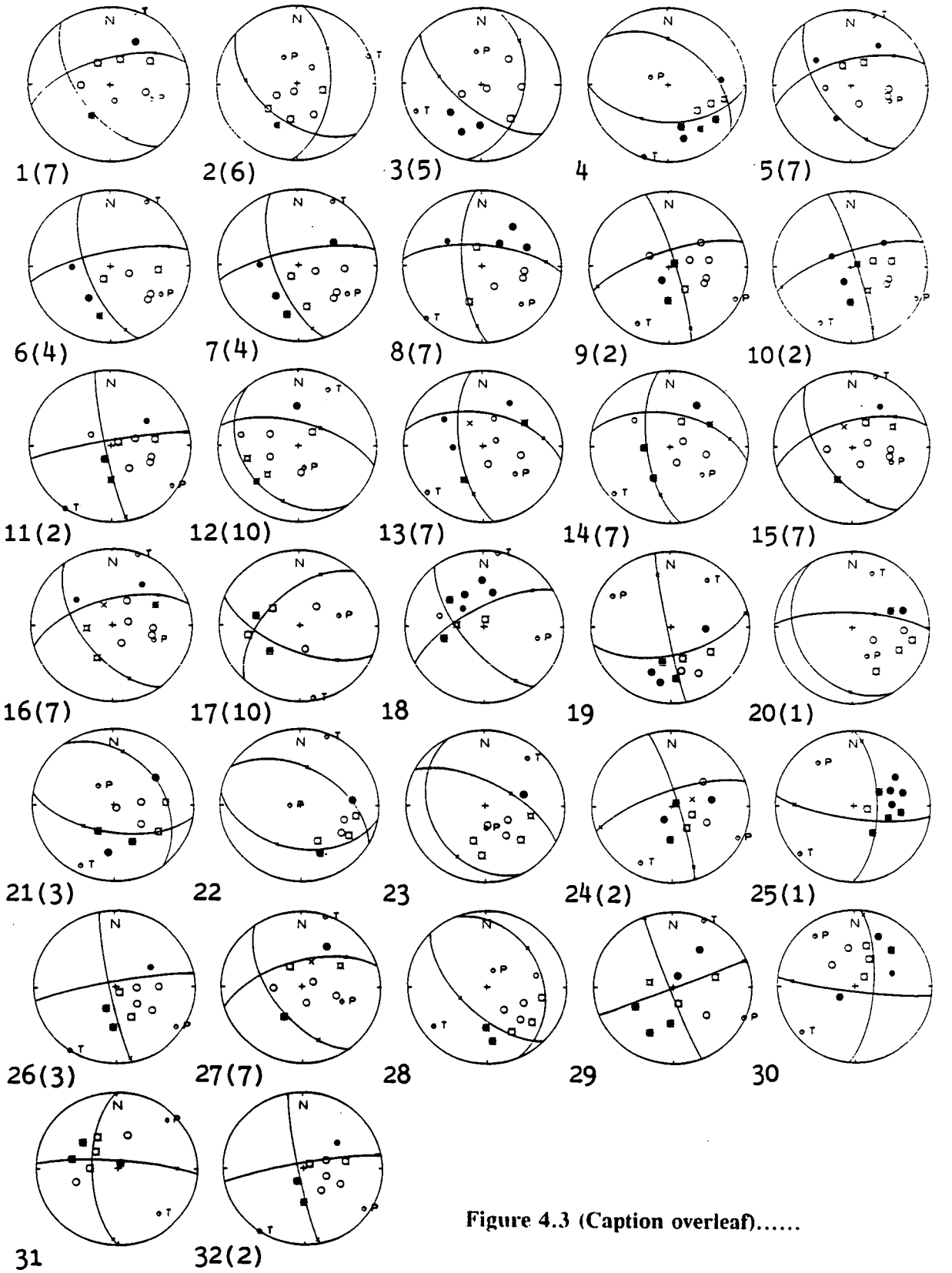

Figure 4.3 (Caption overleaf).....

Caption to Figure 4.3 on preceding page

Figure 4.3 Fault-plane solutions for the 32 best-constrained events from Fig. 4.2, shown on equal-area projections of the upper focal hemisphere. Where applicable, numbers in brackets refer to the number of the cluster in which the event occurs (see Chapter 5). Open and filled circles represent, respectively, dilatational and compressional first motions, smaller circles represent less reliable readings. Crossed circles indicate those stations whose seismograms show a large shear- to *P*-wave amplitude ratio indicating their proximity to a nodal line. Isolated crosses indicate those stations where no *P*-reading was available, and large shear- to *P*-wave amplitude ratios were inferred from the horizontal components. The projections of the slip vectors of the fault- and auxiliary planes are shown as small crosses on the nodal lines. The positions of the compressional (P) and tensional (T) axes are marked.

4.2.2 Mechanisms

The fault-plane solutions shown in Fig. 4.3 show a variety of mechanisms (Lovell *et al.* 1987). Normal faults with varying percentages of dextral strike slip predominate, and constitute about 80 per cent of the total number. There are also several almost pure dextral strike-slip solutions (11, 29 and 32 amongst others). Reverse or thrust fault mechanisms (19, 24 and 31) are less common, and their identification must remain somewhat speculative as fault-plane solutions for these events (with the exception of 31) are poorly constrained. Note that there are almost no pure normal, reverse or strike-slip faults, except, perhaps, no. 29.

4.2.3 Slip vectors

Figure 4.4(a) shows the normals to the fault- and auxiliary-planes (i.e. the possible slip vectors) for the 32 fault-plane solutions of Figure 4.3 plotted on a single composite equal-area projection. With the exception of events 9, 10 and 24, the events have one normal which plots in the north-east quadrant. These normals are grouped around a mean direction of about N60°E (Lovell *et al.* 1987), and because of this strong grouping they are interpreted as slip vectors (Evans *et al.* 1985). The positions of the normals of the three thrusts (nos 19, 24 and 31 of Fig. 4.3) are in the same positions as those found by Evans *et al.* (1985).

4.2.4 Principal axes of stress

The variety of focal mechanisms (Figure 4.3) and locations (Figure 4.2) suggests stress release on a complex array of fault-plane facets in this area. If it is assumed that the same regional stress field drives all these earthquakes, then the principal axes of stress should be common to the mechanisms of all events (Crampin & Booth 1985). Figure 4.4(b) shows the nodal planes of the best-constrained fault-plane solutions superimposed on an equal-area plot of the upper focal hemisphere. The areas of tension (T) and compression (P) common to all solutions are marked, and are in approximately the same position as those in the similar figure of Crampin & Booth (1985),

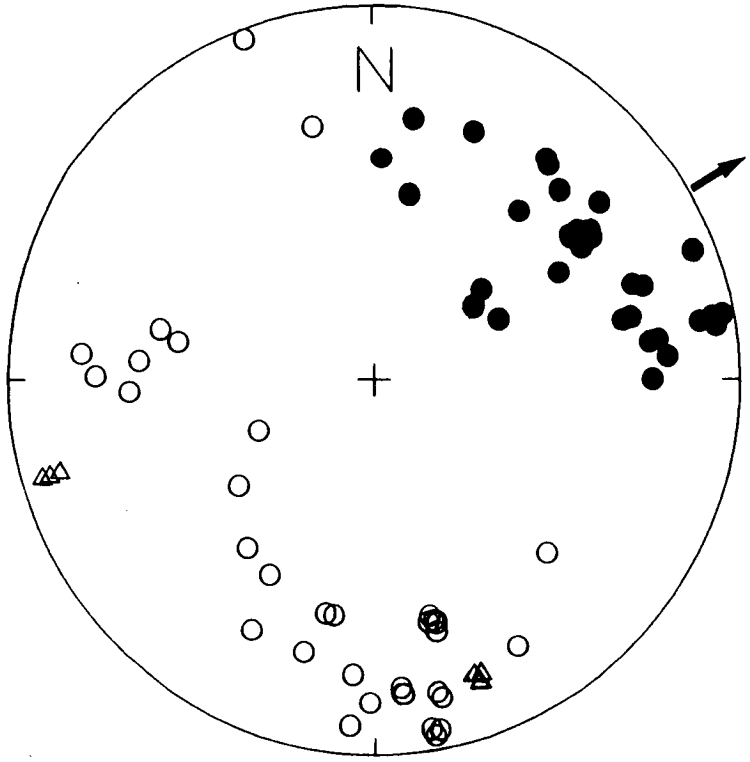

Figure 4.4(a) Fault- and auxiliary-plane normals from 32 fault-plane solutions presented in Fig. 4.3 superimposed on one plot; those in the northeast quadrant, shown as solid circles, are interpreted as slip vectors and their alternates, shown as open circles, are interpreted as fault-plane normals. The normals for the three thrusts are shown as open triangles. The heavy arrow indicates the mean slip vector direction of N60°E.

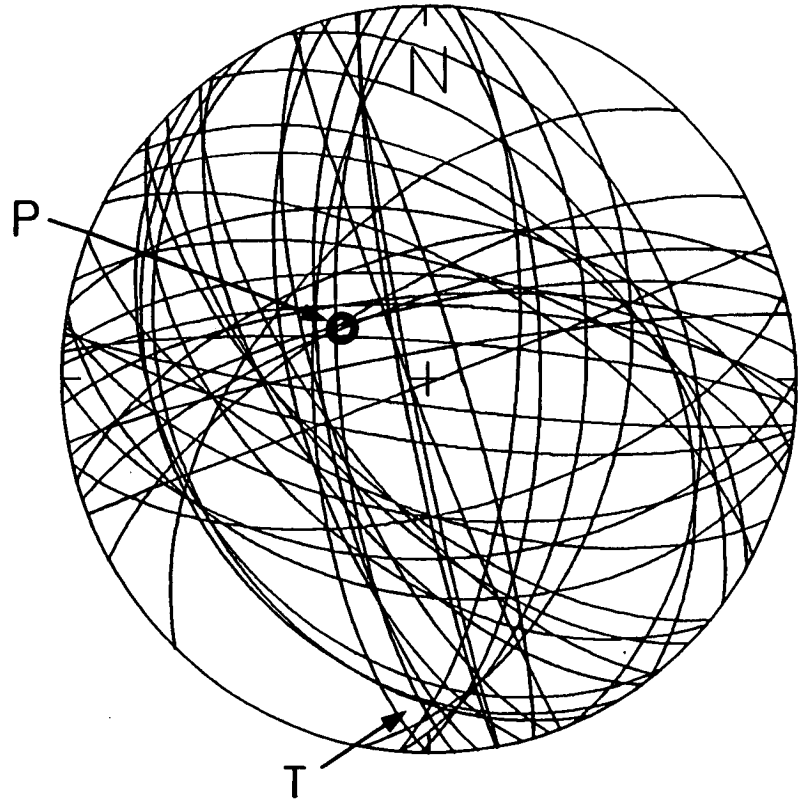

Figure 4.4(b) Nodal lines from the 32 fault-plane solutions in Fig. 4.3 superimposed on one plot. Areas of compression (P) and tension(T) common to each solution are marked.

but more closely constrained (Lovell *et al.* 1987). Additional strong supporting evidence for this argument is provided by the fact that in Figure 4.4(b) the P- and T-axes common to each solution are almost exactly orthogonal. In a strike slip configuration, such as that associated with the North Anatolian Fault, vertical compression is unlikely to be the dominant or driving stress, and the near-vertical compression is likely to be the intermediate stress here. It is concluded that the main driving force of these swarm events is the tensional stress which, in Figure 4.4(b), is constrained to a sub-horizontal direction between N180°E and N190°E. This is consistent with McKenzie's (1969) suggestion that for a shallow earthquake, the maximum stress axis must lie in the dilatational quadrant of the fault-plane solution.

4.3 Discussion and comparison with previous projects

4.3.1 Mechanisms

Identification of the present family of fault planes is somewhat tentative, perhaps because some of the fault-plane solutions are not as well-constrained as those in Fig. 3 of Evans *et al.* (1985). However a pattern emerges from Figs. 4.3 and 4.4(b), although there is some scatter. A predominantly east-west trending, southward-dipping group can be identified together with a north-south striking, westward-dipping family (Lovell *et al.* 1987). These sets are almost orthogonal, and may be interpreted as a conjugate fault system influenced by the same stress-field, and each show slip vectors in the northeast quadrant (Fig. 4.4(a)). This picture is complicated by a small additional group which strikes approximately east-west and dips northwards. These were not previously identified (Lovell *et al.* 1987), but have slip vectors in the northeast quadrant of Fig. 4.4(a), and may be expected to occur in a tensional regime with some uplift in the Marmara area. In addition, Logan (1987) has identified tentatively all these possible fault-plane orientations using a relative relocation method on small clusters of events in the major swarm (discussed further in Chapter 5), but, as pointed out by McKenzie (1969), almost any orientation of fault-planes can be expected.

The apparent lack of pure normal, reverse or strike-slip mechanisms can be explained by the fact that, for shallow earthquakes, movement takes place generally on pre-existing fault planes, or at least on planes of weakness already orientated by the prevailing stress (Bott 1959).

Composite fault-plane solutions were not attempted here, as there is no guarantee that the fault mechanisms are the same within the geographical groupings used, and they may conceal variations of mechanism with time. However, they were used by Evans *et al.* (1985), who demonstrated their validity, when used with care, by the similarity of the solutions obtained by the composite and individual methods.

4.3.2 Slip vectors

The fault-plane mechanisms derived here are similar to those found previously by Evans *et al.* (1985), who suggest that a mixed regime of normal and strike-slip faulting is taking place in the Marmara Sea area, resulting from rotation and internal shearing of the Marmara Block as it is pushed against the bulge of Thrace to the west and northwest of the Marmara area (see Fig. 1.4). The mean slip vector direction of N50°E derived by Evans *et al.* (1985) is consistent with the gradual change westwards of the directions of the slip vectors of teleseismically-determined fault-plane solutions for large earthquakes which have occurred along sections of the NAF. Some of these earthquakes caused surface faulting, from which positive identification of fault planes and thus slip directions could be made. Slip vectors of these large events change from an easterly direction on the NAF in the east of Turkey, through northeast around the study area, and to northwards towards the west of the Marmara Sea. The present mean slip vector direction of N60°E (Lovell *et al.* 1987) is consistent both with previous observations and with the position of the study area on the NAF.

4.3.3 Principal axes of stress and shear-wave polarizations

The tensional stress direction of N10°E (Fig. 4.4(b)) derived from an overlay of the nodal lines from the fault-plane solutions

TDP2, 1980	TDP3, 1984

4.5(a) Fault and auxiliary-plane normals on one plot. Notation as in Fig. 4.4(a).

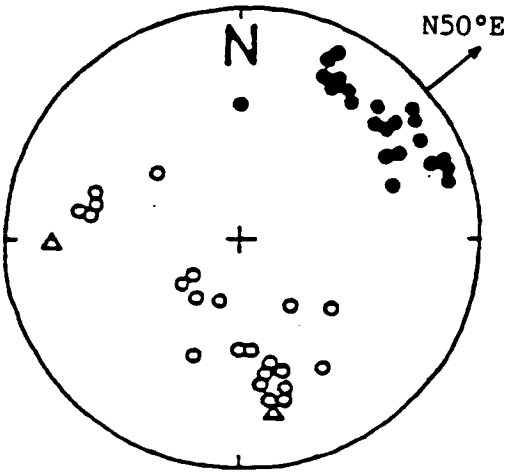

after Evans *et al.* 1985

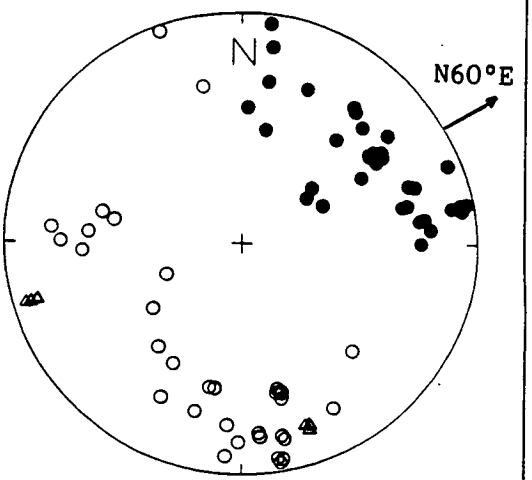

4.5(b) P- & T-axes derived from overlay of nodal lines on one plot. Notation as in Fig. 4.4(b).

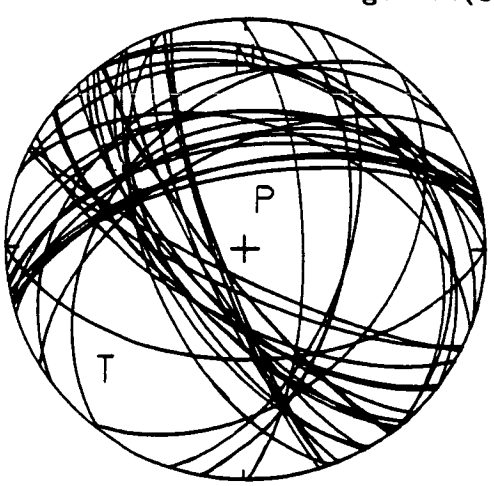

after Crampin & Booth 1985

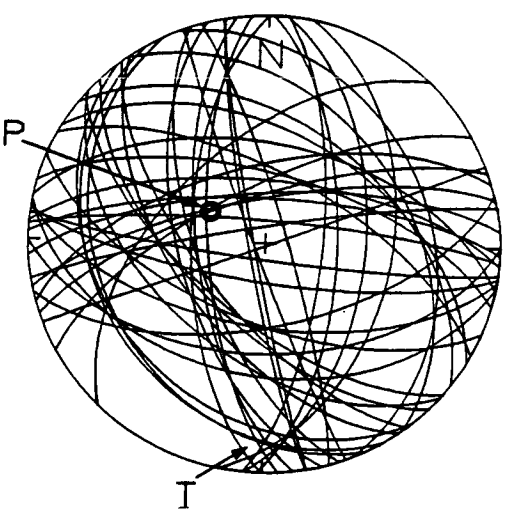

4.5(c) Mean polarization direction of leading split shear-waves (N100°E) and orthogonal minimum compression (max. tension).

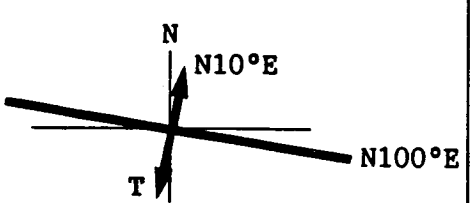

after Crampin & Booth 1985

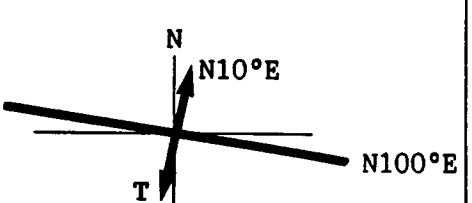

after Chen *et al.* 1987

Figure 4.5 Comparison of results of TDP2 (left) with those of TDP3 (right). Captions above individual figures.

presented in Figure 4.3 agrees closely with that derived by Crampin & Booth (1985), (see comparative Figure 4.5(b)), but is better constrained (Lovell *et al.* 1987). Additionally, it is orthogonal to and consistent with the observed polarizations of the leading split shear-waves whose average was found to be N100°E in all three TDP projects (Crampin & Booth 1985; Chen *et al.* 1987), Figure 4.5(c).

Shear-wave polarizations for only the nine best-constrained fault mechanisms in Fig. 4.3 are shown by Chen *et al.* (1987). However, *all* the fault mechanisms in Figure 4.3 deduced from the *P*-wave data will produce shear-wave polarizations which, after propagation through a distribution of aligned cracks, are consistent with those observed (Dr. D. C. Booth, personal communication, 1987).

4.4 Summary

Results presented in this chapter show that the tectonic regime in the Izmit area has changed little between the periods of operation of the TDP networks (Lovell *et al.* 1987). The pattern of faulting, the dominant stress directions and the shear-wave polarization directions found during TDP3 are consistent with the results of the previous projects. The present results reinforce the conclusions of Crampin & Booth (1985), Evans *et al.* (1985), and Crampin & Evans (1986) that tensional stress provides the driving mechanism for the North Anatolian Fault in this area, and that dominant tensional stress is expected both from the geometry of the movement of the Marmara Block and the tensional features observed at surface.

The Marmara Block (see Chapter 1), is a complex microplate or zone of accommodation located between the Eurasian/Black Sea Plate to the north and the Anatolian Plate to the south (Üçer *et al.* 1985; Evans *et al.* 1985; Crampin & Evans 1986). The position and tectonics of this block have been confirmed by the observations made during TDP3 (Lovell *et al.* 1987). East of the trifurcation point (see Chapter 1) the North Anatolian Fault is a conventional strike-slip fault whose seismicity pattern is characterised by large earthquakes with intervening periods of quiescence. Differing patterns outline the Marmara Block west of this trifurcation point. The northern limit of the Marmara Block is marked by the northern limb of a graben

structure passing westwards through the northern Marmara Sea, representing the pulling away of the Marmara Block from the Eurasia/Black Sea Plate. This line is characterised by continuous swarm activity (Üçer *et al.* 1985). The southern limb of the graben is characterised by a narrow zone of fluctuating swarm activity, such as that described in this thesis. The faulting shown by the pattern of seismicity in this structure represents the internal shearing of the Marmara Block as the southwestwards passage of the Anatolian Plate thrusts and rotates it against the bulge of Thrace on the Eurasian/Black Sea Plate. Dominant tension in this region has been demonstrated by Crampin & Booth (1985), and confirmed here and by Chen *et al.* (1987). The presence of tensional features such as normal faults at surface (Dewey & Şengör 1979) reinforces this deduction.

Swarms of earthquakes such as that described here have marked the epicentres of large earthquakes in the Marmara area in the past. The Izmit swarm area has not experienced a major earthquake for a very long time, and is clearly at risk. This 'seismic gap' evidence demonstrates clearly the fact that continuous and detailed monitoring in this area is of paramount importance in order to observe more closely the seismicity pattern, so that a clearer picture of the seismic hazard may be determined.

Chapter 5

Clustering in space and time

5.1 Introduction

This chapter will deal in some detail with new observations on the behaviour of the earthquake swarm described in the rest of this thesis, and will discuss some profitable lines of research which may increase our knowledge of the processes involved in earthquake genesis.

5.1.1 Earthquake Swarms

According to Richter (1958), earthquake swarms contain sequences of generally small-magnitude events with no large event predominating, and are usually small in areal extent. Swarms have been classified by Mogi (1967) into three types, depending on whether or not they were associated with large earthquakes. Thus, Type 1 swarms contain mainshock/aftershock sequences, Type 2 contain foreshock/mainshock/aftershocks, and Type 3 are not associated with any recognisable large event. In addition, Mogi suggests that Type 3 swarms are characteristic of areas with a highly fractured crust. The definition of Richter (1958) will be adopted here, and swarms recognised as sequences of events with no well-defined main shock.

Earthquake swarms of all types, including those which can be classified as Type 3 (Mogi 1967), have recently become intensively studied, especially for earthquake prediction purposes. They have been widely observed. For instance, they have been reported from the Jan Mayen area of the North Atlantic, Tashkent, and Matsushiro, Japan (Båth 1973), and Lee & Stewart (1981) present an exhaustive list detailing swarms from Japan, the USA, the USSR, China and elsewhere. Nearer home, swarms have been reported from the UK, for example, Glenalmond (Crampin *et al.* 1972), Kintail (Assumpção 1981), and elsewhere in Scotland (Davison 1924; Dollar 1949; Burton & Neilson 1979). Many more examples can be quoted. Some of these swarms have required the installation of a local network or the extension of an

existing one so that they may be better located and recorded.

The behaviour of the three types of earthquake swarms as defined by Mogi (1967) has been explained by Aki (1984) in terms of the properties of the fault surface upon which the earthquake occurs. It is suggested that strong 'patches' on the fault plane can act as either barriers or asperities, depending on the stress levels present and the homogeneity of the rocks. The occurrence of aftershocks after a mainshock (Type 1) can be explained by the breaking of barriers remaining after passage of the main shock. Alternatively, the stress surrounding a strong patch may be relieved by aseismic creep or foreshocks (Type 2), so that stress ultimately concentrates at a strong patch, an asperity, and is released as the main shock when the asperity is broken. Type 3 swarm activity is visualised as the gradual adjustment of the fault zone to concentrated stress by almost continuous, low-magnitude activity. In reality there is probably a complete gradation between the three types.

The relation between the positions of swarms and fault offsets in tensional or extensional areas along strike-slip faults has been pointed out by several authors, for example Sykes (1967), Weaver & Hill (1978) and Barka & Kadinsky-Cade (1988). In each case, swarm activity with or without volcanism could be related to changes in direction of the major fault, and gave rise to differing fault mechanisms. The position of the Izmit swarm in a tensional environment at the eastern end of the Marmara Block is entirely consistent with these observations.

Recent seismic observations have shown that individual faults can generate characteristic earthquakes, that is, earthquakes whose seismograms show a great deal of similarity. Depending on the size of the fault, the seismograms can be similar but varying along the fault, or as here, where the fault dimensions are relatively small, almost identical. The similarity in wave-form between successive earthquakes located in the same area has been described by Tsujiura in a series of papers (ending in Tsujiura 1983). Similar 'earthquake families' have also been identified in the USA (Ishida and Kanamori 1980; Geller and Mueller 1980). This property has been used to derive

the source dimensions, and it will be shown in this chapter that the waveforms of seismograms in the clusters are so similar, if not identical, that they have permitted Logan (1987) to suggest a few tens of metres (sometimes less) as source dimensions of events in this swarm.

5.1.2 Swarms in Anatolia

The swarm-like nature of much of the seismicity of western Anatolia was first described by Üçer *et al.* (1985), who identified the persistent swarm near Izmit which is the subject of this thesis, and who used the seismicity pattern to elucidate the local and regional tectonic regime. Two different kinds of swarm activity were described - continuous and fluctuating. The continuous swarms along the southern shore of the Marmara Sea have been associated with the epicentres of large earthquakes in the past (Üçer *et al.* 1985), and that adds weight to the argument that the Izmit area is a seismic gap (Toksöz *et al.* 1979 and Chapter 1) which can therefore expect a large earthquake in the future. It has been demonstrated in this thesis and elsewhere (Lovell *et al.* 1987) that the Izmit swarm has changed little in character or location for at least six years. The events have local magnitudes typically between about 0.1 and 1.5, with very few above the latter figure, and none exceeding $3.3 M_L$ in the present project (Chapter 3). This type of activity is therefore persistent, and has not been associated with a large earthquake. It remains to be seen whether the anticipated large event will occur within the Izmit swarm, or at least in the Izmit seismic gap (described in Chapter 1).

It has been noted previously that swarm activity is not random. Weaver & Hill (1978) and others have pointed out the association between swarms of activity and major strike-slip faults in tensional regimes, and it is interesting to compare the situations. However, most studies have been conducted on large magnitude earthquakes and using regional networks. Here it will be demonstrated that low-magnitude swarms not detectable by regional networks show the same phenomena, and that further study of such swarms may lead to a better understanding of the processes involved in faulting and earthquake generation.

5.2 Clustering in space

The data sets from all three TDP experiments were examined for clustering. S. B. Üçer and S. Crampin, in an unpublished study, found 15 clusters of varying size in the TDP2 data, and seven clusters were identified in the TDP1 data by the author. This present study has been confined to the more obvious and larger clusters within or very near to the TDP3 network so that confidence may be attached to their locations and good recordings will have been obtained. No doubt additional clusters could be identified from the present large data-set.

5.2.1 Observations

The event locations presented in Figure 2.2 (Chapter 2) showed marked clustering in space. The best-recorded and largest of these events were selected for fault-plane solution analysis; 87 events were chosen and fault-plane solutions for the best of these were discussed in Chapter 4. Here, Figure 5.1 shows these 87 earthquake epicentres and illustrative cross-sections. Time plots are shown in Figure 5.2. It can be seen that the events are located in a swarm in the vicinity of the network, and are confined almost entirely to depths of between seven and 12 km. Within the swarm, the events are seen to occur in well-defined clusters. Ten of the larger and better-located clusters are shown numbered 1 to 10 on Figure 5.1. Evans *et al.* (1985), in a study of the TDP2 data, presented composite fault-plane solutions for four clusters, A-D of their Figure 1. In the present study, these previously-observed clusters are again strongly represented. Although the earthquake epicentres are not coincident, the present fault-plane solutions are generally similar to the previous ones (Chapter 4 and Lovell *et al.* 1987), but show slightly different orientations. It is interesting to note from cross-section WW′ of Figure 5.1, that clusters 1 to 6 form a remarkably linear feature, trending approximately N60°E. This is not far removed from the regional trend of surface features (Evans *et al.* 1985) and may well mark the southern limit of the graben of the NAF.

The seismograms for events in each cluster were compared. In some cases, they showed no real similarity, suggesting that the events were not directly related and that their epicentral proximity was

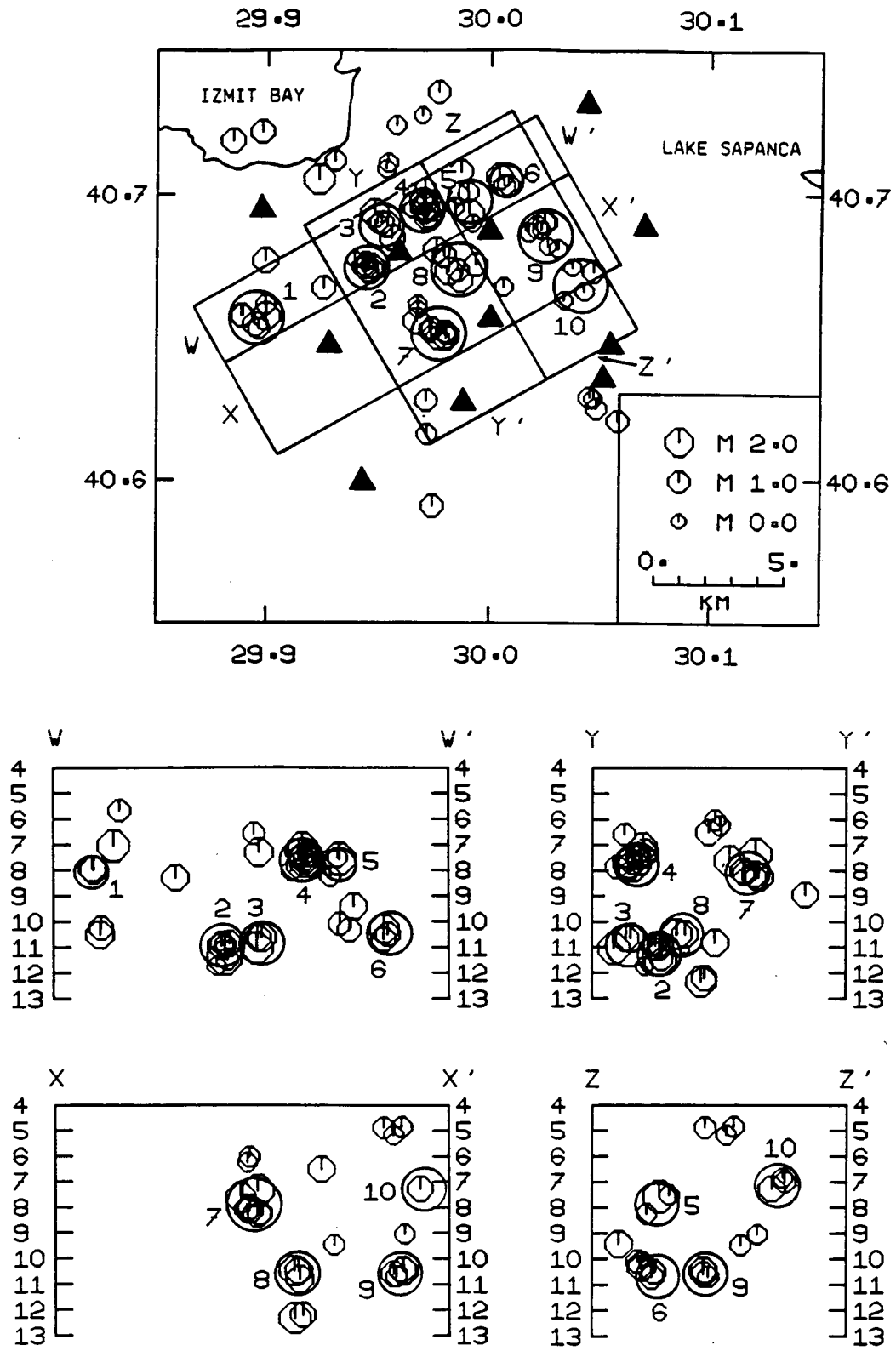

Figure 5.1 (after Lovell *et al.* 1987) Epicentre map and illustrative cross-sections for 87 events with at least six *P*-wave arrivals, showing clusters 1 to 10 (circled). Filled triangles represent TDP3 seismograph stations.

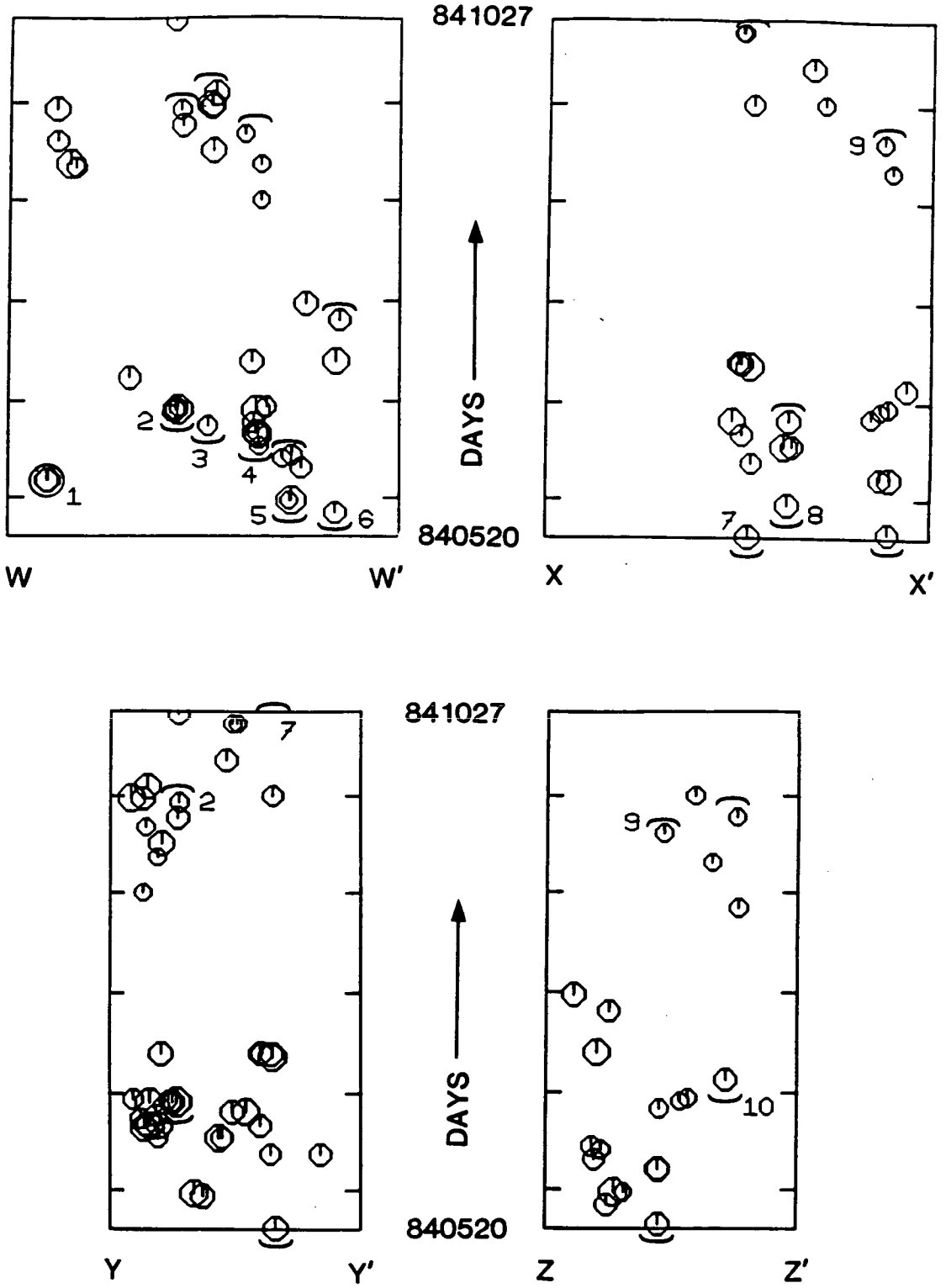

Figure 5.2 (after Lovell *et al.* 1987) Time plots, at the same horizontal scale, for the four cross-sections of Fig. 5.1. Start and finish dates are indicated, ticks denote start of a month. The short-lived clusters are circled, while the long-lived clusters are shown bracketed.

coincidental. In most clusters however, the seismograms showed a striking degree of similarity; some were true doublets. This would be expected for events occurring very close to each other, when the rays to the stations would follow almost identical paths. This similarity facilitated the comparison of seismograms and the derivation of fault-plane solutions for poorly-recorded events. In a few cases a difference of *P*-wave polarity at one station and a consequent slight change of orientation of the fault-plane solution indicated the sensitivity of the network to small changes of epicentre position and fault orientation.

The preceding points are best illustrated by cluster 7 (Figure 5.1). This cluster is well-located within the network, and

Table 5.1 Location data for earthquakes in cluster 7 of Fig. 5.1

Event no. in cluster	Date (y m d)	Time (h m s)	Lat. (°N)	Long. (°E)	Depth km	Magnitude M_L	Fault-plane soln. no. in Fig. 4.3
1′	840507	073928.19	40.651	29.990	8.94	0.2	
2′	840516	055017.79	40.655	29.967	8.65	0.3	
3′	840520	174849.79	40.650	29.980	8.26	1.1	1
4′	840530	052243.66	40.650	29.982	8.22	0.7	
5′	840608	093611.73	40.650	29.982	8.35	0.3	
6′	840609	162800.64	40.649	29.982	8.28	0.9	
7′	840611	172014.45	40.651	29.980	7.69	0.1	
8′	840612	145058.31	40.652	29.980	8.22	0.6	
9′	840618	050220.52	40.650	29.984	8.31	0.0	
10′	840621	010309.52	40.653	29.976	8.30	0.8	5
11′	840625	175332.10	40.655	29.967	7.62	1.4	8
12′	840712	164529.62	40.651	29.980	7.36	1.6	13
13′	840713	030202.18	40.650	29.976	8.13	0.9	14
14′	840627	023604.15	40.652	29.976	7.74	0.4	
15′	840627	034243.08	40.648	29.968	8.30	-0.2	
16′	840713	212331.43	40.652	29.973	8.11	0.7	15
17′	840713	214537.83	40.653	29.973	8.03	1.0	16
18′	840801	035234.34	40.651	29.973	8.39	1.3	
19′	840810	230446.13	40.648	29.975	6.57	0.1	
20′	840812	010613.96	40.650	29.974	7.08	0.6	
21′	840813	171730.81	40.648	29.979	8.43	0.8	
22′	840814	235705.82	40.653	29.974	7.19	0.5	
23′	840818	054854.51	40.654	29.975	7.66	0.6	
24′	840930	105515.95	40.648	29.988	7.61	-0.1	
25′	841001	031014.64	40.651	29.976	7.90	0.6	27
26′	841006	200142.41	40.652	29.975	7.66	0.0	
27′	841021	154513.90	40.653	29.973	8.23	0.4	

Table 5.2 Location data for earthquakes in cluster 1 of Fig. 5.1

Event no. in cluster	Date (y m d)	Time (h m s)	Lat. (°N)	Long. (°E)	Depth km	Magnitude M_L
1	840606	214825.24	40.657	29.889	8.00	1.0
2	840606	223149.48	40.658	29.888	7.94	0.9
3	840911	070540.84	40.661	29.899	5.68	0.4
4	840912	140012.38	40.657	29.899	7.05	1.6
5	840919	180030.31	40.653	29.896	10.25	0.6
6	840929	112301.24	40.654	29.895	10.52	1.1

Table 5.3 Location data for earthquakes in cluster 2 of Fig. 5.1

Event no. in cluster	Date (y m d)	Time (h m s)	Lat. (°N)	Long. (°E)	Depth km	Magnitude M_L
1	840627	173812.38	40.677	29.939	11.74	-0.1
2	840628	203214.60	40.674	29.945	11.44	1.9
3	840628	204507.22	40.675	29.944	10.89	0.5
4	840628	204850.79	40.675	29.944	10.95	1.1
5	840629	025517.73	40.676	29.944	10.94	0.3
6	840924	115201.92	40.674	29.947	10.88	0.9
7	840929	030031.80	40.674	29.947	11.48	0.4
8	841027	022858.88	40.673	29.944	10.97	0.7

Table 5.4 Location data for earthquakes in cluster 3 of Fig. 5.1

Event no. in cluster	Date (y m d)	Time (h m s)	Lat. (°N)	Long. (°E)	Depth km	Magnitude M_L
1	840623	171945.57	40.690	29.949	6.59	0.4
2	840916	131116.51	40.685	29.955	7.32	1.2
3	840930	094117.71	40.690	29.951	10.65	0.9
4	840930	230351.72	40.693	29.948	11.05	1.6
5	841004	021328.58	40.689	29.953	10.63	1.2

Table 5.5 Location data for earthquakes in cluster 4 of Fig. 5.1

Event no. in cluster	Date (y m d)	Time (h m s)	Lat. (°N)	Long. (°E)	Depth km	Magnitude M_L
1	840531	022852.81	40.680	29.976	10.49	1.4
2	840617	013523.89	40.694	29.973	7.77	0.2
3	840620	230902.46	40.697	29.970	7.71	1.4
4	840621	021613.58	40.697	29.970	7.58	0.5
5	840621	022519.46	40.696	29.971	7.56	1.4
6	840621	092113.18	40.693	29.972	7.09	1.2
7	840624	185946.78	40.693	29.970	7.49	0.6
8	840628	071746.25	40.695	29.970	7.82	1.6
9	840713	165527.22	40.692	29.971	7.29	0.9
10	840901	003715.05	40.698	29.970	7.51	0.0
11	840912	003324.80	40.694	29.973	7.32	0.1
12	840921	194451.61	40.695	29.965	8.04	0.1

Table 5.6 Location data for earthquakes in cluster 5 of Fig. 5.1

Event no. in cluster	Date (y m d)	Time (h m s)	Lat. (°N)	Long. (°E)	Depth km	Magnitude M_L
1	840531	131501.39	40.693	29.990	7.57	1.7
2	840531	132853.93	40.690	29.992	7.52	0.1
3	840610	185757.61	40.701	29.990	10.33	0.6
4	840613	215738.26	40.695	29.984	8.24	0.2
5	840614	214807.86	40.700	29.986	10.10	0.5
6	840731	094407.90	40.708	29.987	9.42	1.0

Table 5.7 Location data for earthquakes in cluster 6 of Fig. 5.1

Event no. in cluster	Date (y m d)	Time (h m s)	Lat. (°N)	Long. (°E)	Depth km	Magnitude M_L
1	840527	190818.99	40.703	30.006	10.70	0.7
2	840713	215304.64	40.706	30.004	10.29	1.3
3	840726	045942.93	40.703	30.008	10.50	0.7

Table 5.8 Location data for earthquakes in cluster 8 of Fig. 5.1

Event no. in cluster	Date (y m d)	Time (h m s)	Lat. (°N)	Long. (°E)	Depth km	Magnitude M_L
1	840530	102050.93	40.679	29.979	10.49	1.0
2	840531	022852.81	40.680	29.976	10.49	1.4
3	840617	110548.58	40.673	29.981	12.34	1.5
4	840617	170556.52	40.673	29.985	12.21	0.8
5	840625	154229.59	40.670	29.986	10.82	1.0
6	841012	150726.66	40.675	29.993	6.51	0.9

Table 5.9 Location data for earthquakes in cluster 9 of Fig. 5.1

Event no. in cluster	Date (y m d)	Time (h m s)	Lat. (°N)	Long. (°E)	Depth km	Magnitude M_L
1	840521	195722.99	40.690	30.024	10.42	0.9
2	840607	185457.39	40.688	30.021	10.60	0.8
3	840607	190334.64	40.690	30.025	10.48	1.1
4	840626	001143.44	40.687	30.017	4.88	0.3
5	840628	215029.36	40.682	30.026	5.17	0.1
6	840629	225135.26	40.681	30.031	4.85	0.2
7	840919	202625.71	40.688	30.023	10.69	0.2

Table 5.10 Location data for earthquakes in cluster 10 of Fig. 5.1

Event no. in cluster	Date (y m d)	Time (h m s)	Lat. (°N)	Long. (°E)	Depth km	Magnitude M_L
1	840705	004823.33	40.673	30.047	7.27	0.8
2	840827	112914.38	40.666	30.043	6.99	0.3
3	840910	165953.67	40.674	30.037	9.04	0.1
4	840924	232932.29	40.663	30.034	6.84	0.1

persistent, with over 20 events occurring within a very small volume. Additionally, nine events gave reliable fault-plane solutions, which are presented, together with location data for the cluster in, respectively, Figure 5.3 and Table 5.1. Seismograms recorded at the same station (TE, Fig. 1.11) for the nine events in the three sub-groups of cluster 7 are shown in Figure 5.4. Location details for nine other clusters in the swarm are presented in Tables 5.2 to 5.10, and remarks about cluster 7 apply equally well to these other clusters.

From cross-sections XX′ and YY′ of Figure 5.1 and the location data presented in Table 5.1, it can be seen that cluster 7 contains a sequence of events which occur at almost identical depths and locations. These events can be considered almost coincident even allowing for the possible systematic errors of up to 2 km in locations determined using HYPO71 (Lee & Lahr 1975) when the true regional structure is anisotropic (Doyle *et al.* 1982, see also Chapter 2). This suggests that the events are the result of movement on very small asperities or fault facets, areas perhaps of the order of a few tens of m^2. As would be expected, the closest similarities in seismograms are observed between those events having the closest epicentres. Thus great similarity occurs between three sub-groups of cluster 7, consisting of events 1′ to 10′, 11′ to 13′, and 14′ to 25′ (event numbers with ticks refer to events in Table 5.1, which has been subdivided to illustrate the sub-groups). Events 26′ and 27′ show a greater variation, and are only indirectly related to the rest of the sub-groups. Seismograms for events 3′ and 8′, and for events 16′ and 17′ (Figure 5.4) are almost identical except for amplitude, and there is a close similarity in character between all seismograms in this cluster.

The fault-plane solutions (Figure 5.3) for the events within the three sub-groups of cluster 7 show the expected similarities, but with slight variation in orientation and differences in *P*-wave polarity near nodal lines, for example, between events 11′, 12′ and 13′, especially where noise levels were high, making positive identification of *P*-wave polarities difficult (Chapter 4). The overall similarity between the fault-plane solutions of events in cluster 7 reveals that the nature and orientation of the faulting

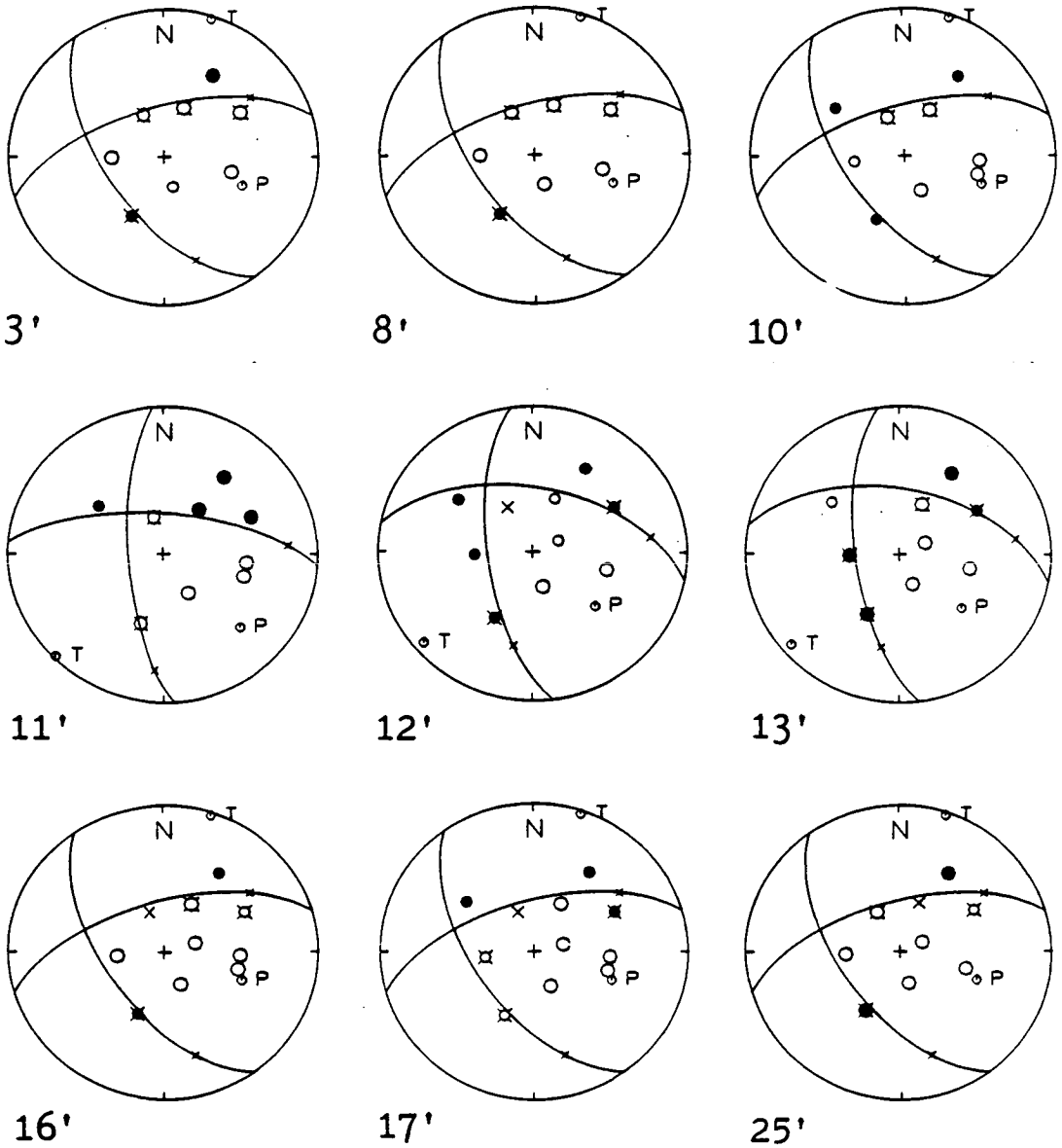

Figure 5.3 (after Lovell *et al.* 1987) Fault-plane solutions for 9 well-recorded events in cluster 7 numbered as in Table 5.1. Notation is as in Figure 4.3, but note the different event numbering.

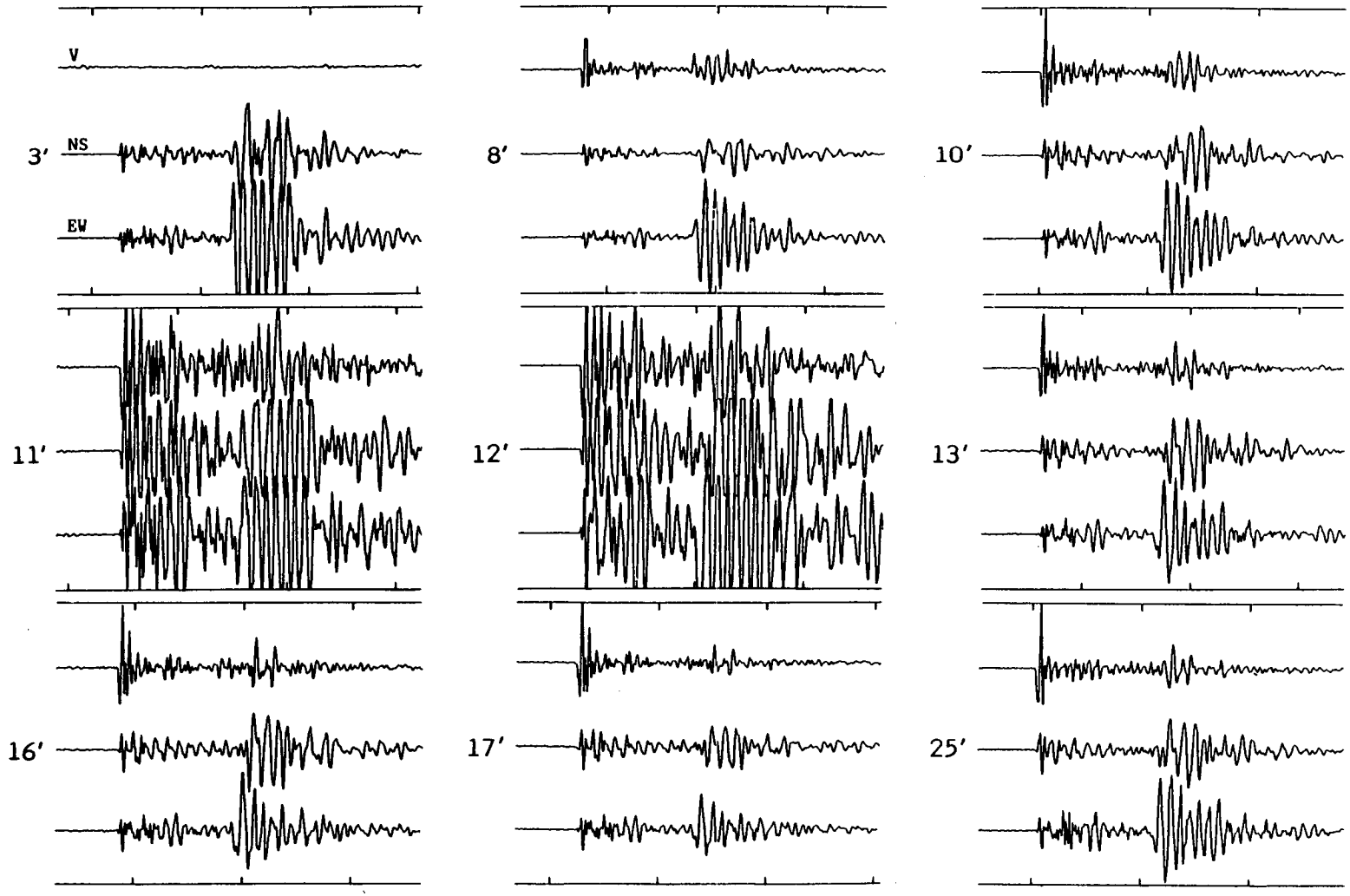

Figure 5.4 (after Lovell *et al.* 1987) Three-component seismograms, recorded at the same station (TE, Fig. 1.11) for the nine events in cluster 7 whose fault-plane solutions are presented in Figure 5.3.

varies little with position in the group. Additionally, as the close cluster of events occurs over a time span of about 5 months, movement on certain facets of fault planes or asperities may take place over considerable periods and is similar in nature throughout this period. This will be discussed in section 5.3.

5.3 Clustering in time

It has been shown in previous chapters that the nature of the swarm activity in this area has been consistent in location, magnitude, and character of faulting for at least six years, and during that time, clustering within the swarm has been observed (Lovell *et al.* 1987). This section will discuss the temporal clustering, not previously observed, and attempt to draw conclusions consistent with the data set which, as discussed previously, represents only a fraction of the time-span of the swarm.

5.3.1 Observations

Figure 5.5 contains histograms showing the overall seismicity level during the TDP3 experiment, together with those showing the activity of three selected clusters from Figure 5.1. Although the overall level of seismicity has decreased recently (S. B. Üçer, personal communication), the general pattern remains similar to that for previous experiments (Chapters 2 & 3, and Lovell *et al.* 1987). Sporadic peaks of activity are superimposed on a generally low background level of activity of a few events per day. The peaks correspond in most cases to outbursts from the more active clusters, for example cluster 1, which briefly shows a level of about 30 events per day (Figure 5.5).

Two distinct types of cluster activity are indicated by the activity histograms in Figure 5.5 (Lovell *et al.* 1987). The first type exhibits short bursts of intense activity of up to 30 events per day for just a few days, as in cluster 1. The magnitudes of these events are quite similar (Table 5.2, which gives details only of the better-recorded events in this cluster) and no clearly-defined main shock can be detected. Such clusters then appear to cease activity abruptly without reactivation, at least over the period of

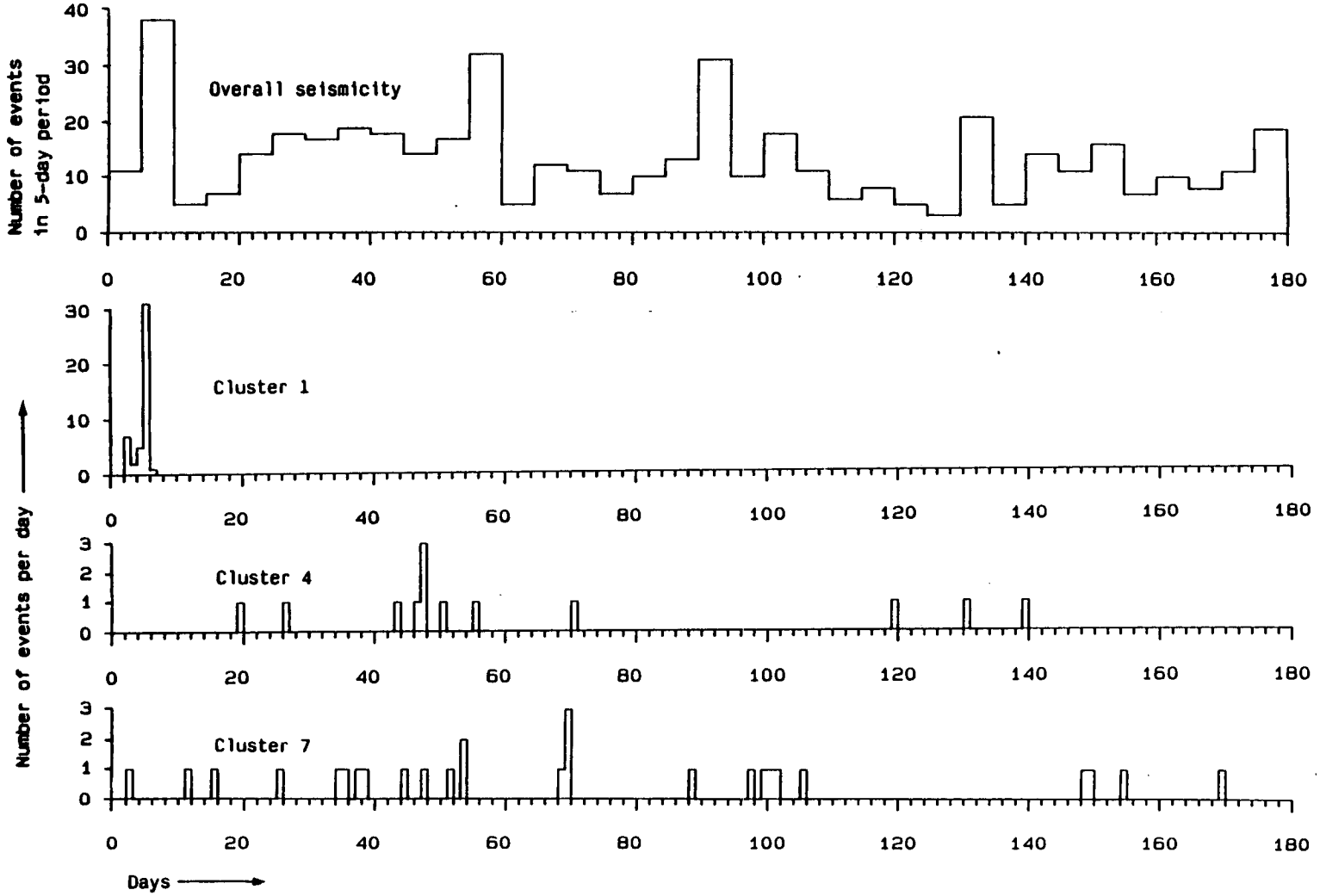

Figure 5.5 (after Lovell *et al.* 1987) Histograms showing overall seismicity during TDP3 and the activity of selected clusters. For the overall seismicity histogram, the number of events in a 5-day period is plotted against that interval, while for the cluster activity histograms the number of events per day is plotted against days. Note that the ordinates are plotted at different scales.

observation. The second type, such as clusters 4 and 7 (Tables 5.5 and 5.1), shows a lower level of just one event every few days or so, but continue in some cases for the whole experimental period. A small change in the seismograms with time can be detected in these clusters, suggesting that activity is migrating very slowly along a fault, that the orientation of the fault is changing slightly, or, as suggested by Chen *et al.* (1987), that the geometry of the microcrack structure changes with time.

Three recording stations (SE, TE and AY, Table 1.1 of Chapter 1) were common to each of the three TDP experiments. An attempt to link the three experiments in time was made initially by comparing seismograms of the clusters in Figure 5.1 with those of the clusters from TDP2 whose epicentres plotted close to the present clusters. The search was extended to a radius of at least 1 km to allow for possible systematic errors in locations due to the slightly different network configurations. A similar comparison between the TDP2 and TDP1 data sets was also made. Apart from a few similarities at stations having characteristic seismograms and other similarities especially in the *P*-waves, in no case were clusters traceable between the three data sets (Lovell *et al.* 1987). It therefore appears that clusters may remain active for several months, but that once activity in one cluster ceases reactivation does not take place.

5.4 Discussion

The properties exhibited by cluster 7 are shown to a greater or lesser extent by all of the clusters in Figure 5.1 and those found in previous experiments (Lovell *et al.* 1987). Although some clusters consist of only a few events, each cluster contains at least two earthquakes whose seismograms are almost identical (doublets) or which show great similarity and whose epicentres are very close. In some cases the activity of the cluster spans only a day or two, but it can occur over a much longer period - up to five months in the present study (Figure 5.2). It is noticeable that sequences of near-identical events usually tend to be spaced over a period of a few days, for example, cluster 1 (Figure 5.5). This suggests that these short bursts of activity represent movement on asperities which either become locked in some way or the particular fault-plane facet

of the asperity becomes eroded, so that subsequent fault movement migrates, possibly to another facet of the same asperity. In cases where a cluster contains sub-groups, the fault-plane solutions for each sub-group are similar but not identical, suggesting that the fault mechanism or orientation varies little with time throughout the cluster. The seismograms for events in the more long-lived clusters may show a slight change with time, suggesting a change in fault orientation, a migration of the epicentres (which is not detectable in the HYPO71 locations), or a change in the crack structure within the rock mass (Chen *et al.* 1987)

In general, very close similarities between seismograms were observed only for short-lived clusters of earthquakes. Although a similarity in general character exists between events which are more widely-spaced in time they do not have identical mechanisms but are very closely related, and probably result from movement on facets of the same asperity. Additionally, as the joint epicentre relocation method has an accuracy of the order of a hundred metres, clusters identified by HYPO71 locations may well show subdivision and therefore more similarity between seismograms on further analysis. It is suggested therefore that seismic activity on the small individual fault planes or asperity facets on which these clusters of events occur is short-lived and exists for periods of the order of weeks or at most a few months (Lovell *et al.* 1987).

Theoretical studies (for example by Aki, 1979 and Israel and Nur, 1979) suggest that stress concentrates along a fault at barriers and asperities. Clusters, or families, of earthquakes with identical or near-identical seismograms (doublets) have been described from Japan (Tsujiura 1983), the USA (Ishida and Kanamori 1980; Geller and Mueller 1980) and elsewhere. Regional networks with station separations typically of 30-100 km have been used, and the events studied have been of greater magnitude than those described here. Clusters of all types have been linked to foreshock and aftershock activity and earthquake prediction, and it seems clear that long-term monitoring is necessary to reveal the relationship between clustering and stress change.

Logan (1987), in an independent study of some of these clusters using a joint epicentral relocation method, reports that the relocated epicentres appear to plot on northward- and southward-dipping planes which strike approximately east-west. Even using this method, however, there was still some doubt, as several clusters were not resolved satisfactorily. It seems reasonable to expect these planes to be fault planes, and they are consistent with individual and composite fault-plane solutions produced for those clusters (see Chapter 4), although as those fault-plane solutions are not well-constrained they are not presented either in Figures 5.3 or 4.3. Additionally, Logan reports that the relocation method has an accuracy of 20 to 30 metres (sometimes less) in this case, and it has been able to subdivide clusters into small sub-groups far more accurately than is possible using purely visual comparison of seismograms.

The results of the study into the clustering phenomenon exhibited by the Izmit microearthquake swarm illustrate the complexity of the movement of the North Anatolian Fault in this region and have revealed something of the fundamental properties of earthquake source regions. It is clear that further, intensive monitoring is required to show up any long-term trends, and that the joint epicentral relocation method is appropriate for further analysis of these clusters. Routine use of such techniques will permit very accurate resolution of the epicentres of cluster activity, and should thus reveal the pattern of this activity in minute detail. Further studies of clusters of all types must ultimately reveal the relationship between clustering and stress change, and improve our understanding of the genesis of earthquakes.

Chapter 6

Summary and suggestions for further study

6.1 Summary

This thesis has dealt in some detail with the historical, geographical and seismotectonic setting within which the three Turkish Dilatancy Projects were carried out. In each project, there has been very close cooperation between staff of the British Geological Survey, Edinburgh, and their colleagues at Kandilli Observatory, Istanbul. This culminated in the third project, TDP3, in which at least ten BGS scientific staff and 5 Turkish counterparts, together with support and technical staff at Kandilli, enjoyed a lengthy period of cooperation. The author is glad to have been associated with the final project and the subsequent data analysis, and has already acknowledged the sources of the help which was so freely given throughout.

The original purpose of the TDP experiments was to investigate the properties of a small swarm of earthquakes located by MARNET in the Izmit seismic gap, and to use the direct shear-waves from this swarm as a natural data set for studies of their properties and for the development of a method of earthquake prediction. The projects have been highly successful. The studies have revealed much of the complex behaviour of shear-waves, enabling succeeding projects to be designed accordingly. They have led to what is thought to be a deterministic method of earthquake prediction and have stimulated a large amount of shear-wave research world-wide, with potential economic importance. They have also revealed much about the complex behaviour in the source regions of the microearthquakes.

The historical and seismotectonic background to the TDP experiments and the full details of the final TDP3 project were described in Chapter 1. The routine analysis of the earthquakes in the swarm, producing locations, magnitudes and fault-plane solutions,

was the subject of Chapters 2 to 4. Studies of the clustering phenomena observed in the Izmit swarm were described in Chapter 5. These results are entirely new, as it is probably the first time that such a low-magnitude earthquake swarm has been so intensively studied with three-component instruments. This may lead to a better understanding of the processes involved in the source regions of small earthquakes, and perhaps, by extension, of those in the source regions of large earthquakes.

The three projects have demonstrated clearly the evolution of the scientific techniques as new discoveries were made and incorporated into the operation of the seismograph networks. In particular, the effect of the free surface on shear-waves was discovered, investigated and incorporated into the operation of the networks which were tailored to take account of the shear-wave window. These shear-wave studies have also led to the hypothesis of EDA (see below). In addition, field and analytical techniques have been refined, and an automatic, digital, event-triggered recording system has been developed and proved in use.

6.1.1 Results of TDP3

The high resolution obtained in the TDP3 project by the use of more three-component instruments than used previously and a more closely-spaced network situated directly above the swarm has enabled the results from the earlier projects to be confirmed and refined (Lovell *et al.* 1987).

The activity of this microearthquake swarm, first located by MARNET, has persisted for at least six years, although there has been some fluctuation of activity at various points within the swarm, and, perhaps, differences in the level of activity from year to year. A comparison of the results from all the TDP experiments has shown that the locations and magnitudes of events in the swarm have changed little during the time in which observations have been carried out (Lovell *et al.* 1987), although it is realised that the durations of observation over the swarm are small in comparison to the lifetime of the swarm.

The principal directions of stress determined in 1979, 1980 and 1984 are almost identical (Lovell *et al.* 1987). Chen *et al.* (1987) report that the mean polarization direction of the leading split shear-waves during TDP3 was N100°E, as it was in TDP1 and TDP2 (Crampin & Booth 1985), and this is in good agreement with stress directions derived independently from the fault-plane solutions. The fault-plane solutions show that the faulting continues to be predominantly normal, but with some strike slip and a few thrust mechanisms, and strikes suggested for the fault-planes are consistent both with previous observations and with those suggested by Logan (1987). This confirms the stress patterns around the Marmara Block suggested by Evans *et al.* (1985) and Crampin & Evans (1986). Temporal variations of delays between split shear-waves recorded during the projects have been reported by Chen *et al.* (1987). These are differential changes of at most about two milliseconds per kilometre of raypath and have major significance as sensitive indicators of the stress behaviour within the fault region, but do not give rise to noticeable effects on locations or fault mechanisms.

The clustering in space and time of events in this swarm has revealed that the pattern of faulting in this area is highly complex, as it has been demonstrated that the Izmit swarm can be considered as many small clusters. It has been possible to suggest time constraints of between a few days and several months for the lifetimes of the asperities or fault-plane facets thought to be responsible for the two types of clustering observed (Lovell *et al.* 1987). It is clear that long-term monitoring will reveal more of the complicated pattern of activity in the earthquake source regions.

6.1.2 Earthquake prediction

In addition to the refinement of previous results and the suggestion of new insight into the complex pattern of faulting discussed above, the Turkish Dilatancy Projects have given an opportunity for the development of the hypothesis of EDA (Crampin 1984; Crampin *et al.* 1984), and the postulation of a scientific and workable method of earthquake prediction (Crampin 1987b). EDA-cracks are thought to be responsible for the shear-wave splitting which has been reported from many areas of the world and from many different

tectonic regimes. It is now recognised that they are ubiquitous in at least the upper 10 to 20 km of the earth's crust (Crampin 1987a).

The suggested earthquake prediction method, although at an early stage, shows great promise. Variations in the delays between split shear-waves caused by morphology changes of stress-influenced EDA-cracks, upon which the method depends, have already been reported from Turkey (Chen *et al.* 1987), and the USA (Peacock *et al.* 1988; Booth *et al.* 1989). The most positive proof has been reported by Crampin *et al.* (1989), who demonstrate that cracks, influenced by stress before an earthquake, returned to their pre-earthquake configuration after the build-up of stress was relieved by the 1986 North Palm Springs earthquake, in California. The potential of the earthquake prediction method is now indisputable, but it remains to be seen whether sufficient funds will be forthcoming for its practicality to be demonstrated.

6.1.3 Further applications of shear-wave research

In addition to the earthquake prediction method and the world-wide recognition of EDA, another important consequence of the ODA-financed TDP experiments has been the recognition that such parameters of the EDA-cracks as their orientation, aspect ratio and their density (number per unit volume) can be deduced from the analysis of shear-waves (particularly those generated by vertical seismic profiling techniques) propagating through them (Crampin 1987a). The economic importance of this has now been realised, particularly by the oil industry, who are at present engaged in increasing amounts of shear-wave research because of its potential to predict the internal structure of hydrocarbon reservoirs remote from the well, and to optimise subsequent extraction. Other important areas of application include the geothermal industry, where efficiency increases can be made by predictions of the fracture orientations which influence fluid flow. There are many more applications in the geological field, such as monitoring rock bursts in mines and the prediction of the properties of potential burial-sites for radioactive waste. The many applications of such research have been reviewed by Crampin (1987a), and doubtless many more will be found in the future.

6.2 Suggestions for further study

As suggested in Chapter 1, there is a need for a comprehensive geological, geophysical and geodetic survey of the Marmara region, with particular emphasis on structure, neotectonic studies and geophysical measurements such as heat flow, which would enable an overall synthesis of the region to be attempted. Such a study of this comparatively poorly-investigated area would not only further our knowledge of the area, but would also enable meaningful comparisons to be made between it and similar, better-studied areas elsewhere. In particular, comparative studies of the Izmit earthquake swarm and others identified elsewhere by MARNET as coinciding with the locations of large earthquakes in the Marmara region, might reveal any similarities or differences which would enhance our understanding of the seismic gap in this area. A long-term and rigorous investigation of the relation between the large events (around 3.0 or 3.5 M_L) occurring in the swarm area would enable their relationship to the swarm to be determined. All such studies would require an investment of finance and resources, and it remains to be seen whether these will be forthcoming.

An improvement of the crustal model is required, although so far the simple isotropic, two-layered model used for all the TDP earthquake locations has proved adequate. However, the more detailed studies of the anisotropy of the crust in the area now being undertaken need a more refined model. Once again this requires investment.

Further studies of the clustering phenomenon observed in the Izmit swarm and elsewhere may contribute to a better understanding of the processes involved, and the movements occurring, in the source regions of large and small earthquakes. The purely visual method of comparing seismograms described here is inadequate for the detailed discrimination of similar events in a cluster, and the relative epicentral relocation method used by Logan (1987) should be used. This has given good results, as described in Chapter 5, and could probably be automated to a certain extent. This method should enable clusters to be split up into their component sub-groups, as it is clear from the discussion in Chapter 5 that the Izmit swarm consists

of many clusters, each of which can be sub-divided into smaller but related clusters. The pattern of movement on these small fault-planes is clearly very complicated, perhaps even more complex than movement in the source regions of large earthquakes. This relocation method is therefore an interesting and potentially critical topic for further research, and would increase our understanding of the fundamental properties of the source regions of earthquakes.

Research into shear-wave and reservoir properties continues, but the earthquake prediction method has yet to be demonstrated to government and the public in a way which will ensure adequate funding (by successfully predicting a large earthquake and minimizing consequent loss of life). Recent earthquakes involving large numbers of civilian casualties may provide the stimulus, as earthquake prediction programmes have, in the past, been stimulated by large earthquakes.

References

Aki, K., 1979. Characterization of barriers on an earthquake fault. *J. Geophys. Res.*, **84**, 6140-6148.

Aki, K., 1984. Asperities, barriers, characteristic earthquakes and strong motion prediction, *J. Geophys. Res.*, **89**, 5867-5872.

Aki, K. & Richards, P., 1980. *Quantitative Seismology; Theory and Methods*, (2 vols), W. H. Freeman, San Francisco.

Allen, C. R., 1975. Geological criteria for evaluating seismicity, *Bull. Geol. Soc. Am.*, **86**, 1041-1057.

Allen, C. R., Amand, P. S., Richter, C. F. & Nordquist, J. M., 1965. Relationship between seismicity and geologic structure in the southern California region. *Bull. Seism. Soc. Am.*, **55**, 753-798.

Ambraseys, N. N., 1970. Some characteristic features of the Anatolian fault zone, *Tectonophys.*, **9**, 143-165.

Ambraseys, N. N. & Zatopek, A., 1969. The Mudurnu Valley, West Anatolia, Turkey, earthquake of 22 July 1967, *Bull. seism. Soc. Am.*, **59**, 521-589.

Ando, M., 1975. Possibility of a major earthquake in the Tokai district, Japan and its pre-estimated seismotectonic effects, *Tectonophys.*, **25**, 69-85.

Assumpção, M., 1981. The NW Scotland earthquake swarm of 1974, *Geophys. J. R. astr. Soc.*, **67**, 577-586.

Bakun, W. H. & Lindh, A. G., 1985. The Parkfield, California, Earthquake Prediction Experiment, *Science*, **229**, **(4714)**, 619-624.

Barka, A. A. & Kadinsky-Cade, K., 1988. Strike-slip fault geometry in Turkey and its influence on earthquake activity, *Tectonics*, **7**, 663-684.

Båth, M., 1973. *Introduction to Seismology*, Birkhäuser Verlag, Basel & Stuttgart.

Båth, M., 1981. Earthquake Magnitude - Recent Research and Current Trends, *Earth Sci. Rev.*, **17**, 315-398.

Beamish, D., 1982. A geomagnetic precursor to the 1979 Carlisle earthquake, *Geophys. J. R. astr. Soc.*, **68**, 531-543.

Beamish, D. & Riddick, J. C., 1985a. TDP3 I. Background to the project, *GRG Report 85/21, British Geological Survey.*

Beamish, D. & Riddick, J. C., 1985b. TDP3 II. Magnetotelluric array instrumentation, *GRG Report 85/22, British Geological Survey.*

Booth, D. C., Crampin, S., Evans, R. & Roberts, G., 1985. Shear-wave

polarizations near the North Anatolian Fault - I. Evidence for anisotropy-induced shear-wave splitting, *Geophys. J. R. astr. Soc.*, **83**, 61-73.

Booth D. C., Crampin, S., Lovell, J. H. & Chiu, J-M., 1989. Temporal changes in shear-wave splitting during an earthquake swarm in Arkansas. *J. Geophys. Res.*, (submitted).

Bott, M. H. P., 1959. The Mechanics of Oblique Slip Faulting, *Geol. Mag.*, **XCV1:2**, 109-117.

Brinkmann, R., 1976. *Geology of Turkey*, Elsevier, Amsterdam, Oxford & New York.

Browitt, C. W. A., Turbitt, T. & Morgan, S. N., 1985. Investigation of British earthquakes using the national monitoring network of the British Geological Survey, in *Earthquake Engineering in Britain*, 33-47, Thomas Telford, London.

Brune, J. N. & Allen, C. R., 1967. A microearthquake survey of the San Andreas fault system in southern California, *Bull. Seism. Soc. Am.*, **57**, 277-296.

Bufe, C. G., 1970. Frequency-magnitude variations during the 1970 Danville earthquake swarm, *Earthquake Notes*, **41**, 3-7.

Burke, K. & Şengör, A. M. C., 1986. Tectonic escape in the evolution of the continental crust, *in* Barazangi, M. & Brown, L. D., eds., Reflection seismology: the Continental Crust, *Amer. Geophys. U. Geodyn. Ser.*, **14**, 41-53.

Burton, P., 1979. Seismic risk in southern Europe through to India examined using Gumbel's third distribution of extreme values, *Geophys. J. R. astr. Soc.*, **59**, 249-280.

Burton, P. & Neilson, G., 1979. Earthquake swarms in Scotland, *Forth Naturalist and Historian*, **4**, 3-26.

Burton, P., McGonigle, R. W., Makropoulos, K. C. & Üçer, S. B., 1984. Seismic risk in Turkey, the Aegean and the eastern Mediterranean: the occurrence of large magnitude earthquakes, *Geophys. J. R. astr. Soc.*, **78:2**, 475-506.

Chen, T-C., Booth, D. C. & Crampin, S., 1987. Shear-wave polarizations near the North Anatolian Fault - III. Observations of temporal changes, *Geophys J. R. astr. Soc.*, **91**, 287-311.

Cooke, P. A. V., Maguire, P. K. H., Laffoley, N. d'A. & Evans, J. R. 1988. Implications of the distribution of seismicity near Lake Bogoria in the Kenyan Rift, *Geophys. J.*, (submitted).

Crampin, S., 1978. Seismic-wave propagation through a cracked solid: polarization as a possible dilatancy diagnostic, *Geophys. J. R. astr. Soc.*, **53**, 467-496.

Crampin, S., 1984. Effective elastic constants for wave propagation in anisotropic media, in *Proc. First Int. Workshop on Seismic Anisotropy, Suzdal, 1982*, Eds S. Crampin, R. G. Hipkin and E. M. Chesnokov, *Geophys. J. R. astr. Soc.*, **76**, 17-28.

Crampin, S., 1987a. Geological and industrial implications of extensive-dilatancy anisotropy, *Nature*, **328**, 491-496.

Crampin, S., 1987b. The basis for earthquake prediction, in *Proc. Second Int. Workshop on Seismic Anisotropy, Moscow, 1985*, eds D. C. Booth, S. Crampin and E. M. Chesnokov, *Geophys. J. R. astr. Soc.*, **91**, 331-347.

Crampin, S. & Booth, D.C., 1985. Shear-wave polarizations near the North Anatolian Fault- II.Interpretation in terms of crack-induced anisotropy, *Geophys. J. R. astr. Soc.*, **83**, 75-92.

Crampin, S. & Evans, R., 1986. Neotectonics of the Marmara Sea region in Turkey, *J. Geol. Soc.*, **143**, 343-348.

Crampin, S. & Üçer, S. B., 1975. The seismicity of the Marmara Sea region of Turkey, *Geophys. J. R. astr. Soc.*, **40**, 269-288.

Crampin, S., Evans, R. & Atkinson, B. K., 1984. Earthquake prediction: a new physical basis, in *Proc. First Int. Workshop on Seismic Anisotropy, Suzdal, 1982*, Eds S. Crampin, R. G. Hipkin and E. M. Chesnokov, *Geophys. J. R. astr. Soc.*, **76**, 147-156.

Crampin, S., Booth, D. C., Evans, R., Peacock, S. & Fletcher, J. B., 1989. Shear-wave splitting: a possible key to earthquake prediction? *J. Geophys. Res.*, (submitted).

Crampin, S., Evans, R., & Üçer, S. B., 1985. Analysis of records of local earthquakes: the Turkish Dilatancy Projects (TDP1 and TDP2), *Geophys. J. R. astr. Soc.*, **83**, 1-16.

Crampin, S., Jacob, A. W. B., Miller, A. & Neilson, G., 1970. The LOWNET radio-linked seismometer network in Scotland, *Geophys. J. R. astr. Soc.*, **21**, 207-216.

Crampin, S., Jacob, A. W. B. & Neilson, G., 1972. The Glenalmond Earthquake Series, February 1970-March 1972, *Nature*, **240**, 233-236.

Davison, C., 1924. *A History of British Earthquakes*, 466pp,

Cambridge University Press.

Dewey, J. W., 1976. Seismicity of Northern Anatolia, *Bull. seism. Soc. Am.*, **66**, 843-868.

Dewey, J. W. & Şengör, A. M. C., 1979. Aegean and surrounding regions: complex multiplate and continuum tectonics in a convergent zone, *Geol. Soc. Am. Bull.*, **90**, 84-92.

Dewey, J. W., Pitman, W. C., Ryan, W. B. F. & Bonnin, J., 1973. Plate tectonics and the evolution of the Alpine system, *Geol. Soc. Amer. Bull.*, **84**, 3137-3180.

Dollar, A. T. J., 1949. Catalogue of Scottish earthquakes of 1916-1949, *Trans. Geol. Soc. Glasgow*, **21**, 283-361.

Doyle, M., McGonigle, R. & Crampin, S., 1982. The effects of crack anisotropy on the hypocentral locations of local earthquakes, *Geophys. J. R. astr. Soc.*, **69**, 137-157.

Doyle, M., Crampin, S., McGonigle, R. & Evans, R., 1985. Joint-inversion of arrival times in a region of dilatancy anisotropy, *Pure & Appl. Geophys.*, **123**, 375-387.

Eaton, J. P., O'Neill, M. E. & Murdock, J. N., 1970. Aftershocks of the 1966 Parkfield-Cholame, California, earthquake: a detailed study. *Bull. Seism. Soc. Am.*, **60**, 1151-1197.

Evans, J. R., 1980. ADC: a program for digitising seismic records into a format suitable for automatic processing, *Brit. Geol. Surv. Glob. Seismol. Rep. No 136.*

Evans, R., 1984. Effects of the free surface on shear wavetrains, *Geophys. J. R. astr. Soc.*, **76**, 165-172.

Evans, J. R., 1986a. A user's guide to ADC and NETFIL, computer programs for use in digitising Geostore tapes, *British Geological Survey Global Seismology Research Group Reports*, in preparation.

Evans, J. R., 1986b. PICK: an interactive program for identifying the arrival times of seismic phases, *British Geological Survey Global Seismology Research Group Reports*, in preparation.

Evans, R., 1989. The effects of the earth's free surface on shear waveforms: observations using a seismometer array, (abs.), JAG meeting on EDA: predicting earthquakes using shear-waves, *Geol. Soc. Newsletter*, **18(2)**, p 26.

Evans, J. R. & Miller, A., 1986. An interface unit for digitisation of geostore tapes, *Brit. Geol. Surv. Glob. Seis. Rep. No.* 278.

Evans, R., Asudeh, I., Crampin, S. & Üçer, S. B., 1985. Tectonics of

the Marmara Sea region of Turkey: new evidence from micro-earthquake fault plane solutions, *Geophys. J. R. astr. Soc.*, **83**, 47-60.

Evans, R., Beamish, D., Crampin, S. & Ucer, S. B., 1987. The Turkish Dilatancy Project (TDP3): multidisciplinary studies of a potential earthquake source region, *Geophys. J. R. astr. Soc.*, **91**, 265-286.

Fedotov, S. A., 1965. On regularities in distribution of strong earthquakes of Kamchatka, Kurile Islands and northeastern Japan. *Tr. Inst. Fiz. Zemli, Akad. Nauk SSSR*, **36**, 66-93.

Fedotov, S. A., 1968. The seismic cycle, quantitative seismic zoning and long term seismic forecasting, In *Seismic Zoning of the USSR*, S. V. Medvedev, ed., 121-150, Science Press, Moscow (English translation, 1976, 133-166).

Foulger, G. & Long, R. E., 1984. Anomalous focal mechanisms: tensile crack formation on an accreting plate boundary, *Nature*, **310**, 43-45.

Geller, R. J. & Mueller, C. S., 1980. Four similar earthquakes in central California, *Geoph. res. Let.*, **7**, 821-824.

Gutenberg, B. & Richter, C. F., 1941. Seismicity of the Earth. *Geol. Soc. Am., Spec. Pap.*, **34**, 1-133.

Hagiwara, T., 1964. Brief description of the project proposed by the earthquake prediction research group of Japan. *Proc. U.S.-Japan Conf. Res. Relat. Earthquake Prediction Probl.*, 10-12.

Ishida, M. & Kanamori, H., 1980. Temporal variation of seismicity and spectrum of small earthquakes preceding the 1952 Kern County, California, earthquake, *Bull. seism. Soc. Am.*, **70**, 509-527.

Israel, M. & Nur, A. M., 1979. A complete solution of a one dimensional propagating fault with nonuniform stress and strength, *J. Geophys. Res.*, **84**, 2223-2234.

Julian, B. R., 1983. Evidence for dyke intrusion earthquake mechanisms near Long Valley caldera, California. *Nature*, **303**, 323-325.

Karnik, V., 1971. *Seismicity of the European Area*, **Part 2**, Reidel, Dordrecht.

Kelleher, J., Sykes, L. & Oliver, J., 1973. Possible criteria for predicting earthquake locations and their application to major

plate boundaries of the Pacific and the Caribbean, *J. Geophys. Res.*, **78**, 2547-2585.

Laubscher, H. & Bernoulli, D., 1977. Mediterranean and Tethys, *in* Nairn, A. E. M., Kanes, W. H. & Stehli, F. G. (eds), *The Ocean Basins and Margins*, **4A**, Plenum, New York & London.

Lee, W. & Lahr, J., 1975. HYP071 (revised): a computer program for determining hypocentre, magnitude and first motion pattern of local earthquakes, *U.S. Geol. Surv., Open File Rept.*, 75-311.

Lee, W. K. H. & Stewart, S. W., 1981. Principles and applications of microearthquake networks. *Advances in Geophysics, Supplement 2*, Saltzman, B. (ed), Academic Press, New York.

Le Pichon, X., & Angelier, J., 1979. The Hellenic arc and trench system: a key to the neotectonic evolution of the Eastern Mediterranean area, *Tectonophys.*, **60**, 1-42.

Logan, A. L. L., 1987. Accurate relative location of similar earthquakes, *Ph.D. thesis*, University of Edinburgh.

Lovell, J. H., Crampin, S., Evans, R. & Üçer, S. B., 1987. Microearthquakes in the TDP swarm, Turkey: clustering in space and time. *Geophys. J. R. astr. Soc.*, **91**, 313-330.

Main, I. G., 1985. Seismotectonics and seismic hazard in areas of differing crustal deformation rates, *Ph.D. thesis*, University of Edinburgh.

Main, I. G. & Burton, P. W., 1988. Seismotectonics and seismic hazard in the Aegean area, *Geophys. J.*, (submitted).

Makris, J., 1976. A dynamical model of the Hellenic Arc deduced from geophysical data, *Tectonophys.*, **36**, 339-346.

Makropoulos, K. C. & Burton, P. W., 1984. Greek tectonics and seismicity. *Tectonophys.*, **106**, 275-304.

Marrow, P. C. & Roberts, G., 1985. Focal mechanisms of aftershocks of the 1979 Carlisle earthquake: a re-interpretation, *Geophys. J. R. astr. Soc.*, **83:3**, 797-803.

McKenzie, D. P., 1969. The relation between fault plane solutions for earthquakes and the directions of the principal stresses, *Bull. seism. Soc. Am.*, **59**, No.2, 591-601.

McKenzie, D. P., 1972. Active tectonics of the Mediterranean region, *Geophys. J. R. astr. Soc.*, **30**, 109-186.

McKenzie, D. P., 1978. Active tectonics of the Alpine-Himalayan belt: the Aegean Sea and surrounding region, *Geophys. J. R. astr. Soc.*, **55**, 217-254.

Meissner, R. & Strehlau, J., 1982. Limits of stresses in continental crusts and their relation to the depth-frequency distribution of shallow earthquakes, *Tectonics*, **1**, 73-89.

Mogi, K., 1967. Earthquakes and fractures, *Tectonophys.*, **5**, 35-55.

Mogi, K., 1969. Relationship between the occurrence of great earthquakes and tectonic structures. *Bull. Earthquake Res. Inst., Univ. Tokyo*, **47**, 429-451.

Ohtake, M., Matumoto, T. & Latham, G. V., 1977. Seismicity gap near Oaxaca, southern Mexico as a probable precursor to a large earthquake. *Pure Appl. Geophys.*, **115**, 375-385.

Pamir, H. N., 1944. Kuzey Anadolu'da bir deprem çizgisi, *Istanb. Univ. Fen. Fak. Mecm. A.*, **7**.

Peacock, S., Crampin, S., Booth, D. C. & Fletcher, J. B., 1988. Shear-wave splitting in the Anza seismic gap, southern California: temporal variations as possible precursors, *J. Geophys. Res.*, **93**, 3339-3356.

Pearce, R. G. 1977. Fault plane solutions using relative amplitudes of *P* and *pP*, *Geophys. J. R. astr. Soc.*, **50**, 381-394.

Pearce, R. G. & Rogers, R. M., 1987. Some comments on the determination of earthquake moment tensors using world-wide seismic data, *Geophys. J. R. astr. Soc.*, **89**, 460 (abstract).

Raleigh, C. B., Bennett, G. T., Craig, H., Hanks, T. C. et al, 1977. Prediction of the Haicheng earthquake, *Eos, Trans. Am. Geophys. Union*, **58**, 236-272.

Richter, C. F., 1935. An instrumental earthquake magnitude scale, *Bull. Seism. Soc. Amer.*, **25**, 1-32.

Richter, C. F., 1958. *Elementary Seismology*, Freeman, San Francisco, California.

Rikitake, T., 1974. Probability of earthquake occurrence as estimated from crustal strain, *Tectonophys.*, **23**, 299-312.

Rikitake, T., 1976. *Earthquake Prediction*, Elsevier, Amsterdam.

Roberts, G., 1985. Shear-wave polarizations from local seismic events, *PhD thesis*, University of Edinburgh.

Russell, M., 1988. Electromagnetic induction studies in an area of active crustal deformation, *PhD thesis*, University of Edinburgh.

Şengör, A. M. C., 1979. The North Anatolian transform fault: its age, offset and tectonic significance, *J. geol. Soc.*, **136**, 269-282.

Şengör, A. M. C., 1984. The Cimmeride Orogenic System and the Tectonics of Eurasia, *Geol. Soc. Am.*, Special Paper 195.

Şengör, A. M. C., & Canitez, N., 1982. The North Anatolian fault, *In: Alpine-Mediterranean Geodynamics, Geodynamic Ser.*, 7, 205-216.

Şengör, A. M. C., & Yilmaz, Y., 1981. Tethyan evolution of Turkey: a plate tectonic approach, *Tectonophys.*, 75, 181-241.

Şengör, A. M. C., Görür, N. & Şaroğlu, F., 1985. Strike-slip faulting and related basin formation in zones of tectonic escape: Turkey as a case study. *S. E. P. M. Spec. Pub. 37*, 227-264.

Stephens, C. D., Lahr, J. C., Fogleman, K. A. & Horner, R. B., 1980. The St. Elias, Alaska earthquake of 28 February 1979: Regional recording of aftershocks and short-term , pre-earthquake seismicity, *Bull. Seism. Soc. Am.*, 70, 1607-1633.

Sykes, L., 1967. Mechanism of Earthquakes and Nature of Faulting on the Mid-Oceanic Ridges, *J. Geophys. Res.*, 72, 2131-2153.

Tapponier, P., Peltzer, G. & Armijo, R., 1986. On the mechanics of the collision between India and Asia, *in* Coward, M. P. & Reis, A. C., eds., Collision Tectonics: *Geol. Soc. Lond. Spec. Pub. 19*, 115-157.

Toksöz, M. N., Shakal, A. F. & Michael, A. J., 1979. Space-time migration of earthquakes along the North Anatolian fault zone and seismic gaps, *Pure appl. Geophys.*, 117, 1258-1270.

Tsujiura, M., 1983. Characteristic frequencies for earthquake families and their tectonic implications: Evidence from earthquake swarms in the Kanto District, Japan, *Pure appl. Geophys.*, 121, 573-600.

Turbitt, T. & Stewart, D. A., 1982. Calibration of the Willmore Mk IIIA Geostore seismic recording system, *Inst. Geol. Sci. Global Seism. Unit Rep. No. 158.*

Üçer, S. B., Crampin, S., Evans, R., Miller, A. & Kafadar, N., 1985. The MARNET radiolinked seismometer network spanning the Marmara Sea, and the seismicity of Western Anatolia, *Geophys. J. R. astr. Soc.*, 83, 17-30.

Utsu, T., 1972a. Large earthquakes near Hokkaido and the expectancy of the occurrence of a large earthquake off Nemuro, *Rep. Coord. Comm. Earthquake Prediction*, 7, 7-13 (in Japanese).

Utsu, T., 1972b. Aftershocks and earthquake statistics, IV, *J. Fac.*

Sci. Hokkaido Univ., **Ser. 7,4**, 1-42.

Utsu, T., 1974. Space-time pattern of large earthquakes occurring off the Pacific coast of the Japanese islands, *J. Phys. Earth*, **22**, 325-342.

Weaver, C. S. & Hill, D. P., 1978. Earthquake swarms and local crustal spreading along major strike-slip faults in California, *Pure appl. Geophys.*, **117**, 51-64.

Zschau, J., Nehl, B., Roth, F. & Noell, U., 1981. Cyclic earthquake activity near Adapazarı, western Turkey, (abstract), *Terra Cognita, special issue Spring 1981*, **33**.

Zschau, J., Işikara, A. M., Berckhemer, H., Bonatz, M. & Meissner, R., 1982. The Turkish/German earthquake prediction research project near Adapazarı, western Turkey, (abstract), *EOS*, **63**, 1272.

Appendix A

Earthquake epicentres determined within the TDP experimental area, 1984.

Earthquake epicentres determined within the TDP3 experimental area, 1984.

Origin							Location parameters						
-Date-			---Time---	Latitude °N	Longitude °E	Depth km	Magn M_L	N	Gap	DM	RMS	ERH	ERZ	Q
84	502	1521	35.34	40.6490	29.9800	7.12	-0.3	7	170	4.6	0.03	0.4	0.4	B1
84	502	18 8	58.45	40.6960	29.9950	9.33	-0.1	6	253	0.9	0.03	0.6	0.4	C1
84	503	452	14.99	40.6588	29.8883	7.93	-0.3	6	286	7.9	0.01	0.3	0.3	C1
84	503	717	35.04	40.6988	29.9817	10.09	-0.2	6	318	1.8	0.01	0.3	0.2	C1
84	503	1219	34.56	40.7775	30.1050	13.56	-0.3	9	334	10.2	0.05	1.1	0.6	C1
84	503	15 6	45.40	40.6565	29.8967	8.13	1.0	12	279	2.7	0.06	0.6	0.5	C1
84	503	1525	6.13	40.6517	29.9000	8.18	0.5	9	275	2.2	0.06	0.8	0.5	C1
84	503	1527	21.50	40.6522	29.9000	8.19	1.0	10	276	2.3	0.05	0.6	0.5	C1
84	503	1540	51.73	40.6573	29.8917	7.33	0.2	9	283	3.1	0.05	0.6	0.7	C1
84	503	1625	27.09	40.6582	29.8950	8.25	0.5	10	281	2.9	0.06	0.6	0.5	C1
84	503	1946	11.72	40.6502	29.9517	2.00	-0.3	6	146	2.1	0.32	0.5	1.0	C1
84	503	20 7	30.41	40.5960	29.9683	7.93	0.1	8	226	2.3	0.04	0.4	0.4	C1
84	503	2232	53.84	40.6547	29.9017	8.22	0.2	9	275	2.2	0.04	0.5	0.4	C1
84	504	059	24.71	40.6572	29.9017	8.19	-0.1	7	275	2.3	0.03	0.5	0.4	C1
84	504	2129	28.68	40.6582	29.8950	7.87	0.9	10	280	2.8	0.08	0.8	0.9	C1
84	505	035	33.08	40.6583	29.9017	6.76	-0.1	7	276	2.4	0.03	0.6	0.7	C1
84	505	1055	48.26	40.6573	29.8967	8.12	0.7	10	280	2.8	0.03	0.3	0.3	C1
84	505	11 3	55.17	40.6558	29.9033	8.40	-0.2	7	275	2.2	0.05	0.8	0.6	C1
84	505	22 4	19.11	40.6582	29.8950	7.89	0.5	11	281	2.9	0.06	0.6	0.6	C1
84	505	2322	29.96	40.6595	29.8950	8.09	0.5	12	282	3.0	0.07	0.6	0.5	C1
84	506	128	44.11	40.7000	29.9817	8.47	-0.1	7	282	1.9	0.02	0.3	0.2	C1
84	506	333	53.44	40.6583	29.9033	8.48	-0.2	7	274	2.2	0.02	0.3	0.3	C1
84	506	350	51.42	40.6560	29.9083	8.53	-0.3	6	270	1.8	0.04	0.7	0.5	C1
84	506	725	32.06	40.6577	29.9067	7.83	0.4	8	272	2.0	0.06	0.8	0.7	C1
84	506	925	57.39	40.6590	29.8967	8.42	0.1	8	279	2.8	0.06	0.7	0.6	C1
84	506	1140	17.94	40.6597	29.8950	7.54	0.0	10	281	2.9	0.06	0.6	0.7	C1
84	506	1142	51.63	40.6587	29.9000	8.10	0.2	7	277	2.5	0.03	0.6	0.7	C1
84	506	1211	5.24	40.6543	29.9050	8.65	-0.1	6	273	2.0	0.02	0.5	0.5	C1
84	506	1212	8.80	40.6612	29.8950	8.35	-0.2	8	282	3.0	0.02	0.3	0.3	C1
84	506	1214	33.54	40.6597	29.8933	8.71	1.3	11	282	3.1	0.03	0.3	0.3	C1
84	506	1215	45.76	40.6572	29.9067	8.48	0.1	8	271	2.0	0.03	0.4	0.4	C1
84	506	1217	27.64	40.6552	29.9050	8.72	0.2	6	272	2.0	0.02	0.4	0.4	C1
84	506	1219	1.59	40.6583	29.8967	8.32	0.8	12	279	2.7	0.03	0.2	0.2	C1
84	506	1221	34.81	40.6585	29.9033	8.03	-0.3	6	274	2.2	0.03	0.7	0.7	C1
84	506	1255	12.41	40.6607	29.8917	8.05	1.0	11	284	3.3	0.08	0.8	0.8	C1
84	506	1257	0.84	40.6592	29.8933	8.02	0.9	12	282	3.0	0.03	0.3	0.3	C1
84	506	13 1	51.81	40.6612	29.8933	8.26	1.2	11	282	3.1	0.04	0.4	0.4	C1
84	506	13 3	5.66	40.6590	29.8950	7.87	0.9	11	281	2.9	0.03	0.3	0.3	C1
84	506	1311	52.99	40.6633	29.8967	8.15	0.5	7	281	3.0	0.03	0.5	0.4	C1
84	506	1313	47.62	40.6588	29.8967	7.68	0.8	10	280	2.8	0.05	0.5	0.5	C1
84	506	1315	16.69	40.6100	30.0367	8.81	0.3	8	241	3.2	0.22	2.3	2.1	C1
84	506	1316	6.85	40.6582	29.9000	7.73	0.5	8	277	2.5	0.03	0.4	0.3	C1
84	506	1319	7.20	40.6610	29.9000	8.45	0.3	8	278	2.6	0.03	0.5	0.4	C1
84	506	1347	51.45	40.6572	29.9050	7.94	0.0	6	273	2.1	0.03	0.7	0.8	C1
84	506	14 0	54.93	40.6610	29.8967	6.92	-0.1	7	281	2.9	0.05	0.9	1.0	C1
84	506	1514	43.22	40.6577	29.9033	8.95	-0.2	6	274	2.2	0.02	0.4	0.4	C1
84	506	1534	27.70	40.6570	29.9017	8.11	-0.1	6	276	2.4	0.03	0.6	0.7	C1
84	506	1820	10.19	40.6602	29.8950	8.18	0.0	10	282	3.0	0.05	0.5	0.6	C1
84	506	1841	51.78	40.6613	29.8950	7.28	-0.3	6	281	3.0	0.04	0.7	1.0	C1
84	506	2154	38.60	40.6570	29.8967	7.81	-0.4	6	280	2.8	0.03	0.6	0.6	C1
84	507	712	33.18	40.6550	29.9083	8.48	0.1	7	270	1.8	0.02	0.4	0.3	C1
84	507	739	28.19	40.6507	29.9883	8.94	0.2	7	172	2.5	0.06	0.9	0.6	B1
84	507	745	10.02	40.6545	29.9050	8.54	-0.3	8	272	1.9	0.04	0.5	0.4	C1
84	507	1724	52.95	40.6600	29.8817	8.02	0.8	10	290	4.0	0.05	0.5	0.6	C1
84	507	1855	2.51	40.6568	29.8917	8.13	0.1	10	283	3.0	0.03	0.3	0.4	C1
84	507	2022	36.49	40.6585	29.8933	8.33	-0.2	6	282	3.1	0.04	1.0	1.1	C1
84	507	2335	36.27	40.6000	29.9667	7.51	0.0	6	211	2.1	0.02	0.3	0.2	C1
84	508	041	28.16	40.7403	30.1483	13.27	0.2	9	330	8.7	0.10	1.8	1.1	C1
84	508	642	25.38	40.6850	29.9767	8.59	0.3	6	213	1.9	0.04	1.0	0.5	C1
84	508	1135	18.86	40.6612	29.8933	8.19	0.6	11	283	3.1	0.04	0.4	0.3	C1
84	508	2032	37.82	40.6290	30.0300	9.92	1.0	10	183	2.0	0.06	0.6	0.5	C1
84	508	2051	26.45	40.6287	30.0367	10.31	0.5	10	197	1.5	0.04	0.4	0.3	C1
84	508	2056	21.74	40.6240	30.0450	10.48	1.5	8	236	1.5	0.04	0.7	0.5	C1
84	508	2110	8.37	40.6263	30.0417	9.89	0.5	10	217	1.4	0.06	0.6	0.4	C1
84	508	2133	2.94	40.6253	30.0383	9.78	0.2	9	211	1.7	0.06	0.7	0.6	C1
84	509	111	43.60	40.6233	30.0433	9.74	0.9	10	233	1.6	0.10	1.0	0.6	C1
84	509	1824	35.01	40.6997	29.9183	9.68	-0.2	6	309	5.7	0.01	0.6	0.4	C1
84	510	247	19.96	40.6870	30.0000	9.65	0.4	9	137	0.2	0.07	0.7	0.5	B1

Earthquake epicentres determined within the TDP3 experimental area, 1984.

Origin							Location parameters					
-Date-	——Time——	Latitude °N	Longitude °E	Depth km	Magn M_L	N	Gap	DM	RMS	ERH	ERZ	Q
84 510	624 10.23	40.6735	30.0400	8.50	0.4	8	119	3.1	0.05	0.5	0.5	B1
84 512	1852 46.50	40.6195	30.0450	10.10	0.1	8	242	5.0	0.10	1.5	1.3	C1
84 513	619 4.56	40.7077	30.0217	10.18	-0.1	8	245	2.9	0.05	0.6	0.4	C1
84 513	1634 34.53	40.7327	29.9333	9.53	0.2	11	289	7.4	0.14	1.5	1.5	C1
84 513	1930 41.48	40.6973	30.0000	9.86	1.1	10	229	1.0	0.06	0.6	0.4	C1
84 514	2017 2.19	40.6837	29.8683	8.03	0.8	9	301	6.3	0.04	0.5	0.7	C1
84 515	1032 51.15	40.6902	30.0133	9.40	0.5	8	252	1.3	0.04	0.5	0.4	C1
84 516	229 27.31	40.7408	29.9300	2.97	-0.2	8	294	10.3	0.78	12.1	69.3	D1
84 516	550 17.79	40.6552	29.9667	8.65	0.3	9	133	3.0	0.07	0.7	0.7	B1
84 516	18 6 49.45	40.6580	29.8900	7.19	0.2	9	280	3.2	0.05	0.5	0.6	C1
84 517	1213 36.29	40.6947	29.9817	9.83	0.1	9	221	1.6	0.03	0.2	0.2	C1
84 518	143 51.55	40.6222	30.0433	10.84	0.6	9	233	1.7	0.03	0.3	0.3	C1
84 518	5 2 29.85	40.6538	29.8967	8.32	-0.1	6	273	2.6	0.02	0.5	0.3	C1
84 518	1013 50.11	40.6972	29.9433	10.97	1.2	13	260	2.2	0.07	0.7	0.5	C1
84 518	12 3 32.47	40.7040	29.9817	9.85	1.0	14	244	2.3	0.06	0.4	0.3	C1
84 520	1748 49.79	40.6495	29.9800	8.26	1.1	13	64	2.4	0.07	0.5	0.5	A1
84 521	747 32.39	40.5912	30.1317	9.42	1.0	12	299	8.5	0.06	0.8	0.8	C1
84 521	8 5 51.26	40.7210	30.1267	6.51	0.3	9	322	6.0	0.03	0.5	0.5	C1
84 521	1957 22.99	40.6900	30.0233	10.42	0.9	13	185	2.1	0.03	0.2	0.2	C1
84 521	2015 38.97	40.7163	29.9250	4.48	0.8	14	285	4.8	0.13	1.0	1.2	C1
84 521	2218 13.70	40.6697	29.9283	8.38	0.0	10	239	2.4	0.04	0.4	0.3	C1
84 521	2234 7.34	40.7168	30.1233	11.15	0.6	14	321	5.5	0.51	5.3	4.0	D1
84 521	2342 42.05	40.6217	30.0417	10.82	0.7	14	231	1.8	0.08	0.6	0.5	C1
84 522	4 6 42.41	40.7222	30.1317	7.42	0.9	14	323	6.3	0.08	0.7	0.6	C1
84 522	410 8.20	40.7137	30.1367	7.60	0.5	14	324	6.3	0.10	1.0	0.9	C1
84 523	652 32.69	40.7113	30.1217	7.88	1.0	11	319	5.0	0.05	0.6	0.4	C1
84 523	956 22.14	40.7157	30.1250	7.63	0.7	11	321	5.5	0.06	0.7	0.5	C1
84 523	1051 40.22	40.7180	30.1267	8.00	0.7	11	321	5.8	0.05	0.6	0.4	C1
84 523	1150 5.21	40.6737	29.9917	10.95	0.0	12	96	1.7	0.04	0.4	0.3	B1
84 523	1155 41.81	40.7117	29.9283	7.98	0.6	11	281	4.2	0.06	0.5	0.4	C1
84 523	1225 58.94	40.7085	29.9250	7.72	0.3	12	281	4.2	0.07	0.7	0.5	C1
84 524	14 7 46.63	40.6502	29.9283	2.00	0.5	6	179	0.2	0.51	0.1	0.1	D1
84 525	348 38.36	40.7118	29.9017	8.48	-0.1	6	320	5.9	0.04	0.9	0.7	C1
84 525	926 9.25	40.7022	29.9100	3.76	0.0	6	314	4.7	0.03	0.5	0.5	C1
84 527	19 8 18.99	40.7028	30.0050	10.70	0.7	13	226	1.7	0.06	0.5	0.4	C1
84 527	1934 8.09	40.6330	30.0300	10.13	-0.2	7	216	3.6	0.03	0.4	0.3	C1
84 527	20 5 26.34	40.6112	30.0933	5.39	-0.1	6	308	9.2	0.11	1.6	2.4	C1
84 528	533 54.48	40.7943	30.1050	12.26	-0.2	7	332	12.0	0.07	2.0	1.9	C1
84 528	1851 49.39	40.6588	30.0817	9.07	0.2	10	244	3.6	0.03	0.3	0.2	C1
84 529	048 16.99	40.7735	30.0600	12.51	0.2	12	315	9.3	0.04	0.5	0.4	C1
84 529	142 35.29	40.6808	29.9233	9.65	0.4	12	267	2.9	0.24	2.1	1.6	C1
84 529	228 43.35	40.7035	29.9067	9.22	-0.2	10	297	5.0	0.04	0.5	0.4	C1
84 529	317 31.16	40.6537	29.9250	9.62	-0.2	10	236	0.6	0.02	0.2	0.1	C1
84 529	412 6.31	40.6543	29.9217	9.25	-0.2	8	241	4.2	0.02	0.3	0.2	C1
84 529	729 5.51	40.7328	30.0533	6.09	0.1	9	289	5.0	0.11	1.3	1.2	C1
84 529	931 43.97	40.5698	29.9817	9.89	0.3	9	277	4.8	0.03	0.3	0.2	C1
84 529	1257 57.83	40.6527	29.9817	7.86	0.0	7	149	2.8	0.04	0.5	0.4	B1
84 529	1410 58.11	40.7912	30.1100	12.24	0.0	8	330	11.8	0.07	1.8	1.8	C1
84 529	2132 41.26	40.6797	29.9783	10.38	0.4	12	146	1.7	0.05	0.4	0.3	B1
84 529	22 8 42.04	40.6775	29.9783	10.59	-0.2	6	146	1.8	0.02	0.5	0.2	B1
84 529	2214 57.97	40.6815	29.9683	10.43	0.0	8	168	0.8	0.03	0.4	0.3	B1
84 530	517 49.28	40.6810	29.9767	10.22	0.4	11	157	1.6	0.05	0.5	0.3	B1
84 530	522 43.66	40.6503	29.9817	8.22	0.7	11	99	2.5	0.07	0.5	0.5	B1
84 530	8 2 8.72	40.6800	29.9783	10.31	0.8	12	148	1.8	0.05	0.4	0.3	B1
84 530	1020 50.93	40.6785	29.9783	10.49	1.0	13	139	1.7	0.05	0.4	0.3	B1
84 530	1035 0.23	40.6788	29.9783	10.46	0.5	13	142	1.7	0.04	0.4	0.3	B1
84 530	1310 14.36	40.6790	29.9783	10.50	1.1	13	143	1.7	0.04	0.3	0.2	B1
84 530	2357 44.73	40.7163	30.1250	7.37	0.2	10	321	5.6	0.04	0.5	0.3	C1
84 531	228 52.81	40.6808	29.9750	10.50	1.4	14	157	1.4	0.05	0.4	0.3	B1
84 531	655 12.35	40.7203	30.1250	7.86	0.2	10	321	5.8	0.08	1.0	1.1	C1
84 531	7 3 36.66	40.7142	30.1400	7.66	0.7	14	325	6.5	0.11	1.1	0.9	C1
84 531	920 38.60	40.6553	29.9383	5.45	0.6	8	185	1.2	0.56	2.3	2.5	D1
84 531	1315 1.39	40.6932	29.9900	7.57	1.7	11	210	0.9	0.06	0.6	0.7	C1
84 531	1328 53.93	40.6898	29.9917	7.52	0.1	12	199	0.7	0.10	0.7	0.6	C1
84 531	2250 58.00	40.7073	29.9867	9.20	0.0	8	246	2.4	0.11	2.5	1.0	D1
84 601	0 8 11.56	40.6898	29.9983	9.48	0.0	13	196	0.2	0.23	1.5	1.5	C1
84 601	210 1.55	40.7215	29.9300	8.56	0.4	8	301	5.1	0.06	1.1	0.9	C1
84 601	218 5.96	40.7227	29.9300	8.39	0.1	8	302	5.2	0.06	1.2	1.0	C1

Earthquake epicentres determined within the TDP3 experimental area, 1984.

Origin							Location parameters						
-Date-			---Time---	Latitude °N	Longitude °E	Depth km	Magn M_L	N	Gap	DM	RMS	ERH	ERZ	Q
84	601	1034	15.16	40.6973	30.0417	5.52	0.6	12	214	2.4	0.15	1.0	1.1	C1
84	601	11	8 40.65	40.7278	29.9550	7.66	0.3	8	305	5.2	0.05	1.0	0.7	C1
84	601	1148	43.37	40.7083	29.9250	9.22	0.8	8	291	4.1	0.06	1.2	0.8	C1
84	601	1556	30.00	40.7035	29.8917	2.44	0.7	9	296	6.1	0.08	1.0	2.4	C1
84	601	1937	20.73	40.6807	29.9783	10.48	0.6	12	152	1.8	0.06	0.5	0.4	B1
84	602	136	2.00	40.6872	29.9883	7.41	0.4	10	188	1.0	0.05	0.4	0.4	C1
84	602	2	5 36.35	40.5887	29.9700	10.48	0.0	7	247	2.7	0.01	0.1	0.1	C1
84	602	320	9.80	40.5890	29.9717	10.28	0.1	10	246	2.8	0.03	0.3	0.2	C1
84	602	330	35.89	40.5868	29.9750	10.33	0.1	7	249	3.2	0.01	0.3	0.1	C1
84	603	1549	16.03	40.6622	30.0067	7.91	0.1	14	77	3.0	0.07	0.4	0.5	A1
84	603	2328	3.38	40.6587	29.8867	7.76	0.7	14	283	3.6	0.04	0.3	0.3	C1
84	605	1147	55.44	40.7122	30.0050	12.11	0.1	12	246	2.7	0.06	0.5	0.5	C1
84	606	1059	8.11	40.6760	29.8500	11.42	0.1	9	306	7.1	0.02	0.3	0.2	C1
84	606	2148	25.24	40.6573	29.8883	8.00	1.0	14	282	3.4	0.04	0.3	0.3	C1
84	606	2231	49.48	40.6575	29.8867	7.94	0.9	14	282	3.5	0.04	0.3	0.3	C1
84	606	2233	13.73	40.6580	29.8917	7.88	0.1	9	279	3.2	0.03	0.5	0.3	C1
84	607	1	3 59.79	40.6558	29.8933	8.05	0.1	10	276	2.9	0.03	0.3	0.3	C1
84	607	1	9 22.96	40.6502	29.9283	2.00	-0.1	8	179	0.2	0.33	1.4	1.2	C1
84	607	152	44.85	40.5892	30.0517	12.84	-0.2	10	270	5.3	0.05	0.6	0.4	C1
84	607	329	12.46	40.6637	29.9617	8.28	-0.1	7	169	3.4	0.03	0.5	0.4	B1
84	607	941	6.91	40.7843	30.1283	13.37	0.5	11	330	11.6	0.11	1.8	1.4	C1
84	607	1023	23.65	40.5908	29.9733	9.06	0.9	11	240	2.9	0.02	0.2	0.1	C1
84	607	1854	57.38	40.6887	30.0200	10.63	0.8	14	179	1.8	0.05	0.4	0.3	B1
84	607	1857	22.69	40.6860	30.0200	10.19	0.2	11	166	1.8	0.06	0.5	0.4	B1
84	607	19	3 34.64	40.6903	30.0233	10.48	1.1	13	187	2.1	0.05	0.4	0.4	C1
84	607	19	9 44.56	40.6912	30.0233	10.20	0.0	12	191	2.2	0.05	0.4	0.4	C1
84	607	2210	19.22	40.7145	29.9433	8.81	0.0	8	291	3.9	0.04	0.7	0.5	C1
84	608	134	9.68	40.6888	30.0333	10.65	0.3	12	179	2.9	0.05	0.4	0.3	B1
84	608	326	54.67	40.6905	30.0200	10.38	0.0	9	188	1.9	0.02	0.2	0.1	C1
84	608	936	11.73	40.6497	29.9817	8.35	0.3	9	148	2.4	0.04	0.4	0.3	B1
84	608	2017	21.09	40.6537	29.8967	7.31	0.1	6	272	2.6	0.02	0.5	0.5	C1
84	609	255	6.75	40.6567	29.8883	8.02	1.0	12	281	3.3	0.04	0.3	0.2	C1
84	609	412	1.66	40.6562	29.8950	8.20	0.5	9	276	2.9	0.04	0.5	0.3	C1
84	609	1449	39.81	40.7287	29.9233	10.06	0.2	9	315	6.1	0.03	0.5	0.3	C1
84	609	1628	0.64	40.6488	29.9817	8.28	0.9	11	64	2.3	0.08	0.6	0.6	A1
84	609	2051	6.56	40.6547	29.8933	8.31	-0.1	9	276	2.9	0.03	0.4	0.3	C1
84	610	430	36.52	40.7095	29.9300	7.11	0.7	10	278	3.9	0.08	1.0	0.6	C1
84	610	919	5.03	40.6898	30.0000	2.00	-0.1	6	249	0.2	0.72	0.2	0.1	D1
84	610	1857	57.61	40.7007	29.9883	10.33	0.6	13	230	1.6	0.07	0.5	0.4	C1
84	610	1935	34.90	40.7008	30.0017	9.59	0.0	8	282	1.4	0.04	0.5	0.4	C1
84	610	2139	30.47	40.6997	29.9917	9.79	0.1	12	226	1.4	0.06	0.5	0.4	C1
84	610	2141	17.22	40.6943	29.9967	9.60	0.0	11	209	0.7	0.08	0.8	0.6	C1
84	611	1440	52.40	40.7193	29.9883	12.30	0.4	14	262	3.6	0.07	0.6	0.4	C1
84	611	1720	14.45	40.6510	29.9800	7.69	0.1	8	145	2.6	0.05	0.5	0.4	B1
84	611	22	6 44.99	40.6885	30.0200	10.25	0.2	12	179	1.8	0.07	0.5	0.4	B1
84	612	8	2 0.66	40.7207	29.8983	8.36	0.8	14	299	6.7	0.09	0.8	0.7	C1
84	612	937	28.94	40.6277	29.9700	8.94	0.8	14	132	1.4	0.05	0.3	0.3	B1
84	612	1450	58.31	40.6515	29.9800	8.22	0.6	12	83	2.7	0.04	0.2	0.2	A1
84	612	15	7 12.73	40.6875	30.0150	10.68	0.1	8	173	1.3	0.03	0.4	0.3	B1
84	612	15	8 15.25	40.6862	30.0167	10.38	0.1	13	166	1.6	0.11	0.7	0.6	B1
84	613	951	34.73	40.7275	29.9683	7.40	0.0	8	274	5.1	0.02	0.5	0.3	C1
84	613	2157	38.26	40.6955	29.9833	8.24	0.2	13	222	1.5	0.09	0.7	0.5	C1
84	614	033	57.55	40.6942	29.9850	7.97	0.1	8	216	1.4	0.04	0.5	0.3	C1
84	614	229	13.32	40.6465	29.9267	12.29	0.2	12	214	0.2	0.03	0.3	0.2	C1
84	614	331	52.40	40.7893	30.0967	14.02	0.0	8	328	11.3	0.04	1.0	1.2	C1
84	614	2148	7.86	40.6998	29.9850	10.10	0.5	14	231	1.7	0.06	0.4	0.3	C1
84	615	036	28.64	40.7763	30.1033	14.03	0.0	12	327	10.0	0.06	0.8	0.6	C1
84	615	2032	13.62	40.6008	29.9633	7.65	0.2	11	207	1.9	0.03	0.3	0.2	C1
84	615	2210	50.20	40.7247	29.9650	9.09	0.4	12	273	5.0	0.24	2.2	1.9	C1
84	616	159	21.22	40.7283	29.9533	9.78	-0.2	7	305	5.3	0.05	1.0	0.8	C1
84	617	135	23.89	40.6937	29.9717	7.77	0.2	14	232	1.9	0.08	0.5	0.5	C1
84	617	136	36.62	40.6942	29.9767	7.67	0.1	10	227	2.0	0.06	0.5	0.5	C1
84	617	11	5 48.59	40.6727	29.9800	12.31	1.5	14	106	2.1	0.04	0.4	0.3	B1
84	617	11	6 54.74	40.6793	29.9750	12.55	0.1	12	147	1.5	0.08	0.7	0.5	B1
84	617	1319	23.29	40.6747	29.9783	12.49	0.1	12	117	1.8	0.04	0.4	0.3	B1
84	617	17	5 56.52	40.6735	29.9850	12.21	0.8	14	106	2.0	0.04	0.3	0.2	B1
84	617	2041	16.95	40.6063	29.9850	11.21	0.0	11	201	2.5	0.03	0.3	0.2	C1
84	618	155	18.43	40.6990	29.9833	7.82	-0.2	6	237	1.8	0.04	1.4	0.8	C1

Earthquake epicentres determined within the TDP3 experimental area, 1984.

Origin						Location parameters						
-Date-	---Time---	Latitude °N	Longitude °E	Depth km	Magn M_L	N	Gap	DM	RMS	ERH	ERZ	Q
84 618	5 2 20.52	40.6502	29.9833	8.31	0.0	9	155	2.4	0.04	0.5	0.4	B1
84 618	1456 0.61	40.7047	29.9017	4.10	0.1	7	299	5.4	0.06	1.0	1.5	C1
84 618	2021 41.39	40.6512	29.8800	8.73	0.1	10	287	4.0	0.03	0.5	0.4	C1
84 618	2119 47.11	40.7217	29.8967	8.07	1.0	14	299	6.9	0.08	0.7	0.7	C1
84 619	2328 11.68	40.6917	30.0717	2.00	0.4	11	289	0.2	1.03	2.6	2.0	D1
84 620	437 33.01	40.6637	30.0033	10.05	0.1	7	170	2.7	0.03	0.6	0.5	B1
84 620	1517 24.13	40.6112	30.0700	11.59	0.5	12	264	3.3	0.04	0.4	0.3	C1
84 620	1834 10.01	40.7062	29.9633	10.34	-0.1	6	278	2.8	0.00	0.2	0.1	C1
84 620	2140 7.77	40.7032	30.1450	10.40	1.1	12	325	6.6	0.03	0.3	0.2	C1
84 620	23 9 2.48	40.6955	29.9700	7.62	1.4	13	239	1.9	0.07	0.5	0.5	C1
84 621	1 3 9.52	40.6532	29.9750	8.30	0.8	8	128	2.9	0.02	0.2	0.2	B1
84 621	216 13.56	40.6978	29.9700	7.62	0.5	12	242	2.2	0.07	0.5	0.4	C1
84 621	225 19.41	40.6952	29.9700	7.75	1.4	13	239	1.9	0.07	0.5	0.5	C1
84 621	921 13.22	40.6912	29.9717	6.94	1.2	14	226	1.6	0.06	0.4	0.3	C1
84 622	1454 41.58	40.6898	30.0167	7.63	0.4	10	187	1.5	0.08	0.8	0.6	C1
84 622	1750 35.48	40.6987	29.9867	9.66	0.2	9	227	1.6	0.05	0.6	0.4	C1
84 622	2219 34.28	40.7075	29.9100	7.76	0.8	13	298	5.0	0.08	0.6	0.6	C1
84 623	011 17.37	40.7138	30.0200	10.26	0.1	11	247	3.3	0.05	0.5	0.3	C1
84 623	1719 45.57	40.6898	29.9483	6.59	0.4	12	248	1.3	0.09	0.7	0.6	C1
84 623	1720 19.86	40.7305	30.0033	8.81	0.0	8	274	4.7	0.05	0.8	0.6	C1
84 624	1855 14.75	40.6917	29.9617	7.80	0.1	12	259	1.2	0.03	0.3	0.2	C1
84 624	1859 46.78	40.6933	29.9700	7.49	0.6	16	236	1.7	0.07	0.4	0.4	C1
84 624	19 2 18.28	40.6960	29.9617	7.64	0.0	9	274	1.7	0.03	0.4	0.3	C1
84 624	1930 38.95	40.6967	29.9617	7.97	0.1	10	264	1.8	0.04	0.4	0.3	C1
84 625	054 10.06	40.6740	29.9867	8.32	0.1	11	107	1.9	0.04	0.3	0.3	B1
84 625	448 3.98	40.7057	29.9667	7.47	0.1	10	253	2.8	0.05	0.7	0.4	C1
84 625	819 0.23	40.7287	30.0517	4.82	3.3	8	284	4.6	0.06	3.4	3.3	D1
84 625	825 54.98	40.7793	30.0950	13.34	1.2	14	326	10.2	0.07	0.9	0.7	C1
84 625	830 33.77	40.7765	30.1067	12.96	0.8	15	327	10.1	0.11	1.4	1.2	C1
84 625	836 15.33	40.7808	30.0917	13.19	0.8	12	325	10.3	0.06	0.8	0.8	C1
84 625	945 41.04	40.7822	30.0867	13.06	1.1	13	324	10.4	0.05	0.7	0.6	C1
84 625	1520 7.04	40.7735	30.1017	13.45	1.4	14	326	9.7	0.08	1.0	0.7	C1
84 625	1542 29.59	40.6697	29.9850	10.82	1.0	14	92	2.3	0.05	0.4	0.3	B1
84 625	1549 5.89	40.6722	29.9900	11.09	0.0	8	108	1.9	0.03	0.4	0.3	B1
84 625	1753 32.10	40.6555	29.9667	7.62	1.4	13	148	2.9	0.05	0.3	0.4	B1
84 625	1810 45.25	40.5607	30.1167	2.03	0.0	7	315	10.1	0.08	3.4	26.1	D1
84 625	2253 41.92	40.6950	29.9650	7.61	0.1	8	251	1.7	0.03	0.5	0.3	C1
84 625	2258 16.56	40.6937	29.9717	7.23	0.0	10	246	1.8	0.05	0.5	0.4	C1
84 626	011 43.44	40.6865	30.0167	4.88	0.3	11	168	1.5	0.07	0.4	0.5	B1
84 626	146 5.41	40.6528	29.9583	7.45	0.2	10	221	3.1	0.05	0.5	0.4	C1
84 626	927 33.21	40.7280	30.0317	10.93	0.1	10	273	5.2	0.08	1.1	0.8	C1
84 626	10 2 23.25	40.6902	30.0433	6.95	-0.1	7	184	2.3	0.03	0.5	0.4	C1
84 626	2024 28.57	40.7902	30.1117	12.34	1.2	15	330	11.7	0.09	1.1	1.0	C1
84 627	236 4.15	40.6520	29.9750	7.74	0.4	12	71	2.8	0.07	0.5	0.5	A1
84 627	342 43.08	40.6478	29.9667	8.30	-0.2	10	130	2.8	0.12	1.0	0.9	B1
84 627	1711 21.95	40.7012	29.9950	9.16	0.2	9	227	1.5	0.06	0.7	0.4	C1
84 627	1738 12.38	40.6772	29.9383	11.74	-0.1	11	239	1.7	0.07	0.8	0.5	C1
84 628	717 46.25	40.6955	29.9700	7.82	1.6	15	240	1.9	0.08	0.5	0.5	C1
84 628	2032 14.60	40.6740	29.9450	11.44	1.9	14	207	1.4	0.07	0.6	0.5	C1
84 628	2038 34.26	40.6732	29.9467	11.09	0.1	12	217	3.2	0.06	0.6	0.4	C1
84 628	2045 7.22	40.6748	29.9433	10.89	0.5	16	217	1.5	0.07	0.5	0.4	C1
84 628	2048 50.79	40.6747	29.9433	10.95	1.1	16	216	1.5	0.06	0.4	0.4	C1
84 628	21 5 49.68	40.6723	29.9467	10.83	0.8	15	190	1.3	0.06	0.5	0.3	C1
84 628	2150 29.36	40.6818	30.0250	5.17	0.1	11	149	2.3	0.09	0.5	0.8	B1
84 629	255 17.73	40.6765	29.9433	10.94	0.3	15	224	1.3	0.06	0.5	0.3	C1
84 629	1157 4.07	40.7022	29.9700	7.86	0.5	13	248	2.5	0.07	0.5	0.4	C1
84 629	1558 34.20	40.6820	29.9733	7.02	-0.1	6	168	1.2	0.05	1.1	0.7	C1
84 629	2251 35.26	40.6810	30.0300	4.85	0.2	10	146	2.8	0.06	0.4	0.7	B1
84 629	2329 56.72	40.6642	29.9283	7.82	0.0	8	231	1.7	0.03	0.3	0.3	C1
84 630	016 17.17	40.6790	29.9500	11.02	-0.1	9	222	0.7	0.07	0.8	0.5	C1
84 630	912 49.29	40.7140	29.9267	6.78	0.5	9	295	4.5	0.05	0.5	0.6	C1
84 630	22 9 45.49	40.6917	30.0717	2.00	0.1	8	289	0.2	0.87	0.8	0.6	D1
84 701	623 16.38	40.6950	29.9617	7.53	0.1	8	272	1.6	0.03	0.3	0.2	C1
84 701	1039 7.13	40.6385	30.0517	5.65	0.4	10	203	0.2	0.46	2.3	1.6	D1
84 703	1416 50.36	40.7763	30.1083	12.78	1.6	16	327	10.1	0.09	1.2	1.3	C1
84 703	1425 4.10	40.7803	30.1100	12.37	1.2	14	328	10.6	0.08	1.1	1.3	C1
84 703	1937 29.06	40.7810	30.0983	13.41	0.6	14	327	10.4	0.07	0.9	0.7	C1
84 703	2334 17.60	40.7777	30.1067	13.53	1.3	15	327	10.2	0.08	1.1	0.9	C1

Earthquake epicentres determined within the TDP3 experimental area, 1984.

Origin -Date-	-Time-	Latitude °N	Longitude °E	Depth km	Magn M_L	Location parameters N	Gap	DM	RMS	ERH	ERZ	Q
84 704	016 19.42	40.6722	29.9467	10.79	0.2	15	193	1.4	0.07	0.6	0.4	C1
84 704	236 53.19	40.7167	30.0100	11.44	0.0	13	253	3.3	0.07	0.7	0.5	C1
84 704	1811 6.28	40.7803	30.1117	12.63	0.0	8	331	10.7	0.05	1.4	1.2	C1
84 704	2228 21.39	40.6743	30.0633	8.71	0.3	14	181	1.8	0.08	0.6	0.5	C1
84 705	048 23.33	40.6730	30.0467	7.27	0.8	14	128	2.7	0.07	0.4	0.4	B1
84 705	216 7.29	40.6965	29.9783	7.66	-0.1	11	236	2.0	0.08	0.7	0.6	C1
84 706	925 29.66	40.7783	30.0950	12.63	0.3	11	328	10.1	0.07	1.3	1.0	C1
84 706	1737 1.65	40.6735	29.8983	6.52	0.8	9	284	3.7	0.09	1.2	1.4	C1
84 706	2025 35.62	40.6715	30.0000	9.65	0.3	10	110	1.5	0.07	0.9	0.6	B1
84 707	612 30.47	40.6798	29.9450	12.34	0.4	14	234	1.1	0.08	0.8	0.6	C1
84 707	1734 40.03	40.6760	29.9483	11.78	-0.1	8	201	0.9	0.03	0.4	0.3	C1
84 708	534 23.75	40.6642	29.9267	8.32	0.4	11	235	1.7	0.07	0.6	0.5	C1
84 708	922 38.86	40.6672	29.9250	8.31	0.9	13	247	2.1	0.06	0.5	0.5	C1
84 708	1157 28.68	40.6708	29.9450	10.86	-0.1	10	191	1.5	0.08	1.0	0.7	C1
84 708	1511 37.70	40.6742	29.8917	5.35	-0.1	8	306	4.1	0.12	1.5	1.6	C1
84 708	1817 58.58	40.6723	29.9400	11.56	0.1	11	215	1.8	0.06	0.7	0.4	C1
84 708	1828 11.13	40.7787	30.1133	13.09	-0.3	8	331	10.5	0.03	0.9	0.7	C1
84 709	415 13.07	40.6867	30.0217	10.63	0.3	12	169	1.9	0.09	0.8	0.6	B1
84 709	12 5 54.08	40.6717	29.9483	10.69	0.5	12	184	1.3	0.06	0.7	0.4	C1
84 709	2130 54.03	40.6733	29.9167	6.49	0.4	12	271	2.9	0.06	0.4	0.4	C1
84 710	357 3.90	40.6767	29.8983	6.57	1.2	14	285	4.0	0.07	0.6	0.4	C1
84 710	1222 3.36	40.6855	30.0200	9.97	1.7	12	163	1.8	0.07	0.6	0.5	B1
84 711	1911 19.39	40.7247	29.9767	10.01	0.6	12	270	5.1	0.09	1.1	0.8	C1
84 712	027 51.52	40.6880	29.9867	8.25	0.5	10	196	2.5	0.10	1.0	0.7	C1
84 712	919 46.55	40.7878	30.1250	12.37	0.5	11	330	11.8	0.10	1.8	1.5	C1
84 712	1645 29.62	40.6507	29.9783	7.36	1.6	13	65	1.9	0.06	0.4	0.5	A1
84 713	3 2 2.18	40.6495	29.9750	8.13	0.9	15	68	2.2	0.07	0.4	0.4	A1
84 713	1655 27.22	40.6915	29.9700	7.29	0.9	16	230	1.6	0.07	0.4	0.3	C1
84 713	2123 31.43	40.6518	29.9717	8.11	0.7	17	75	2.4	0.08	0.4	0.4	A1
84 713	2145 37.83	40.6527	29.9733	8.03	1.0	17	75	2.3	0.07	0.4	0.4	A1
84 713	2153 4.64	40.7060	30.0033	10.29	1.3	17	234	2.0	0.08	0.6	0.4	C1
84 713	2353 28.05	40.5963	30.1217	11.06	0.7	17	295	7.5	0.10	1.0	0.9	C1
84 714	10 4 13.17	40.6718	30.0000	9.71	0.3	15	75	1.6	0.09	0.6	0.5	A1
84 715	20 5 46.38	40.7515	30.0283	10.06	0.5	12	312	7.5	0.12	1.6	1.5	C1
84 715	2141 19.92	40.7038	29.9550	5.62	0.0	8	274	2.6	0.06	0.7	0.6	C1
84 717	4 3 16.38	40.6898	30.0000	2.00	1.3	7	278	0.2	1.22	3.0	2.7	D1
84 717	2046 17.80	40.6802	29.8917	2.00	0.2	6	290	9.1	0.04	0.8	5.2	D1
84 717	2346 16.15	40.6748	29.9267	6.78	0.2	6	266	6.3	0.01	0.4	0.4	C1
84 718	025 48.71	40.6818	29.8983	4.73	1.0	8	287	8.5	0.06	1.2	2.0	C1
84 718	220 2.03	40.6758	29.9050	6.07	0.3	8	280	8.0	0.05	1.3	1.5	C1
84 718	5 2 45.91	40.6898	30.0000	2.00	0.2	6	324	0.2	1.07	0.5	0.3	D1
84 719	617 41.39	40.6640	30.0367	7.83	0.5	9	185	3.2	0.06	0.7	0.6	C1
84 720	2 1 59.43	40.6772	29.9417	10.32	-0.2	6	254	1.5	0.06	2.1	0.7	C1
84 720	2145 3.17	40.6555	29.8600	5.51	0.0	8	300	8.7	0.06	1.2	1.7	C1
84 721	2332 56.43	40.5713	29.9717	9.32	-0.2	10	290	4.1	0.10	1.3	1.1	C1
84 722	716 52.35	40.7503	29.9650	6.58	0.3	8	301	7.5	0.07	1.3	1.5	C1
84 722	914 34.95	40.7402	29.9667	7.35	0.6	10	295	6.4	0.07	1.0	0.8	C1
84 722	1510 49.82	40.7003	29.9833	7.89	0.5	9	235	1.9	0.06	0.9	0.4	C1
84 722	1743 22.76	40.5922	30.1383	9.92	0.1	12	302	9.0	0.12	1.6	1.7	C1
84 723	838 20.55	40.6710	29.9367	10.36	0.1	14	219	2.1	0.08	0.7	0.5	C1
84 723	1237 31.13	40.7050	29.9217	8.41	1.9	12	281	4.0	0.06	0.7	0.9	C1
84 723	1629 42.45	40.6582	29.9367	7.92	0.1	12	180	1.3	0.05	0.4	0.4	B1
84 723	1929 36.00	40.7310	29.9117	8.27	-0.1	9	311	6.8	0.09	1.3	1.2	C1
84 723	2323 26.34	40.6665	29.9450	8.34	0.2	13	175	1.9	0.08	0.6	0.5	B1
84 724	1356 30.61	40.6925	29.9933	9.46	0.4	14	206	0.7	0.08	0.6	0.4	C1
84 725	1742 40.02	40.7288	30.0117	14.39	0.1	9	301	7.0	0.08	1.8	1.0	C1
84 725	2044 31.02	40.6725	29.9500	12.03	0.1	11	182	1.2	0.10	1.3	0.7	C1
84 725	21 2 51.87	40.6445	29.9983	2.53	0.1	10	107	1.5	0.08	0.4	0.6	B1
84 726	217 48.02	40.7073	30.0100	10.66	0.0	12	235	2.3	0.07	0.7	0.5	C1
84 726	456 3.95	40.7003	30.0050	10.32	0.8	14	220	4.5	0.06	0.5	0.4	C1
84 726	459 42.93	40.7030	30.0067	10.50	0.7	14	226	4.8	0.06	0.5	0.4	C1
84 726	12 0 14.13	40.6953	30.0083	10.98	0.3	11	207	4.2	0.09	1.0	0.6	C1
84 727	222 52.12	40.6978	30.0083	10.69	0.8	12	213	4.5	0.07	0.7	0.5	C1
84 727	1531 44.80	40.7537	30.0233	13.24	0.1	10	296	8.1	0.07	1.5	0.8	C1
84 728	336 31.55	40.7417	30.0233	12.44	0.2	11	287	6.3	0.09	1.5	0.7	C1
84 728	19 6 47.05	40.7152	30.0767	10.37	0.2	12	304	2.9	0.07	0.7	0.5	C1
84 728	22 8 40.82	40.7178	30.0717	10.43	0.3	11	297	3.1	0.05	0.6	0.3	C1
84 729	013 6.87	40.6385	30.0517	2.00	-0.5	6	282	0.2	0.61	0.5	0.4	D1

Earthquake epicentres determined within the TDP3 experimental area, 1984.

Origin							Location parameters						
-Date-			---Time---	Latitude °N	Longitude °E	Depth km	Magn M_L	N	Gap	DM	RMS	ERH	ERZ	Q
84	729	632	32.65	40.7192	30.0750	10.10	0.8	13	302	3.3	0.08	0.8	0.5	C1
84	729	8 3	14.54	40.7123	29.9833	10.22	0.9	13	255	4.1	0.06	0.6	0.5	C1
84	729	859	14.90	40.6213	30.0533	9.73	0.7	13	246	1.7	0.06	0.5	0.4	C1
84	729	1129	2.80	40.6990	29.9850	10.23	0.7	11	230	3.0	0.06	0.7	0.5	C1
84	729	1238	43.81	40.6820	30.0633	9.58	0.6	11	165	1.0	0.06	0.6	0.4	B1
84	729	14 4	4.47	40.6470	29.9067	13.67	0.1	7	291	1.7	0.04	0.8	0.4	C1
84	729	20 8	9.30	40.7243	29.9467	8.84	0.3	9	279	4.9	0.12	2.0	1.3	C1
84	729	2136	33.55	40.7203	30.0750	10.75	0.3	12	303	3.4	0.09	1.1	0.6	C1
84	729	2229	13.36	40.7252	30.0750	10.62	1.5	16	304	3.9	0.08	0.8	0.5	C1
84	729	2338	38.33	40.7882	29.9750	9.94	-0.1	7	309	11.3	0.07	2.5	2.7	D1
84	730	950	41.80	40.7540	29.9650	11.57	0.7	12	293	8.1	0.11	1.4	1.0	C1
84	730	951	11.74	40.7680	29.9733	9.68	0.3	10	300	9.1	0.12	1.5	1.5	C1
84	730	1029	36.04	40.7473	29.9733	12.12	0.5	10	288	7.5	0.10	1.4	1.1	C1
84	730	1157	1.79	40.6930	29.9867	9.47	0.3	11	212	1.2	0.09	0.9	0.6	C1
84	730	1324	14.44	40.6987	29.9683	7.41	0.5	13	244	2.2	0.09	0.7	0.5	C1
84	730	1643	59.72	40.7258	29.9267	7.84	0.2	9	304	5.6	0.10	1.4	1.2	C1
84	731	023	3.65	40.5825	30.1367	8.97	0.6	13	302	9.4	0.11	1.4	1.6	C1
84	731	135	59.37	40.7853	30.0083	2.00	0.1	7	323	12.3	0.13	3.1	26.9	D1
84	731	944	7.90	40.7078	29.9867	9.42	1.0	15	247	2.4	0.05	0.4	0.3	C1
84	731	1033	15.43	40.7193	29.9867	9.05	-0.3	11	262	3.6	0.07	0.8	0.5	C1
84	731	2149	30.32	40.7107	29.9800	9.08	0.5	15	254	3.0	0.08	0.6	0.4	C1
84	731	2158	18.05	40.6568	29.9400	3.92	0.5	11	159	1.5	0.07	0.4	0.5	B1
84	801	048	39.65	40.7087	29.9817	9.43	1.0	14	251	3.7	0.05	0.4	0.3	C1
84	801	051	20.09	40.7133	29.9817	9.06	0.6	15	256	3.1	0.07	0.6	0.4	C1
84	801	1 0	28.32	40.7105	29.9867	9.59	0.9	16	252	2.7	0.07	0.6	0.4	C1
84	801	114	43.50	40.7178	29.9867	9.36	-0.2	12	261	3.4	0.06	0.6	0.4	C1
84	801	116	25.13	40.6455	29.9767	7.98	-0.1	9	108	2.1	0.07	0.6	0.6	B1
84	801	158	43.96	40.7073	29.9767	8.80	0.1	13	251	2.9	0.08	0.7	0.5	C1
84	801	210	40.38	40.7093	29.9867	9.34	0.3	14	288	2.5	0.06	0.5	0.4	C1
84	801	223	55.22	40.7120	29.9850	9.13	-0.1	12	254	2.9	0.06	0.6	0.4	C1
84	801	352	34.34	40.6508	29.9717	8.39	1.3	15	74	2.4	0.07	0.4	0.3	A1
84	801	449	13.64	40.7127	29.9883	9.22	0.4	14	292	2.9	0.04	0.4	0.2	C1
84	801	533	52.43	40.7237	29.9883	8.92	0.2	10	299	4.0	0.05	0.7	0.5	C1
84	801	1416	56.86	40.7073	30.0067	6.84	0.3	8	280	5.0	0.12	1.8	2.0	C1
84	801	1540	23.96	40.7272	29.9417	8.57	0.4	12	283	5.3	0.08	0.8	0.7	C1
84	801	1646	44.48	40.7012	29.9683	7.24	-0.1	9	247	2.4	0.09	0.9	0.7	C1
84	801	1853	36.81	40.7047	30.0050	10.43	0.4	15	230	1.9	0.07	0.5	0.4	C1
84	801	22 5	26.05	40.7198	30.0717	10.82	0.2	14	303	3.3	0.08	0.8	0.5	C1
84	802	255	24.41	40.7132	30.0050	9.02	0.0	8	316	2.8	0.05	0.8	0.4	C1
84	802	648	10.86	40.6665	29.9250	7.80	0.1	10	242	2.0	0.08	0.8	0.7	C1
84	802	1038	42.48	40.7095	29.9833	8.83	0.0	11	251	2.7	0.08	0.8	0.5	C1
84	802	12 3	54.70	40.7142	29.9883	8.56	0.0	14	256	3.0	0.06	0.5	0.4	C1
84	802	1210	29.05	40.7163	29.9867	8.87	0.3	14	259	3.3	0.07	0.6	0.5	C1
84	802	13 2	15.97	40.6588	29.9350	8.22	0.2	11	184	1.4	0.09	0.8	0.6	C1
84	802	1328	54.12	40.5800	30.1383	7.85	-0.2	6	303	13.5	0.10	3.6	7.3	D1
84	802	18 1	54.85	40.6832	30.0667	7.82	1.2	15	177	0.8	0.06	0.4	0.3	B1
84	803	220	29.57	40.6708	30.0600	4.68	0.4	13	172	2.3	0.10	0.5	0.7	B1
84	803	812	46.01	40.7070	29.9233	8.20	1.7	15	282	4.1	0.06	0.5	0.4	C1
84	803	1944	47.21	40.6845	30.0183	10.16	1.6	14	176	3.4	0.06	0.5	0.4	B1
84	804	223	43.23	40.6890	30.0217	10.18	0.0	8	181	2.0	0.07	0.9	0.6	C1
84	804	515	57.48	40.7013	29.9467	7.00	0.0	6	272	2.4	0.06	1.1	0.8	C1
84	804	15 5	22.97	40.6858	30.0283	4.31	0.8	14	166	2.5	0.08	0.4	0.5	B1
84	804	2027	22.74	40.7053	29.8817	6.84	1.0	15	300	7.0	0.09	0.8	0.9	C1
84	805	2 1	49.56	40.6420	30.0517	2.00	-0.1	11	179	0.6	0.85	2.9	3.3	D1
84	805	19 4	41.32	40.6853	30.0317	9.42	0.3	13	164	2.9	0.05	0.4	0.4	B1
84	806	1817	0.83	40.6877	29.9950	11.95	0.0	9	185	0.4	0.08	0.8	0.6	C1
84	806	2220	37.34	40.7052	29.9217	8.07	1.7	15	281	4.1	0.07	0.6	0.5	C1
84	807	639	10.47	40.6522	29.8667	7.53	1.1	16	296	5.1	0.08	0.7	0.7	C1
84	807	8 1	1.64	40.6560	29.8650	6.46	0.7	12	297	8.4	0.05	0.5	0.7	C1
84	807	2044	34.16	40.7197	29.9233	8.37	1.2	12	292	5.2	0.06	0.7	0.6	C1
84	807	2128	12.92	40.7238	30.0717	9.68	0.4	12	299	3.8	0.06	0.6	0.5	C1
84	808	8 3	22.54	40.6723	29.9250	5.86	0.2	6	252	2.6	0.02	0.4	0.3	C1
84	808	1530	1.31	40.6270	30.0433	9.71	0.4	9	224	1.2	0.06	0.7	0.5	C1
84	809	1220	11.84	40.6502	29.8667	5.91	0.4	10	295	5.0	0.10	1.2	1.4	C1
84	809	1625	0.33	40.7438	30.0383	13.54	0.4	12	292	6.5	0.08	1.0	0.8	C1
84	810	853	19.41	40.7020	29.9867	10.66	0.2	7	235	3.4	0.06	1.3	0.7	C1
84	810	1816	1.94	40.6597	29.9933	10.67	0.2	10	105	0.6	0.06	0.6	0.5	B1
84	810	2113	14.20	40.6807	30.0617	6.96	0.6	11	157	1.2	0.06	0.5	0.5	B1

Earthquake epicentres determined within the TDP3 experimental area, 1984.

Origin							Location parameters						
-Date-		---Time---		Latitude °N	Longitude °E	Depth km	Magn M_L	N	Gap	DM	RMS	ERH	ERZ	Q
84	810	23 4	46.13	40.6478	29.9750	6.57	0.1	10	81	2.4	0.03	0.3	0.4	A1
84	810	2317	23.01	40.6290	30.0433	9.45	0.9	11	211	1.1	0.06	0.6	0.5	C1
84	810	2321	3.85	40.6257	30.0450	8.30	-0.2	6	237	4.9	0.03	0.6	0.7	C1
84	811	820	58.35	40.6410	30.0233	9.06	0.1	7	135	2.3	0.13	1.4	2.0	C1
84	811	15 5	0.17	40.6657	30.0383	6.81	0.3	10	118	3.4	0.09	0.7	1.0	B1
84	811	1839	24.27	40.6868	29.9617	9.51	0.4	11	233	0.7	0.06	0.6	0.5	C1
84	811	2220	23.79	40.6920	30.0817	12.52	0.5	10	297	1.1	0.06	0.7	0.5	C1
84	812	1 6	13.96	40.6495	29.9733	7.08	0.6	10	71	2.4	0.04	0.3	0.5	A1
84	812	3 2	0.39	40.6905	30.0000	9.19	-0.2	7	271	0.3	0.03	0.5	0.4	C1
84	812	2320	29.60	40.6612	30.0383	5.89	0.2	13	121	2.9	0.04	0.2	0.3	B1
84	813	050	54.00	40.6743	29.8533	10.03	0.0	13	305	6.8	0.06	0.6	0.7	C1
84	813	327	31.11	40.6958	29.9883	9.69	0.2	12	217	1.2	0.07	0.6	0.5	C1
84	813	841	40.86	40.6665	29.9533	8.16	-0.2	11	143	1.6	0.08	0.7	0.5	B1
84	813	9 8	16.24	40.7088	29.9217	3.25	0.5	12	293	4.3	0.06	0.5	0.7	C1
84	813	1717	30.81	40.6478	29.9783	8.43	0.8	11	83	2.1	0.06	0.5	0.6	A1
84	813	2351	45.08	40.7665	30.0467	11.67	0.9	10	309	8.7	0.07	1.4	1.1	C1
84	814	918	50.41	40.7788	30.0950	12.20	0.5	9	328	10.1	0.06	1.4	1.6	C1
84	814	1747	19.07	40.6097	29.9667	9.77	0.4	10	178	2.4	0.05	0.5	0.4	B1
84	814	918	50.41	40.7788	30.0950	12.20	0.5	9	328	10.1	0.06	1.4	1.6	C1
84	814	1747	19.08	40.6102	29.9683	9.66	0.4	10	177	2.5	0.08	0.9	0.7	B1
84	814	2052	49.63	40.6327	30.0217	10.32	-0.3	8	259	2.9	0.07	1.8	0.7	C1
84	814	2246	1.70	40.6257	30.0517	10.63	0.8	11	241	1.2	0.05	0.6	0.6	C1
84	814	2357	5.82	40.6528	29.9733	7.19	0.5	10	74	2.3	0.03	0.2	0.4	A1
84	815	1754	13.14	40.6968	30.0033	9.29	0.3	12	212	1.0	0.06	0.6	0.6	C1
84	816	954	14.21	40.7297	30.0300	8.37	0.6	7	275	5.3	0.02	0.6	0.3	C1
84	816	2318	26.76	40.6943	30.0250	8.78	0.9	9	202	2.4	0.08	1.1	0.8	C1
84	817	829	58.76	40.6992	30.0333	9.83	0.0	10	216	3.2	0.07	1.0	0.5	C1
84	817	1354	14.98	40.7040	30.0317	9.72	0.5	9	228	3.3	0.07	1.1	0.7	C1
84	817	2336	42.95	40.7048	29.9917	8.28	-0.3	8	236	1.9	0.11	1.4	1.0	C1
84	818	548	54.51	40.6538	29.9750	7.66	0.6	7	130	2.1	0.05	0.6	0.7	B1
84	819	2043	46.62	40.7225	29.9300	9.86	0.9	10	291	5.2	0.09	1.3	0.9	C1
84	820	1733	5.28	40.7007	30.1300	10.07	0.6	10	332	5.2	0.08	1.3	0.9	C1
84	820	1749	56.08	40.7358	30.0417	11.22	0.0	7	286	5.6	0.11	1.9	1.4	C1
84	821	723	27.91	40.6703	29.8583	2.00	0.0	6	303	8.5	0.05	1.5	8.5	D1
84	821	1217	0.74	40.6763	29.9400	10.82	0.1	10	251	1.6	0.06	0.9	0.5	C1
84	821	1950	10.26	40.6997	30.0833	8.62	0.1	9	327	1.6	0.10	1.2	0.8	C1
84	822	1634	38.65	40.6728	29.9467	10.75	0.1	8	223	1.3	0.06	1.0	0.7	C1
84	822	2126	26.84	40.6917	30.0517	9.49	0.9	9	192	1.5	0.09	1.3	0.8	C1
84	823	149	52.58	40.6577	29.9183	6.36	0.0	7	249	4.2	0.07	1.3	0.9	C1
84	823	3 2	23.50	40.6777	29.9767	8.43	0.0	6	218	2.2	0.05	1.1	0.9	C1
84	825	344	11.18	40.6267	30.0483	10.13	0.7	14	238	1.1	0.04	0.4	0.3	C1
84	825	2048	16.90	40.6872	30.0383	8.32	1.0	12	171	2.6	0.03	0.2	0.2	B1
84	826	759	49.06	40.6942	30.0250	8.52	0.2	12	266	2.4	0.05	0.4	0.4	C1
84	827	1129	14.38	40.6630	30.0383	7.10	0.3	11	117	3.1	0.06	0.4	0.5	B1
84	827	1148	14.12	40.6672	30.0333	10.29	0.3	11	105	3.7	0.08	0.5	0.6	B1
84	827	2219	51.21	40.6697	29.9567	10.01	0.4	13	142	1.3	0.04	0.3	0.3	B1
84	828	326	20.15	40.6385	30.0517	2.00	-0.1	6	203	0.2	0.39	1.8	1.2	D1
84	828	2017	14.32	40.7285	29.9650	13.23	1.0	12	276	5.3	0.05	0.5	0.5	C1
84	829	2343	39.28	40.6945	29.9933	14.16	-0.3	9	211	3.4	0.11	1.3	0.9	C1
84	830	357	33.31	40.7083	30.0000	10.01	1.7	13	239	2.2	0.04	0.4	0.3	C1
84	830	415	37.41	40.6315	30.0450	9.31	0.3	14	207	0.8	0.05	0.3	0.3	C1
84	830	9 6	29.64	40.6965	29.9733	7.54	0.7	13	238	2.2	0.05	0.4	0.3	C1
84	830	2215	30.55	40.6400	29.9600	2.00	0.0	6	167	4.6	0.52	0.7	1.8	D1
84	901	037	15.10	40.6937	29.9683	7.49	0.0	12	238	1.6	0.05	0.4	0.4	C1
84	903	1413	9.08	40.7048	29.9433	7.91	0.9	12	279	2.9	0.02	0.2	0.1	C1
84	904	1959	57.48	40.6283	30.0467	9.73	0.7	11	230	1.0	0.06	0.5	0.4	C1
84	906	331	8.95	40.7460	29.9950	6.59	0.0	11	311	6.4	0.04	0.6	0.6	C1
84	907	2011	11.77	40.6520	29.8700	9.19	1.1	15	293	4.8	0.03	0.3	0.3	C1
84	908	246	35.04	40.6683	29.9700	8.27	-0.2	9	169	2.7	0.03	0.4	0.3	B1
84	908	627	33.45	40.6280	30.0450	8.79	0.7	14	224	1.1	0.03	0.3	0.2	C1
84	909	2145	54.77	40.7427	29.9900	6.44	0.1	9	309	6.1	0.08	1.0	1.0	C1
84	910	315	15.83	40.7435	30.0917	10.60	0.0	12	318	6.2	0.04	0.5	0.5	C1
84	910	1524	13.05	40.6873	30.0417	7.99	0.1	12	178	2.4	0.06	0.4	0.4	B1
84	910	1659	53.86	40.6887	30.0400	7.61	0.1	11	178	2.5	0.02	0.2	0.2	B1
84	910	1812	32.56	40.6888	30.0883	4.61	0.3	11	294	1.5	0.05	0.4	0.4	C1
84	910	1817	4.32	40.6563	29.9033	7.80	0.0	10	266	2.1	0.04	0.5	0.3	C1
84	910	2023	17.34	40.7318	29.9833	7.84	1.3	14	275	5.0	0.08	0.7	0.6	C1
84	910	22 7	25.49	40.7280	29.9817	7.49	0.8	13	272	4.6	0.05	0.5	0.3	C1

Earthquake epicentres determined within the TDP3 experimental area, 1984.

Origin							Location parameters						
-Date-	——Time——		Latitude °N	Longitude °E	Depth km	Magn M_L	N	Gap	DM	RMS	ERH	ERZ	Q
84 910	2310	13.93	40.7342	29.9833	7.11	-0.1	8	306	5.3	0.06	0.8	0.6	C1
84 911	038	29.94	40.7275	29.9017	8.41	-0.2	11	311	7.0	0.05	0.7	0.6	C1
84 911	130	33.60	40.7182	29.9667	9.26	-0.3	8	297	4.2	0.07	0.8	0.7	C1
84 911	7 5	40.81	40.6598	29.9000	5.96	0.4	12	273	2.6	0.04	0.3	0.3	C1
84 911	714	28.74	40.6592	29.9117	4.79	-0.2	9	260	1.8	0.05	0.5	0.5	C1
84 911	1920	6.17	40.7310	29.9833	7.39	0.3	13	274	4.9	0.07	0.5	0.5	C1
84 911	2253	47.11	40.6790	29.8983	3.57	1.0	15	286	4.1	0.09	0.6	0.7	C1
84 911	2254	15.72	40.6827	29.9083	2.00	-0.1	8	283	4.1	0.06	1.0	1.3	C1
84 911	2351	15.10	40.6813	29.9133	2.69	0.3	9	279	3.8	0.05	0.6	0.6	C1
84 912	033	24.75	40.6948	29.9733	7.50	0.1	13	233	2.0	0.06	0.4	0.4	C1
84 912	13 2	7.98	40.6768	29.8950	4.31	0.4	7	302	4.1	0.06	0.9	1.1	C1
84 912	14 0	12.62	40.6602	29.9067	5.38	1.6	13	266	2.2	0.04	0.3	0.3	C1
84 912	1814	51.66	40.6797	29.9050	2.09	0.4	13	282	3.9	0.06	0.5	0.7	C1
84 912	1822	14.18	40.6808	29.9517	11.01	0.6	15	227	0.5	0.04	0.3	0.2	C1
84 912	2253	46.31	40.6557	29.9017	5.85	-0.2	8	269	2.3	0.03	0.4	0.4	C1
84 914	1842	23.55	40.6983	29.9067	5.17	1.1	13	294	4.8	0.06	0.5	0.5	C1
84 915	332	34.80	40.7158	29.9250	8.91	1.0	13	297	4.7	0.04	0.4	0.3	C1
84 916	1311	16.53	40.6827	29.9550	7.20	1.2	15	229	0.3	0.05	0.3	0.3	C1
84 916	20 3	40.05	40.6912	29.9533	10.40	0.1	15	245	1.2	0.05	0.4	0.3	C1
84 917	013	24.24	40.6940	29.9750	6.95	0.1	13	228	2.1	0.06	0.4	0.4	C1
84 918	139	6.74	40.6920	29.9600	10.04	-0.3	11	247	1.2	0.06	0.6	0.4	C1
84 918	844	35.22	40.6942	29.9583	10.24	-0.2	11	254	1.5	0.04	0.4	0.3	C1
84 918	1256	41.52	40.6212	30.0200	10.50	0.2	14	194	2.8	0.05	0.4	0.3	C1
84 918	18 6	46.50	40.6963	29.9583	10.23	-0.1	9	258	1.7	0.04	0.4	0.3	C1
84 918	2236	58.95	40.6095	29.9633	10.12	-0.2	10	174	2.1	0.05	0.4	0.4	B1
84 919	135	44.06	40.7105	29.9100	7.09	0.1	14	291	5.2	0.10	0.9	0.8	C1
84 919	18 0	30.31	40.6523	29.8917	10.00	0.6	13	277	3.0	0.05	0.4	0.4	C1
84 919	2026	25.73	40.6882	30.0217	10.55	0.2	14	178	1.9	0.04	0.3	0.3	B1
84 920	447	49.55	40.7387	29.9800	8.57	0.3	13	281	5.8	0.07	0.7	0.6	C1
84 920	1853	55.39	40.7185	29.8700	6.74	0.3	8	305	8.5	0.10	1.7	2.3	C1
84 920	1854	29.67	40.7185	29.8833	8.43	1.1	12	302	7.6	0.07	0.8	0.8	C1
84 921	027	54.33	40.7080	29.9500	8.51	0.3	12	265	3.1	0.04	0.4	0.3	C1
84 921	028	31.10	40.7105	29.9517	8.87	0.2	12	266	3.3	0.06	0.7	0.4	C1
84 921	1944	51.64	40.6930	29.9667	7.91	0.1	11	238	1.5	0.06	0.7	0.4	C1
84 921	2141	41.99	40.6728	29.9200	8.92	-0.1	10	267	2.8	0.03	0.4	0.3	C1
84 922	1 5	44.67	40.6518	29.9017	10.14	0.2	14	266	2.1	0.04	0.4	0.2	C1
84 922	139	4.43	40.5722	29.9900	10.95	0.6	14	272	5.1	0.07	0.7	0.4	C1
84 922	1756	1.31	40.6772	30.0717	2.00	0.9	11	206	1.4	0.82	2.0	2.7	D1
84 922	2023	1.50	40.6157	30.0500	5.33	0.0	11	249	2.4	0.05	0.4	0.4	C1
84 924	050	32.62	40.6127	30.0467	8.24	-0.3	8	249	2.7	0.18	3.2	1.7	D1
84 924	234	21.56	40.7297	29.9383	8.63	0.0	12	286	5.7	0.08	0.8	0.7	C1
84 924	816	13.80	40.7270	29.9417	10.36	0.8	13	304	5.3	0.15	1.5	1.2	C1
84 924	1152	1.95	40.6747	29.9483	10.67	0.9	14	196	1.1	0.04	0.3	0.2	C1
84 924	2126	40.40	40.7223	29.9917	9.28	1.6	13	265	3.8	0.07	0.7	0.7	C1
84 924	2211	6.51	40.6857	30.0517	8.65	0.0	11	158	1.5	0.04	0.4	0.4	B1
84 924	2318	50.37	40.6957	29.9167	2.26	0.3	12	287	3.9	0.15	1.2	2.1	C1
84 924	2329	32.39	40.6630	30.0350	6.08	0.1	10	110	3.0	0.02	0.2	0.3	B1
84 925	1236	51.53	40.6642	29.9667	7.83	0.3	10	94	2.0	0.03	0.3	0.2	B1
84 925	1456	53.46	40.7247	30.0083	8.60	0.1	9	299	4.1	0.04	0.6	0.4	C1
84 926	1618	19.23	40.6887	30.0517	9.43	0.7	13	175	1.5	0.05	0.4	0.3	B1
84 927	17 2	29.22	40.6592	29.9267	6.21	0.3	8	230	1.2	0.04	0.4	0.4	C1
84 928	859	57.96	40.6810	29.9367	6.50	-0.1	8	249	1.8	0.02	0.3	0.3	C1
84 929	3 0	31.89	40.6728	29.9467	10.87	0.4	14	196	1.3	0.04	0.3	0.3	C1
84 929	1123	1.33	40.6505	29.8983	10.16	1.1	15	269	2.4	0.06	0.5	0.4	C1
84 929	1941	52.99	40.6205	29.9383	9.41	-0.1	8	203	2.2	0.25	3.4	2.6	D1
84 929	22 1	30.69	40.6817	30.0233	11.10	0.1	9	246	3.4	0.04	0.6	0.3	C1
84 930	941	17.80	40.6868	29.9550	10.26	0.9	13	239	0.7	0.03	0.3	0.2	C1
84 930	1055	15.95	40.6483	29.9867	7.61	-0.1	8	168	2.2	0.04	0.5	0.4	B1
84 930	1655	54.95	40.6973	30.0217	9.25	-0.1	8	210	4.2	0.03	0.4	0.5	C1
84 930	1742	6.42	40.6655	30.0533	7.10	0.2	11	159	3.0	0.05	0.4	0.5	B1
84 930	1745	43.31	40.6697	29.9417	8.42	-0.1	8	228	1.9	0.04	0.5	0.4	C1
84 930	23 3	51.83	40.6918	29.9567	10.53	1.6	12	244	1.2	0.03	0.3	0.3	C1
841001	227	23.47	40.6685	30.0033	9.32	0.2	12	77	1.2	0.03	0.2	0.3	A1
841001	310	14.64	40.6505	29.9750	7.90	0.6	11	84	2.2	0.03	0.3	0.3	A1
841001	1022	18.60	40.6672	30.0033	9.28	0.1	11	75	2.4	0.04	0.3	0.3	A1
841001	2051	5.60	40.6638	30.0033	9.71	-0.1	10	126	0.8	0.03	0.2	0.3	B1
841002	013	0.79	40.7088	29.9917	10.43	0.0	10	244	2.3	0.03	0.4	0.4	C1
841002	12 6	52.04	40.6605	29.9200	6.30	0.2	8	251	1.5	0.02	0.3	0.2	C1

Earthquake epicentres determined within the TDP3 experimental area, 1984.

Origin						Location parameters					
-Date-	---Time---	Latitude °N	Longitude °E	Depth km	Magn M_L	N	Gap	DM	RMS	ERH	ERZ	Q
841003	1448 2.13	40.7102	29.9333	6.95	0.6	13	277	3.9	0.06	0.5	0.4	C1
841004	213 28.67	40.6892	29.9517	9.95	1.2	14	244	1.0	0.05	0.4	0.3	C1
841004	354 30.36	40.6053	29.8767	7.10	0.1	11	303	5.5	0.03	0.3	0.3	C1
841004	644 39.48	40.6923	29.9517	10.28	0.4	11	272	1.4	0.03	0.3	0.2	C1
841004	1852 56.18	40.6913	29.9583	10.36	0.6	13	241	1.2	0.03	0.3	0.3	C1
841006	17 9 25.34	40.7010	30.1200	10.19	-0.3	7	331	4.5	0.04	0.8	0.7	C1
841006	20 1 42.41	40.6522	29.9733	7.66	0.0	10	123	2.2	0.02	0.2	0.2	B1
841006	21 6 25.05	40.7248	29.9600	8.94	0.3	13	303	4.9	0.06	0.6	0.5	C1
841006	2327 40.62	40.5452	29.9750	7.45	0.1	7	303	6.7	0.04	0.9	0.7	C1
841007	347 35.70	40.6502	29.8517	7.22	-0.2	7	303	6.4	0.10	2.3	2.5	C1
841007	12 5 16.17	40.6917	30.1417	9.27	0.1	9	323	6.1	0.03	0.4	0.3	C1
841007	2145 1.74	40.6503	29.8717	8.37	1.0	11	296	4.7	0.04	0.5	0.5	C1
841007	23 5 1.71	40.6758	29.9517	10.17	-0.3	7	217	3.7	0.02	0.6	0.4	C1
841008	222 23.21	40.6705	29.9617	8.69	-0.3	7	186	3.7	0.03	0.7	0.5	C1
841008	648 20.91	40.6892	30.0533	8.57	0.5	10	178	1.4	0.03	0.4	0.3	B1
841008	1137 9.90	40.6668	29.9567	7.70	-0.1	10	185	3.3	0.06	0.5	0.6	C1
841008	1220 58.24	40.6860	30.0267	9.17	0.0	6	167	2.3	0.02	0.4	0.5	B1
841008	1721 56.45	40.7118	29.8617	6.53	0.2	10	312	9.0	0.05	0.8	1.3	C1
841009	022 59.91	40.7175	29.9617	9.56	0.6	11	295	4.5	0.07	0.7	0.6	C1
841009	1545 33.73	40.6912	29.9783	7.74	0.1	11	228	1.7	0.07	0.6	0.5	C1
841009	2321 21.70	40.7137	30.0683	10.41	-0.1	12	294	2.6	0.08	0.8	0.8	C1
841010	1415 16.68	40.6892	29.9600	10.20	0.9	11	240	3.3	0.05	0.5	0.4	C1
841010	1439 29.79	40.6518	29.8917	9.54	0.3	8	318	3.0	0.03	0.5	0.4	C1
841010	1717 51.26	40.6787	29.9033	2.42	0.3	9	283	3.9	0.11	1.1	1.7	C1
841011	928 44.55	40.6160	30.0583	8.60	0.2	10	254	2.4	0.06	0.7	0.4	C1
841011	1636 34.05	40.7220	29.9583	8.73	0.2	12	300	4.6	0.06	0.6	0.4	C1
841012	015 41.32	40.7168	29.9300	8.54	-0.1	9	297	4.6	0.07	1.0	0.8	C1
841012	15 7 26.66	40.6747	29.9900	6.36	0.9	15	100	1.6	0.04	0.2	0.2	B1
841013	024 49.08	40.6952	29.9017	7.45	1.0	15	291	5.1	0.08	0.7	0.5	C1
841014	015 28.31	40.7128	29.8667	9.68	0.0	10	311	8.5	0.06	0.8	0.9	C1
841014	1619 43.43	40.6973	29.9400	7.57	-0.2	8	270	2.4	0.03	0.5	0.3	C1
841014	20 0 16.32	40.6303	30.0467	8.94	0.4	9	229	0.8	0.06	0.6	0.5	C1
841014	20 1 19.55	40.6328	30.0450	9.21	0.7	12	198	0.7	0.05	0.4	0.3	C1
841014	2355 1.36	40.6783	29.9850	7.37	-0.2	10	128	1.5	0.06	0.5	0.4	B1
841015	6 3 39.78	40.5643	29.9883	8.29	0.2	11	282	5.6	0.07	0.7	0.7	C1
841015	1243 4.79	40.6280	30.0433	9.13	0.4	12	232	4.7	0.04	0.4	0.4	C1
841015	2151 26.18	40.7203	29.8667	8.92	0.0	8	307	9.5	0.07	1.1	1.2	C1
841015	2242 49.64	40.6893	30.0783	4.27	0.1	8	286	0.8	0.04	0.4	0.4	C1
841016	8 8 6.23	40.6537	29.9050	8.79	0.4	11	263	1.9	0.05	0.4	0.4	C1
841016	1056 17.92	40.6268	30.0483	9.66	0.5	12	237	1.1	0.06	0.5	0.5	C1
841017	727 9.85	40.6898	30.0050	2.00	0.1	9	194	0.5	0.75	3.8	2.9	D1
841018	153 25.73	40.6940	29.8950	7.06	1.1	13	293	5.6	0.06	0.5	0.5	C1
841018	1120 39.77	40.6267	30.0417	8.55	-0.1	6	216	1.4	0.04	0.7	0.6	C1
841019	2 2 52.76	40.6705	29.8567	10.74	0.4	11	304	6.4	0.04	0.5	0.4	C1
841019	630 37.11	40.6552	29.9300	6.25	0.2	10	200	0.8	0.03	0.3	0.2	C1
841019	1119 11.66	40.6688	29.9133	12.76	0.4	9	268	2.5	0.04	0.6	0.4	C1
841019	1625 26.85	40.7175	29.8700	6.60	0.7	15	305	8.4	0.08	0.8	1.0	C1
841019	1717 5.20	40.6667	29.9100	12.52	0.2	12	268	2.4	0.09	1.1	0.6	C1
841019	1733 57.68	40.6620	29.8717	7.92	-0.2	10	295	4.9	0.08	1.3	0.8	C1
841020	5 6 58.93	40.6287	30.0483	9.40	0.4	14	236	0.9	0.13	0.9	0.8	C1
841020	2046 32.55	40.6758	29.9450	7.89	-0.1	13	217	1.3	0.07	0.6	0.4	C1
841021	1545 13.90	40.6535	29.9717	8.23	0.4	14	77	2.4	0.06	0.4	0.4	A1
841021	1635 19.16	40.6768	30.0650	9.49	0.6	13	184	1.5	0.08	0.8	0.4	C1
841022	358 50.78	40.6288	30.0483	9.92	1.0	14	236	0.9	0.08	0.7	0.5	C1
841022	437 37.41	40.6300	30.0433	9.72	0.0	12	213	1.0	0.07	0.6	0.4	C1
841022	1141 10.83	40.7697	30.0533	11.06	0.3	7	312	9.0	0.08	1.7	1.8	C1
841023	235 45.98	40.6937	29.9583	9.99	0.0	15	245	1.4	0.08	0.7	0.5	C1
841023	1817 7.60	40.6258	30.0533	9.27	-0.2	10	243	5.7	0.11	1.5	1.4	C1
841023	1932 49.76	40.6170	29.9733	7.76	0.5	14	164	1.7	0.06	0.4	0.4	B1
841023	2020 15.92	40.7268	30.0033	6.90	0.2	15	269	4.3	0.09	0.6	0.8	C1
841023	21 7 56.93	40.7258	30.0083	6.63	0.9	14	267	4.3	0.05	0.4	0.4	C1
841023	2119 3.15	40.7402	30.0250	5.09	0.1	11	309	6.2	0.06	0.7	0.9	C1
841023	2130 43.04	40.6138	29.9300	5.71	-0.2	12	212	1.8	0.06	0.4	0.4	C1
841024	338 28.26	40.6597	29.9683	6.07	0.1	15	89	2.5	0.07	0.4	0.4	A1
841024	338 34.60	40.6607	29.9733	5.46	0.0	14	80	2.3	0.10	0.5	0.6	A1
841024	4 5 6.21	40.6620	29.9667	6.42	0.2	15	96	2.2	0.07	0.4	0.4	B1
841024	538 39.84	40.7315	30.0083	6.31	0.3	11	274	4.9	0.05	0.8	0.6	C1
841024	1958 0.85	40.6502	29.8833	8.56	-0.2	10	284	3.7	0.05	0.6	0.6	C1

Earthquake epicentres determined within the TDP3 experimental area, 1984.

Origin						Location parameters						
-Date-	---Time---		Latitude °N	Longitude °E	Depth km	Magn M_L	N	Gap	DM	RMS	ERH	ERZ	Q
841024	2138	13.73	40.6243	30.0550	9.57	-0.2	14	245	1.4	0.19	1.4	1.1	C1
841024	2229	15.96	40.6825	29.9600	11.63	-0.4	9	223	3.4	0.06	1.0	0.5	C1
841025	1050	1.01	40.6318	30.0433	9.87	0.3	13	202	0.8	0.08	0.6	0.5	C1
841025	1724	40.78	40.7792	30.1067	12.94	0.4	13	328	10.4	0.08	1.3	1.1	C1
841026	618	19.17	40.6958	29.9567	10.65	0.7	16	248	1.7	0.07	0.6	0.4	C1
841026	648	49.82	40.6502	29.8517	4.14	0.3	11	303	6.4	0.06	0.7	1.3	C1
841026	1636	40.64	40.6287	30.0467	9.57	0.2	16	227	1.0	0.07	0.5	0.4	C1
841026	2040	35.50	40.6282	30.0483	9.49	0.2	15	235	1.0	0.09	0.6	0.5	C1
841027	1	9 20.32	40.7852	30.1167	13.04	0.7	14	330	11.3	0.08	1.2	0.9	C1
841027	228	58.93	40.6717	29.9467	10.72	0.7	16	188	1.4	0.07	0.5	0.4	C1
841027	634	42.45	40.6570	29.9133	11.66	-0.3	12	256	1.5	0.05	0.4	0.3	C1
841027	737	11.72	40.5837	30.1317	8.28	0.0	13	301	9.0	0.11	1.1	1.6	C1
841027	812	4.16	40.6240	30.0450	9.31	0.0	15	237	1.5	0.07	0.5	0.4	C1
841027	938	14.54	40.6553	29.8967	10.26	0.4	16	272	2.6	0.07	0.6	0.4	C1
841028	340	5.27	40.6537	29.9300	6.86	-0.4	9	193	0.6	0.08	0.7	0.6	C1
841028	442	59.08	40.6018	30.1100	10.33	0.6	15	289	6.4	0.09	0.8	0.6	C1
841029	244	6.92	40.7068	30.0083	9.91	1.1	16	234	2.2	0.06	0.4	0.3	C1
841029	628	3.02	40.6738	29.9517	8.37	-0.3	16	180	1.0	0.05	0.3	0.3	C1
841029	1836	48.63	40.7182	30.0117	11.10	0.2	12	255	3.5	0.07	0.7	0.6	C1
841029	1838	47.41	40.7172	30.0150	11.28	0.4	14	253	3.5	0.07	0.6	0.4	C1
841029	1839	14.84	40.7108	30.0133	10.94	-0.1	14	241	2.8	0.04	0.3	0.2	C1
841029	1843	36.56	40.7130	30.0100	11.38	0.0	13	246	2.9	0.05	0.4	0.3	C1
841029	1844	18.12	40.7158	30.0133	11.39	0.1	14	251	3.3	0.07	0.6	0.5	C1
841031	222	11.62	40.6898	29.9517	9.32	1.7	9	265	3.9	0.04	0.6	0.5	C1
841031	229	1.29	40.6902	29.9533	9.53	1.0	9	265	3.9	0.04	0.5	0.5	C1
841031	245	48.30	40.6917	29.9517	9.86	0.7	9	266	4.0	0.03	0.4	0.3	C1
841031	344	37.11	40.6902	29.9533	9.53	1.0	9	264	3.8	0.04	0.6	0.5	C1

Appendix B

The author's contribution to TDP3

This appendix contains details of the author's contribution to the TDP3 project, and of papers, reports, and various oral presentations of material which forms the basis for this thesis. Copies of the paper and two internal reports are bound into the end of the thesis as Appendix C.

B.1 The author's contribution

The author was part of a BGS team which carried out the third Turkish Dilatancy Project in 1984. The author was involved from an early planning stage, was primarily responsible for the logistic arrangements, and undertook a seven-month period of foreign service in Turkey installing and maintaining the networks. The bulk of the data processing and preliminary interpretation (locations, magnitudes, fault-plane solutions etc.), and the preparation of archives and additional specialised plots for use by other team members when the team returned to Edinburgh was also the author's responsibility.

Throughout this analytical work, carried out under the overall supervision of Dr. S. Crampin, the author relied heavily on the expertise of Dr. J. R. Evans for day-to-day discussion, help and guidance. As a result of discussion with Dr. Crampin and BGS line management, it was agreed that the author could use these BGS earthquake data, together with additional private research on fault-plane solutions and clustering, as the basis for a thesis. This research was also guided by Dr. Crampin but again with much discussion with Dr. Evans and Dr. A. L. L. Logan.

The results of the TDP3 experiment were written up by the author as one of a series published by BGS staff on the TDP projects (section B.2), and presented at various conferences (section B.4), and are used here with the permission of the co-authors. In addition, a symposium presenting the results of the TDP projects and their application to earthquake prediction was organised at BGS, Edinburgh, chiefly by the author, and financed by the Overseas Development Administration. Internal reports on this symposium were written by the author for submission to outside journals and are bound into

Appendix C at the back of this thesis by permission of Director, BGS; they have not been referenced in the text.

B.2 Published papers

Lovell, J. H., Crampin, S., Evans, R. & Üçer, S. B., 1987. Microearthquakes in the TDP swarm, Turkey: clustering in space and time. *Geophysical Journal of the Royal Astronomical Society*, **91**, 313-330. (Appendix C)

Lovell, J. H., 1988. A possibility for earthquake prediction? *Geology Today*, **4(4)**, 139-141.

Lovell, J. H., 1988. Symposium on a technique for earthquake prediction and monitoring *in situ* stress. *British Geologist*, **14(1)**, 16.

B.3 Internal reports

Lovell, J. H., Stuart Crampin, Russ Evans & Balamir Üçer, 1987a. Microearthquakes in the TDP swarm, Turkey: clustering in space and time. *Global Seismology Research Group Report No. 336, Aug 1987.* (submitted to *Geophys. J. R. astr. Soc.*)

Lovell, J. H., 1987b. Report on a symposium on Earthquake Prediction held at BGS, Edinburgh 28 June - 1 July 1987. *Global Seismology Research Group Report No. 342, Sept 1987.* (submitted to Geology Today).

Lovell, J. H., 1987c. Symposium on a technique for earthquake prediction and monitoring *in situ* stress. *Global Seismology Research Group Report No. 343, Sept 1987.* (submitted to British Geologist).

B.4 Oral presentations

B.4.1 UKGA11, Durham

Lovell, J. H., Crampin, S. & Evans, R., 1987. Clustering in space

and time of microearthquakes in a swarm in Turkey. *Geophysical Journal of the Royal Astronomical Society*, **89**, p 464 (abs.).

B.4.2 ODA-sponsored symposium held at BGS, Edinburgh, 29 June - 1 July 1987, entitled "Extensive-dilatancy anisotropy: an important new tool for earthquake prediction"

Lovell, J. H., Crampin, S. & Evans, R., 1987. Clustering in space and time of microearthquakes in a swarm in Turkey.

Appendix C

Published Papers

Lovell, J. H., Crampin, S., Evans, R. & Üçer, S. B., 1987. Microearthquakes in the TDP swarm, Turkey: clustering in space and time. *Geophysical Journal of the Royal Astronomical Society*, **91**, 313-330.

Lovell, J. H., 1987b. Report on a symposium on Earthquake Prediction held at BGS, Edinburgh 28 June - 1 July 1987. *Global Seismology Research Group Report No. 342, Sept 1987.* (also published in *Geology Today*).

Lovell, J. H., 1987c. Symposium on a technique for earthquake prediction and monitoring *in situ* stress. *Global Seismology Research Group Report No. 343, Sept 1987.* (also published in *British Geologist*).

Geophys. J. R. astr. Soc. (1987) **91**, 313–330

Microearthquakes in the TDP swarm, Turkey: clustering in space and time

John Lovell, Stuart Crampin and Russ Evans *British Geological Survey, Murchison House, West Mains Road, Edinburgh EH9 3LA, Scotland, UK*

S. Balamir Üçer *Kandilli Observatory and Centre for Development in Space and Earth Science, Çengelköy, Istanbul, Turkey.*

Accepted 1987 July 28. Received 1987 July 27; in original form 1987 March 12

Summary. The third occupation (experiment TDP3) of recording sites above a persistent swarm of microearthquakes near the North Anatolian Fault, with a larger seismic network and over a longer period of time, confirms and refines previous observations with greater resolution. The greater resolution in earthquake locations has revealed marked clustering in time and space. Many, perhaps most, of the earthquakes belong to clusters, where successive earthquakes originate in a very small volume and have similar fault mechanisms. Such studies allow the progression of seismic activity of small earthquakes to be followed in some detail, and may reveal features which are hidden in larger and more complex earthquake sequences.

1 Introduction

A swarm of small earthquakes near the North Anatolian Fault (NAF) in Turkey was monitored during the Turkish Dilatancy Projects, TDP1 in 1979, TDP2 in 1980 (Crampin et al. 1985) and TDP3 in 1984 (Evans et al. 1987). The persistent swarm of microearthquakes is associated with the southern limb of a graben structure beneath the hills south-east of Izmit, at the eastern end of the Marmara Sea (Fig. 1). Here the nature of the North Anatolian Fault (NAF) changes, and it has been suggested (Evans et. al. 1985) that this is a key area for understanding the complex tectonics of Western Anatolia. East of the Marmara Sea, the North Anatolian Fault is a prominent, east-west trending dextral strike-slip fault. With an offset of up to 90km, it separates the massive Eurasian-Black Sea plate to the north from the westward-migrating Anatolian plate to the south and forms a well-defined zone of parallel rifts with associated tensional features (pull-apart basins, sag ponds etc.). For a fuller description of the NAF the reader is referred to Dewey & Şengör (1979), Şengör (1979) and Şengör

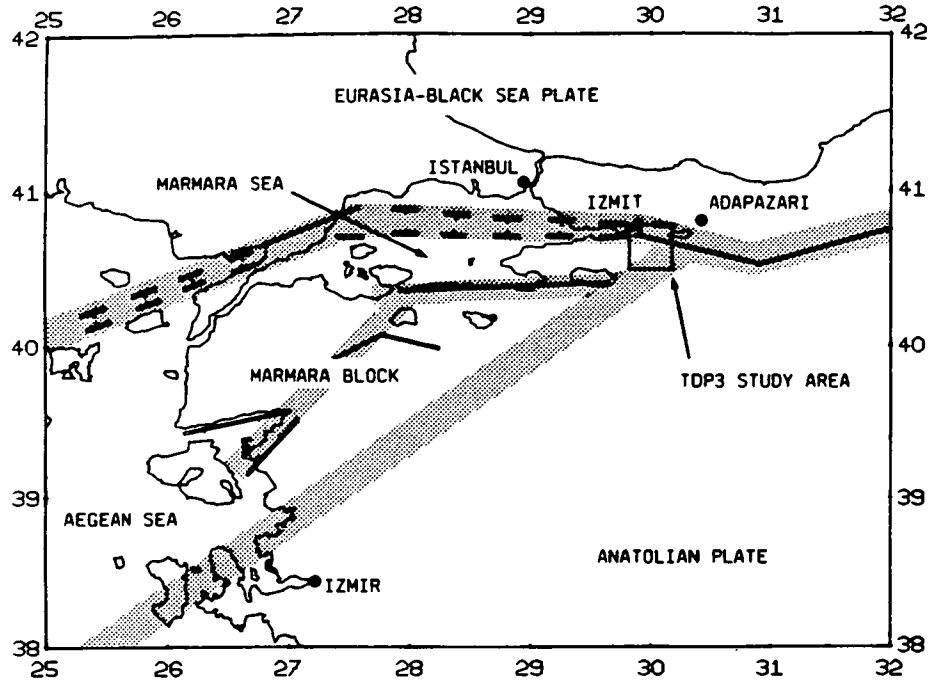

Figure 1. Location and simplified tectonics of TDP3 study area. Seismic lineations outlining the Marmara Block are shown stippled; solid and dashed lines show the trace of the North Anatolian Fault and its subsidiary faults on land and under water respectively (after Crampin & Evans 1986).

& Canitez (1982).

The nature of the NAF changes at the eastern extremity of the Marmara Sea. On the basis of their associated seismicity, three distinct lineations have been recognized radiating from this area (Crampin & Üçer 1975; Üçer et al. 1985). The northern branch of the NAF continues in a direct line westwards as a graben structure, enclosing Lake Sapanca, Izmit Bay and a deep trough in the Marmara Sea. It reappears as a south-west trending, strike-slip fault on the north-west shore of the Marmara Sea, and continues into the Aegean Sea as a deep trough. The middle lineation follows the southern shore of the Marmara Sea westwards, changing strike to south-west towards the western extremity of the sea. Although it is less well-defined seismically than the other two lineations, it is well defined by surface geology (Dewey & Şengör 1979). The southern lineation strikes south-west, following the line of the Izmir-Ankara ophiolite suture zone, (Şengör & Yilmaz 1981).

Recognition of these three seismically-defined lineations has led Evans et al. (1985) and Crampin & Evans (1986) to postulate the existence of the Marmara Block (Fig. 1) as a distinct seismotectonic unit. This wedge-shaped zone of accommodation is trapped between the Eurasian and Anatolian

Plates, and is being rotated and sheared by the westward movement of the Anatolian Plate. Seismicity associated with the Marmara Block is typically low-magnitude and persistent, and displays marked clustering. Its character is therefore somewhat different from that of the rest of western Anatolia, which typically displays the more usual foreshock/mainshock/aftershock sequences, and suggests that the Marmara Block behaves as a discrete tectonic unit (Crampin & Evans 1986). Crampin & Booth (1985) conclude that sub-horizontal tension provides the main driving force for movement on the NAF in this area, and this is confirmed by the geometry of the plate motions (Crampin & Evans 1986).

2 The Turkish Dilatancy Projects

Throughout history the NAF has been the location of many large earthquakes. Various authors have described its seismicity (Pamir 1944; Ambraseys & Zatopek 1969; Ambraseys 1970; Crampin & Üçer 1975; Dewey 1976; Toksöz et al. 1979) and it has been noted that these earthquakes form a westward-migrating sequence but with an area of quiescence around Izmit Bay. Toksöz et al. (1979) suggest that this area is a seismic gap, where a significant earthquake can be expected in the future.

Since 1971, the British Geological Survey (formerly the Institute of Geological Sciences) and the Centre for Research and Development in Space and Earth Science of Boğaziçi University, Istanbul (formerly Kandilli Observatory) have collaborated in seismological research in the Marmara Sea area. MARNET (Üçer et al. 1985), a permanent telemetered network of single-component seismograph stations, has monitored the area since 1978 and was augmented during the summers of 1979, 1980 and 1984 by temporary networks of closely-spaced, three-component stations (Turkish Dilatancy Projects TDP1, TDP2, and TDP3, respectively). These networks monitored the low-magnitude swarm activity in the Izmit Bay area, (Fig. 1). The earthquakes were used as sources of shear-waves for the investigation of shear-wave splitting, diagnostic of extensive-dilatancy anisotropy or EDA (Crampin 1978; Crampin et al. 1980, 1985). EDA is now recognised for shear-waves propagating in the crust in many areas of the world (Crampin 1987). The TDP3 project deployed up to 15 three-component stations in a more closely-spaced network than TDP1 or TDP2, and recorded earthquakes for a six-month period in summer 1984. Over seven hundred local events were located using HYP071 (Lee & Lahr, 1975). The level, magnitude and distribution of the seismicity recorded during TDP3 are very similar to those recorded in the two previous experiments. MARNET, however, which records only the largest

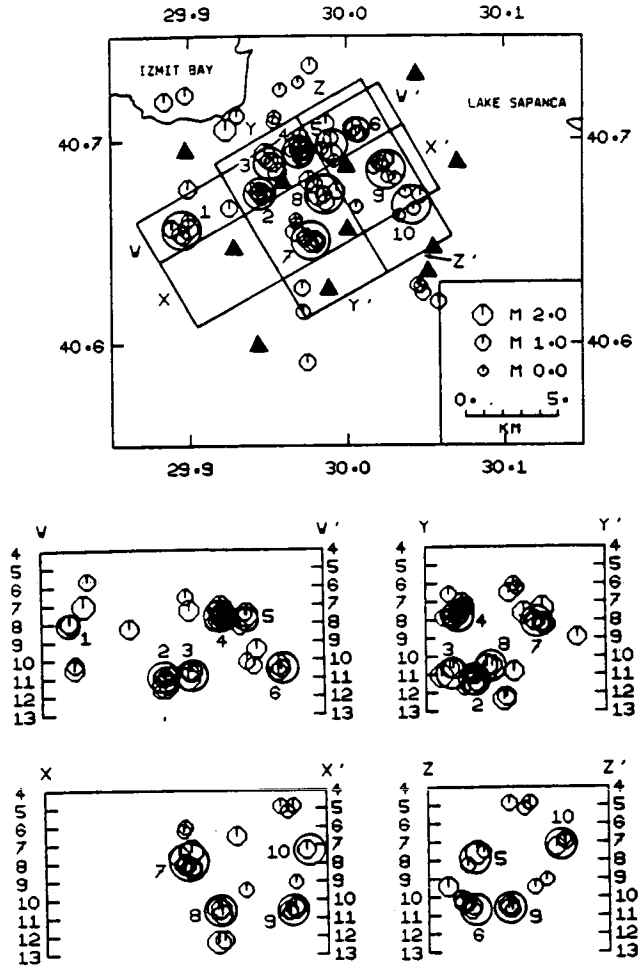

Figure 2(a). Epicentre map and illustrative cross-sections for the 87 events with at least six P-wave arrivals, showing clusters 1 to 10 (circled). Filled triangles represent TDP3 seismograph stations.

events in the swarm, indicates that there has been a slight decrease in overall activity during the period 1979-1984. Fig. 2(a) shows the epicentres and cross-sections of the 87 best-located local events having at least six P-wave arrivals.

3 Fault-plane solutions

Fault-plane solutions were constructed for the 87 earthquakes of Fig. 2(a). In general, these events were the largest and best-located, although unambiguous P-wave arrivals were not always present. In such cases nodal lines were drawn near to stations whose seismograms showed the high S- to P-wave amplitude ratios which often indicate the proximity of a nodal plane. A number of events gave well-constrained solutions, and fault-plane solutions for 32 of these are shown in Fig. 3. These events are

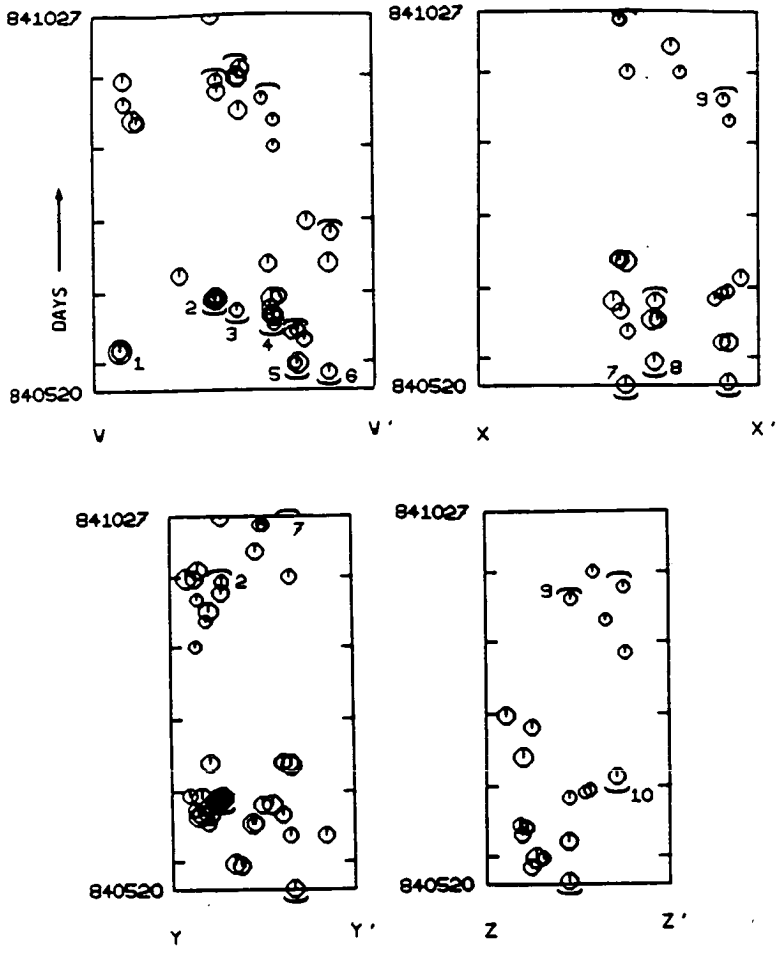

Figure 2(b). Time plots, at the same horizontal scale, for the four cross-sections of Fig. 2(a). Start and finish dates are indicated, ticks denote start of a month. The short-lived clusters are circled, while the long-lived clusters are shown bracketed.

distinguished by having generally larger magnitudes and better azimuthal distributions of P-wave arrivals.

3.1 OBSERVATIONS

Mechanisms

The fault-plane solutions show a variety of mechanisms. Normal faults with varying percentages of strike slip predominate but there are several almost pure dextral strike-slip solutions (11, 29 and 32, amongst others). Reverse fault mechanisms (19, 24 and 31) are less common, and their identification must remain somewhat speculative as fault-plane solutions for these events (with the exception of 31) are not well-constrained.

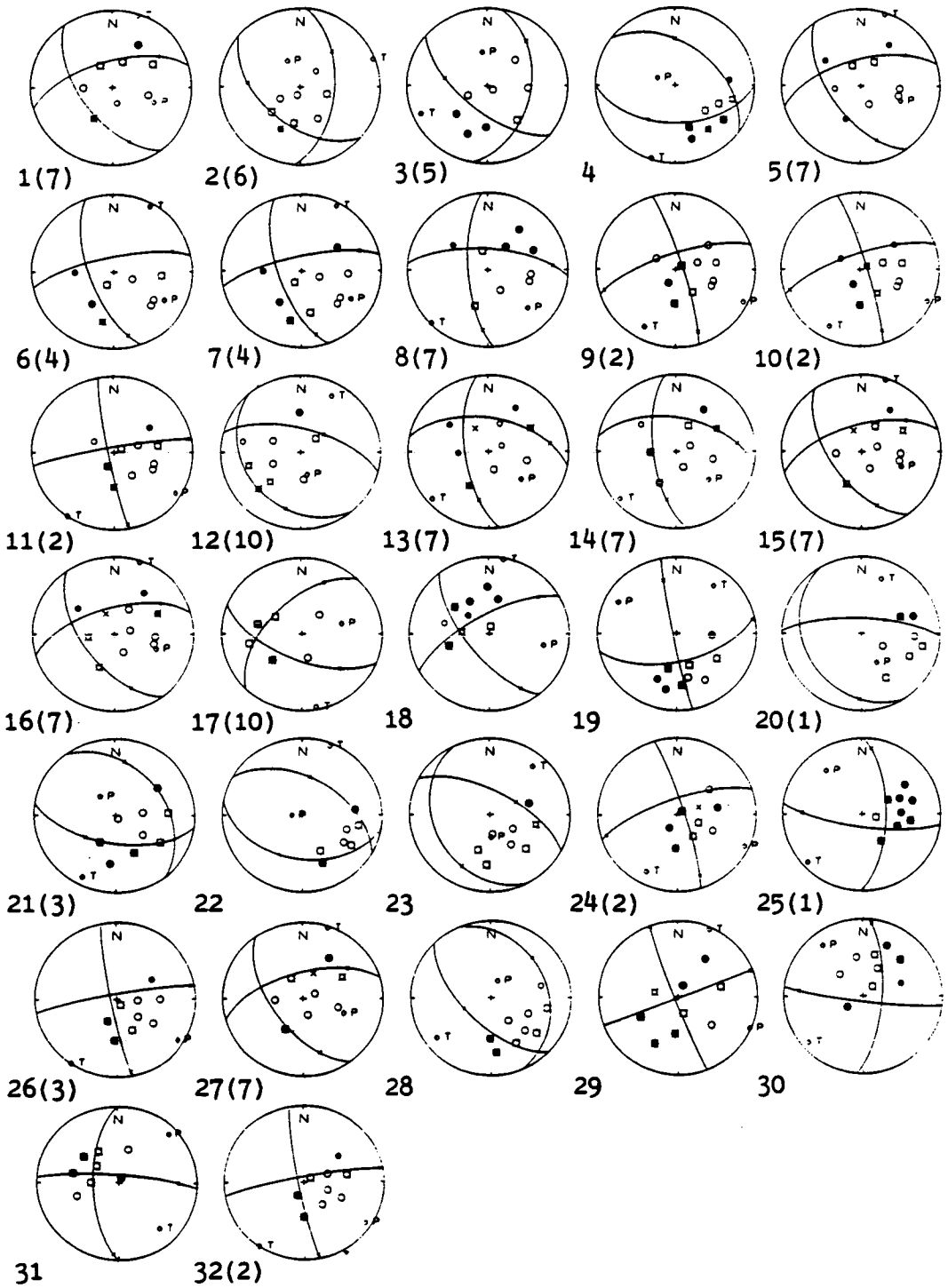

Figure 3. Individual fault-plane solutions for the 32 best-constrained events from Fig. 2(a). Where applicable, the number of the cluster in Fig. 2(a) in which the event occurs has been included in brackets. Data are shown on equal-area projections of the upper focal hemisphere. Open and filled circles

(Continued on opposite page..)

Slip vectors

Fig. 4(a) shows the normals to the fault- and auxiliary-planes (that is the possible slip vectors) for the 32 fault-plane solutions of Fig. 3 plotted on a single composite equal-area projection. With the exception of events 9, 10 and 24, the events have one normal which plots in the north-east quadrant. These normals are grouped around a mean direction of about N 60°E, and, because of this grouping, are interpreted as slip vectors (Evans *et al.* 1985).

Principal axes of stress

The variety of focal mechanisms (Fig. 3) and locations (Fig. 2a) suggests stress release on a complex array of fault-plane facets. If we assume that the same regional stress field drives all these earthquakes, then the principal axes of stress will be common to the mechanisms of all events (Crampin & Booth 1985). Fig. 4(b) shows the nodal planes of the best-constrained fault-plane solutions superimposed on an equal-area plot of the upper focal hemisphere. The areas of tension (T) and compression (P) common to all solutions are marked, and are in approximately the same position as, but more closely constrained than, those in the similar figure of Crampin & Booth (1985). In a strike slip configuration, vertical compression is unlikely to be the dominant or driving stress, and the near-vertical compression is likely to be the intermediate stress here. We conclude that the main driving force of these swarm events is the tensional stress which in Fig. 4(b) is constrained to a sub-horizontal direction N 180°E to N 190°E. This tensional stress direction is orthogonal to, and consistent with, the observed polarizations of the leading split shear-waves whose average is N 100°E in all three TDP projects (Crampin & Booth 1985; Chen *et al.* 1987). Furthermore, dominant tensional stress is expected from the geometry of the movement of the Marmara Block and the tensional features observed at surface in the area (Crampin & Evans 1986).

(Fig. 3, contd.)
represent, respectively, dilatational and compressional first motions, and smaller circles indicate less reliable readings. Crossed circles indicate those stations whose seismograms show a large *S*- to *P*-wave amplitude ratio, indicating proximity to a nodal line. Isolated crosses indicate those stations where no *P*-reading was available and large *S*- to *P*-wave amplitude ratios were inferred from the horizontal components. The projections of the slip vectors of the fault- and auxiliary planes are shown as small crosses on the nodal lines. The positions of compressional (P) and tensional (T) axes are marked.

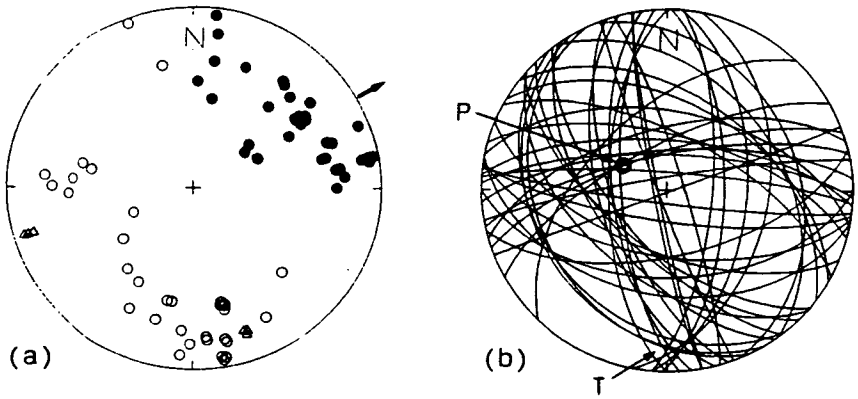

Figure 4. (a) Fault and auxiliary plane normals for the 32 fault-plane solutions in Fig. 3 superimposed on one plot; those in the north-east quadrant, shown as solid circles, are interpreted as slip vectors and their alternates, shown as open circles, are interpreted as fault-plane normals. The normals for the three thrusts are shown as open triangles. The heavy arrow indicates the mean slip vector direction of N 60°E. (b) Nodal lines for the 32 fault-plane solutions in Fig. 3 superimposed on one plot. Those areas of compression (P) and tension (T) common to each solution are marked.

3.2 DISCUSSION AND COMPARISON WITH PREVIOUS EXPERIMENTS

The fault-plane mechanisms derived here are similar to those found previously by Evans et al. (1985), who suggest that a mixed regime of normal and strike-slip faulting is taking place in the Marmara Sea area, resulting from rotation and shearing of the Marmara Block. Their mean slip vector direction (N 50°E) is consistent with the gradual change westwards of the directions of the slip vectors of teleseismically-determined fault-plane solutions for large earthquakes which have occurred along sections of the NAF. Some of these earthquakes caused surface faulting, from which positive identification of fault planes and thus slip directions could be made. The slip vectors change from an easterly direction on the NAF in the east of Turkey, through north-east around the study area, and to northwards towards the west of the Marmara Sea. The present mean slip vector direction of N 60°E is consistent both with previous observations and with the position of the study area on the NAF.

Identification of the present family of fault planes is somewhat tentative, perhaps because some of the fault-plane solutions are not as well-constrained as those of Evans et al. (1985). However, a pattern emerges from Figs. 3 and 4(b). A predominantly east-west trending, southward-dipping group can be identified, and the north-south striking, westward-dipping family of Evans et al. (1985) is again represented. This

picture is complicated by a series which strikes approximately east-west and dips northwards. These may be expected to occur in a tensional regime with some uplift in the Marmara area. Although Chen et al. (1987) only show results for the nine best-constrained mechanisms for which shear-wave polarizations are observed, all the mechanisms in Fig. 3 deduced from the P-wave data will produce shear-wave polarizations which, after propagation through a distribution of aligned cracks, are consistent with those observed (D.C. Booth, personal communication).

4 Clustering in space and time

Similarity in the wave-form of seismic waves from successive earthquakes located in the same area has been described by Tsujiura in a series of papers (see Tsujiura 1983). These earthquake families have also been described from the USA (Ishida and Kanamori 1980; Geller and Mueller 1980). Weaver & Hill (1978) have pointed out the association between swarms of activity and major strike-slip faults in tensional regimes. However, these

Table 1. Location data for earthquakes in cluster 7 of Fig. 5.

Event no. in cluster	Date (y m d)	Time (h m s)	Lat. (°N)	Long. (°E)	Depth (km)	Magnitude M_L	Fault-plane soln. no. in Fig. 3
1′	840507	073928.19	40.651	29.990	8.94	0.5	
2′	840516	055017.79	40.655	29.967	8.65	0.6	
3′	840520	174849.79	40.650	29.980	8.26	1.4	1
4′	840530	052243.66	40.650	29.982	8.22	1.0	
5′	840608	093611.73	40.650	29.982	8.35	0.6	
6′	840609	162800.64	40.649	29.982	8.28	1.2	
7′	840611	172014.45	40.651	29.980	7.69	0.4	
8′	840612	145058.31	40.652	29.980	8.22	0.9	
9′	840618	050220.52	40.650	29.984	8.31	0.3	
10′	840621	010309.52	40.653	29.976	8.30	1.1	5
11′	840625	175332.10	40.655	29.967	7.62	1.7	8
12′	840712	164529.62	40.651	29.980	7.36	1.9	13
13′	840713	030202.18	40.650	29.976	8.13	1.2	14
14′	840627	023604.15	40.652	29.976	7.74	0.7	
15′	840627	034243.08	40.648	29.968	8.30	0.1	
16′	840713	212331.43	40.652	29.973	8.11	1.0	15
17′	840713	214537.83	40.653	29.973	8.03	0.0	16
18′	840801	035234.34	40.651	29.973	8.39	1.6	
19′	840810	230446.13	40.648	29.975	6.57	0.4	
20′	840812	010613.96	40.650	29.974	7.08	0.9	
21′	840813	171730.81	40.648	29.979	8.43	1.1	
22′	840814	235705.82	40.653	29.974	7.19	0.8	
23′	840818	054854.51	40.654	29.975	7.66	0.9	
24′	840930	105515.95	40.648	29.988	7.61	0.2	
25′	841001	031014.64	40.651	29.976	7.90	0.9	27
26′	841006	200142.41	40.652	29.975	7.66	0.3	
27′	841021	154513.90	40.653	29.973	8.23	0.7	

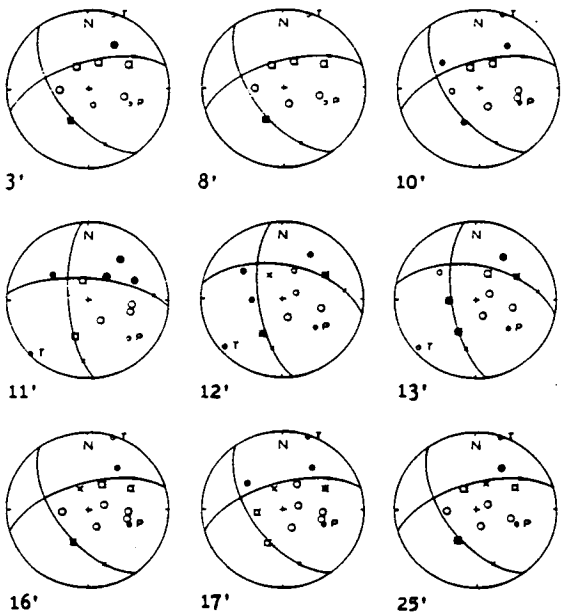

Figure 5. Fault-plane solutions for nine well-recorded events in cluster 7 numbered as in Table 1. Notation is as in Fig. 3, but note different event numbering.

studies have been conducted on large magnitude earthquakes and using regional networks. Here we demonstrate that low-magnitude swarms not detectable by regional networks show the same phenomena.

4.1 CLUSTERING IN SPACE

Earthquake epicentres shown on the map and cross-sections of Fig. 2(a) exhibit strong clustering and their focal depths are confined almost entirely to between seven and 11 km. These clusters are numbered 1 to 10 on Fig. 2(a). Evans et al. (1985) presented composite fault-plane solutions for four clusters, A-D of their Fig. 1. In the present study, these previously-observed clusters are again strongly represented. Although the earthquake epicentres are not coincident, the present fault-plane solutions are generally similar to the previous ones, but show slightly different orientations. It is interesting to note from cross-section WW' of Fig. 2(a), that clusters 1 to 6 form a remarkably linear feature, trending approximately N 60°E. This is related to the regional trend of surface features and may well mark the southern limit of the graben of the NAF.

Data sets from previous TDP experiments were examined for clustering. S. Crampin and S.B. Üçer, in an unpublished study, found 15 clusters of varying size in the TDP2 data, and seven clusters have been found in the TDP1 data by the present authors. No doubt additional clusters could be

identified from the present large data-set, but we have confined our study to the more obvious and larger clusters.

The seismograms for events in each cluster were compared. In some cases, they showed no real similarity, suggesting that the events were not directly related and that their epicentral proximity was coincidental. In most clusters however, the seismograms showed a striking degree of similarity, and some were true doublets. This would be expected for events occurring very close to each other, when the rays to the stations would follow almost identical paths. This similarity enabled us to compare seismograms and thus derive fault-plane solutions for poorly-recorded events. In a few cases, a difference of P-wave polarity at one station and a consequent slight change of orientation of the fault-plane solution indicated the sensitivity of the network to small changes of epicentre position and fault orientation.

These points are well illustrated by cluster 7 (Fig. 2a). This cluster is well-located within the network, and persistent, with over 20 events occurring within a very small volume. Additionally, nine events gave reliable fault-plane solutions, which are presented, together with location data for the cluster in, respectively, Fig. 5 and Table 1. Seismograms recorded at the same station for the nine events in the three sub-groups of cluster 7 are shown in Fig. 6.

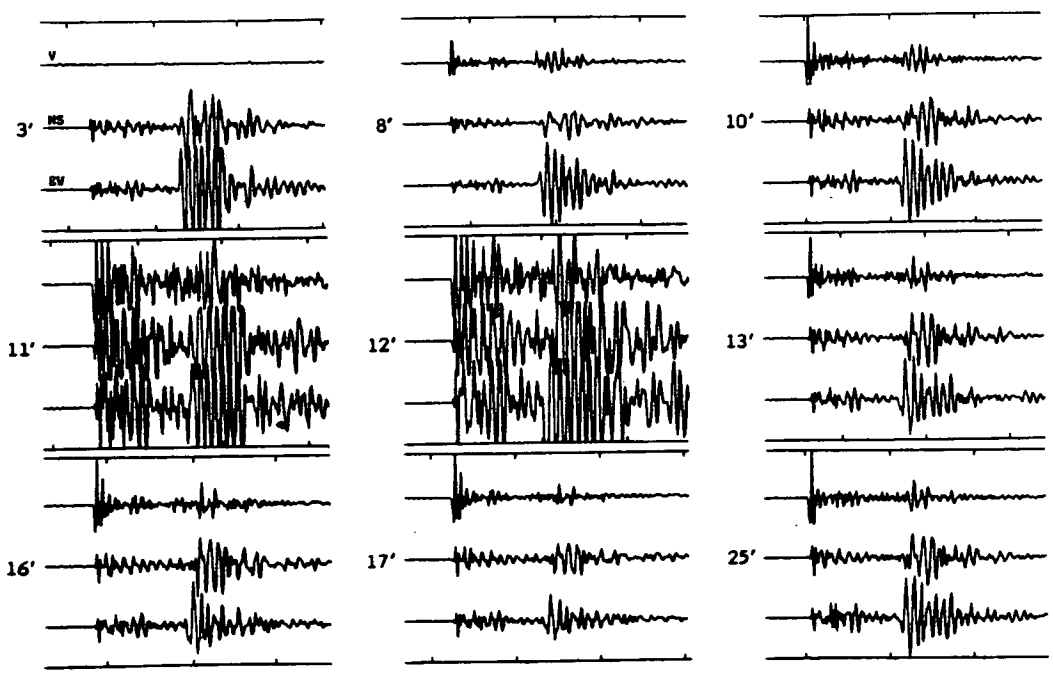

Figure 6. Three-component seismograms, recorded at the same station, for the nine events in cluster 7 whose fault-plane solutions are presented in Fig. 5.

From cross-sections XX′ and YY′ of Fig. 2(a) and the location data presented in Table 1 it can be seen that cluster 7 contains a sequence of events which occur at almost identical depths and locations. These events can be considered almost coincident even allowing for the possible systematic errors of up to 2km in locations determined using HYPO71, when the true regional structure is anisotropic (Doyle et al. 1982). This suggests that they are the result of movement on very small asperities or fault facets, areas perhaps of the order of a few tens of m^2. As would be expected, the closest similarities in seismograms were observed between those events having the closest epicentres. Thus great similarity occurred between three sub-groups of cluster 7, consisting of events 1′ to 10′, 11′ to 13′, and 14′ to 25′ (event numbers with ticks refer to events in Table 1, which has been subdivided to illustrate the sub-groups). Events 26′ and 27′ show a greater variation, and are only indirectly related to the rest of the sub-groups. Seismograms for events 3′ and 8′, and for events 16′ and 17′ (Fig. 6) were almost identical except for amplitude, and there was a close similarity in character between all seismograms in this cluster, (for example, compare those from events 10′, 13′ and 25′). The fault-plane solutions (Fig. 5) for the events within these three sub-groups of cluster 7 show the expected similarities, but with slight variation in orientation and differences in P-wave polarity near nodal lines, for example, between events 11′, 12′ and 13′, especially where noise levels were high, making positive identification of P-wave polarities difficult. The overall similarity between the fault-plane solutions of events in cluster 7 reveals that the nature and orientation of the faulting varies little with position in the group. Additionally, as the close cluster of events occurs over a time span of about five months, movement on certain facets of fault planes or asperities may take place over considerable periods and is similar in nature throughout this period.

4.2 CLUSTERING IN TIME

The swarm activity in this area has shown clustering for at least five years. Fig. 7 contains histograms showing the overall seismicity level during the TDP3 experiment, together with those showing the activity of three selected clusters from Fig. 2(a). Although the overall level of seismicity has decreased recently, the general pattern remains similar to that for previous experiments. Sporadic peaks of activity are superimposed on a generally low background level of activity of a few events per day. The peaks correspond in most cases to outbursts from the more active clusters, for example cluster 1, which briefly shows a level of about 30 events per day (Fig. 7).

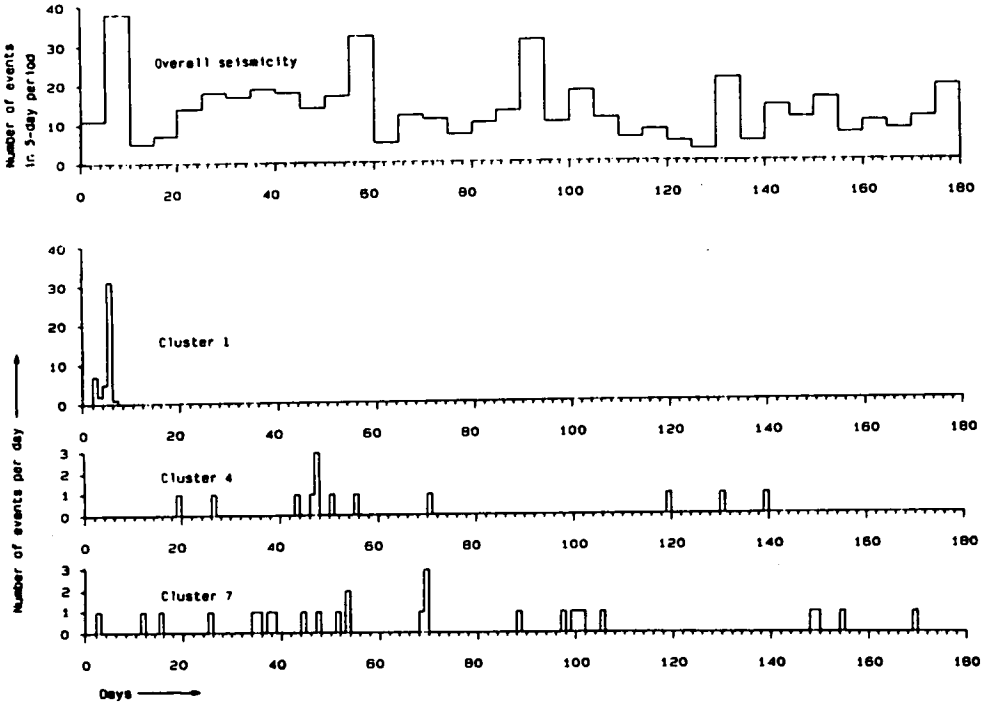

Figure 7. Histograms showing overall seismicity during TDP3 and the activity of selected clusters. For the overall seismicity histogram, the number of events in a five-day period is plotted, while for the cluster activity histograms the number of events per day is plotted. Note that the ordinates are plotted at different scales.

Two distinct types of cluster activity are indicated by the activity histograms in Fig. 7. The first type exhibits short bursts of intense activity of up to 30 events per day for just a few days, as in cluster 1. Such clusters then appear to cease activity abruptly without reactivation, at least over the period of observation. The second type, such as clusters 4 and 7, shows a lower activity level of a few events every few days or so, but continuing in some cases for the whole experimental period. A small change in the seismograms with time can be detected in these clusters, suggesting that activity is migrating very slowly along a fault, that the orientation of the fault is changing slightly, or, as suggested by Chen et. al. (1987), that the geometry of the microcrack structure changes with time.

Three recording stations were common to each of the three TDP experiments. We attempted to link the three experiments in time initially by comparing seismograms of the clusters in Fig. 2(a) with those of the clusters from TDP2 whose epicentres plotted close to the present clusters. The search was extended to a radius of about 1 km. to allow for possible

systematic errors in locations due to the slightly different station configurations. A similar comparison between the TDP2 and TDP1 data sets was also made. Apart from a few similarities at stations having characteristic seismograms and other similarities especially in the P-waves, in no case could clusters be traced between all three data sets. It therefore appears that clusters may remain active for several months, but that once activity in one cluster ceases reactivation does not usually occur.

4.3 CLUSTERS - DISCUSSION

The properties exhibited by cluster 7 are shown to a greater or lesser extent by all of the clusters in Fig. 2(a) and those found in previous experiments. Although some clusters consist of only a few events, each cluster contains at least two earthquakes whose seismograms are almost identical (doublets) or which show great similarity and whose epicentres are very close. In some cases the activity of the cluster spans only a day or two, but it can occur over a much longer period - up to five months in the present study (Fig. 2b). It is noticeable that sequences of near-identical events usually tend to be spaced over a period of a few days, for example, cluster 1 (Fig. 7). This suggests that these short bursts of activity represent movement on asperities which either become locked in some way or the particular fault-plane facet of the asperity becomes eroded, so that subsequent fault movement migrates, possibly to another facet of the same asperity. In cases where a cluster contains sub-groups, the fault-plane solutions for each sub-group are similar but not identical, suggesting that the fault mechanism or orientation varies little with time throughout the cluster. The seismograms for events in the more long-lived clusters may show a slight change with time, suggesting a change in fault orientation, a migration of the epicentres (which is not detectable in the HYPO71 locations), or a change in the crack structure within the rock mass (Chen *et al.* 1987)

In general, very close similarities between seismograms were observed only for short-lived clusters of earthquakes. Although a similarity in general character exists between events which are more widely-spaced in time, they do not have identical mechanisms but are very closely related, and probably result from movement on facets of the same asperity. Additionally, as joint epicentre relocation methods have an accuracy of the order of a hundred metres (Logan 1987), clusters identified by HYPO71 locations may well show subclustering on further analysis. We suggest therefore that seismic activity on the small individual fault planes, or asperity facets, on which these clusters of events occur is short-lived, existing for periods of the order of weeks or at most a few months.

Theoretical studies (for example by Aki 1979 and Israel and Nur 1979) suggest that stress concentrates along a fault at barriers and asperities. Clusters, or families, of earthquakes with identical or near-identical seismograms (doublets) have been described from Japan (Tsujiura 1983) and the USA (Ishida and Kanamori 1980; Geller and Mueller 1980). Regional networks with station separations typically of 30-100km. have been used, and the events studied have been of greater magnitude than those described here. These clusters have been linked to foreshock activity and earthquake prediction, and it seems clear that long-term monitoring is necessary to reveal the relationship between clustering and stress change.

Logan (1987), in an independent study of some of the TDP clusters using a joint epicentral relocation method, reports that the relocated epicentres appear to plot on northward- and southward-dipping planes which strike approximately east-west. It seems reasonable to expect these planes to be fault planes, and they are consistent with composite fault-plane solutions produced for those clusters, although as the fault-plane solutions are not well-constrained they are not presented in Fig. 3. Additionally, he reports that the relocation method has an accuracy of a few tens of metres, and has been able to subdivide clusters into small sub-groups far more accurately than is possible using purely visual comparison of seismograms. It seems likely that routine use of such techniques will permit very accurate resolution of the epicentres of cluster activity, and thus reveal the pattern of activity in great detail.

5 Conclusions

The activity of the TDP microearthquake swarm has persisted for at least five years, although there has been some fluctuation of activity at various points within the swarm. The use in the present experiment of more three-component stations in a more closely-spaced network has allowed previous results to be confirmed and refined. The principal directions of stress determined in 1979, 1980 and 1984 are almost identical, and Chen *et al.* (1987) report that the mean polarization direction of the leading split shear-waves during TDP3 is still N 100°E, as it was in TDP1 and TDP2 (Crampin & Booth, 1985). The fault-plane solutions show that the faulting continues to be predominantly normal, but with some strike slip and a few thrust mechanisms, confirming the stress patterns around the Marmara Block identified by Evans *et al.* (1985) and Crampin & Evans (1986). Note that the temporal variations of delays between split shear-waves, reported by Chen *et al.* (1987), are differential changes of at most 3 milliseconds km^{-1} over five years. These small differential changes do not give rise to noticeable effects on locations or fault-plane mechanisms, but have major significance

as sensitive indicators of the stress behaviour within the fault region.

This is probably the first time that small clusters of earthquakes have been identified and located with such a closely-spaced, small-aperture network. Cluster activity has been occurring in this area for many years in response to the particular stress pattern. Many, if not most, earthquakes in this swarm belong to such clusters. We suggest that analysis of the behaviour of such clusters may be important for earthquake source studies because it allows the behaviour of small earthquakes to be studied in great detail, and may lead in turn to a better understanding of the behaviour at the source of large earthquakes.

Acknowledgements

We would like to thank the staff of Kandilli Observatory of Boğaziçi University, Istanbul, for their help in conducting the fieldwork on which this study is based, and also the staff of the British Council in Ankara and Istanbul for their invaluable assistance with the documentation and logistics. This work was supported by the UK Overseas Development Administration and the Natural Environment Research Council, with some indirect support provided by US Geological Survey Contract No. 14-08-0001-G1169. It is published with the approval of the Director of the British Geological Survey (NERC).

References

Aki, K., 1979. Characterization of barriers on an earthquake fault, *J.geophys. Res.*, 84, 6140-6148.

Ambraseys, N.N., 1970. Some characteristic features of the Anatolian Fault Zone, *Tectonophys.*, 9, 143-165.

Ambraseys, N.N. & Zatopek, A., 1969. The Mudurnu Valley, West Anatolia, Turkey, earthquake of 22 July 1967, *Bull.seism.Soc.Am.*, 59, 521-589.

Chen, T., Booth, D.C. & Crampin, S., 1987. Shear-wave polarizations near the North Anatolian Fault - III. Observations of temporal changes, *Geophys. J.R.astr.Soc.*, 91, this issue.

Crampin, S., 1978. Seismic-wave propagation through a cracked solid: polarization as a possible dilatancy diagnostic, *Geophys.J.R.astr.Soc.*, 53, 467-496.

Crampin, S., 1987. Geological and industrial implications of extensive-dilatancy anisotropy, *Nature*, 328, 491-496.

Crampin, S. & Booth, D.C., 1985. Shear-wave polarizations near the North Anatolian Fault - II. Interpretation in terms of crack-induced anisotropy, *Geophys.J.R.astr.Soc.*, 83, 75-92.

Crampin, S. & Evans, R., 1986. Neotectonics of the Marmara Sea region in Turkey, *J.geol.Soc.*, 143, 343-348.

Crampin, S., Evans, R. & Üçer, S.B., 1985. The analysis of records of local earthquakes: the Turkish Dilatancy Projects (TDP1 and TDP2), *Geophys. J.R.astr.Soc.*, **83**, 1-16.

Crampin, S., Evans, R., Üçer, S.B., Doyle, M., Davis, J.P., Yegorkina, G.V. & Miller, A., 1980. Observations of dilatancy-induced polarization anomalies and earthquake prediction, *Nature*, **286**, 874-877.

Crampin, S. & Üçer, S.B., 1975. The seismicity of the Marmara Sea region of Turkey, *Geophys.J.R.astr.Soc.*, **40**, 269-288.

Dewey, J.W., 1976. Seismicity of Northern Anatolia, *Bull.seism.Soc.Am.*, **90**, 84-92.

Dewey, J.W. & Şengör, A.M.C., 1979. Aegean and surrounding regions: complex multiplate and continuum tectonics in a convergent zone, *Bull.geol. Soc.Am.*, **90**, 84-92.

Doyle, M., McGonigle, R. & Crampin, S., 1982. The effects of crack anisotropy on the hypocentral locations of local earthquakes, *Geophys.J.R.astr.Soc.*, **69**, 137-157.

Evans, R., Asudeh, I., Crampin, S. & Üçer, S.B., 1985. Tectonics of the Marmara Sea region of Turkey: new evidence from micro-earthquake fault plane solutions, *Geophys.J.R.astr.Soc.*, **83**, 47-60.

Evans, R., Beamish, D., Crampin, S. & Üçer, S.B., 1987. The Turkish Dilatancy Project (TDP3): multidisciplinary studies of a potential earthquake source region, *Geophys.J.R.astr.Soc.*, **91**, this issue.

Geller, R.J. & Mueller, C.S., 1980. Four similar earthquakes in central California, *Geoph.res.Let.*, **7**, 821-824.

Ishida, M. & Kanamori, H., 1980. Temporal variation of seismicity and spectrum of small earthquakes preceding the 1952 Kern County, California, earthquake, *Bull.seism.Soc.Am.*, **70**, 509-527.

Israel, M. & Nur, A.M., 1979. A complete solution of a one dimensional propagating fault with nonuniform stress and strength, *J.geophys.Res.*, **84**, 2223-2234.

Lee, W. & Lahr, J., 1975. HYPO71 (revised): a computer program for determining hypocentre, magnitude and first motion pattern of local earthquakes, *U.S.Geol.Surv., Open File Rept.*, 75-311.

Logan, A.L.L., 1987. Accurate relative location of similar earthquakes, *Ph.D. thesis*, University of Edinburgh.

Pamir, H.N., 1944. Kuzey Anadolu'da bir deprem çizgisi, *Istanb.Üniv.Fen. Fak.Mecm.A*, **7** (in Turkish).

Şengör, A.M.C., 1979. The North Anatolian transform fault: its age, offset and tectonic significance, *J.geol.Soc.*, **136**, 269-282.

Şengör, A.M.C., & Canitez, N., 1982. The North Anatolian fault. In: *Alpine-Mediterranean Geodynamics, Geodynamic Ser.*, **7**, 205-216.

Şengör, A.M.C., & Yilmaz, Y., 1981. Tethyan evolution of Turkey: a plate tectonic approach, *Tectonophys.*, **75**, 181-241.

Tsujiura, M., 1983. Characteristic frequencies for earthquake families and their tectonic implications: Evidence from earthquake swarms in the Kanto District, Japan, Pure appl.Geophys., 121, 573-600.

Toksöz, M.N., Shakal, A.F. & Michael, A.J., 1979. Space-time migration of earthquakes along the North Anatolian fault zone and seismic gaps, Pure appl.Geophys., 117, 1258-1270.

Üçer, S.B., Crampin, S., Evans, R., Miller, A. & Kafadar, N., 1985. The MARNET radiolinked seismometer network spanning the Marmara Sea, and the seismicity of Western Anatolia, Geophys.J.R.astr.Soc., 83, 17-30.

Weaver, C.S. & Hill, D.P., 1978. Earthquake swarms and local crustal spreading along major strike-slip faults in California. Pure appl. Geophys., 117, 51-64.

GLOBAL SEISMOLOGY

Report No. 342

Report on a symposium on Earthquake Prediction held at BGS, Edinburgh 28 June - 1 July 1987

by

J.H. Lovell

September 1987

Global Seismology Research Group
British Geological Survey
Murchison House
West Mains Road
EDINBURGH
EH9 3LA

031 667 1000

Article for submission to Geology Today 7/9.87 - GEOLGY.REP

Report on a symposium on Earthquake Prediction held at BGS, Edinburgh, 28 June - 1 July 1987

John H. Lovell, Global Seismology Research Group, British Geological Survey, Edinburgh

A powerful new technique for earthquake prediction and monitoring in situ stress was presented by the Global Seismology Research Group of the British Geological Survey at a recent symposium in Edinburgh. The technique also has potential applications to the mining, hydrocarbon, and geothermal industries.

Introduction

Papers presented by BGS at a symposium held recently at BGS, Edinburgh, described new techniques for monitoring stress by analyzing the effects of stress-aligned microcracks on seismic shear-wave propagation. The work, partially financed by the Overseas Development Administration, involved three separate field projects recording earthquakes near the North Anatolian fault, in north-west Turkey. The projects monitored a swarm of microearthquakes on a facet of the North Anatolian Fault, one of the Earth's major strike-slip faults, separating the Black Sea and Anatolian Plates. The high-quality digital shear-wave data stimulated Stuart Crampin and his colleagues at BGS to suggest the hypothesis of extensive-dilatancy anisotropy and develop the programs and techniques necessary for its interpretation.

Extensive-Dilatancy Anisotropy and Shear-wave splitting

Most, if not all, of the Earth's crust is permeated by distributions of fluid-filled cracks, microcracks, and preferentially oriented pore-space, which can vary in size from microns up to joint dimensions. In general, these cracks are aligned by tectonic stress into parallel, vertical orientations, and the phenomenon is called *extensive-dilatancy anisotropy* or *EDA*. Such aligned EDA-cracks cause the elastic properties of the rockmass to vary with direction so that it becomes effectively anisotropic to seismic wave propagation. In particular, shear-waves radiated from earthquakes or artificial sources entering such an anisotropic region split into two or more components, each component having different velocities and polarizations of particle motion.

This phenomenon is called shear-wave splitting and is analogous to the optical anisotropy or birefringence observed in many minerals. The split components have different velocities of propagation, so in time they separate and introduce a characteristic signature into the three-dimensional particle motion, as shown in Figure 1. The polarization direction of the leading (faster) split shear-wave is parallel to the direction of maximum compression of the tectonic stress. When these waves are recorded using three-component seismometers, the methods developed by BGS can be used to estimate the geometry of the cracks and hence monitor the behaviour of the stress aligning the cracks.

Shear-wave splitting has been observed above small earthquakes in many parts of the world whenever suitable three-component seismograms are available. It has now been observed above earthquakes in Turkey, Japan, Kenya, the USA, the USSR, the UK, and elsewhere. It has also been reported above acoustic events in geothermal experiments, in shear-wave reflection surveys for hydrocarbon exploration and production, and in shear-wave vertical-seismic-profiles or VSPs in hydrocarbon and geothermal reservoirs. (VSPs are recordings of a source at the surface by geophones down a borehole.) It is clear that crack-induced anisotropy is a very common feature of at least the upper 10 or 20 km of the Earth's crust.

The distributions of EDA-cracks in the Earth's crust are relatively inaccessible to direct physical observations. Approaching the *in situ* cracks by drilling, for example, would disturb the stress regime and possible modify the crack geometry irretrievably. The most direct way to examine these cracks is by analyzing shear-waves that have propagated through the cracked rockmass. The preferred technique involves displaying the three-component seismograms in polarization diagrams, so that shear-wave splitting can be identified and the behaviour of the particle motion analyzed. Polarization diagrams are seismograms displayed in mutually orthogonal cross-sections of the three-dimensional particle motion, as in Figure 2. They are the most convenient way to analyze shear-waves with the interpretation techniques developed at BGS.

Application to earthquake prediction

The behaviour of stress before earthquakes is not well understood. At present, very limited observations of shear-wave splitting suggest that stress increases

before an earthquake without any significant change of direction. Such increases in stress cause the EDA-cracks to become "bowed", as indicated in Figure 3, without necessarily affecting the number of cracks, their length, or their orientation. Such bowing modifies the delay between the split shear-waves propagating through the cracked rock. The polarization of the leading split shear-wave is unaffected, but the time-delay between the split shear-waves changes in a distinctive patterns that can be recognized by analyzing polarization diagrams. Such subtle changes can be accurately measured with the above techniques and have been identified in the Anza seismic gap in southern California and (less clearly) in the Izmit gap in Turkey.

It is suggested that such methods are a powerful technique for directly monitoring stress changes before earthquakes. Routine earthquake prediction would require long-term monitoring of high-risk vulnerable areas (such as the San Andreas Fault in California) using earthquakes, or, preferably, shear-wave VSPs, where the behaviour of split shear-waves would be routinely examined at some appropriate time interval. A picture of the behaviour of stress could be built up, and appropriate further action taken if changes were noted. Results reported so far from the Anza seismic gap in California and from the Izmit seismic gap in Turkey (where large earthquakes are expected in the future) are encouraging. Temporal variations in stress have been detected in both areas, pointing the way to routine earthquake prediction.

Other applications for monitoring EDA

Monitoring the behaviour of EDA-cracks by analyzing shear-wave splitting offers a real opportunity for accurate and routine earthquake prediction. It also has other important industrial applications. Within the last year or two, oil companies have realized the importance of shear waves for identifying the alignment and geometry of cracks and fractures in reservoirs. A better knowledge of the internal structure of crack and fracture alignments in hydrocarbon reservoirs would enable the extraction efficiency to be maximized and secondary and tertiary extraction optimized. Similar considerations apply in the field of geothermal heat extraction, and there are other applications to monitoring of rockbursts in mines, and the investigation of crack and fracture patterns in radioactive waste repositories, unstable slopes, and mine overburdens.

Conclusions

Earthquake studies by BGS have led to the development of the hypothesis of EDA and the possibility of monitoring *in situ* stress by analyzing the effects of EDA-crack geometry on shear-wave splitting. This has applications to earthquake prediction and a wide variety of other industrial and geological problems. These results were received with great interest by delegates at the seminar, and BGS hopes to collaborate with several of them on further research. As yet, this work is in its infancy, but as more people become aware of its potential, the investigation of the Earth's crust using repeatable, shear-wave sources should become routine, and lead to considerable industrial and environmental benefits.

Suggestions for further reading

Crampin, S. 1987. The basis for earthquake prediction, *Geophys.J.R.Astr.Soc.* (in press).

Crampin, S. 1987. Geological and industrial implications of extensive-dilatancy anisotropy, *Nature*, **328**, pp 491-496.

Figure captions

Figure 1. Schematic diagram shoving a shear-wave passing through a region of parallel, vertical, liquid-filled EDA-cracks which have been aligned parallel to the direction of maximum compressional stress. The shear-wave is split into two phases, where the leading (faster) split shear-wave is polarized parallel to the maximum compressional stress. These distinctive features are preserved in the emergent wave, and can be studied using the techniques outlined in this article.

Figure 2. Examples of three-component seismograms and polarization diagrams for the shear-wave arrivals in the numbered time-windows marked above the seismograms. The seismograms are rotated into (V)ertical, and horizontal (R)adial and (T)ransverse components. The polarization diagrams are labelled (U)p, (D)own and (L)eft and (R)ight when looking from the source to the receiver, and (T)owards and (A)way from the source. The abrupt changes in direction of the shear-wave particle motion, typical of anisotropy-induced shear-wave splitting, are marked by arrowheads on the horizontal polarization diagrams.

Figure 3. Schematic diagram shoving the bowing of cracks by an increase in stress. This bowing modifies the time-delay between the split shear-waves in particular patterns that can be recognized by analyzing the split shear-waves.

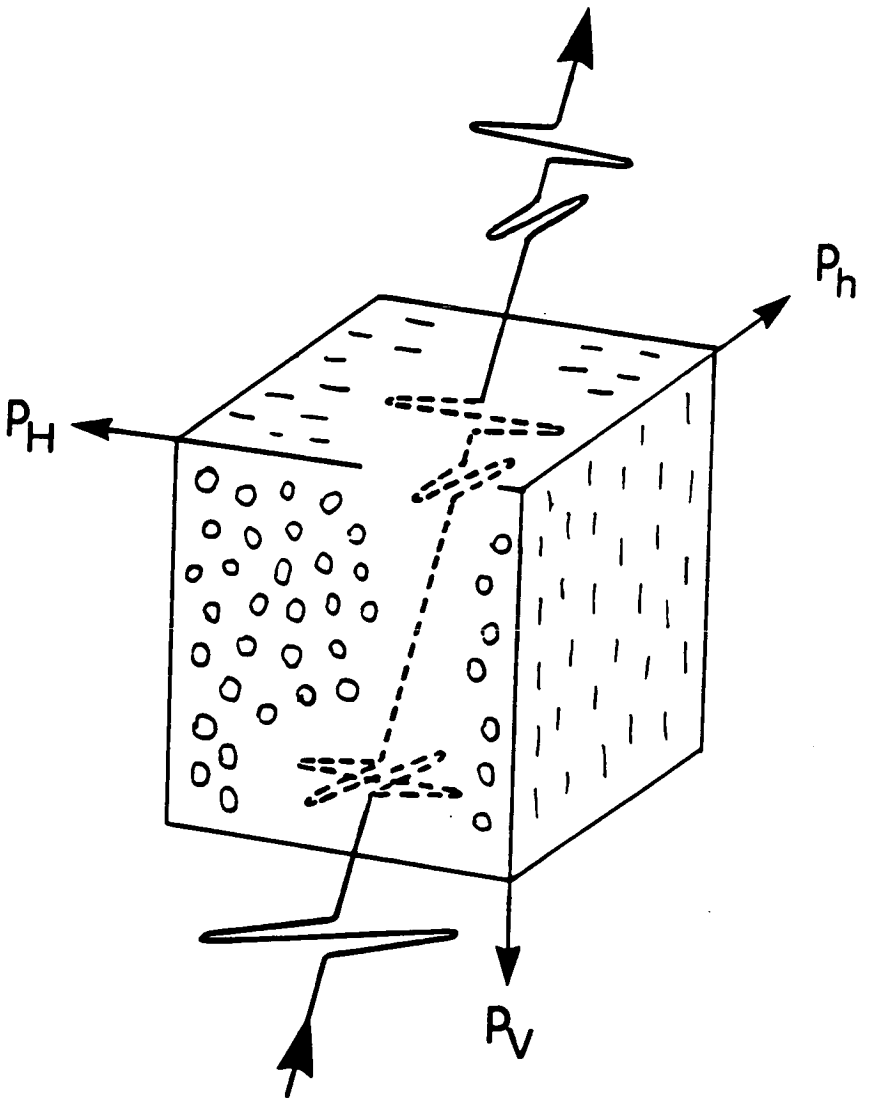

$$P_H \sim P_V \gg P_h$$

Figure 1

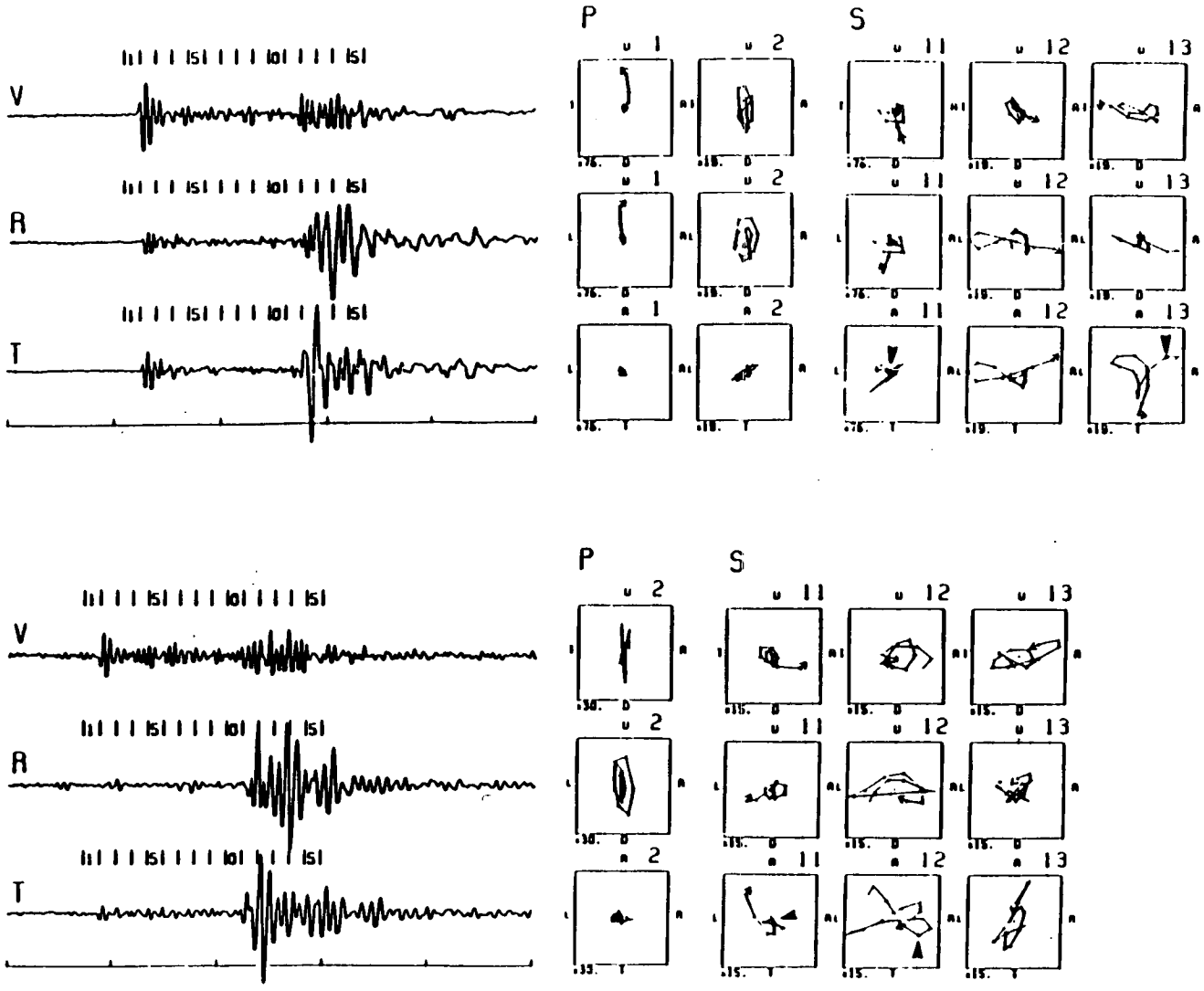

Figure 2

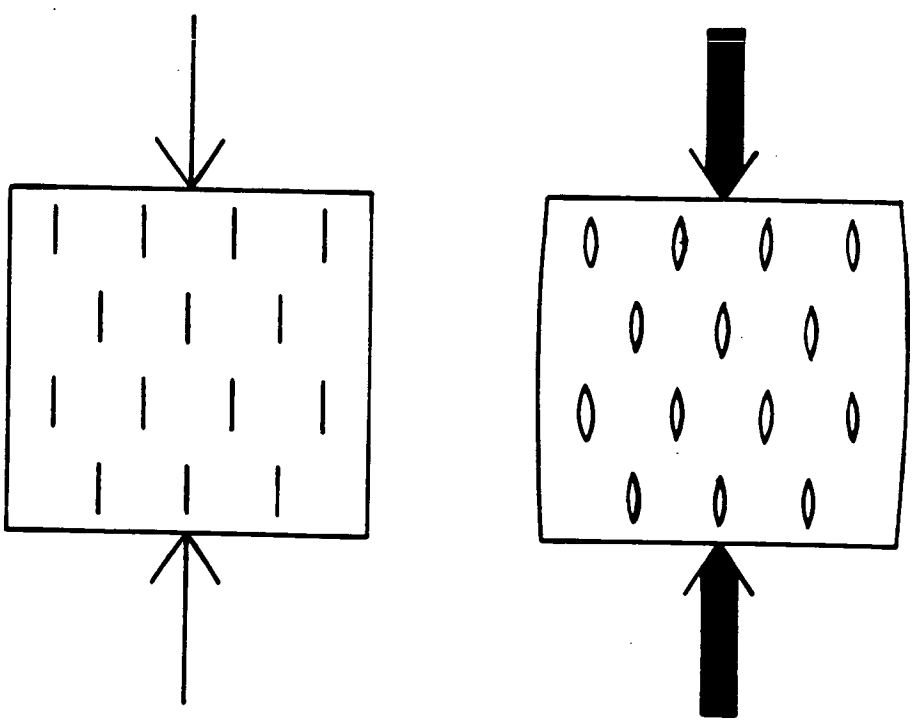

Figure 3

GLOBAL SEISMOLOGY

Report No. 343

Symposium on a technique for earthquake prediction and monitoring in situ stress

by

J.H. Lovell

September 1987

Global Seismology Research Group
British Geological Survey
Murchison House
West Mains Road
EDINBURGH
EH9 3LA

031 667 1000

SYMPOSIUM ON A TECHNIQUE FOR EARTHQUAKE PREDICTION AND MONITORING IN SITU STRESS

John H. Lovell, Global Seismology Research Group, British Gelogical Survey, Edinburgh

At a symposium held recently at the British Geological Survey, Edinburgh, thirty delegates from the UK and elsewhere heard staff of the BGS describe a new method for earthquake prediction which also has wide-ranging applications in the hydrocarbon and geothermal industries and other geological investigations. The symposium was sponsored by the Overseas Development Administration who funded much of the research upon which it was based.

Since 1979, the Global Seismology Research Group of BGS has investigated earthquakes near the Marmara Sea, NW Turkey. A persistent swarm of microearthquakes, caused by movement on the North Anatolian Fault, has been monitored during three separate field experiments evolving as the techniques were developed. The large amount of high-quality digital data acquired during these projects has enabled the BGS team, led by Stuart Crampin and colleagues, to develop the hypotheses and sophisticated computer procedures required for the detailed shear-wave analysis in the earthquake prediction technique.

The hypothesis of Extensive-Dilatancy Anisotropy or EDA was developed by modelling the propagation of seismic shear-waves (*S*-waves) through cracked rock. Observations obtained in Turkey could only be explained by the shear-waves propagating through regions of parallel, vertical, liquid-filled cracks aligned by tectonic stress. These regions of stress-aligned EDA-cracks have subtle effects on the propagation of shear-waves. When a shear-wave enters a region of EDA-cracks, it splits into two or more phases with different velocities and polarization directions which are fixed by the direction of propagation through the cracked rock. This phenomenon is called shear-wave splitting, and is analogous to the optical birefringence observed in many minerals. Shear-wave splitting has now been reported in differing rock types and differing tectonic environments from many parts of the world, including the UK, France, Japan, Kenya, Turkey, the USA, and the USSR, and it appears that most of the Earth's crust down to a depth of at least 10 or 20 km is pervaded by EDA-cracks, and is anisotropic to shear-waves. The split shear-waves travel

at different velocities in the cracked rock. Consequently, they separate with time and introduce a characteristic signature into the three-dimensional particle motion of the shear wavetrain. This is illustrated schematically in Figure 1. The distinctive signature is preserved once the shear wave has left the cracked region, and can be identified at any point along its path by the techniques discussed during the symposium. Moreover, the leading, or faster, split shear-wave is polarized in a direction parallel to the maximum compressional stress. This polarization direction can be easily measured, and used to estimate the direction of stress.

For analysis, the three-component seismograms are rotated into vertical, and horizontal radial and transverse components, and plotted in mutually orthogonal cross-sections of the three-dimensional particle motion called polarization diagrams. The time delays between the split shear-waves, and the directions of polarization of the leading split shear-waves, can be accurately measured directly from these diagrams. These measurements can be modelled to determine the crack density (the degree of anisotropy) and the stress orientation controlling the crack geometry. The crack dimensions are sensitive to changes of stress, and it was demonstrated that stress change before earthquakes could be detected by following the behaviour of the time delays between split shear-waves. This is the basis of the earthquake prediction technique, which requires continuous monitoring of high-risk areas, using natural earthquakes or, preferably, repeated vertical-seismic-profiles (VSPs), where a source of shear waves at the surface is recorded down a borehole. Changes of shear-wave delays and hence of the stress controlling the crack geometry could then be identified and other appropriate action taken as deemed necesary. This method offers a real possibility of accurate earthquake prediction. Encouraging results were reported from the Anza seismic gap, in California, where a large earthquake is expected. Measurement of shear-wave delays over a number of years has shown a temporal increase, indicating a local build-up of stress.

The applications of monitoring EDA-cracks for the hydrocarbon and geothermal industries were demonstrated. A knowledge of the crack orientation and crack density within the source rock would enable industry to plan extraction in the most optimum ways, and many oil companies have recently become interested in shear-wave analysis.

Delegates at the symposium received these nev ideas with enthusiasm, and it is

hoped that several new long-term collaborative projects will be initiated in the near future between BGS and foreign institutes.

Figure caption

Figure 1. Schematic illustration of shear-wave splitting. A shear-wave entering a region of aligned cracks, necessarily splits into two phases with different polarizations and different velocities which insert a characteristic signature into the three-dimensional particle motion. This signature is preserved for an subsequent uncracked segment of the path.

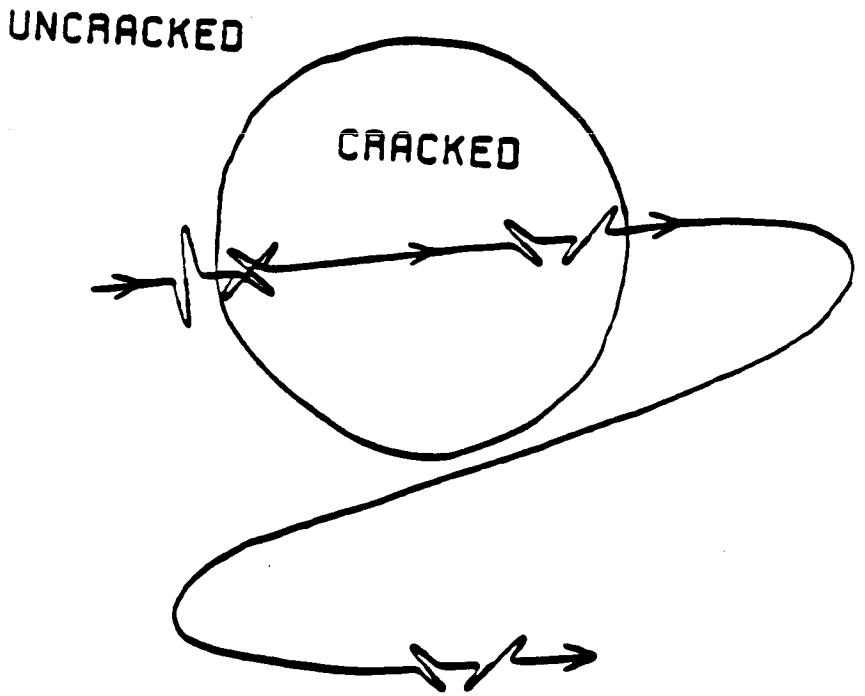

FIG. 1.